ADSORPTION AND TRANSPORT PROPERTIES OF OXIDIZED MULTI-WALLED CARBON NANOTUBES

by

Jin Yang

A dissertation submitted to Johns Hopkins University in conformity with the requirements for the degree of Doctor of Philosophy

Baltimore, Maryland

March 2014

ABSTRACT

This work established quantitative relationships between the surface composition of oxidized multi-walled carbon nanotubes (O-MWCNTs) and their adsorption and transport properties under varying aquatic chemical conditions.

The effects of aquatic and surface chemistry on adsorption properties of O-MWCNTs for Zn^{2+} and Ni^{2+} were found consistent with expectations based on prior study, and were similar to aggregated and dispersed O-MWCNTs. New studies revealed, however, a significant effect of O-MWCNT solid-to-liquid ratio on measured adsorption isotherms. Although causes of such effects remain poorly understood, these results have important environmental implications.

Transport of various O-MWCNTs through silica glass bead media was studied in columns under conditions of steady flow and pulse inputs. These studies revealed that O-MWCNT transport was affected by aquatic and surface chemistry in ways generally consistent with theories of electrostatic interactions between surfaces. Dissolved Ca^{2+} destabilized O-MWCNTs more than Na^{+} and diminished the impact of O-MWCNT surface chemistry on transport. NOM at low concentrations (<4 mg-C/L) significantly stabilized O-MWCNTs under most conditions, including high ionic strength (IS) (10 mM Ca^{2+} or 100 mM Na^{+}).

For experiments when clean-bed filtration (CBF) dominated removal (i.e., pulse-input injections), the mathematical relationship between k_d and approach velocity followed expectations of interception theory and suggested that CNT length is the relevant length scale for prediction of collisions. For step-input conditions and considering both breakthrough curves and in-situ concentrations of O-MWCNTs, models

based on CBF and incorporating additional mechanisms of straining, site-blocking, and multilayer deposition (ripening) were developed. Model sensitivity studies revealed that at IS < 40 mM, site-blocking and straining were more important to model than other mechanisms. At higher IS (≥ 60 mM), CBF and ripening were the only important mechanisms to consider. At IS = 40 mM, site-blocking, straining and ripening were all important to consider. Thus, IS is a key variable controlling which mechanisms must be considered when modeling O-MWCNT interactions with silica-based porous media.

Overall, findings from this study have furthered the understanding of O-MWCNTs in terms of their transport and adsorption properties. The results and associated model development can improve interpretation and simulation of O-MWCNTs behavior in aquatic systems.

Dissertation Readers:

Dr. William Ball, Johns Hopkins University (advisor)

Dr. Edward Bouwer, Johns Hopkins University

Dr. Kai Loon Chen, Johns Hopkins University

Dr. Howard Fairbrother, Johns Hopkins University

Dr. Alan Stone, Johns Hopkins University

ACHNOWLEDGEMENTS

First and foremost, I would like to express my deepest gratitude to my advisor Dr. William Ball, who has always been supportive and helpful. Bill has constantly encouraged me to think independently and critically. Every time I thought I have found answers to a problem, Bill asked questions that I could not answer right away. Bill has also helped me with my writing skill with great patience.

I would also like to thank my committee members. Dr. Howard Fairbrother provided me the opportunity to work in his lab for more than two years. Howard acted as a second advisor during my dissertation research and provided tremendous help in experimental design and data processing. I appreciate him for always being available when I had questions or came across obstacles in my experiments. Dr. Kai Loon Chen also helped me in many ways in my research, especially colloidal related theories. Dr. Alan Stone was always the one to turn to when I had questions regarding aquatic chemistry and he always had inspiring answers in return. Dr. Edward Bouwer gave me valuable advises in our weekly Ball/Bouwer meetings and provided generous help when I came across problems. I appreciate all the committee members for devoting their time for my committee meeting, defense and thesis reading.

Other current and previous faculty members of DoGEE also helped me a lot. The late Dr. Charlie O'Melia provided useful suggestions on my transport experiments. Dr. Markus Hilpert answered a lot of my questions in hydrology. Dr. Lynn Roberts nicely granted me the opportunity to TA for her where I learnt much. Dr. Seth Guikema and his postdoc Allison Reilly helped me improve my skill with modeling and coding.

In addition to faculty members from DoGEE, I also want to express my sincere gratitude to Dr. Stephane Ngueleu Kamangou and his advisors Prof. Olaf Cirpka and Prof. Peter Grathwohl from University of Tuebingen in Germany, Dr. Kenneth Livi from Departments of Earth and Planetary Sciences and Biology, and Professor Nathalie Tufenkji from McGill University for their help and suggestions on my experiments and simulation.

Friends and colleagues from DoGEE and Dr. Fairbrother's group all deserve and are with my sincere gratitude. Dr. Hyunhee Cho taught me how to do adsorption measurements in an accurate way. Dr. Billy Smith initially set up the column system. Dr. Julie Bitter helped me a lot in lab and has edited my writing for numerous times. David Goodwin helped me with both the column and adsorption experiments. Zhifeng Yan, Dr. Zhi Shi, Dr. Nathan Boland, Dr. Kevin Wepasnick, Mike Barkley, Dr. Chip Elliot, Dr. Yongseok Hong, Dr. Amar Wadhawan, Dr. Katie Parry, Dr. Yaqi You, Dr. Phillip Flanders, Dr. Samantha Rosenberg, Dr. Peng Yi, Li Tang, Dr. An Huynh, and Pavlo Bohutskyi have all provided me lots of help with my experiments. Laura McDonald, Dano Wilusz, Chris Kelly, and Miranda Gallagher helped me a lot with my writing. My lab assistants Hannah Kim, Alex Dang, Chenqi Xie, Debjani Mallick, Peter Mellott, Gene Patrick Geronimo, and Cynthia Chambers have also contributed significantly to my research.

I would also like to thank current and previous front office staff Keith Ritchie Adena Rojas, Christine Kavanagh, Robert Francisco, Denise Nowlin, Vicky Moreira, and Joyce Moody. My research would not go so smoothly without their help and my lab would not last for a month without help from Keith.

Especially, I want to express my gratitude to DoGEE family for the anonymous donation for my cat Daidai (Tara) when she had a severe accident and big surgery. I was caught by surprise and was so touched by their great kindness and compassion.

I also want to thank my other friends and colleagures Dr. Yuqi Li, Dr. Meredith Erb, Stephanie Lau, Xiaomeng Xia, Dr. Jing Chen, Dr. Shawn Li, Xin Tang, Dr. Chang Lang, Dr. Lijun Xia, Dr. Yang Li, Man Li, XinXing Zhang, Jing Li, Dr. Yajing Zhang, Yao Li, Ting Zhang, Ying Zhang, and Dr. Jun Zhong for making my Ph.D. Journey fun.

Last but not the least, I would like to thank my family. My parents, Daquan Yang and Xiaojuan Zhu, have raised me and supported me all these years. Their constant encouragement and stimulation propelled me through my early education, and ultimately resulted in my pursuit of a scientific career today. I would not be the person I am without their devotion. They also generously provided me with funds for my first year of studies as a Master's student here at Johns Hopkins. I also want to thank my husband Xiaolei Zhu. Xiaolei is beside me and absolutely supportive at all times. My Ph.D. journey was sometimes stressful and he was always there when I could not handle the situation on my own. I would not have gained the PhD without him.

TABLE OF CONTENTS

LIST OF TABLES

LIST OF FIGURES

Chapter 1. Introduction

1.1 Properties and Applications of Carbon Nanotubes

Carbon nanotubes (CNTs) are "needle-like hollow tubes" made of cylindrical sheets of graphene.[1] CNTs include both single-walled carbon nanotubes (SWCNTs), which contain only one graphitic layer, and multi-walled carbon nanotubes (MWCNTs), which contain two or more (often between 7-10) concentric layers of graphitic sheets with an interlayer distance of ~3.4 Å.[1, 2] CNTs range from 2 to 30 nm in diameter and up to 1 μm or more in length, as based on direct observation with TEM.[1-5] Since their discovery, CNTs have been well known for their unique seamless cylindrical structure with nano-scale diameters and graphene rolls with three possible primary rolling patterns.[1-3] The unique structure leads to remarkable properties such as large surface area to volume ratios, high aspect ratios, low densities, high mechanical and tensile strengths, high electric and thermal conductivity, strong non-linear optical property, high hydrogen storage potentials, high adsorbency and antimicrobial property compared to other materials.[3, 4, 6-9] For instance, the values of Young's modulus for CNTs are exceptionally high,[10] and it has been reported that the strength-to-weight ratio of SWCNTs is 460 times that of steel.[8]

The novel physicochemical properties of CNTs, as given by their unique structure and overall chemical composition, have led to various commercial applications of CNTs and their derivatives in a variety of fields. For instance, CNTs are used as proximal probe tips of scanning tunneling microscope (STM) due to their small size, high electrical conductivity and high modulus.[11] They can also be used as nanotweezers to handle

nanoclusters by moving them as well as probing their electronic structure.[12] CNTs not only exhibit high electrical conductivity, but their electrical conductivity can also be changed significantly by exposure to certain gases such as NO_2 or NH_3,[13] making them an excellent choice for chemical sensors. Moreover, CNTs have been added into composite materials such as polymer matrices to either enhance the strength and modulus of the composite materials[14] or to serve as antimicrobial agents.[15, 16] The high strength and resilience of the resulting composite materials that contain CNTs have been used in fields of plastic manufacture and automobile manufacture. Other composite materials, such as membranes and polymers, have been used in water purification systems due to their antimicrobial property. CNTs are also viable as candidates for the storage of H_2, as relevant to the promotion of H_2 as a new fuel source.[17-19] A high degree of H_2 storage in CNTs has been reported in experimental literature,[17-19] although theoretical explanations for such phenomena are still incomplete. [17-19]

1.2 Production of CNTs

Because of their wide range of current and potential future applications, production of CNTs has increased exponentially in recent years.[17] According to a report from Innovation Research and Products Inc. (iRAP), the production capacity for nanocarbon products, including SWCNTs, MWCNTs, fullerenes, graphene, carbon nanofibers and nanodiamonds, has increased from 996 tons in 2008 to 4065 tons in 2010.[17] This number is expected to exceed 12,300 tons in 2015 with a production value of roughly $1.3 billion.[17] The production of SWCNTs and MWCNTs has been predicted to increase at a compound annual growth rate of 32.5% starting in 2010 and reaching 14,110 tons by 2016.[20] MWCNTs, with an annual production about two times higher than

SWCNTs, are expected to dominate the product market for at the least next two years because of their lower production cost and availability in large quantities.[21]

1.3 Possible Risks to the Environment from CNT Production and Use

The rapid growth in CNT production is undoubtedly accompanied by elevated potential risks for the natural environment, including surface and ground water systems. Although pathways for release of CNTs are still under investigation,[22-24] and accurate detection and quantification in actual matrices is still not possible, it is reasonable to assume that during the processes of production, application and disposal, CNTs can access aqueous environments through municipal and industrial wastewater, solid waste leachate, precipitation from the atmosphere following air pollution events, or from direct input via spills or misuse.[25] Aqueous contamination may also occur as the result of long-term degradation of the commercial materials into which CNTs are embedded.[22-24] As a new material, the potential hazards of CNTs to humans, other organisms and the ecosystem are not yet fully understood, but biomagnifications through aquatic ecosystems is a concern, including the possibility of toxic accumulations. In fact, some potentially harmful human health effects of MWCNTs have already been reported by some investigators.[26, 27] For instance, Sayes *et al.*[26] reported that suspended SWCNTs selectively deposited on the membranes of human dermal fibroblasts (HDF). Another research group, Patlolla *et al*.,[28] reported that MWCNTs induced the viability loss of HDF through DNA damage.

Given these concerns, and the importance of transport as a potential exposure pathway, CNT behavior in aquatic systems is important to understand. The so-called pristine CNTs (i.e., CNTs whose surface have not been modified after initial production)

are mostly hydrophobic and unstable in water systems, limiting their ability to travel long distances in natural environments.[9, 29] On the other hand, however, CNT surfaces are often subjected to oxidation through intentional functionalization processes.[9, 29] The existence of hydrophilic groups such as oxides on CNT surfaces have been shown to dramatically influence their environmentally relevant properties, especially stability in aqueous systems.[29, 30] In addition to chemical incorporated oxygen functional groups, adsorbed natural organic matter (NOM) has also been reported to significantly stabilize CNTs in aqueous system.[31-35] Such modifications can thus significantly increase the risk of CNTs.

In addition, CNTs' large specific surface area, which, together with surface oxides, enhances their ability to strongly interact with other chemicals in their vicinity, creating the possibility for their presence to substantially change the distribution, availability and transport properties of other contaminants such as heavy metals and organic compounds.[26, 36] Previously established risk estimation of these other types of contaminants may therefore need to be re-evaluated and possibly altered for situations when CNTs are present.

Overall, the unknown effects of CNTs on the environment and on other contaminants are concerns that need to be addressed through proper research.

1.4 Motivation for This Research

1.4.1 *The Need to Study the Fate and Transport of CNTs*

CNT fate and transport studies are necessary for the estimation of their potential risks to environmental and human receptors. These studies are essential for the establishment of a comprehensive understanding of overall risk, as needed to establish an

appropriate regulatory system. In this regard, it is important to recognize the fate of CNTs is heavily dependent on their aggregation, deposition, and transport properties, all of which will be strongly affected by CNT surface chemistry and the surrounding aquatic chemistry.[29-31, 34]

As mentioned above, CNT surfaces are often oxidized in the process of production to increase their stability in polar solvents[37-42] or to improve their bioavailability as drug delivery carriers.[43] Surface oxides can also be introduced onto the surface of CNTs inadvertently as a result of purification processes used in industry or due to incidental exposure to oxidizing agents such as UV radiation and/or ozone.[26, 29] The degree of surface functionalization as well as the nature and different distribution of functional groups grafted onto the surface of CNTs varies significantly with the type and intensity of the oxidation processes, and these properties will in turn alter the aggregation and transport properties of CNTs.[26, 29]

In the aqueous environment, MWCNTs with surface oxides such as hydroxyl and carboxylic acid groups on their surface will be negatively charged under typical environmental conditions, e.g. pH 6-8, which will affect their interactions with other MWCNTs, particles in suspension or collector surfaces that they encounter. It is well known that electrostatic repulsive forces between like-charged particles will be affected by changes in pH and ionic strength (IS).[29, 44] Changing these factors will either increase (with increasing pH) or screen (with increasing IS) the negative charges on the CNT surface and therefore change the nature and compressed thickness of the diffuse layer of ions surrounding each particle. Early attempts to quantitatively describe such phenomena were provided by Derjaguin-Landau[45, 46] and Verwey-Overbeek[47] and have been further

developed by others over time.[48] The basic theory describing the balance of electrostatic interactions and shorter-range chemical forces is now generally referenced as DLVO theory, although more complex models have also been developed to supplement this theory with regard to more complex and short-range interactions.[49] The situation can be especially complex in the presence of surfactant molecules or other polymeric or macromolecular adsorbents such as NOM, which can attach to the particles or collectors causing particles to experience additional steric and electrostatic interactions with each other and other surfaces. Thus, the aggregation, deposition, and transport behavior of colloidal particles will be significantly changed by the presence of such materials. [50, 51]

In the past, colloidal aggregation and transport have been studied extensively through both experimental and modeling approaches.[52-55] However, because the properties of CNTs are in many ways unique relative to other colloids, new studies are needed to better understand their environmental fate in water.

1.4.2 *The Need to Study the Interactions of CNTs with Other Contaminants*

To fully investigate the potential risk of CNTs, we have to better understand not only their environmental fate, but also their potential associations with other pre-existing chemicals and the mutual impacts of such associations on the movements of both CNTs and other chemicals. When considering their interactions with other contaminants, sorption properties are important to understand, including the influences of both CNT surface chemistry and the surrounding aquatic chemistry.[56, 57] CNTs are now well known to be good adsorbents for hydrophobic organic chemicals (HOCs) as well as heavy metal contaminants.[57-61] With the rapidly growing production of CNTs, there is an increased

likelihood of CNTs to adsorb those contaminants and therefore alter their distributions and movement.

1.5 Recent Studies of the Aggregation, Transport and Adsorption Properties of CNTs

1.5.1 *Homo-Aggregation of CNTs*

Homo-aggregation of CNTs has been studied intensively in the past several years.[34, 35, 62-64] Such studies have revealed a major impact of pH and IS on the aggregation properties of CNTs in a manner that is qualitatively consistent with DLVO theory.[29] Calcium and NOM have also been shown to play an important role in affecting the aggregation behavior of CNTs via specific ion interactions and the steric effect, respectively.[34, 64] The effect of surface chemistry on the homo-aggregation of oxidized-MWCNTs (O-MWCNTs) has also been studied.[29, 35] For example, Smith *et al*.[29] studied the effect of NaCl concentration, pH value and surface chemistry on the aggregation kinetics of O-MWCNTs using time resolved dynamic light scattering (TR-DLS). The authors reported accelerated aggregation of MWCNTs with increasing NaCl concentration or decreasing pH, while O-MWCNTs at higher surface oxygen concentration showed higher stability at identical aquatic conditions. Hyung *et al.*[31] reported that for any given mass of added MWCNT powder, the concentration of well-dispersed MWCNTs in solution increased systematically with concentration of Suwannee River natural organic matter (SRNOM). Smith *et al.*[35] discovered that NOM at concentrations as low as 0.5 dissolved organic carbon/L (DOC/L) was able to enhance the stability of O-MWCNT dispersions and that these effects occurred even in the

presence of Ca^{2+} and in a manner largely independent of O-MWCNT surface oxygen concentration.[35]

1.5.2 *Hetero-Aggregation of CNTs*

In environments where multiple colloidal particles exist, hetero-aggregation may take place.[65] Because of the ubiquitous presence of naturally occurring colloidal particles, the hetero-aggregation process plays a more important role in determining the fate and transport of CNTs than homo-aggregation in natural environments.[66] However, fewer studies regarding hetero-aggregation were conducted compared to those for homo-aggregation. Huynh *et al.*[65] investigated the hetero-aggregation of MWCNTs (negatively charged) with hematite nanoparticles (HemNPs, positively charged) with varied CNT/HemNP mass concentration ratios (CNT/HemNP) using TR-DLS. They reported that the rate of hetero-aggregation first increased with increasing CNT/HemNP untill the ratio reached 0.0316, where the hetero-aggregation rate was 3.3 times of the HemNP homo-aggregation rate.[65] The further increase in the CNT/HemNP, on the other hand, caused a dramatic drop in the hetero-aggregation rate, possibly due to a blocking mechanism.[65] The authors also reported that the maximum hetero-aggregation rate decreased with increasing concentration of humic acid.[65] Lin *et al*.[67] investigated the hetero-aggregation of amidine and sulfate latex particles and silica particles over a range of varied IS and pH. Results indicated that the hetero-aggregation of opposite charged colloidal particles increased slowly with decreasing IS, and the pH value of the system did not show significant effect on the aggregation rate.[67]

1.5.3 *Deposition and Transport of CNTs*

Compared to homo-aggregation, deposition and transport of CNTs, like hetero-aggregation, has been less thoroughly studied. In this context, deposition refers to the process of colloidal attachment onto surfaces of a large material. Transport, on the other hand, refers to a more general and complex set of processes that affect the movement of colloidal particles in the solid environment. In this specific study, my focus is on O-MWCNT transport through porous media.

For the direct study of colloidal particle deposition, Quartz Crystal Microbalance with Dissipation Monitoring (QCM-D) has been widely applied. In experiments using QCM-D, colloidal particles are deposited onto the surface of a piece of quartz crystal. This approach isolates deposition of colloidal particles from other interactions and therefore provides a more controllable system so that the mechanism may be tractable. The oversimplified condition, however, also leads to relatively less practical results compared to alternative approaches. Yi *et al.*[68] studied the deposition of O-MWCNTs with two different surface oxygen concentrations onto quartz crystals using QCM-D and reported that O-MWCNTs with higher surface oxygen concentrations exhibited a lower deposition rate onto quartz in the presence of only Na^+. In the presence of Ca^{2+}, however, MWCNTs with both high and low surface oxygen concentrations showed similar deposition rates that were significantly higher than those observed in the presence of Na^+.

For studies of CNT transport, packed columns are commonly used. This approach better simulates many aspects of the actual subsurface aquifer and is therefore able to provide information that is more directly relevant to real-world conditions than QCM-D. Nevertheless, no direct and continuous measurement can be obtained in experiments

conducted using packed columns. Results obtained with this approach also have lower accuracy due to the complexity of the media and the influence of relatively less well controlled hydrodynamic processes compared to QCM-D. Prior investigations of CNT transport through porous media have been conducted mostly with natural soil or quartz sand systems, and none have quantified attachment efficiency as a function of both surface and solution chemistry.[63, 69-73] Wang *et al.*[63] passed NOM-stabilized MWCNT and SWCNT dispersions through sand packed columns at varied KCl and $CaCl_2$ concentrations and observed that substantial mass fractions of CNTs passed through the column at KCl concentrations up to 1 mM and $CaCl_2$ up to 0.1 mM. Jaisi *et al.*[69, 70] studied the transport of O-SWCNTs through quartz sand as a function of IS and found that O-SWCNT transport followed predictions of conventional deposition theory under most conditions for quartz sand[70], while straining was the primary means of O-SWCNT deposition on soils under all conditions.[69] The authors also reported that NOM presence can substantially decrease rates of SWCNT deposition onto quartz sand in the presence Ca^{2+}.[70] Wang *et al.* [71] studied functionalized MWCNT tube-length effects on transport through quartz sand and reported that straining played an important role. These investigators observed spatial retention profiles that deviated substantially from expectations based on simple first-order removal, and therefore attachment efficiencies could not be estimated. O'Carroll *et al.*[72] investigated and modeled the impact of MWCNT tube diameter on transport through quartz sands. They reported that all tested MWCNTs were readily mobile under typical conditions of subsurface aquifers, but MWCNTs with smaller diameters were less mobile than their larger counterparts. Liu *et al.*[73] studied the effect of flow velocity on the transport of O-MWCNTs through columns

packed with soda-lime glass beads or quartz sands reporting that approach velocity had a significant effect on O-MWCNT retention. Significant increase of O-MWCNT breakthrough (20% - 30%) was observed when the approach velocity was increased from 0.42 m/d to 4 m/d.[73]

1.5.4 *Adsorption Properties of CNTs*

The adsorption of heavy metals as well as organic compounds onto CNTs has been studied intensively in last decades.[33, 34, 56, 60, 74-78] Studies on this issue have been conducted for two primary reasons. The first of these is to evaluate if CNTs could serve as strong adsorbents to remove organics and heavy metals from water and wastewater as might be applicable, for example, to be incorporated in fixed bed, membranes, or other unit processes of treatment facilities.[79, 80] For example, Peng *et al*.[61] and Lu *et al*.[57] reported CNTs had the ability to effectively achieve the complete removal of 1,2-dichlorobenzene and trihalomethanes from water at low application doses. Lu and Chiu [44] showed that the specific adsorption capacity of NaClO-treated CNTs for Zn^{2+} was higher than that of powdered activated carbon. Cho *et al*.[60] reported that the adsorption capacity of MWCNTs (used as received) was higher than that of natural char and lower than activated carbon. A second reason to study adsorption ability of CNTs for trace organics and metals is to understand the implications of CNT presence on the fate, transport, and risk associated with these other contaminants.[56] The focus of this study is the adsorption of heavy metals onto O-MWCNTs because of the ubiquitous presence and non-degradable property of trace metals.[44, 81]

Prior studies have also reported research of O-MWCNTs as adsorbents for metals, including studies on the effects of aquatic and surface chemistry. More specifically, Cho

et al.[56] reported that IS, pH, and the co-presence of multiple metals all had strong effects on adsorption properties of MWCNTs for Zn^{2+} and Cd^{2+}.[56] Likewise, Cho *et al.*[56] as well as Li *et al*.[82] showed that the surface oxidation degree of CNTs had significant effects on their capacity to adsorb metallic contaminants, with increasing surface oxidation degree leading to increasing adsorption capacity. In particular, carboxyl groups have been shown to have a particularly strong adsorption ability for divalent metallic cations. Although there have been numerous studies regarding CNT adsorption of heavy metals, most studies have been conducted at CNT mass concentrations ranging from ~0.1 g/L to ~ 10 g/L.[83] Considering that concentrations of CNTs in natural systems are not expected to be greater than parts per million level (1 mg/L) or lower, there is need for more studies using CNTs at environmentally relevant concentrations.

1.6 Research Questions

Given the assumption that CNTs will access aquatic environments, there is need to better understand their potential impacts in these environments. In order to estimate the environmental impacts that CNTs may have in water systems, it is important to understand their fate and transport as well as their interactions with other contaminants, which is the primary research question addressed in this work. More specifically, the research questions in this work include:

- What are the adsorption properties of O-MWCNTs for Ni^{2+} and Zn^{2+} and effects of experimental conditions, including aquatic chemistry, surface chemistry, and adsorbent concentration (solid-to-liquid ratio)?
- What are the transport properties of O-MWCNTs through simulated porous media (soda-lime spherical glass beads) and what are the effects of changes in

experimental conditions, including effects due to changes of pH, ionic strength, cation species, and O-MWCNT surface oxygen concentration and functional group distribution?

- What are the removal mechanisms of O-MWCNTs passing through porous media and the contributions of each mechanism under varied experimental conditions?

1.7 Objectives and Outline

The overall objectives of this work were to establish quantitative relationships between the surface composition of MWCNTs and their sorption and transport properties under varying aquatic chemical conditions. Both theoretical and experimental approaches were used in order to better estimate these properties. Mathematical models and computations were applied to test whether the hypothesized conceptual understanding was useful for interpreting and predicting experimental observations. Specific objectives are listed below by chapter.

Chapter 2 contains results from studies of the adsorption of MWCNTs for divalent cations (Zn^{2+} and Ni^{2+}). The effects of surface chemistry and aquatic chemistry on MWCNT adsorption properties were studied using both experimental approaches and mathematical modeling. Adsorption experiments were also conducted at varied solid-to-liquid ratios (S/L), including those usually used in prior research and in water treatment facilities and those relevant to possible MWCNT concentrations in natural water systems. The studies revealed a surprising effect of S/L on the adsorption property of MWCNTs, and a possible explanation was proposed.

Chapter 3 contains methods and results relating to studies of the impacts of both surface and solution chemistry on MWCNT deposition during transport through silica-

based media. In order to accurately measure deposition rates in the absence of blocking or straining (i.e., to maintain "clean-bed" conditions), a well-defined system of uniform spherical collectors was applied. Studies were conducted on O-MWCNTs with five different oxygen contents in varied solution chemistries. Solution chemistry variables include IS, pH, SRNOM concentration and type of cation in the feed solution (Na^+ or Ca^{2+}).

Chapter 4 contains methods and results relating to the investigation of the transport mechanisms of MWCNTs on silica based porous media as conducted through the analysis of both temporal breakthrough curves and retention profiles obtained after completion of transport experiments. Mathematical models that combine a standard formation of clean bed filtration model with additional models were composed to account for other removal mechanisms such as site-blocking, ripening and straining are provided. These models were applied to the interpretation of the experimental results.

In Chapter 5, the sensitivity of the mathematical models developed in Chapter 4 is analyzed and the physical meaning of each term in the models is discussed in detail. The advantages and disadvantages of each mathematical approach and the contributions of each deposition mechanism are also analyzed.

Finally, Chapter 6 contains the major conclusions from this work as well as discussion of the significance of the results toward a better understanding of the potential environmental implication and application of this new nano-material. Possible directions of future work are also suggested.

1.8 Cited References

1. Iijima, S., Helical Microtubules of Graphitic Carbon. *Nature* **1991,** *354*, (6348), 56-58.

2. Dresselhaus, M. S.; Dresselhaus, G.; Eklund, P. C., Science of Fullerenes and Carbon Nanotubes. Academic Press: San Diego, 1996; p xviii, 965 p.

3. Ebbesen, T. W., Carbon Nanotubes. *Annual Review of Materials Science* **1994,** *24*, (1), 235-264.

4. Gallagher, M. J.; Chen, D.; Jacobsen, B. P.; Sarid, D.; Lamb, L. D.; Tinker, F. A.; Jiao, J.; Huffman, D. R.; Seraphin, S.; Zhou, D., Characterization of Carbon Nanotubes by Scanning Probe Microscopy. *Surface Science* **1993,** *281*, (3), L335-L340.

5. Ebbesen, T. W.; Hiura, H.; Fujita, J.; Ochiai, Y.; Matsui, S.; Tanigaki, K., Patterns in the Bulk Growth of Carbon Nanotubes. *Chemical Physics Letters* **1993,** *209*, (1-2), 83-90.

6. Klaine, S. J.; Alvarez, P. J. J.; Batley, G. E.; Fernandes, T. F.; Handy, R. D.; Lyon, D. Y.; Mahendra, S.; Mclaughlin, M. J.; Lead, J. R., Nanomaterials in the Environment: Behavior, Fate, Bioavailability, and Effects. *Environ Toxicol Chem* **2008,** *27*, (9), 1825-1851.

7. Kreupl, F.; Graham, A. P.; Duesberg, G. S.; Steinhogl, W.; Liebau, M.; Unger, E.; Honlein, W., Carbon Nanotubes in Interconnect Applications. *Microelectron Eng* **2002,** *64*, (1-4), 399-408.

8. Lekas, D. The Project on Emering Nanotechnologies; Washington D.C., 2005.

9. Sinnott, S. B.; Andrews, R., Carbon Nanotubes: Synthesis, Properties, and Aplications. Taylor & Francis: London, 2010.

10. Treacy, M. M. J.; Ebbesen, T. W.; Gibson, J. M., Exceptionally High Young's Modulus Observed for Individual Carbon Nanotubes. *Nature* **1996,** *381*, (6584), 678-680.

11. Dai, H. J.; Hafner, J. H.; Rinzler, A. G.; Colbert, D. T.; Smalley, R. E., Nanotubes as Nanoprobes in Scanning Probe Microscopy. *Nature* **1996,** *384*, (6605), 147-150.

12. Wong, S. S.; Woolley, A. T.; Odom, T. W.; Huang, J. L.; Kim, P.; Vezenov, D. V.; Lieber, C. M., Single-Walled Carbon Nanotube Probes for High-Resolution Nanostructure Imaging. *Appl Phys Lett* **1998,** *73*, (23), 3465-3467.

13. Kong, J.; Franklin, N. R.; Zhou, C. W.; Chapline, M. G.; Peng, S.; Cho, K. J.; Dai, H. J., Nanotube Molecular Wires as Chemical Sensors. *Science* **2000,** *287*, (5453), 622-625.

14. Qian, D.; Dickey, E. C.; Andrews, R.; Rantell, T., Load Transfer and Deformation Mechanisms in Carbon Nanotube-Polystyrene Composites. *Appl Phys Lett* **2000,** *76*, (20), 2868-2870.

15. Aslan, S.; Loebick, C. Z.; Kang, S.; Elimelech, M.; Pfefferle, L. D.; Van Tassel, P. R., Antimicrobial Biomaterials Based on Carbon Nanotubes Dispersed in Poly(Lactic-Co-Glycolic Acid). *Nanoscale* **2010,** *2*, (9), 1789-1794.

16. Ahmed, F.; Santos, C. M.; Vergara, R. a. M. V.; Tria, M. C. R.; Advincula, R.; Rodrigues, D. F., Antimicrobial Applications of Electroactive Pvk-Swnt Nanocomposites. *Environ Sci Technol* **2012,** *46*, (3), 1804-1810.

17. Parish, A. Production and Application of Carbon Nanotubes, Carbon Nanofibers, Fullerenes, Graphene and Nanodiamonds: A Global Technology Survey and Market Analysis; Innovative research and products (iRAP), Inc: 2011.

18. Rzepka, M.; Lamp, P.; De La Casa-Lillo, M. A., Physisorption of Hydrogen on Microporous Carbon and Carbon Nanotubes. *Journal of Physical Chemistry B* **1998,** *102*, (52), 10894-10898.

19. Wang, Q.; Johnson, J. K., Molecular Simulation of Hydrogen Adsorption in Single-Walled Carbon Nanotubes and Idealized Carbon Slit Pores. *The Journal of Chemical Physics* **1999,** *110*, (1), 577-586.

20. Patel, V. Global Carbon Nanotubes Market - Industry Beckons. http://www.nanowerk.com/spotlight/spotid=23118.php

21. Thayer, A. M., Carbon Nanotubes by the Metric Ton. *Chemical & Engineering News* **2007,** *85*, (46), 29-35.

22. Mueller, N. C.; Nowack, B., Exposure Modeling of Engineered Nanoparticles in the Environment. *Environ Sci Technol* **2008,** *42*, (12), 4447-4453.

23. Nowack, B.; Bucheli, T. D., Occurrence, Behavior and Effects of Nanoparticles in the Environment. *Environ Pollut* **2007,** *150*, (1), 5-22.

24. Petosa, A. R.; Jaisi, D. P.; Quevedo, I. R.; Elimelech, M.; Tufenkji, N., Aggregation and Deposition of Engineered Nanomaterials in Aquatic Environments: Role of Physicochemical Interactions. *Environ Sci Technol* **2010,** *44*, (17), 6532-6549.

25. Koelmans, A. A.; Nowack, B.; Wiesner, M. R., Comparison of Manufactured and Black Carbon Nanoparticle Concentrations in Aquatic Sediments. *Environ Pollut* **2009,** *157*, (4), 1110-1116.

26. Sayes, C. M.; Liang, F.; Hudson, J. L.; Mendez, J.; Guo, W. H.; Beach, J. M.; Moore, V. C.; Doyle, C. D.; West, J. L.; Billups, W. E.; Ausman, K. D.; Colvin, V. L., Functionalization Density Dependence of Single-Walled Carbon Nanotubes Cytotoxicity in Vitro. *Toxicology Letters* **2006,** *161*, (2), 135-142.

27. Nemmar, A.; Hoet, P. H. M.; Vanquickenborne, B.; Dinsdale, D.; Thomeer, M.; Hoylaerts, M. F.; Vanbilloen, H.; Mortelmans, L.; Nemery, B., Passage of Inhaled Particles into the Blood Circulation in Humans. *Circulation* **2002,** *105*, (4), 411-414.

28. Patlolla, A.; Knighten, B.; Tchounwou, P., Multi-Walled Carbon Nanotubes Induce Cytotoxicity, Genotoxicity and Apoptosis in Normal Human Dermal Fibroblast Cells. *Ethnicity & disease 20*, (1 Suppl 1), S1-65-72.

29. Smith, B.; Wepasnick, K.; Schrote, K. E.; Cho, H. H.; Ball, W. P.; Fairbrother, D. H., Influence of Surface Oxides on the Colloidal Stability of Multi-Walled Carbon Nanotubes: A Structure-Property Relationship. *Langmuir* **2009,** *25*, (17), 9767-9776.

30. Yang, J.; Bitter, J. L.; Smith, B. A.; Fairbrother, D. H.; Ball, W. P., Transport of Oxidized Multi-Walled Carbon Nanotubes through Silica Based Porous Media: Influences of Aquatic Chemistry, Surface Chemistry, and Natural Organic Matter. *Environ Sci Technol* **2013,** *47*, (24), 14034-14043.

31. Hyung, H.; Fortner, J. D.; Hughes, J. B.; Kim, J. H., Natural Organic Matter Stabilizes Carbon Nanotubes in the Aqueous Phase. *Environ Sci Technol* **2007,** *41*, (1), 179-184.

32. Lin, D. H.; Tian, X. L.; Wu, F. C.; Xing, B. S., Fate and Transport of Engineered Nanomaterials in the Environment. *J Environ Qual* **2010,** *39*, (6), 1896-1908.

33. Hou, L.; Zhu, D. Q.; Wang, X. M.; Wang, L. L.; Zhang, C. D.; Chen, W., Adsorption of Phenanthrene, 2-Naphthol, and 1-Naphthylamine to Colloidal Oxidized Multiwalled Carbon Nanotubes: Effects of Humic Acid and Surfactant Modification. *Environ Toxicol Chem* **2013,** *32*, (3), 493-500.

34. Hyung, H.; Kim, J. H., Natural Organic Matter (Nom) Adsorption to Multi-Walled Carbon Nanotubes: Effect of Nom Characteristics and Water Quality Parameters. *Environ Sci Technol* **2008,** *42*, (12), 4416-4421.

35. Smith, B.; Yang, J.; Bitter, J. L.; Ball, W. P.; Fairbrother, D. H., Influence of Surface Oxygen on the Interactions of Carbon Nanotubes with Natural Organic Matter. *Environ Sci Technol* **2012,** *46*, (23), 12839-12847.

36. Oberdorster, G.; Oberdorster, E.; Oberdorster, J., Nanotoxicology: An Emerging Discipline Evolving from Studies of Ultrafine Particles. *Environmental Health Perspectives* **2005,** *113*, (7), 823-839.

37. Marrs, B.; Andrews, R.; Pienkowski, D., Multiwall Carbon Nanotubes Enhance the Fatigue Performance of Physiologically Maintained Methyl Methacrylate-Styrene Copolymer. *Carbon* **2007,** *45*, (10), 2098-2104.

38. Breuer, O.; Sundararaj, U., Big Returns from Small Fibers: A Review of Polymer/Carbon Nanotube Composites. *Polymer Composites* **2004,** *25*, (6), 630-645.

39. Vaisman, L.; Marom, G.; Wagner, H. D., Dispersions of Surface-Modified Carbon Nanotubes in Water-Soluble and Water-Insoluble Polymers. *Advanced Functional Materials* **2006,** *16*, (3), 357-363.

40. Sluzarenko, N.; Heurtefeu, B.; Maugey, M.; Zakri, C.; Poulin, P.; Lecommandoux, S., Diblock Copolymer Stabilization of Multi-Wall Carbon Nanotubes in Organic Solvents and Their Use in Composites. *Carbon* **2006,** *44*, (15), 3207-3212.

41. Bourlinos, A. B.; Georgakilas, V.; Zboril, R.; Dallas, P., Preparation of a Water-Dispersible Carbon Nanotube-Silica Hybrid. *Carbon* **2007,** *45*, (10), 2136-2139.

42. Liu, P., Modifications of Carbon Nanotubes with Polymers. *European Polymer Journal* **2005,** *41*, (11), 2693-2703.

43. Yusof, A. M.; Buang, N. A.; Yean, L. S.; Ibrahim, M. L., The Use of Multi-Walled Carbon Nanotubes as Possible Carrier in Drug Delivery System for Aspirin. In *Nanoscience and Nanotechnology*, Rusop, M.; Soga, T., Eds. 2009; Vol. 1136, pp 390-394.

44. Stumm, W.; Morgan, J. J., Aquatic Cheistry: Chemical Equilibria and Rates in Natural Waters. John Wiley & Sons, Inc: New York, 1996.

45. Derjaguin, B., On the Repulsive Forces between Charged Colloid Particles and on the Theory of Slow Coagulation and Stability of Lyophobe Sols. *Transactions of the Faraday Society* **1940,** *35*, (0), 203-215.

46. Derjaguin, B.; Landau, L., Theory of the Stability of Strongly Charged Lyophobic Sols and of the Adhesion of Strongly Charged-Particles in Solutions of Electrolytes. *Prog Surf Sci* **1941,** *14*, 633.

47. Verwey, E. J. W.; Overbeek, J. T. G., Theory of the Stability of Lyophobic Colloids. *Journal of Colloid Science* **1948,** *10*, (2), 224-225.

48. Tufenkji, N.; Elimelech, M., Correlation Equation for Predicting Single-Collector Efficiency in Physicochemical Filtration in Saturated Porous Media. *Environ Sci Technol* **2004,** *38*, (2), 529-536.

49. Westall, J.; Hohl, H., Comparison of Electrostatic Models for the Oxide-Solution Interface. *Adv Colloid Interfac* **1980,** *12*, (4), 265-294.

50. O'melia, C. R., Particle-Particle Interactions in Aquatic Systems. *Colloid Surface* **1989,** *39*, (1), 255-271.

51. Au, K. K.; Penisson, A. C.; Yang, S.; O'melia, C. R., Natural Organic Matter at Oxide/Water Interfaces: Complexation and Conformation. *Geochimica et Cosmochimica Acta* **1999,** *63*, (19-20), 2903-2917.

52. Tobiason, J. E.; Omelia, C. R., Physicochemical Aspects of Particle Removal in Depth Filtration. *J Am Water Works Ass* **1988,** *80*, (12), 54-64.

53. Elimelech, M.; Omelia, C. R., Effect of Particle Size on Collision Efficiency in the Deposition of Brownian Particles with Electrostatic Energy Barriers. *Langmuir* **1990,** *6*, (6), 1153-1163.

54. Hahn, M. W.; O'melia, C. R., Deposition and Reentrainment of Brownian Particles in Porous Media under Unfavorable Chemical Conditions: Some Concepts and Applications. *Environmental Science and Technology* **2004,** *38*, (1), 210-220.

55. Veerapaneni, S.; Wiesner, M. R., Role of Suspension Polydispersivity in Granular Media Filtration. *Journal of Environmental Engineering* **1993,** *119*, (1), 172-190.

56. Cho, H. H.; Wepasnick, K.; Smith, B. A.; Bangash, F. K.; Fairbrother, D. H.; Ball, W. P., Sorption of Aqueous Zn[Ii] and Cd[Ii] by Multiwall Carbon Nanotubes: The Relative Roles of Oxygen-Containing Functional Groups and Graphenic Carbon. *Langmuir* **2010,** *26*, (2), 967-981.

57. Lu, C.; Chung, Y. L.; Chang, K. F., Adsorption of Trihalomethanes from Water with Carbon Nanotubes. *Water Res* **2005,** *39*, (6), 1183-1189.

58. Li, Q. L.; Yuan, D. X.; Lin, Q. M., Evaluation of Multi-Walled Carbon Nanotubes as an Adsorbent for Trapping Volatile Organic Compounds from Environmental Samples. *J Chromatogr A* **2004,** *1026*, (1-2), 283-288.

59. Bond, T. C.; Streets, D. G.; Yarber, K. F.; Nelson, S. M.; Woo, J. H.; Klimont, Z., A Technology-Based Global Inventory of Black and Organic Carbon Emissions from Combustion. *Journal of Geophysical Research D: Atmospheres* **2004,** *109*, (14).

60. Cho, H. H.; Smith, B. A.; Wnuk, J. D.; Fairbrother, D. H.; Ball, W. P., Influence of Surface Oxides on the Adsorption of Naphthalene onto Multiwalled Carbon Nanotubes. *Environ Sci Technol* **2008,** *42*, (8), 2899-2905.

61. Peng, X.; Li, Y.; Luan, Z.; Di, Z.; Wang, H.; Tian, B.; Jia, Z., Adsorption of 1,2-Dichlorobenzene from Water to Carbon Nanotubes. *Chemical Physics Letters* **2003,** *376*, (1-2), 154-158.

62. Saleh, N. B.; Pfefferle, L. D.; Elimelech, M., Influence of Biomacromolecules and Humic Acid on the Aggregation Kinetics of Single-Walled Carbon Nanotubes. *Environmental Science and Technology* **2010,** *44*, (7), 2412-2418.

63. Wang, P.; Shi, Q.; Liang, H.; Steuerman, D. W.; Stucky, G. D.; Keller, A. A., Enhanced Environmental Mobility of Carbon Nanotubes in the Presence of Humic Acid and Their Removal from Aqueous Solution. *Small* **2008,** *4*, (12), 2166-2170.

64. Saleh, N. B.; Pfefferle, L. D.; Elimelech, M., Aggregation Kinetics of Multiwalled Carbon Nanotubes in Aquatic Systems: Measurements and Environmental Implications. *Environmental Science and Technology* **2008,** *42*, (21), 7963-7969.

65. Huynh, K. A.; Mccaffery, J. M.; Chen, K. L., Heteroaggregation of Multiwalled Carbon Nanotubes and Hematite Nanoparticles: Rates and Mechanisms. *Environ Sci Technol* **2012,** *46*, (11), 5912-5920.

66. Chen, K. L.; Smith, B. A.; Ball, W. P.; Fairbrother, D. H., Assessing the Colloidal Properties of Engineered Nanoparticles in Water: Case Studies from Fullerene C-60 Nanoparticles and Carbon Nanotubes. *Environ Chem* **2010,** *7*, (1), 10-27.

67. Lin, W.; Kobayashi, M.; Skarba, M.; Nu, C. D.; Galletto, P.; Borkovec, M., Heteroaggregation in Binary Mixtures of Oppositely Charged Colloidal Particles. *Langmuir* **2006,** *22*, (3), 1038-1047.

68. Yi, P.; Chen, K. L., Influence of Surface Oxidation on the Aggregation and Deposition Kinetics of Multiwalled Carbon Nanotubes in Monovalent and Divalent Electrolytes. *Langmuir* **2011,** *27*, (7), 3588-3599.

69. Jaisi, D. P.; Elimelech, M., Single-Walled Carbon Nanotubes Exhibit Limited Transport in Soil Columns. *Environ Sci Technol* **2009,** *43*, (24), 9161-9166.

70. Jaisi, D. P.; Saleh, N. B.; Blake, R. E.; Elimelech, M., Transport of Single-Walled Carbon Nanotubes in Porous Media: Filtration Mechanisms and Reversibility. *Environ Sci Technol* **2008,** *42*, (22), 8317-8323.

71. Wang, Y. G.; Kim, J. H.; Baek, J. B.; Miller, G. W.; Pennell, K. D., Transport Behavior of Functionalized Multi-Wall Carbon Nanotubes in Water-Saturated Quartz Sand as a Function of Tube Length. *Water Res* **2012,** *46*, (14), 4521-4531.

72. O'carroll, D. M.; Liu, X.; Mattison, N. T.; Petersen, E. J., Impact of Diameter on Carbon Nanotube Transport in Sand. *J Colloid Interf Sci* **2013,** *390*, 96-104.

73. Liu, X. Y.; O'carroll, D. M.; Petersen, E. J.; Huang, Q. G.; Anderson, C. L., Mobility of Multiwalled Carbon Nanotubes in Porous Media. *Environ Sci Technol* **2009,** *43*, (21), 8153-8158.

74. Bystrzejewski, M.; Pyrzynska, K., Kinetics of Copper Ions Sorption onto Activated Carbon, Carbon Nanotubes and Carbon-Encapsulated Magnetic Nanoparticles. *Colloid Surface A* **2011,** *377*, (1-3), 402-408.

75. Chen, C. L.; Wang, X. K., Adsorption of Ni(Ii) from Aqueous Solution Using Oxidized Multiwall Carbon Nanotubes. *Ind Eng Chem Res* **2006,** *45*, (26), 9144-9149.

76. Chen, G. C.; Shan, X. Q.; Wang, Y. S.; Pei, Z. G.; Shen, X. E.; Wen, B.; Owens, G., Effects of Copper, Lead, and Cadmium on the Sorption and Desorption of Atrazine onto and from Carbon Nanotubes. *Environ Sci Technol* **2008,** *42*, (22), 8297-8302.

77. Chen, W.; Duan, L.; Wang, L. L.; Zhu, D. Q., Adsorption of Hydroxyl- and Amino-Substituted Aromatics to Carbon Nanotubes. *Environ Sci Technol* **2008,** *42*, (18), 6862-6868.

78. Gotovac, S.; Yang, C. M.; Hattori, Y.; Takahashi, K.; Kanoh, H.; Kaneko, K., Adsorption of Polyaromatic Hydrocarbons on Single Wall Carbon Nanotubes of Different Functionalities and Diameters. *J Colloid Interf Sci* **2007,** *314*, (1), 18-24.

79. Lu, C. S.; Chiu, H.; Liu, C. T., Removal of Zinc(Ii) from Aqueous Solution by Purified Carbon Nanotubes: Kinetics and Equilibrium Studies. *Ind Eng Chem Res* **2006,** *45*, (8), 2850-2855.

80. Wang, X.; Chen, C.; Hu, W.; Ding, A.; Xu, D.; Zhou, X., Sorption of 243am(Iii) to Multiwall Carbon Nanotubes. *Environ Sci Technol* **2005,** *39*, (8), 2856-2860.

81. Akpor, O. B.; Muchie, M., Remediation of Heavy Metals in Drinking Water and Wastewater Treatment Systems: Processes and Applications. *Int J Phys Sci* **2010,** *5*, (12), 1807-1817.

82. Li, Y. H.; Wang, S.; Luan, Z.; Ding, J.; Xu, C.; Wu, D., Adsorption of Cadmium(Ii) from Aqueous Solution by Surface Oxidized Carbon Nanotubes. *Carbon* **2003,** *41*, (5), 1057-1062.

83. Rao, G. P.; Lu, C.; Su, F., Sorption of Divalent Metal Ions from Aqueous Solution by Carbon Nanotubes: A Review. *Sep Purif Technol* **2007,** *58*, (1), 224-231.

Chapter 2. Adsorption of Zn^{2+} and Ni^{2+} onto Oxidized Multi-Walled Carbon Nanotubes: Effects of Aquatic and Surface Chemistry, O-MWCNT Aggregation State and Solid-to-Liquid Ratio

ABSTRACT

The interaction of heavy metals with oxidized multi-walled carbon nanotubes (O-MWCNTs) is of great importance not only for the evaluation of O-MWCNTs as possible sorbents in water and treatment facilities, but also for considering the implication of O-MWCNTs as contaminants of emerging concern in natural environments where metal co-contaminants may adsorb onto the surface of O-MWCNTs and have their transport be either facilitated or retarded by association with mobile or retained CNTs, respectively. Studies were conducted on the equilibrium adsorption relationships between O-MWCNTs of varying surface chemistry for two divalent metallic cations, Zn^{2+} and Ni^{2+}. Effects of aquatic chemistry, competing organic adsorbate, O-MWCNT aggregation state and solid-to-liquid ratio (S/L) were all investigated. Results showed that the adsorption capacity of O-MWCNTs for the metallic ions increased with increasing pH and decreasing ionic strength (IS). O-MWCNTs with higher surface oxygen content exhibited higher adsorption capacity for the two metals in a manner consistent with prior results of others and also consistent with a two-site Langmuir adsorption model developed in previous study.[1] The presence of naphthalene did not substantially affect the adsorption of Zn^{2+} onto O-MWCNTs as expected from our hypothesis that the two solutes sorb at

different locations on O-MWCNT surfaces. Comparative studies of adsorption with previously dried O-MWCNT powders relative to carefully dispersed suspensions of individual MWCNTs revealed no statistical difference between adsorption capacities, suggesting that similar adsorption mechanisms were at play with either aggregation state. The S/L, on the other hand, exhibited significant effect on the adsorption of Zn^{2+} onto O-MWCNTs with greater impact on sorption affinity (i.e., isotherm slope at low concentration) rather than on maximum sorption capacity. Although similar results have been long reported in a variety of adsorbate-adsorbent systems, the reason for these results in many systems (including this one) is yet to be understood.

2.1 Introduction

In order to better estimate the risk of hazardous dissolved solutes in water systems, one needs to understand their fate, which is often very strongly affected by their tendency to accumulate at solid-water interfaces.[2] Heavy metals such as aluminum, chromium, nickel, copper, zinc, cadmium, mercury and lead are common aquatic contaminants[3] and have been found to have significant effects on aquatic life and human health because of their toxicity and carcinogeneicity.[4] Properties of heavy metals and their behavior in the environment have been extensively studied.[2, 5] Although naturally occurring concentrations of dissolved heavy metals in natural environments is usually very low (10^{-11} - 10^{-7} M),[2, 6] heavy metal fluxes to water resources have increased due to human activities and incidents of high concentration are occurring with increasing frequency.[2]

Carbon nanotubes (CNTs) have been found to have high adsorption capacity for heavy metals, especially when the tubes's surfaces are functionalized with more reactive

species, such as electron-donating (e.g., oxygen-containing) groups.[1, 7-11] For example, Lu *et al*.[2] showed that the specific adsorption capacity of NaClO treated CNTs for Zn^{2+} was higher than that of powdered activated carbon (PAC). CNTs are therefore being viewed as a new carbon based material that has substantial potential as adsorbents for the removal of heavy metals in water and wastewater treatment.[12, 13] In this context, it is important to fully understand the interaction of CNTs of varying surface functionality with the to-be treated contaminants.

The strong tendency of heavy metals to accumulate at the solid (CNT)-water interfaces also has implications for the role of CNTs as contaminants of emerging concern in natural environments. In aquatic systems where CNTs are present, additional solid surfaces are available for the accumulation of heavy metals. Such surfaces can serve to either facilitate or retard the movement of the metal adsorbates in a manner that will depend on the relative mobility of the adsorbate species and the adsorbent solids (CNTs).[2] As discussed elsewhere in this dissertation (Chapters 3 and 4), such mobility can depend on both the surface chemistry and aggregation state of the CNTs, as well as on the chemical composition of the aqueous solution. Therefore, the addition of CNTs to these matrices will add new challenges to the modeling and prediction of the fate of these heavy metals.

In recent years, the adsorption of heavy metals onto CNTs has been studied for both of the previously mentioned reasons – that is, (1) to estimate the ability of CNTs to serve as alternative water treatment materials for removal of heavy metals[12-14] and (2) to predict the interactions of CNTs with heavy metals in natural aquatic systems to assess the risk of CNTs as novel contaminants. Factors affecting metal adsorption onto CNTs

include the chemical properties of the dissolved metal species, the surface chemistry of the CNTs, the presence of potentially competing co-adsorbates such as co-existing metal cations or organic compounds, and general conditions of aquatic chemistry such as pH, ionic strength (IS), and temperature.

General conditions of aquatic chemistry, including IS and pH, have been reported to affect the adsorption capacity of CNTs for heavy metals in a way consistent with theoretical prediction.[1, 7, 8, 11, 15] Chen and Wang [7] investigated the adsorption of Ni^{2+} onto oxidized multi-walled CNTs (O-MWCNTs) as a function of pH and IS. Results indicated the adsorption of Ni^{2+} was strongly affected by pH and slightly dependent on IS, where the adsorbed amount of Ni^{2+} increased with increasing pH or decreasing IS.[7] Li *et al*.[8] studied the effects of pH and IS on the adsorption of Pb^{2+}, Cu^{2+}, and Cd^{2+} onto CNTs and also reported increasing adsorption capacity with decreasing IS and increasing pH. Meanwhile, adsorbed amount of heavy metal is found to increase with increasing solution temperature, indicating that the adsorption is an endothermic process.[15-18]

In addition to aquatic chemistry, CNT surface properties have also been shown to significantly affect CNT adsorption of heavy metals.[9, 14, 19, 20] Cho *et al*.[19] quantified the atomic oxygen concentration as well as the distribution of functional groups on the surface of O-MWCNTs and reported that the adsorption capacity of O-MWCNTs for Zn^{2+} was positively correlated to the surface oxygen content of O-MWCNTs, and especially to the concentration of carboxylic groups. Li *et al*.[9] studied the adsorption of Cd^{2+} onto O-MWCNTs of various types and found that the adsorption capacity of the as-grown CNTs was significantly lower than that of CNTs treated with H_2O_2, HNO_3, or $KMnO_4$.

The existence of competing adsorbates is another factor that has been reported to affect the adsorption capacity of CNTs for a given heavy metal species.[8, 21-23] Li *et al*.[8] reported that maximum capacity values (q_m, mg/g) of CNTs for Pb^{2+}, Cu^{2+} and Cd^{2+}, as estimated through the fitting of a Langmuir isotherm model, were 97.1, 28.5 and 10.9, respectively in single-solute systems but these values decreased substantially to 34.1, 17.0 and 3.3 mg/g in tri-adsorbate systems, where all three adsorbates were simultaneously present. Hsieh and Tsai[23] conducted similar competitive adsorption study for Pb^{2+}, Cu^{2+} and Cd^{2+} onto lab-grown CNTs and reported dramatic decrease of Pb^{2+} adsorption and slight decrease on Cu^{2+} and Cd^{2+} adsorption capacity in the tri-adsorbate system compared to that in the single-adsorbate system. Such competitive effect among cationic adsorbates can be explained by the ion-exchange adsorption mechanism proposed by several researchers for adsorptions of metals onto CNTs.[7, 21] On the other hand, "organic adsorbates" are perhaps less likely to compete with cations. In regard to polycyclic aromatic hydrocarbons (PAHs), for example, multiple studies have postulated that π-π bonding is a dominant adsorption mechanism.[19, 24] Because π-π bonding occurs at non-functionalized sites and cation adsorption occurs at functionalized sites, we might therefore expect little competition for adsorption sites to occur among PAHs and metal cations. Very few studies, however, have been conducted on this topic.[25] Chen *et al*.[25] investigated the effect of metallic ions (Cu^{2+}, Pb^{2+}, Cd^{2+}) on the adsorption of atrazine onto CNTs and reported the suppressing effect of metallic ions on the atrazine adsorption. Competition between cations and compounds other than HOCs on adsorption onto CNTs was also occasionally reported.[22] Diaz-Flores *et al*.[22] investigated the competitive adsorption of Cd^{2+} and phenol on modified N-doped CNTs and found that increasing

concentration of Cd^{2+} decreases the phenol adsorption.[22] The presence of phenol was found to increase the adsorption of Cd^{2+},[22] presumably because of the addition of new negatively charged functional groups.

Among the numerous studies regarding the adsorption of heavy metals onto CNTs, very few studies have been carried out to investigate adsorption properties at environmentally relevant (i.e., low) concentrations of O-MWCNTs or under conditions where O-MWCNTs were in a highly dispersed (*i.e.*, unaggregated) state in suspension. Instead, most studies to date have been conducted at CNT mass concentrations ranging from ~ 0.1 g/L to ~ 10 g/L with powdered (aggregated) CNTs and in the absence of any deliberate efforts to disperse them.[1, 26] Considering that concentrations of CNTs in natural systems are not expected to be greater than 1 mg/L, and that CNTs may enter the environment in a more highly dispersed state, there is need for more studies using dispersed CNTs at environmentally relevant concentrations. To date, such studies have been limited to adsorbates other than heavy metals. For example, Zhang *et al*. (2009)[27] and Zhang *et al*.(2012)[28] have shown that dispersed CNTs exhibit higher adsorption capacity for synthetic organic chemicals (such as pyrene) than do CNTs added as bulk powders.

To the best of our knowledge, however, the effect of CNT concentration on the adsorption of metal ions has not been previously reported. Based on prior studies of metal ion adsorption by clays, sands and other environmental materials, however, there are good reasons to believe that the adsorbent concentration in solution (i.e., the so-called solid-to-liquid ratio, or S/L) can have an important effect on metal adsorption properties.[29-31] In particular, much higher adsorption capacity has been observed when

low adsorbent concentrations were applied.[29-31] Prior literature has described this as a solid-to-liquid ratio (S/L) effect. Since this effect cannot be explained by current thermodynamic equilibrium theory, previous studies have usually attributed it to artificial interference (i.e., artifacts) in experimental methods. McKinley *et al.*[31] have summarized these as follows: (1) adsorption by colloids that have a much higher adsorption capacity and remain suspended in the aqueous phase after centrifugation or filtration;[32-35] (2) competition for adsorbate by "complexing agents" (particularly organic carbon) desorbed from the adsorbent;[33-36] (3) competition of different species of adsorbates;[36, 37] (4) increased solid aggregation (e.g., flocculation) to produce a net decrease in readily available adsorption sites;[32, 37-40] and (5) uncounted chemical reactions such as precipitation.[41]

In considering metal adsorption on CNTs, the fourth artifact considered above seems to be the most likely, and would suggest that the issues of S/L effect and aggregation (dispersion state) are intimately entwined. Irrespective of cause, however, the presence of a real and important S/L effect on the measurement of metal adsorption onto CNTs could have important environmental implications. More specifically, we would expect that the adsorption capacity of CNTs at low concentrations in the environment would be much higher than that estimated from isotherms obtained in the laboratory at high S/L.

The purpose of the work described in this chapter was to investigate the interaction between metallic ions and O-MWCNTs in well-mixed batch reactors. In this study, equilibrium adsorption and kinetics studies were conducted using both as-received (aggregated) O-MWCNT powders and O-MWCNTs that had been deliberately

disaggregated and dispersed in solution through controlled sonication, and with the level of dispersion confirmed by independent means. Adsorption isotherms were obtained for Zn^{2+} and Ni^{2+} on O-MWCNTs with surface oxygen concentrations ranging from 5.1% to 8.0%. Effects of surface chemistry and aggregation state of CNTs, aquatic chemistry (pH and IS), competing adsorbate of organic compound (naphthanene), and S/L in experimental systems were all studied. In order to independently study the effect of aggregation state on O-MWCNT adsorption ability without the interference of an S/L effect, adsorption experiments were conducted using both well-dispersed and non disaggregated (powdered) O-MWCNTs (preparation method described below) at the same solid-to-liquid ratio. On the other hand, experiments using either non disaggregated or dispersed O-MWCNTs were conducted at multiple S/L to investigate the S/L effect. F400 PAC was also studied to evaluate whether the S/L effect was present with this larger and more traditionally well studied adsorbent material.

2.2 Experimental Methods

2.2.1 *Preparation of Adsorbents*

O-MWCNTs. MWCNTs powders (diameter = 15 ± 5 nm, length = 1 - 5 μm, < 5% metal content according to thermogravimetric analysis, 95% carbon purity, provided by manufacturer) were purchased from NanoLabs, Inc.. 18% w/w HNO_3 as well as a combination of $KMnO_4$ and H_2SO_4 were used to oxidize MWCNTs in our own laboratories, following previously described methods[1, 42, 43] in order to obtain O-MWCNTs at two different surface oxygen concentrations. In the functionalization process, MWCNTs were mixed with oxidants (HNO_3 or $KMnO_4$-H_2SO_4 mixture), and then sonicated, refluxed, purified and dried sequentially.[43] $KMnO_4$ and H_2SO_4 were

employed as oxidants because this method was known to produce O-MWCNTs with high surface oxygen concentration within which carboxylic groups ($-COO^-$) showed a relatively higher concentration. All functionalized O-MWCNTs were purified using 4 M NaOH and 1 M HCl solution sequentially after the acid treatment to remove amorphous carbon generated in the oxidation process following the method described by Smith *et al.*[44]

Activated carbon. Granular activated carbon (GAC, F400) purchased from Calgon Carbon Corporation (Pittsburgh, PA) was pulverized and passed through a 200 (75 μm) mesh sieve. These PAC particles with $d \leq 75$ μm were then used as adsorbents in the adsorption studies.

2.2.2 *Characterization of Adsorbents*

The total surface oxygen concentrations as well as the distributions of surface oxygen functional groups of O-MWCNTs used in this work were determined using X-ray photoelectron spectroscopy (XPS) (PHI 5400 system) in conjunction with chemical derivatization methods.[45, 46] All the measurements for O-MWCNTs used in this study were conducted by colleagues from the Johns Hopkins University Department of Chemistry (Kevin Wepasnick and David Goodwin). Specific surface areas of both batches of O-MWCNTs were measured using BET surface area analyzer. The length distributions of O-MWCNTs oxidized using the same methods as in this study, have been reported in our prior publications.[43, 44] No significant difference in length distribution was found for O-MWCNTs with varied surface oxygen concentrations.[43, 44] The total surface oxygen concentrations and specific surface area (BET measurement) of F400 PAC used in this study have been reported elsewhere.[1]

2.2.3 *Preparation of dispersed and non-disaggregated O-MWCNTs*

O-MWCNTs that were used in the powdered state obtained after the functionalization and subsequent drying process are hereafter referred to as Aggregated O-MWCNTs if they were used directly without disaggregation. In experiments involving dispersed O-MWCNTs, suspensions of O-MWCNTs (at both surface oxygen concentrations) were prepared using a method described in our prior publications,[43, 44, 47] where O-MWCNTs (2 - 12 mg) were added to 200 mL of de-ionized (DI) water and then sonicated (Branson 1510, 70 W) for 20 hours. For the O-MWCNTs with the lower surface oxygen concentration, it was necessary to keep the pH value between 9 and 10 to achieve a stable stock suspension. After sonication, the suspension was centrifuged at 1000 rpm for 5 minutes to remove any non-suspended O-MWCNTs bundles as well as some colloidal glass particles that were found to have been etched from the wall of the flask during sonication. The resulting suspensions (also referred to as "dispersions" below) were collected and subjected to another 5 min sonication. The hydrodynamic diameters (D_h) of the O-MWCNTs in all prepared stock solutions were measured using dynamic light scattering (DLS). The final O-MWCNT concentration in a given suspension was determined by measuring its absorbance at 270 nm. Preliminary experiments showed good linear relationships ($R^2 > 0.999$) between the absorbance at 270 nm and the mass concentrations for the O-MWCNTs used in this study.

2.2.4 *Preparation of Adsorbates*

Analytical-grade $Zn(NO_3)_2{\cdot}6H_2O$, $Ni(NO_3)_2{\cdot}6H_2O$, $NaNO_3$ were purchased from Sigma-Aldrich and used to prepare stock solutions. Naphthalene was also purchased from Sigma-Aldrich and used together with Zn^{2+} in the preparation of several stock solutions

for competitive sorption experiments. 0.01 M NaOH or 0.01 M HNO_3 were used to adjust the pH of solutions. $NaNO_3$ was used throughout the study for IS adjustment. For most experiments, no pH-buffering agent was added to solutions in order to prevent possible effects on aggregation of the MWCNT dispersions or on the adsorption process. It has been reported previously that the pH value has negligible effect on the adsorption of Zn^{2+} onto O-MWCNTs – batch experiments showed that q_e was steady to within ±15% between pH 5.0 and pH 7.0, where carboxyl groups on the surface of adsorbents are all deprotonated considering the pKa of carboxylic groups were mostly below 4.[1, 48] In experiments where the pH values needed to be precise, $NaHCO_3$ were used to maintain the pH of the solutions at pH 7.1 ± 0.1. The total concentrations of the adsorbate as well as the aquatic chemistry of the stock solutions (IS, pH) varied in different experiments. Details can be found in the following section.

2.2.5 *Adsorption Experiments*

In adsorption experiments where aggregated O-MWCNTs or PAC were used as adsorbents, these materials were weighed using an analytical balance (Mettler Toledo AT261). Extra care was taken to minimize the effect of static electricity by using aluminum foil to cover all plastic surfaces of containers and waiting for a constant time (3 min) for the analytical balance to stabilize at each reading. After weighing the adsorbents, stock solutions containing Zn^{2+} or Ni^{2+} at varied concentrations and designed IS were added into the containers. For experiments in which dispersed O-MWCNTs were used as adsorbents, a secondary stock dispersion of O-MWCNTs was prepared by diluting the O-MWCNTs stock solutions with Milli-Q water. Secondary stock solutions were prepared with metal ion concentrations and IS that were 10 times the target values.

Prior study in our group has also revealed that the effect of pH on the adsorption of Zn^{2+} was negligible at pH > 6,[1] so no buffer was applied in experiments involving Zn^{2+} and the initial pH of all solutions/dispersions were adjusted to 6.5 ± 0.3. For experiments with Ni^{2+}, 5 mM $NaHCO_3$ was used as buffer and pH was adjusted to be 7.0 ± 0.1. 0.01 – 1 M NaOH and HNO_3 were applied for pH adjustment and $NaNO_3$ was applied for IS adjustment. To initiate the adsorption experiments, secondary stock solutions of adsorbate and secondary stock dispersions of O-MWCNTs were mixed in a 1:9 ratio. Note that the pH and IS for all solutions and dispersions were adjusted right before the mixing step. After the mixing step, the resulting mixtures of adsorbate solutions with either aggregated or dispersed MWCNTs were shaken in dark at a constant temperature of 23 ± 0.5 ^{o}C using an end-over-end rotator. Although the adsorption of Zn^{2+} onto O-MWCNTs reaches equilibrium quickly and is not believed to be light sensitive, all experiments in the current study were nonetheless kept in the dark during the full course of a 48-hour rotation, with the time chosen in order to keep the experimental conditions consistent with those required for the PAC.[6] In kinetic studies the shaking time was as specified subsequently in this chapter. All experiments except the ones involving naphthalene were conducted using polypropylene tubes. When naphthalene was employed, borosilicate glass ampoules were used after acid wash (0.01 M HNO_3). Preliminary experiments were first conducted to test all of the containers used in this study, which comprised both polypropylene tubes with nominal volumes of 5 mL, 15 mL, and 50 mL, and borosilicate glass ampoules with nominal volumes of 5 mL. Results showed that all containers had negligible adsorption of Zn^{2+} or Ni^{2+}.

a. Kinetics study of Zn^{2+} adsorption onto aggregated and dispersed O-MWCNTs

O-MWCNTs at O% of 5.1% and 8.0% were employed in the kinetics study. In these experiments, mixtures of O-MWCNTs and Zn^{2+} solutions were prepared using the methods described above and shaken for a designated amount of time, ranging from 5 minutes to 48 hours. For experiments in which dispersed O-MWCNTs were used, the hydrodynamic diameters (D_h) of these diluted dispersions were also measured at the time of final sampling using dynamic light scattering (DLS). DLS was conducted immediately after sampling by diluting an aliquot of the mixture to ~ 0.1 mg/L O-MWCNT dispersion.

b. Adsorption experiments to investigate pH effect

3 mg Pristine MWCNTs or F400 PAC were added into 5 mL solutions to investigate the effect of solution pH. Ni^{2+} at concentrations ranging from 0.1 – 3.0 mM was used as a single adsorbate. 5 mM $NaHCO_3$ was used as a buffer and the solution pH was adjusted to be 7.1 ± 0.1 using 0.01 M NaOH or HNO_3, with NaNO3 then added as necessary to achieve the finally desired IS of 10 mM Experiments at a lower pH value were conducted without any buffer and the final pH of those experiments was measured to be 5.2 ± 0.2. IS was maintained at 10 mM for these experiments as well.

c. Adsorption experiments to investigate IS effect

Mixtures containing 0.427 g/L dispersed 8.0% O-MWCNT and Zn^{2+} at concentrations ranging from 0.003 to 0.03 mM were used to investigate IS effects. The total IS of those mixtures were adjusted to be 1 mM or 10 mM. The initial pH values were adjusted to 6.5 ± 0.3 using 0.01 M NaOH or 0.01 M HNO_3. The final pH of these experiments ranged from pH 5.8 – pH 6.4.

d. Adsorption experiments to investigate O-MWCNT surface chemistry effect

Solutions containing Zn^{2+} ranging from 0.2 – 3 mM were mixed with O-MWCNTs with total surface oxygen concentrations of 5.1%, 5.4%, 6.3% and 7.1% to study the effects of O-MWCNT surface chemistry on adsorption. IS in this study was kept at 10 mM. No buffer was used and the initial pH was adjusted to be 6.5 ± 0.3. Final pH of this study ranged from pH 5.8 – pH 6.4.

e. Adsorption experiment to investigate S/L and aggregation effects

8.0% O-MWCNT and 5.1% O-MWCNT at both aggregated and dispersed forms as well as PAC were all used as adsorbents to study Zn^{2+} sorption at varied S/L. Details for the experimental setup are summarized in **Table 2.1**. The initial pH values for all experiments in this section were adjusted to 6.5 ± 0.3. Final pH of these experiments ranged from pH 5.8 – pH 6.4. Total IS was kept at 10 mM throughout the experiments.

Table 2.1. Summary of adsorption experimental parameters

adsorbent	Aggregation state	Solid-to-liquid ratios (S/L), g/L
8.0% O-MWCNTs	Dispersed	0.016
		0.031
		0.061
	Aggregated	0.061
		0.143
		0.429
		0.714
5.1% O-MWCNTs	Dispersed	0.016
		0.031
		0.061
	Aggregated	0.061
		0.143
PAC	Aggregated	0.143
		0.429
		0.714

As shown in **Table 2.1**, both aggregated and dispersed O-MWCNTs were applied in experiments at the S/L of 0.061 g/L. This is the only solid-to-liquid ratio with sufficiently large CNT mass for the aggregated O-MWCNTs powder to be accurately measured out using an analytical balance (0.9 ± 0.1 mg per sample) and with a sufficiently low solid concentration to allow the maintenance of stable O-MWCNT dispersion that do not

2.2.6 *Measurement of Adsorbate Concentrations*

At the end of the specified equilibration period, all samples from the sorption experiments were removed from the rotator and solutions were passed through a 0.20 μm nylon filter (Corning Inc.). I then measured the pH as well as aqueous concentrations of Zn^{2+} in the filtrate. Preliminary experiments were conducted in systems without CNT addition and these results confirmed negligible (< 1%) uptake of Zn^{2+} by the filter. In order to test the filtration efficiency of the filter, O-MWCNT dispersions were prepared in pure Milli-Q water at the lowest (0.016 g/L) and highest (0.061 g/L) concentrations used in this study. These were passed through the same nylon filter and the filtrate was scanned from 200 nm to 800 nm using UV-Vis. Results showed that negligible amount of O-MWCNTs in the dispersion passed through the filters (99.8% removal). The concentrations of Zn^{2+} (C_e in equilibrium experiments and C_t in kinetic experiments) in the filtrates were measured using inductively coupled plasma mass spectrometry (ICP-MS, ELAN DRC II, PerkinElmer) or atomic absorption spectroscopy (AAS, AAnalyst 100, PerkinElmer). The solid (adsorbed) concentration of Zn^{2+} at equilibrium, q_e (mmol/g), was calculated using **Eq. 2.1** below:

$$q_e = \frac{(C_0 - C_e)V}{M} \qquad \textbf{Eq. 2.1}$$

where C_0 is the initial aqueous concentration of Zn^{2+} (mM); V is the volume of solution (L); and M is the mass of adsorbent (O-MWCNT or PAC, g).

In studies of kinetics, the instantaneous aqueous Zn^{2+} concentration at time t, C_t was measured and the instantaneously adsorbed concentration of Zn^{2+} at time t, q_t, was calculated using **Eq. 2.1** as well.

2.2.7 *Mathematical Modeling of Adsorption Isotherms*

The Langmuir isotherm model, as shown in **Eq. 2.2**, was used to fit all adsorption isotherms and was the primary tool for quantitative comparison of results. The following "single-site" form of the model was fit to data in a manner designed to minimize the sum of unweighted squared errors between observed data and model values (solver in Excel):

$$q_e = \frac{C_e K_L q_{\max}}{1 + K_L C_e} \qquad \textbf{Eq. 2.2}$$

where q_{max} is the maximum sorption capacity (mmol/g) and K_L is the adsorption affinity (mM^{-1}). Because the regression results using linearization or least squared regression with weighted squared errors were similar to the results obtained with the currently applied method, these two methods were not applied in this study.

In addition to the traditional Langmuir isotherm, a two-site Langmuir isotherm model as shown in **Eq. 2.3** was also applied to fit the experimental results. Cho *et al.*[1]

$$q_e = \frac{C_e K_{L,\ graphene}\ q_{\max,\ graphene}}{1 + K_{L,graphene}\ C_e} + \frac{C_e K_{L,COOH}\ q_{\max,\ COOH}}{1 + K_{L,COOH}\ C_e} \qquad \textbf{Eq. 2.3}$$

have shown that the quantity of carboxylic groups on the surface of O-MWCNTs correlates strongly with the adsorption capacity of O-MWCNTs, while the other

functional groups, *i.e.*, carbonyl, hydroxyl and non-identified residue, show comparatively negligible correlation. The correlation between carboxylic groups and the adsorption capacity of O-MWCNTs also revealed a positive intercept, indicating adsorption of Zn^{2+} onto the surface of O-MWCNTs where carboxylic groups were absent. Graphene accounts for over 90% of the carbon on the surface of O-MWCNTs. Therefore, we assumed that the graphene and carboxylic groups served as the two dominant types of adsorption sites. Note that the contribution of the graphene surfaces is also significant only because of their high relative contribution to surface area despite their low unit adsorption ability for metal ions. On the other hand, although carboxylic groups have a much lower relative surface concentration compared to that of the graphene sheet, but show much stronger affinity to Zn^{2+}, leading to high adsorption capacity. More details regarding the two-site Langmuir model have been provided previously by Cho *et al.*[1]

2.3 Results and Discussions

2.3.1 *Characterization of O-MWCNTs*

The total atomic oxygen concentrations on the surface of studied O-MWCNTs as well as the relative percentages of different oxygen containing functional groups are summarized in **Table 2.2**. Also included in **Table 2.2** is the total surface oxygen

Table 2.2. Surface oxygen concentrations and oxide distribution of adsorbents*

Treatment method	O_T%	O_{COOH}%	$O_{C=O}$%	O_{OH}%	O_{others}%
18% HNO_3	5.1	2.0	2.9	0.6	-0.5
25% HNO_3	8.0	2.2	1.9	0.6	0.7
43% HNO_3	8.0	2.6	1.4	0.7	1.6
53% HNO_3	8.0	2.8	1.1	0.7	2.6
$KMnO_4/H_2SO_4$	8.0	3.6	1.4	0.7	2.3
PAC	8.0	N/A	N/A	N/A	N/A

***** The XPS measurement in conjunction with chemical derivatization methods was conducted in Chemistry Department by Kevin Wapasnick and David Goodwin.

concentration of PAC (sieved through mesh 200) applied in this study. The values of surface oxygen in these O-MWCNTs were 5.1%, 5.4%, 6.3%, 7.1%, and 8.0%, respectively. The surface oxygen concentration for PAC was 8.0%. For the 5.1% and 8.0% O-MWCNTs, the percentages of oxygen associated with carboxyl groups were estimated to be 2.0% and 3.6%, respectively. The measured BET surface area for 8.0% O-MWCNT and PAC were 228.4 ± 0.6 m^2/g, and 1004.0 ± 0.1 m^2/g respectively. It has been shown from our previous study that O-MWCNTs oxidized using HNO_3 or $KMnO_4/H_2SO_4$ exhibited statistically identical surface area compared to their pristine counterpart.[1] Therefore, it is reasonable to assume that 5.1% O-MWCNT exhibits surface area of 228 m^2/g. DLS measurement showed that the hydration diameter D_h of the dispersed O-MWCNTs involving in this study was 163 ± 5 nm, which was similar to those measured in our previous studies, where the existence of individually dispersed nanoparticles in solution was shown using TEM and AFM.[43]

2.3.2 *Kinetic Study of O-MWCNT Adsorption*

The adsorption kinetics of Zn^{2+} onto dispersed and aggregated O-MWCNTs is shown in **Figure 2.1**. The adsorption of Zn^{2+} onto dispersed or aggregated O- MWCNTs were both apparently complete within less than 30 minutes.. For the dispersed O-MWCNTs, the adsorption kinetics figure reaches a plateau within 5 minutes. For the aggregated O-MWCNTs, the time required to reach a plateau was relatively longer, but still under 30 minutes. Due to the experimental limitation, quantitative analysis was not conducted for the kinetic experiments. It is noteworthy, however, that pseudo-second

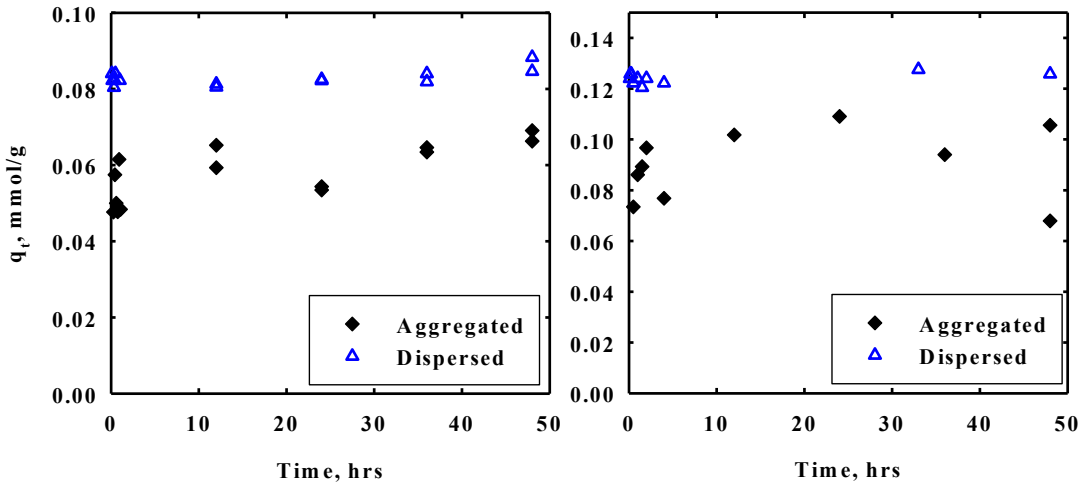

Figure 2.1 Kinetic study for the adsorption of Zn^{2+} onto (a) 5.1% O-MWCNTs and (b) 8.0% O-MWCNTs at the solid-to-liquid ratio of 0.061g/L. Both aggregated and dispersed O-MWCNTs were employed. Experiments were conducted without any additional buffer and the final pH and ionic strength were 5.8 – 6.4 and 10 mM, respectively.

order kinetics model as shown in **Eq. 2.4** was reported to be the best fit by numerous prior investigators who also studied heavy metal adsorption onto carbon nanotubes.[12, 15-18, 49, 50]

$$\frac{t}{q_t} = \frac{1}{k_2 q_e^2} + \frac{t}{q_e} \qquad \textbf{Eq. 2.4}$$

where q_t [M/M] and q_e [M/M] are the amounts of Zn^{2+} adsorbed onto O-MWCNTs at time t and at equilibrium, respectively, and k2 is the pseudo-second-order rate constant (M/(M·T))

2.3.3 *Effects of pH and ionic strength*

The pH value and IS of solutions were varied in the adsorption experiments and both factors exhibited significant effects.

a. Effect of pH

As shown in **Figure 2.2**, the adsorption of pristine MWCNTs exhibited

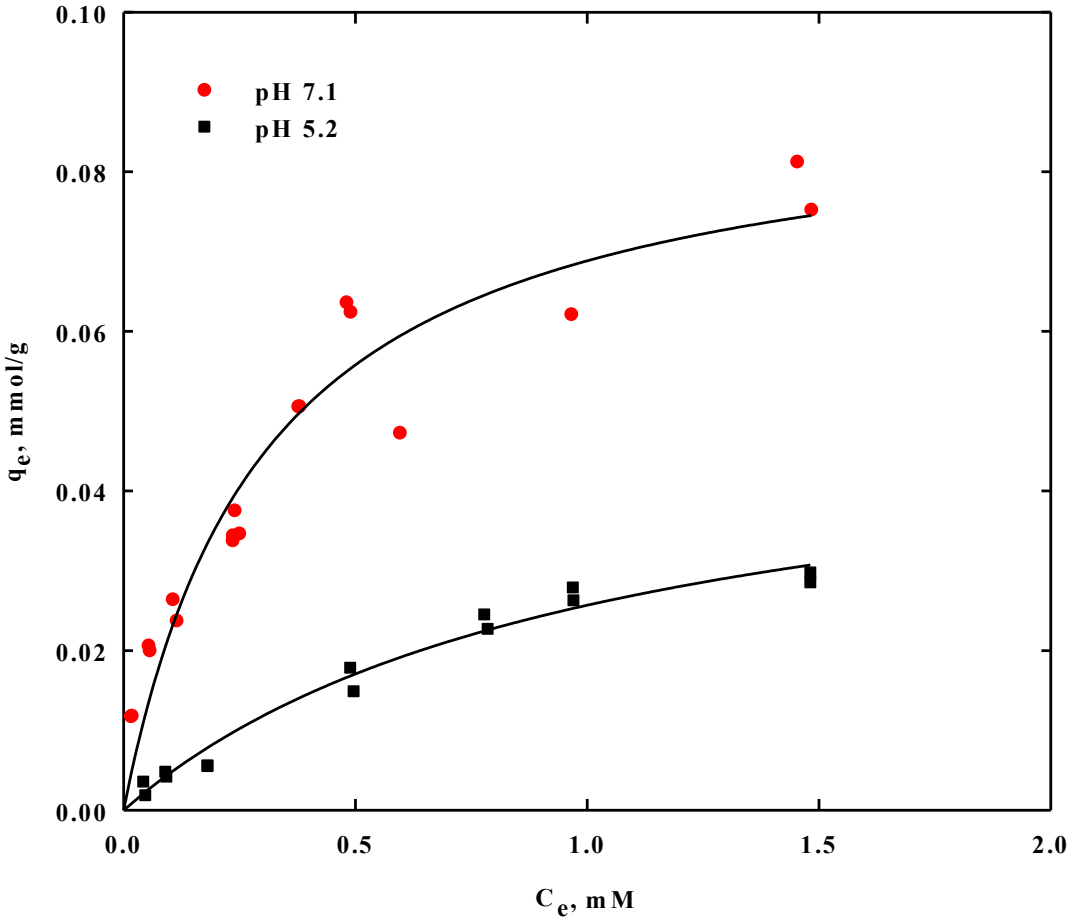

Figure 2.2. Adsorption isotherms of Ni^{2+} onto pristine MWCNTs at pH values of 5.2 ± 0.3 and 7.1 ± 0.1. 5 mM $NaHCO_3$ was applied as a buffer at pH 7.1. Experiments were conducted without any buffer at pH 5.2. IS was maintained at 10 mM with $NaNO_3$ for all experiments conducted for this purpose.

significantly larger adsorption ability towards Ni^{2+} at pH 7.1 than at pH 5.2. At pH 7.1, both the initial isotherm slope (affinity) and the ultimately approached plateau (adsorption capacity) of the isotherm are larger than those at pH 5.2.

The extent of difference is larger than what was previously reported by Cho *et al.*,[1] who found that pH had negligible effect on the adsorption of Zn^{2+} (<15% change in q_e) for both pristine and O-MWCNTs at pH 5.0 – 7.0. It is noteworthy, however, that pH 5.0 was the lower limit of the pH range in the study of Cho *et al.*[1] and that this value is

within a pH range where high sensitivity to pH is likely and, in particular, at a pH where significant decreases on Zn^{2+} adsorption with pH begin to occur. Given the different species of cations being studied (Ni^{2+} here versus Zn^{2+} in Cho *et al*) and that there is relatively large variation of pH value (± 0.3) in both studies owing to the absence of buffer at pH 5.0, the noted differences of results are not especially surprising. Morever, the large difference in adsorption capacity at these two pH values, as observed in this study, is also consistent with expectations based on deprotonization of carboxylic groups on the surface of MWCNTs at higher pH. In order to avoid the interference of pH in subsequent studies, all experiments involving Ni^{2+} were conducted at pH 7.0. When Zn^{2+} was applied, no buffer was applied and the final pH lied between 5.8 to 6.4, where the pH effect was observed to be negligible, as is consistent with the prior findings of Cho *et al.*[1].

b. Effect of ionic strength

IS effects on the adsorption of metal cations by O-MWCNTs has been reported previously mostly with aggregated CNTs [6-8, 11, 16] and these results were confirmed by our studies for dispersed forms of O-MWCNTs. As shown in **Figure 2.3**, higher adsorption capacity of dispersed O-MWCNTs for Zn^{2+} was observed at IS of 1 mM than that at IS of 10 mM.

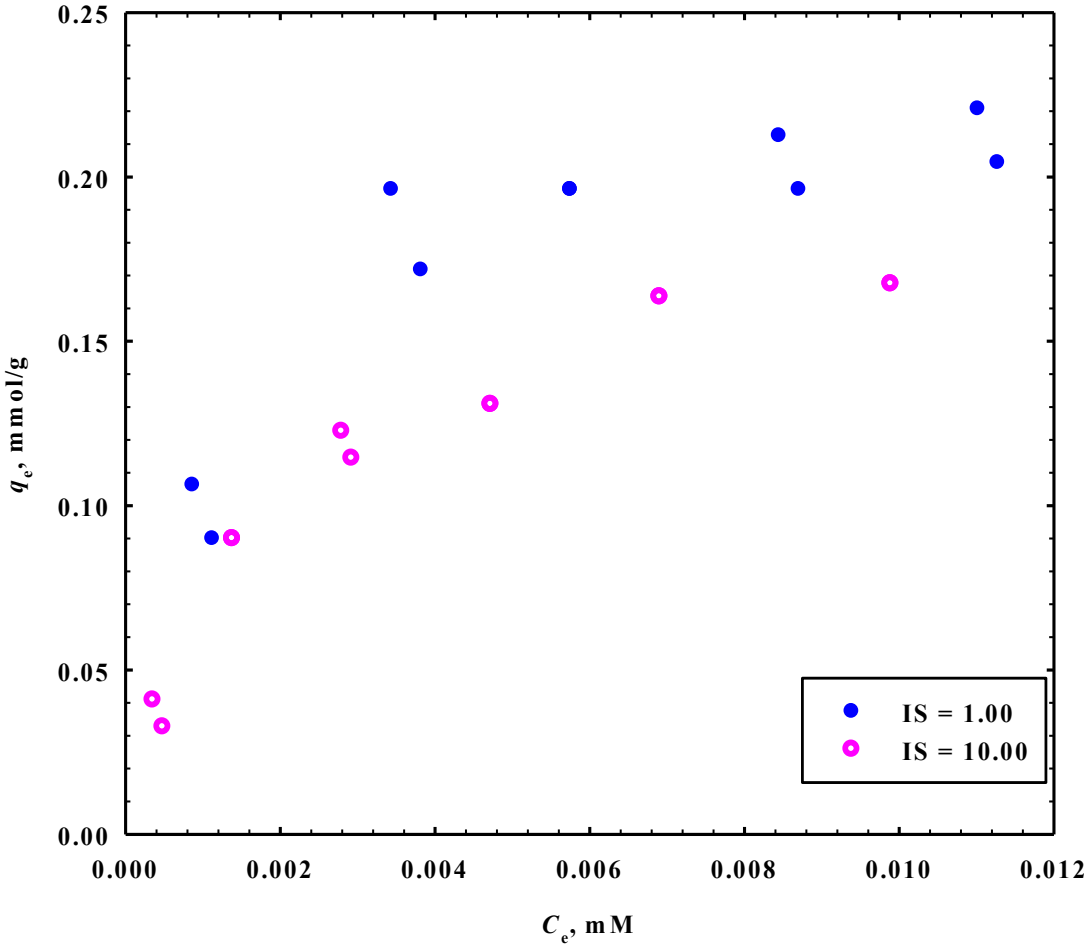

Figure 2.3 Adsorption isotherms of Zn^{2+} onto 8.0% O-MWCNTs at varied IS. Experiments were conducted without any buffer at a final pH of 5.8-6.4.

2.3.4 *Effect of Competing Organic Compound*

As shown in **Figure 2.4**, the adsorption of Zn^{2+} onto 8.0% O-MWCNTs was not affected by the additional 5 mg/L naphthalene. Prior study in our lab using O-MWCNTs (provided by the same manufacturer and passed through the same functionalization

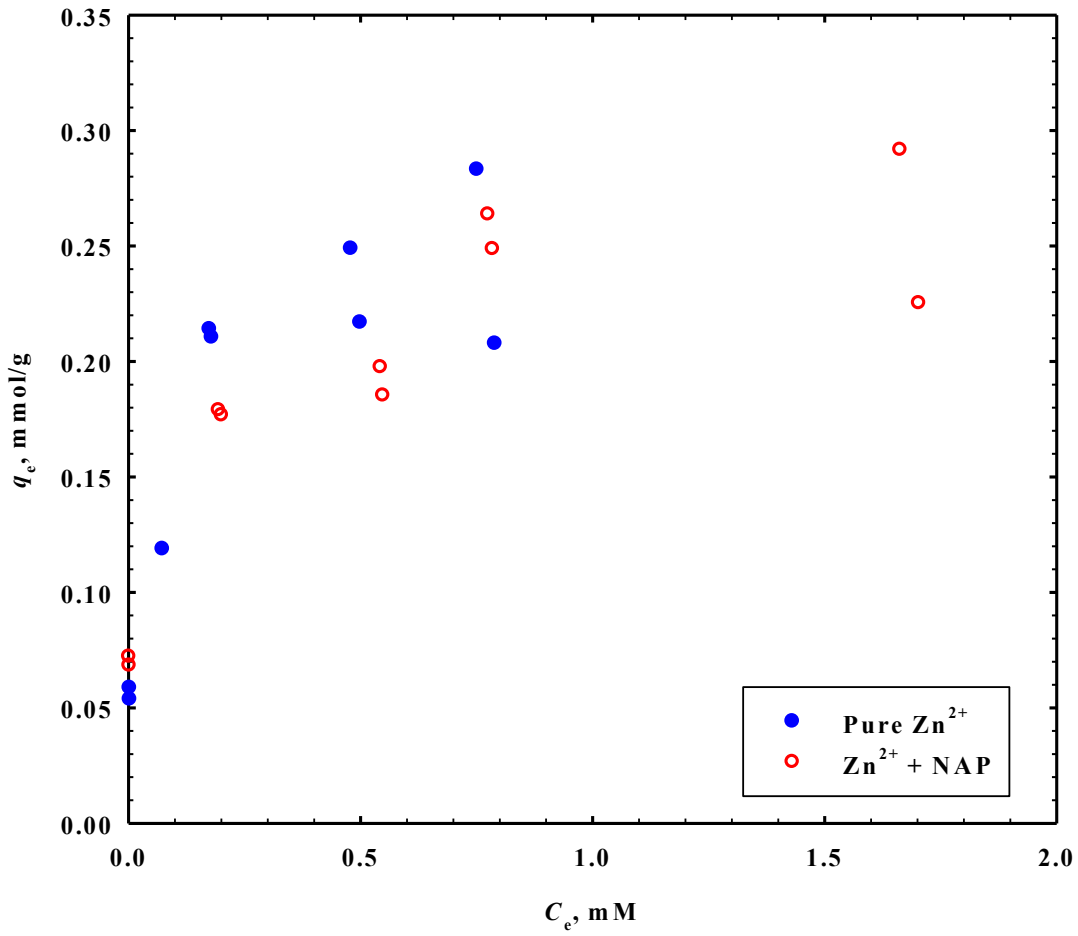

Figure 2.4 Adsorption isotherms of Zn^{2+} onto 8.0% O-MWCNTs in the presence and absence of 5 mg/L naphthalene. Experiments were conducted without any buffer at a final pH of 5.8-6.4

process) showed that the equilibrated adsorbed naphthalene was~ 44 mg/g for 7.4% O-MWCNTs and ~ 31 mg/g 8.9% O-MWCNTs in a single-solute system.[19] Even if the adsorbed amount of naphthalene was suppressed by the presence of Zn^{2+}, the presence of naphthalene in the system should still have a noticeable effect on the adsorption capacity of O-MWCNTs for Zn^{2+}. These results therefore may indicate that metallic ions and hydrophobic organic compounds adsorb onto O-MWCNTs with different adsorption mechanisms. This finding is consistent with those reported in previous studies where ion

exchange was found to be the primary mechanism for metallic ion adsorption and π -π interaction was the primary mechanism for the adsorption of organic compounds.[7, 19, 25, 51]

2.3.5 *Effect of Surface Chemistry*

The concentration of oxygen functional groups on the surfaces of O-MWCNTs is shown to have a significant effect on the adsorption of divalent ions(**Figure 2.5**).

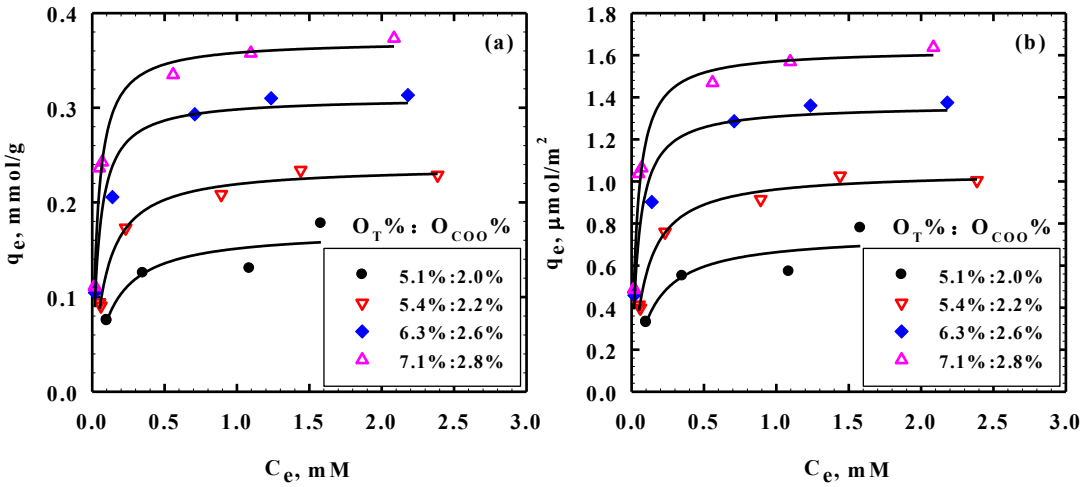

Figure 2.5 Adsorption of Zn^{2+} onto O-MWCNTs at varied total oxygen concentrations as well as carboxylic group concentrations. Experiments were conducted at the S/L of 0.43 g/L without any buffer and the final pH and ionic strength were 5.8 - 6.4 and 10 mM, respectively. The (a) mass normalized and (b) surface area normalized equilibrated solid concentration (q_e) were both shown. All data were fitted using single-site Langmuir model.

O-MWCNTs with higher total oxygen concentrations and higher concentrations of carboxylic groups exhibited higher adsorption capacity. All isotherms could be well fit by the traditional Langmuir isotherm model. The parameters are summarized in **Table 2.3**.

Table 2.3. Fit parameters for the four isotherms shown in **Figure 2.5** as based upon fitting of the one-site Langmuir isotherm model.

O_T% of O-MWCNTs	q_{max}(mmol/g)	q_{max}(mmol/m^2)	K_L(mM^{-1})	R^2
5.1%	0.17	0.75	7.68	0.879
5.4%	0.24	1.05	11.25	0.989
6.3%	0.31	1.36	23.41	0.967
7.1%	0.37	1.63	27.21	0.983

In **Figure 2.5**, the adsorbed concentration q_e is shown in units of mmol/g as well as μmol/m^2. The former is more commonly seen in literature and can help researchers more practically consider the required amount of adsorbent needed in a packed bed or batch study to reach a specific equilibrium concentration. The latter (μmol/m^2), on the other hand, is more useful for considering the adsorption mechanism since the number of adsorption sites will scale with the surface area of the adsorbent. Although the BET measured surface area is an inexact measure of the actual contact area available for adsorption in solution, normalization of the adsorbed concentration with the surface area one can still provide a possibly better qualitative method for comparing the adsorption ability per unit site among varied adsorbents.

In addition to the traditional Langmuir model, a two-site Langmuir model as described above and in Cho *et al.*[1] was also applied in this study to mathematically analyze the role of carboxyl functional groups. As discussed previously, we hypothesize that carboxylic groups and graphene are two primary site types on the surface of O-MWCNTs interacting with Zn^{2+} based on the high correlation between carboxylic group concentration and the adsorption capacity of O-MWCNTs in linear regression and the positive intercepts of the regression.[1] The four experimental data were then fitted altogether with eight q_{max} (two for each type of O-MWCNTs) and two K_L (one attributed to graphene and the other to carboxylic groups for all O-MWCNTs employed). The fit parameters are shown in **Table 2.4** and the data were replotted with the two-site Langmuir model in **Figure 2.6**.

Table 2.4. Fit parameters for four isotherms shown in **Figure 2.5** using two-site Langmuir isotherm model with fixed K_L (constants of affinity).

O_T% of O-MWCNTs	$q_{max,COOH}$ ($\mu mol/m^2$)	$q_{max,Graphene}$ ($\mu mol/m^2$)	$K_{L,COOH}$ (μM^{-1})	$K_{L,\ Graphene}$ (μM^{-1})	R^2
5.1%	0.13	0.61	0.053	0.0054	0.879
5.4%	0.33	0.73			0.984
6.3%	0.81	0.60			0.991
7.1%	0.83	0.64			0.808

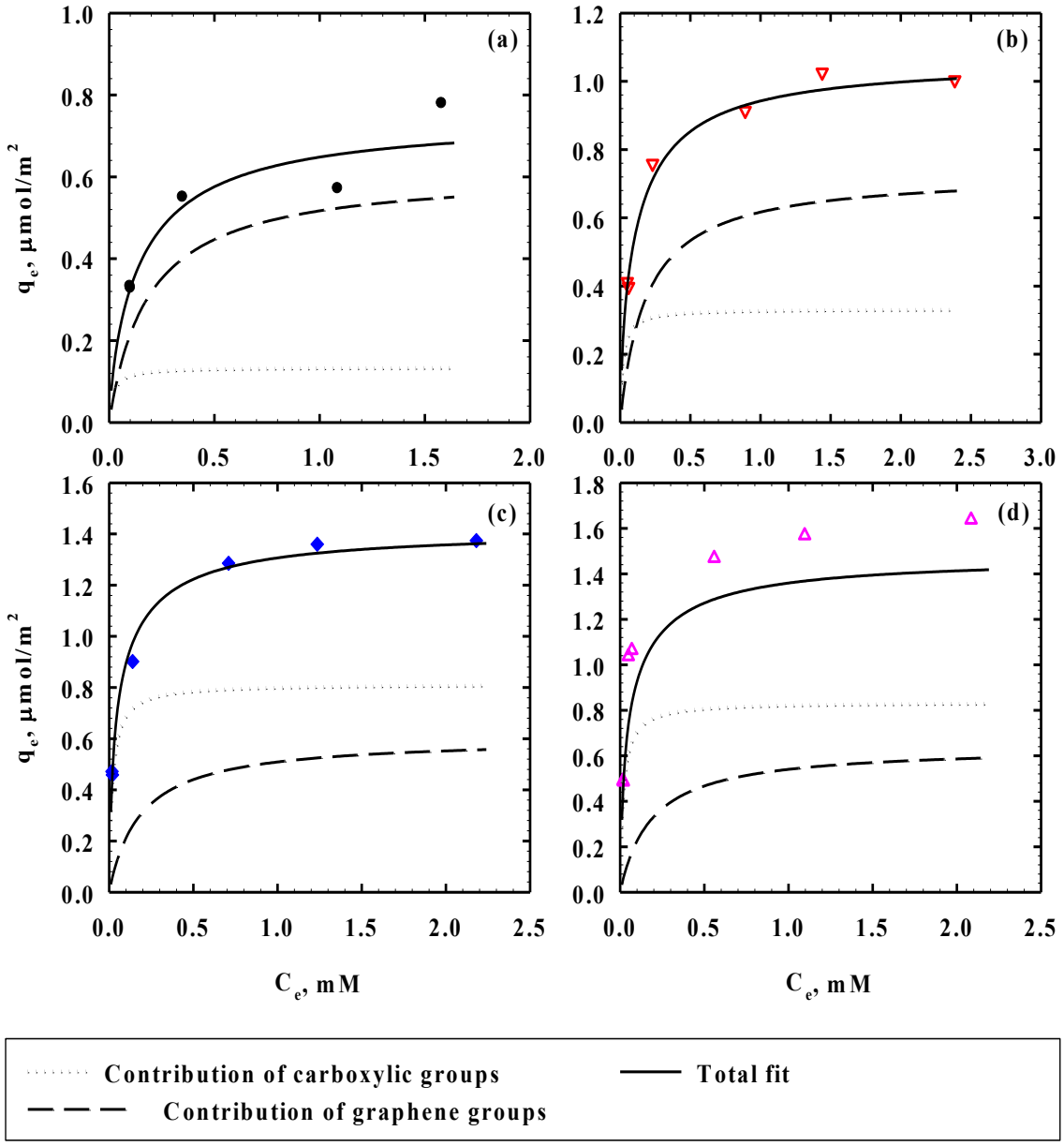

Figure 2.6 Two-site Langmuir isotherm fit of adsorption isotherms shown in Figure 2.5. The isotherms shown were obtained using (a) 5.1% O-MWCNTs, (b) 5.4% O-MWCNTs, (c) 6.4% O-MWCNTs and (d) 7.1% O-MWCNTs.

The two-site Langmuir model fit the experimental results reasonably well. These results are consistent with-the previous findings of Cho *et al.*[1], who reported that the adsorption capacity of O-MWCNTs comprises contributions primarily from graphene

and carboxylic groups on the surface. As shown in **Table 2.4**, the obtained q_{max} and k_L are in the same order of magnitude as those obtained in Cho *et al.*[1], within factors of roughly 2 and 5, respectively. These findings suggest that the O-MWCNTs used in this study have similar properties as those used in the previous study of our group. Note that some differences are in fact expected. Although both materials were obtained using similar oxidizing methods and on starting materials from the same supplier, they do represent different batches of CNTs and were prepared at different times.

The obvious effect of surface oxygen content of O-MWCNTs not only exhibited on aggregated O-MWCNTs, but also showed when dispersed O-MWCNTs were used as shown in **Figure 2.7**. These experimental results were also well fit using one-site

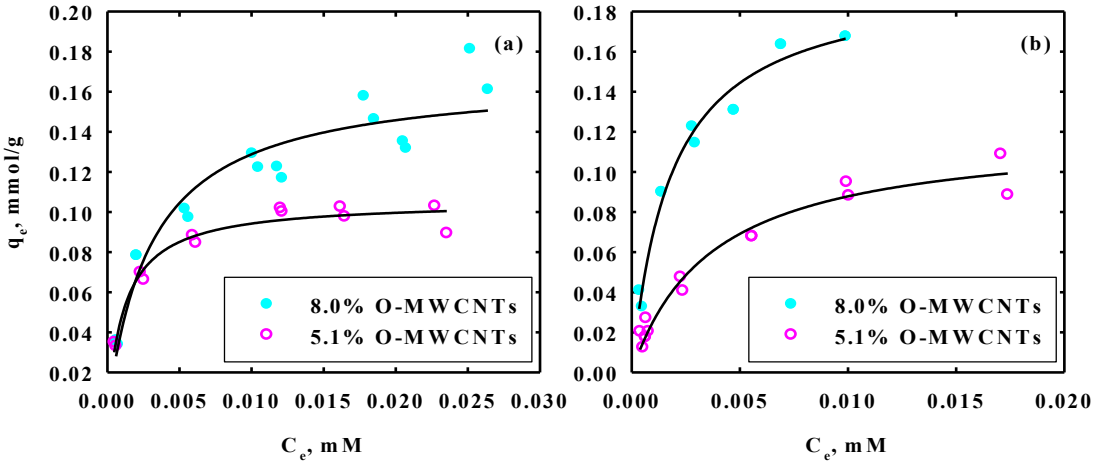

Figure 2.7 Adsorption of Zn^{2+} onto dispersed O-MWCNTs at varied total oxygen concentrations. Experiments were conducted at the S/L of (a) 0.061 g/L and (b) 0.016 g/L. No buffer was employed and the final pH and ionic strength were 5.8 ± 0.2 and 10 mM, respectively.

Langmuir isotherm model, indicating similar favorable (concave downward) isotherm shapes that may also have adsorption plateaus at high C_e. Two-site Langmuir isotherm

model was not applied on these results due to the relatively small pool of the data reservoir.

2.3.6 *Effect of Aggregation States*

As mentioned above, it is important to investigate the possible differences between the dispersed and aggregated O-MWCNTs in their interactions with divalent cations. In the current study we tested the adsorption of Zn^{2+} ions onto 8% and 5% O-MWCNTs at the solid-to-liquid ratio of 0.061 g/L in both completely dispersed and aggregated form. Initial hydrodynamic particle sizes of O-MWCNTs dispersions were tested to be ~160 nm for 5.1% O-MWCNTs and ~163 nm for 8.0% O-MWCNTs, which are typical particle sizes for completely dispersed O-MWCNTs.[44] Even at the low S/L used, obvious aggregation was observed right after mixing the 5.1% O-MWCNT dispersion with the Zn^{2+} testing solution. On the other hand, the 8.0% O-MWCNT dispersion exhibited greater stability, with most material staying well dispersed throughout the equilibrium time (48 hours) and with only a few aggregated particles attached to the wall of containers. DLS measurement of the dispersions showed that the majority of 8.0% O-MWCNT dispersion had the size of ~ 180 nm but the size of 5.1% O-MWCNT dispersion increased to over 400 nm in 10 min.

Figure 2.8 shows the adsorption isotherms for both 5.1% and 8.0% O-MWCNT

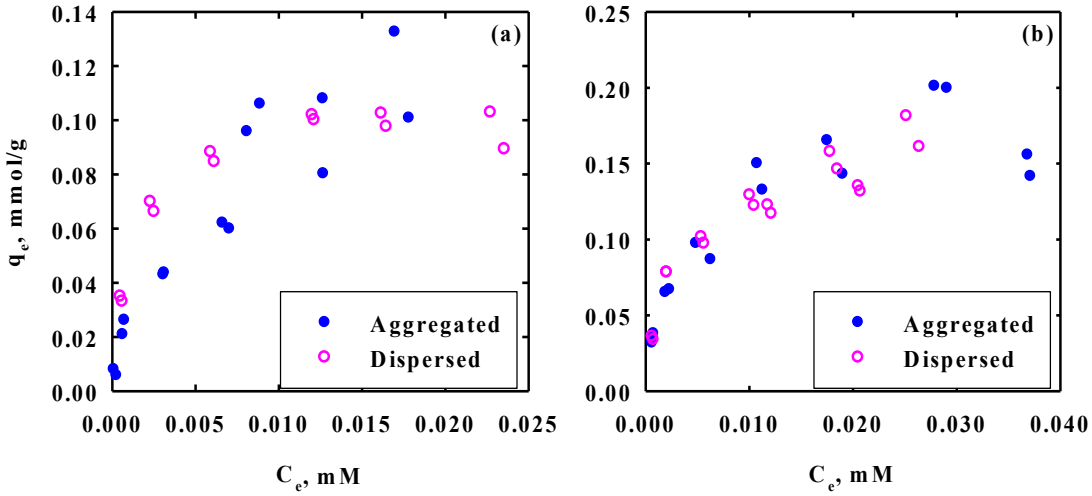

Figure 2.8 Adsorption of Zn^{2+} onto (a) 5.1% O-MWCNTs and (b) 8.0% O-MWCNTs at S/L of 0.061 g/L. Both aggregated and dispersed O-MWCNTs were used as sorbents. No buffer was used in the experiments and the final pH and ionic strength were 5.8 ± 0.2 and 10 mM, respectively.

in both dispersed and aggregated (powdered) forms. For O-MWCNTs at 5.1%O and 8.0%O, there is no statistical difference in their adsorption isotherms between aggregated and dispersed forms at the same solid-to-liquid ratio. These results may indicate there is no significant difference in adsorption mechanism between O-MWCNTs that are still in their initial aggregated state and those being sonicated and well dispersed. These results are also consistent with the observation in our previous study that the aggregation state of O-MWCNTs, per se, does not appear to have a major effect on their adsorption abilities.[1] One may notice that, within the lower equilibrium concentration range of 0.002 – 0.01 mM, the dispersed O-MWNTs exhibited slightly higher adsorbed concentration, which was also shown in the kinetics study (**Figure 2.1**). However, this difference was no longer obvious when C_e > 0.01 mM and therefore did not cause the estimated adsorption capacity of the dispersed O-MWCNTs to be statistically higher than that of the aggregated O-MWCNTs. These findings were different from those of Zhang *et*

al.(2012)[28] and Zhang *et al*. (2009)[27], both of whom reported a significant increase of adsorption capacity for CNTs while dispersed. It is noteworthy, however, that they focused on adsorption of organic compounds onto CNTs and to the best of our knowledge, no study has been conducted to investigate the effect of aggregation state on heavy metal adsorption onto CNTs. We therefore postulate that aggregation state is of great importance when the adsorption mechanism is π - π bonding because the effective surface area increases when CNTs are dispersed. When ion exchange is the primary mechanism, as in heavy metal adsorption, the aggregation state no longer plays an important role in determining the adsorption capacity of CNTs because the availability of carboxylic groups, which serve as ion exchange sites on CNT surfaces, is not limited by CNT aggregation state.

2.3.7 *Effect of Solid-to-Liquid Ratio in the System*

As noted above, the aggregation state of the O-MWCNTs does not appear to have any major effect on the adsorption capacity of O-MWCNTs for the conditions of this study. The solid-to-liquid ratio, on the other hand, showed significant effect on the adsorption characteristics of both types of O-MWCNTs. **Figure 2.9** shows the adsorption

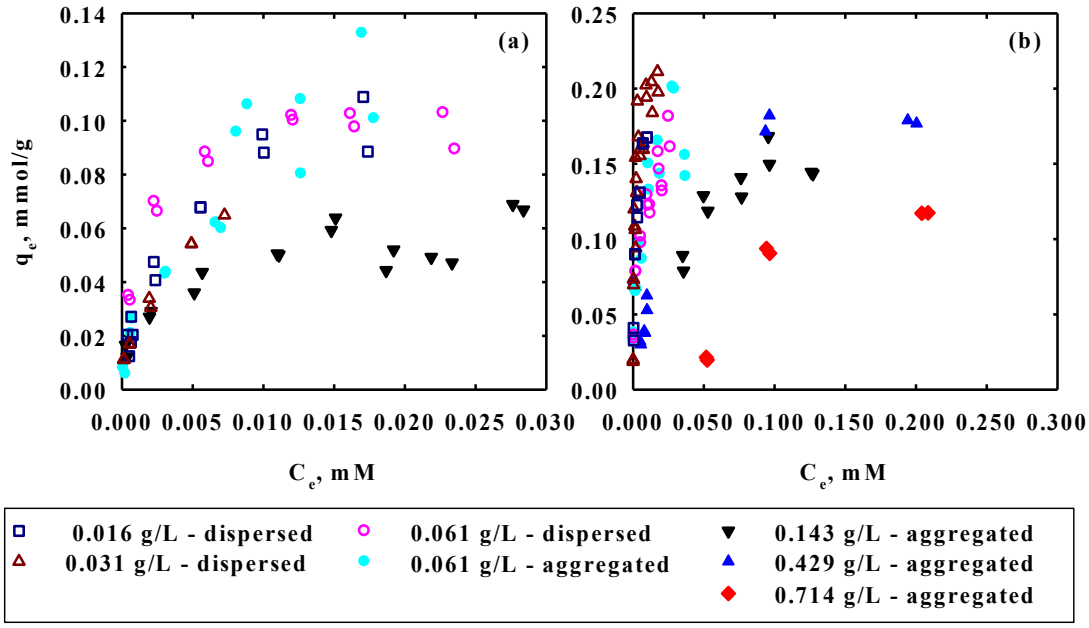

Figure 2.9 Adsorption of Zn^{2+} onto (a) 5.1% O-MWCNTs and (b) 8.0% O-MWCNTs at varied solid-to-liquid ratios as well as aggregation states. Experiments were conducted without any buffer, and the final pH and ionic strength were 5.8 ± 0.2 and 10 mM, respectively.

of Zn^{2+} onto both 5.1% and 8.0% O-MWCNTs at the solid-to-liquid ratios ranging from 0.016 g/L to 0.714 g/L. For both types of O-MWCNTs, isotherms obtained at lower solid-to-liquid ratios are significantly higher than those obtained at relatively higher solid-to-liquid ratios. For reasons previously discussed, aggregated O-MWCNTs can only be used in experiments at solid-to-liquid ratios above 0.061 g/L and dispersed O-MWCNTs can only be employed in experiments at solid-to-liquid ratios below 0.061 g/L. Therefore, a change of aggregation state of O-MWCNTs was unavoidable over the large range of solid-to-liquid ratios studied here. Under the assumption of no differences associated with aggregation state (based on the evidence obtained at 0.061 g/L), it is reasonable to compare the adsorption isotherms shown in **Figure 2.9**, despite the varied aggregation state. Since isotherms for low solid-to-liquid ratios (mostly dispersed O-

MWCNTs) have a much lower range of equilibrated concentration C_e, all isotherms obtained by using dispersed O-MWCNTs have been replotted in **Figure 2.10**. In order to

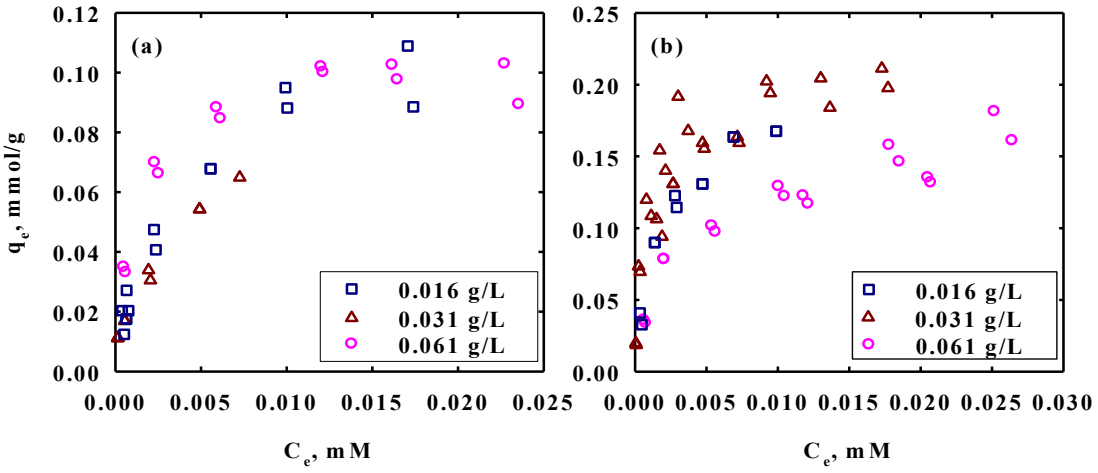

Figure 2.10 Adsorption of Zn^{2+} onto dispersed (a) 5.1% O-MWCNTs and (b) 8.0% O-MWCNTs at varied solid-to-liquid ratios. Experiments were conducted without any buffer, and the final pH and ionic strength were 5.8 – 6.4 and 10 mM, respectively.

further compare the adsorption of O-MWCNTs at different solid-to-liquid ratios, two example isotherms for 8.0% O-MWCNTs at the solid to liquid ratio of (a) 0.429 g/L and (b) 0.031 g/L are shown in Figure 2.11. Both isotherms were well fit using single-site Langmuir isotherms.

It can be seen from **Figure 2.9** and **Figure 2.10** that the effect of S/L is most obvious at higher S/L. For 5.0% O-MWCNTs, such effect cannot be seen below 0.061 g/L, and for 8.0% O-MWCNTs, the effect cannot be seen below 0.031 g/L. This finding further indicates that aggregation state is not the reason for the S/L effect, since in that case, we would expect less S/L effect for the high oxidized tubes at low S/L range. However, the opposite was observed. The strong effect of S/L, however, can be easily observed, for example, between S/L of 0.429 g/L and 0.031 g/L as shown in **Figure 2.11**.

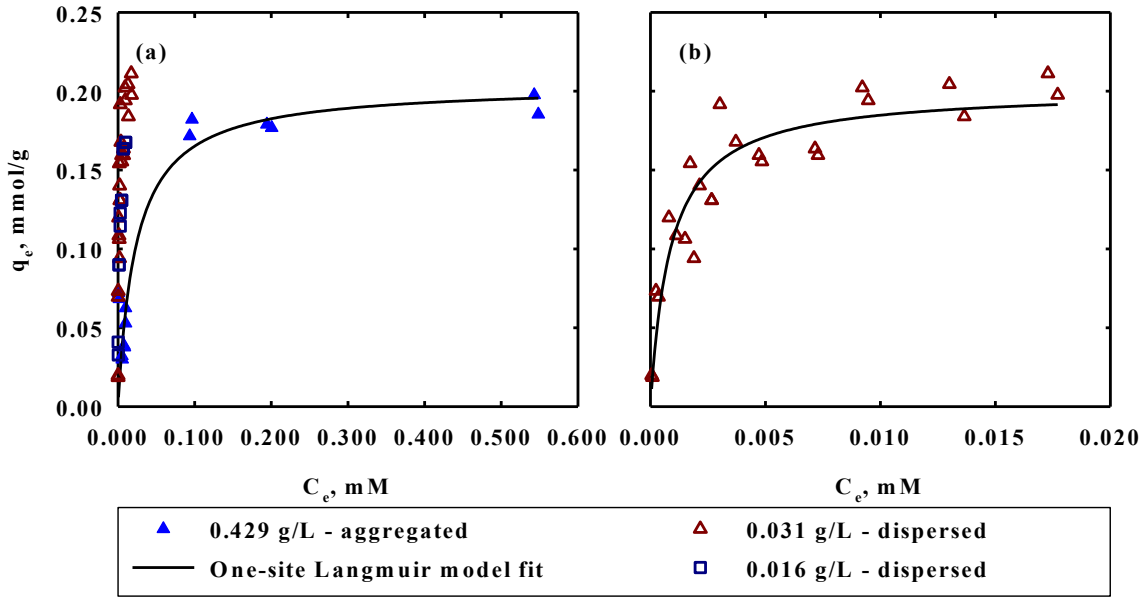

Figure 2.11 Adsorption of Zn^{2+} onto 8.0% O-MWCNTs at the solid-to-liquid ratios of (a) 0.429 g/L and lower S/L and (b) 0.031 g/L. Experiments were conducted without any buffer and the final pH and ionic strength were 5.8 - 6.4 and 10 mM, respectively.

It is clear from this figure that both isotherms reached plateaus at similar height, although the isotherm created at a lower S/L (Figure 2.11(b)) reaches the plateau at an equilibrium concentration around 30 times lower than that created at a higher solid-to-liquid ratio. **Figure 2.9** and **Figure 2.11(a)** also show that much steeper slopes can be observed for isotherms obtained at low S/L than those obtained at high S/L. This finding is in contrast to expectations based on the possibility of site blockage due to aggregation,[30, 52, 53] where the adsorption capacity (the level of plateau) was expected to be different instead of the affinity (the slope of the curve before reaching the plateau). Overall, the mechanistic cause of the S:L effect with CNTs, as with the similarly large effects previously adsorbed with metal adsorption to quartz and clays[30, 52, 53] remains uncertain.

In order to better understand the adsorption properties of CNTs, all isotherms obtained in the study of S/L effect were fit using one-site Langmuir isotherm model.

Maximum adsorption capacity, q_{max}, and adsorption affinity K_L obtained from the fitting are summarized in **Table 2.5**. Parameters obtained for 8.0% O-MWCNTs are also shown

Table 2.5 Fit parameters of isotherms shown in **Figure 2.9** and **Figure 2.13** using one-site Langmuir model.

	8%		5.1%		AC	
solid-to-liquid ratio	q_{max}	K_L	q_{max}	K_L	q_{max}	K_L
0.016	0.1972	545.8	0.1204	269		
0.031	0.2011	1133	0.08207	387.4		
0.061	0.168	328.1	0.1056	827		
0.061	0.1942	225	0.1678	119.8		
0.143	0.2751	14.01	0.00625	412.6		
0.429	0.245	27.34			0.066	0.782
0.714	0.2619	3.116			0.104	0.545

in **Figure 2.12**, where they are plotted as a function of the corresponding S/L. As shown

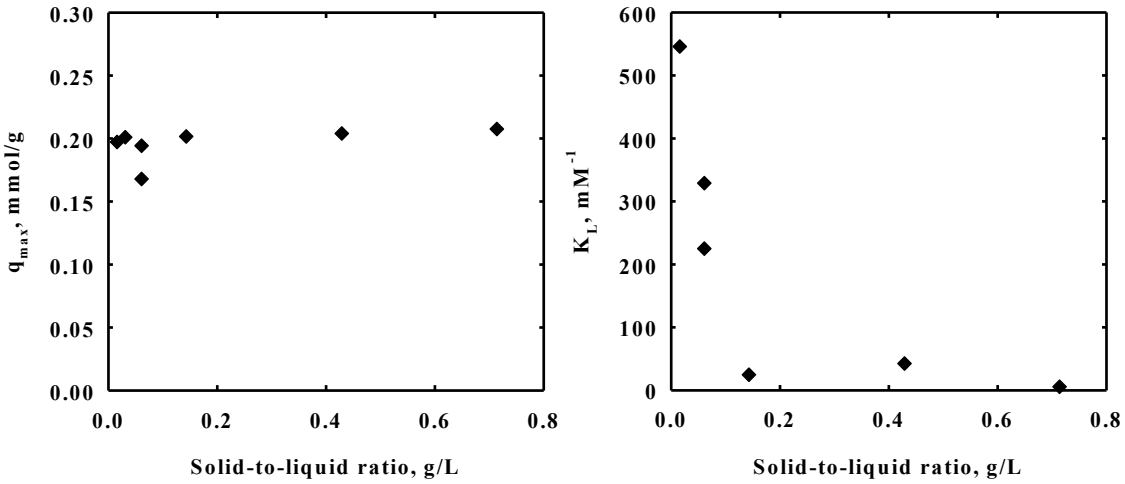

Figure 2.12 Fit parameters of experimental data in **Figure 2.9**(b) using one-site Langmuir model. Both (a) the maximum adsorption capacity and (b) the affinity constant K_L are plotted as a function of solid-to-liquid ratio.

in **Figure 2.12**, the maximum adsorption capacity q_{max} keeps roughly constant when the S/L increases by more than 10 times. On the other hand, the affinity K_L, decreases dramatically from ~ 0.54 μM^{-1} to ~ 0.0031 μM^{-1}. These results clearly show the negative

correlation between the affinity of the adsorption sites on the surface of O-MWCNTs to Zn^{2+} and the solid-to-liquid ratio of the system. As previously noted, however, the fundamental mechanism causing such strong inverse relationship remains unclear.

One concern in the above regard is that our work may somehow be affected by experimental artifacts that cause an "appearance" of S:L effects where they do not exist. In order to evaluate the possibility of such artifact, and under the assumption that S:L effects should not affect sorption with a microporous material such as PAC, we conducted additional studies of Zn^{2+} sorption with PAC at S:L values of 0.429 g/L and 0.714 g/L). Note that, since PAC cannot be dispersed into aqueous solution as O-MWCNTs. It is not possible to accurately measure lower PAC mass additions, and experiments at lower solid-to-liquid ratio were not possible without using impractically large aqueous volumes. The isotherms obtained using PAC were therefore limited to the S:L ranges as given above. The resulting data, as with the prior CNT results, were fit using one-site Langmuir model. The fitted parameters are summarized in **Table 2.5**. As evident from the values in this table and as shown in **Figure 2.13**, the S/L has negligible

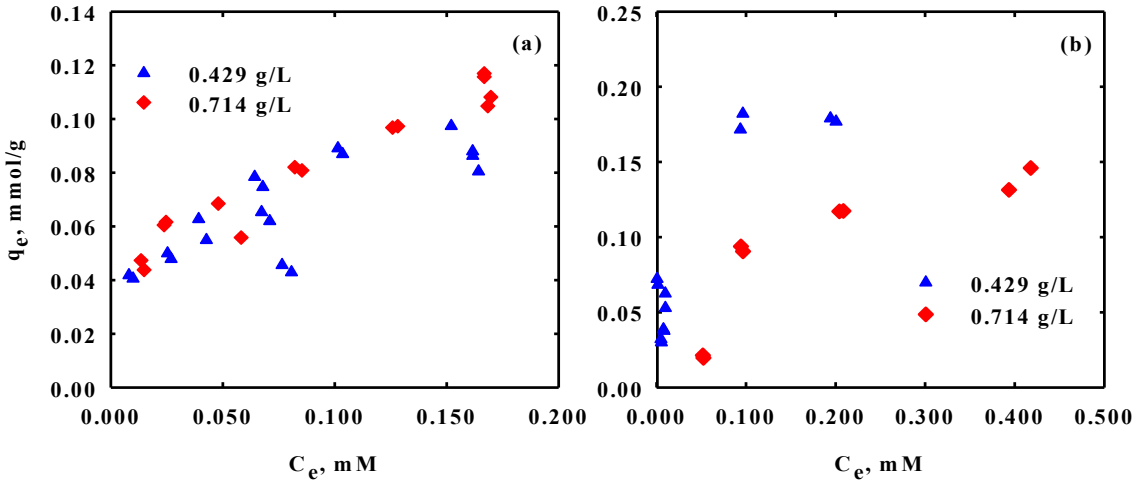

Figure 2.13 Adsorption of Zn^{2+} onto (a) PAC and (b) 8.0% O-MWCNTs at varied solid-to-liquid ratios. Experiments were conducted without any buffer and the final pH and ionic strength were 5.8 -6.4 and 10 mM, respectively.

effect on adsorption experiments using PAC as adsorbents. This is in direct contrast to the strong inverse relationship previously discussed for the 8.0% O-MWCNTs. This investigation indicates that the S/L effect is not a universal phenomenon throughout all types of adsorbents and suggests against the possibility of experimentally artificial factors causing our observations with CNTs. In addition, the results also suggest that the S/L effect may indeed relate in some way to the fact that adsorption with O-MWCNTs occurs on external surfaces of individual particles (with variable surface-volume ratios as affected by solid-liquid ratio), whereas adsorption onto surfaces of PAC occurs on pore walls that are internal to these microscopically porous materials, and which are, thus, less likely to be affected by the proximity of other particles. Nonetheless, however – and as already emphasized in prior discussion – we remain uncertain as to why adsorption affinity to external surfaces is so heavily affected by solid-liquid ratio, even while aggregated state (per se) seems to have relatively little effect.

2.4 Implication of the Study

The meaning of the results is twofold. First, this study investigated the potential of CNTs as a new water treatment candidate. The large surface area and surface functional groups make CNTs a good candidate as adsorbent for heavy metal removal. Our study quantified the relationship between various functional groups, especially carboxyl groups and unit-adsorbed amount of heavy metals on CNT surfaces. We also developed a two-site Langmuir model for CNTs with varied surface oxygen concentrations. These results, together with previous studies using traditional adsorbents, such as PAC, provided quantitatively evaluation for CNT as a potential contaminant treatment material. Second, this study has broadened our knowledge on the interactions between CNTs, as novel materials, and heavy metals. O-MWCNTs at low concentrations exhibited a significantly larger adsorption capacity for divalent metal ion adsorption. This finding is of great importance in estimating the effect of CNTs on the transport and distribution of heavy metals in the water and groundwater systems.

2.5 Cited References

1. Cho, H. H.; Wepasnick, K.; Smith, B. A.; Bangash, F. K.; Fairbrother, D. H.; Ball, W. P., Sorption of Aqueous Zn[Ii] and Cd[Ii] by Multiwall Carbon Nanotubes: The Relative Roles of Oxygen-Containing Functional Groups and Graphenic Carbon. *Langmuir* **2010,** *26*, (2), 967-981.

2. Stumm, W.; Morgan, J. J., Aquatic Cheistry: Chemical Equilibria and Rates in Natural Waters. John Wiley & Sons, Inc: New York, 1996.

3. Ipcs, International Programme on Chemical Safety. World Health Organization: Geneva, 1988.

4. Purdom, P. W., Environmental Health. Academic Press: New York, 1980.

5. Moore, J. W.; Sutherland, D. J., Distribution of Heavy-Metals and Radionuclides in Sediments, Water, and Fish in an Area of Great Bear Lake Contaminated with Mine Wastes. *Arch Environ Con Tox* **1981,** *10*, (3), 329-338.

6. Jacques Buffle, R. R. D., Chemical and Biological Regulation of Aquatic Systems. Lewis Publishers: Chelsea, 1991.

7. Chen, C. L.; Wang, X. K., Adsorption of Ni(Ii) from Aqueous Solution Using Oxidized Multiwall Carbon Nanotubes. *Ind Eng Chem Res* **2006,** *45*, (26), 9144-9149.

8. Li, Y. H.; Ding, J.; Luan, Z. K.; Di, Z. C.; Zhu, Y. F.; Xu, C. L.; Wu, D. H.; Wei, B. Q., Competitive Adsorption of Pb^{2+}, Cu^{2+} and Cd^{2+} Ions from Aqueous Solutions by Multiwalled Carbon Nanotubes. *Carbon* **2003,** *41*, (14), 2787-2792.

9. Li, Y. H.; Wang, S.; Luan, Z.; Ding, J.; Xu, C.; Wu, D., Adsorption of Cadmium(Ii) from Aqueous Solution by Surface Oxidized Carbon Nanotubes. *Carbon* **2003,** *41*, (5), 1057-1062.

10. Liao, Q.; Sun, J.; Gao, L., Adsorption of Chlorophenols by Multi-Walled Carbon Nanotubes Treated with Hno_3 and Nh_3. *Carbon* **2008,** *46*, (3), 553-555.

11. Qiu, K. D.; Li, W. B., Adsorption of Hexavalent Chromium Ions on Multi-Wall Carbon Nanotubes in Aqueous Solution. *Acta Phys-Chim Sin* **2006,** *22*, (12), 1542-1546.

12. Lu, C. S.; Chiu, H.; Liu, C. T., Removal of Zinc(Ii) from Aqueous Solution by Purified Carbon Nanotubes: Kinetics and Equilibrium Studies. *Ind Eng Chem Res* **2006,** *45*, (8), 2850-2855.

13. Wang, X.; Chen, C.; Hu, W.; Ding, A.; Xu, D.; Zhou, X., Sorption of 243am(Iii) to Multiwall Carbon Nanotubes. *Environ Sci Technol* **2005,** *39*, (8), 2856-2860.

14. Wu, C. H., Studies of the Equilibrium and Thermodynamics of the Adsorption of Cu^{2+} onto as-Produced and Modified Carbon Nanotubes. *J Colloid Interf Sci* **2007,** *311*, (2), 338-346.

15. Vukovic, G. D.; Marinkovic, A. D.; Colic, M.; Ristic, M. D.; Aleksic, R.; Peric-Grujic, A. A.; Uskokovic, P. S., Removal of Cadmium from Aqueous Solutions by Oxidized and Ethylenediamine-Functionalized Multi-Walled Carbon Nanotubes. *Chem Eng J* **2010,** *157*, (1), 238-248.

16. Lu, C. Y.; Liu, C. T.; Su, F. S., Sorption Kinetics, Thermodynamics and Competition of Ni^{2+} from Aqueous Solutions onto Surface Oxidized Carbon Nanotubes. *Desalination* **2009,** *249*, (1), 18-23.

17. Vukovic, G. D.; Marinkovic, A. D.; Skapin, S. D.; Ristic, M. D.; Aleksic, R.; Peric-Grujic, A. A.; Uskokovic, P. S., Removal of Lead from Water by Amino Modified Multi-Walled Carbon Nanotubes. *Chem Eng J* **2011,** *173*, (3), 855-865.

18. Luo, C.; Wei, R. Y.; Guo, D.; Zhang, S. F.; Yan, S. Q., Adsorption Behavior of Mno_2 Functionalized Multi-Walled Carbon Nanotubes for the Removal of Cadmium from Aqueous Solutions. *Chem Eng J* **2013,** *225*, 406-415.

19. Cho, H. H.; Smith, B. A.; Wnuk, J. D.; Fairbrother, D. H.; Ball, W. P., Influence of Surface Oxides on the Adsorption of Naphthalene onto Multiwalled Carbon Nanotubes. *Environ Sci Technol* **2008,** *42*, (8), 2899-2905.

20. Kuo, C. Y., Water Purification of Removal Aqueous Copper (Ii) by as-Grown and Modified Multi-Walled Carbon Nanotubes. *Desalination* **2009,** *249*, (2), 781-785.

21. Gao, Z. M.; Bandosz, T. J.; Zhao, Z. B.; Han, M.; Qiu, J. S., Investigation of Factors Affecting Adsorption of Transition Metals on Oxidized Carbon Nanotubes. *J Hazard Mater* **2009,** *167*, (1-3), 357-365.

22. Diaz-Flores, P. E.; Lopez-Urias, F.; Terrones, M.; Rangel-Mendez, J. R., Simultaneous Adsorption of Cd^{2+} and Phenol on Modified N-Doped Carbon Nanotubes: Experimental and Dft Studies. *J Colloid Interf Sci* **2009,** *334*, (2), 124-131.

23. Hsieh, S. H.; Horng, J. J.; Tsai, C. K., Growth of Carbon Nanotube on Micro-Sized Al_2o_3 Particle and Its Application to Adsorption of Metal Ions. *J Mater Res* **2006,** *21*, (5), 1269-1273.

24. Ma, J. P.; Xiao, R. H.; Li, J. H.; Yu, J. B.; Zhang, Y. Q.; Chen, L. X., Determination of 16 Polycyclic Aromatic Hydrocarbons in Environmental Water Samples by Solid-Phase Extraction Using Multi-Walled Carbon Nanotubes as Adsorbent Coupled with Gas Chromatography-Mass Spectrometry. *J Chromatogr A* **2010,** *1217*, (34), 5462-5469.

25. Chen, G. C.; Shan, X. Q.; Wang, Y. S.; Pei, Z. G.; Shen, X. E.; Wen, B.; Owens, G., Effects of Copper, Lead, and Cadmium on the Sorption and Desorption of Atrazine onto and from Carbon Nanotubes. *Environ Sci Technol* **2008,** *42*, (22), 8297-8302.

26. Rao, G. P.; Lu, C.; Su, F., Sorption of Divalent Metal Ions from Aqueous Solution by Carbon Nanotubes: A Review. *Sep Purif Technol* **2007,** *58*, (1), 224-231.

27. Zhang, S. J.; Shao, T.; Bekaroglu, S. S. K.; Karanfil, T., The Impacts of Aggregation and Surface Chemistry of Carbon Nanotubes on the Adsorption of Synthetic Organic Compounds. *Environ Sci Technol* **2009,** *43*, (15), 5719-5725.

28. Zhang, X.; Kah, M.; Jonker, M. T. O.; Hofmann, T., Dispersion State and Humic Acids Concentration-Dependent Sorption of Pyrene to Carbon Nanotubes. *Environ Sci Technol* **2012,** *46*, (13), 7166-7173.

29. Honeyman, B. D.; Balistrieri, L. S.; Murray, J. W., Oceanic Trace Metal Scavenging: The Importance of Particle Concentration. *Deep-Sea Res.* **1988,** *35*, (2), 227 - 246.

30. Di Toro, D. M.; Mahony, J. D.; Kirchgraber, P. R.; O'byrne, A. L.; Pasquale, L. R.; Piccirilli, D. C., The Effects of Nonreversibiliy, Particle Concentration, and Ionic Strength on Heavy Metal Sorption. *Environmental Science and Technology* **1986,** *20*, (1), 55 - 61.

31. Mckinley, J. P.; Jenne, E. A., Experimental Investigation and Review of the "Solids Concentration" Effect in Adsorption Studies. *Environmental Science and Technology* **1991,** *25*, (12), 2082 - 2087.

32. Li, Y. H.; Burkhardt, L.; Buchholtz, M.; Ohara, P.; Santschi, P. H., Partition of Radiotracers between Suspended Particles and Seawater. *Geochimica Et Cosmochimica Acta* **1984,** *48*, (10), 2011-2019.

33. Gschwend, P. M.; Wu, S. C., On the Constancy of Sediment Water Partition-Coefficients of Hydrophobic Organic Pollutants. *Environ Sci Technol* **1985,** *19*, (1), 90-96.

34. Voice, T. C.; Rice, C. P.; Weber, W. J., Effect of Solids Concentration on the Sorptive Partitioning of Hydrophobic Pollutants in Aquatic Systems. *Environ Sci Technol* **1983,** *17*, (9), 513-518.

35. Voice, T. C.; Weber, W. J., Sorbent Concentration Effects in Liquid Solid Partitioning. *Environ Sci Technol* **1985,** *19*, (9), 789-796.

36. Higgo, J. J. W.; Rees, L. V. C., Adsorption of Actinides by Marine-Sediments - Effect of the Sediment Seawater Ratio on the Measured Distribution Ratio. *Environ Sci Technol* **1986,** *20*, (5), 483-490.

37. Chang, C. C. Y.; Davis, J. A.; Kuwabara, J. S., A Study of Metal-Ion Adsorption at Low Suspended-Solid Concentrations. *Estuar Coast Shelf S* **1987,** *24*, (3), 419-424.

38. Grover, R.; Hance, R. J., Effect of Ratio of Soil to Water on Adsorption of Linuron and Atrazine. *Soil Sci* **1970,** *109*, (2), 136-&.

39. Santschi, P. H., Factors Controlling the Biogeochemical Cycles of Trace-Elements in Fresh and Coastal Marine Waters as Revealed by Artificial Radioisotopes. *Limnol Oceanogr* **1988,** *33*, (4), 848-866.

40. Nyffeler, U. P.; Li, Y. H.; Santschi, P. H., A Kinetic Approach to Describe Trace-Element Distribution between Particles and Solution in Natural Aquatic Systems. *Geochimica Et Cosmochimica Acta* **1984,** *48*, (7), 1513-1522.

41. Avotins, P.; Jenne, E. A., Time Stability of Dissolved Mercury in Water Samples .2. Chemical Stabilization. *J Environ Qual* **1975,** *4*, (4), 515-519.

42. Hiura, H.; Ebbesen, T. W.; Tanigaki, K., Opening and Purification of Carbon Nanotubes in High Yields. *Advanced Materials* **1995,** *7*, (3), 275-276.

43. Smith, B.; Wepasnick, K.; Schrote, K. E.; Cho, H. H.; Ball, W. P.; Fairbrother, D. H., Influence of Surface Oxides on the Colloidal Stability of Multi-Walled Carbon Nanotubes: A Structure-Property Relationship. *Langmuir* **2009,** *25*, (17), 9767-9776.

44. Smith, B.; Wepasnick, K.; Schrote, K. E.; Bertele, A. H.; Ball, W. P.; O'melia, C.; Fairbrother, D. H., Colloidal Properties of Aqueous Suspensions of Acid-Treated, Multi-Walled Carbon Nanotubes. *Environ Sci Technol* **2009,** *43*, (3), 819-825.

45. Langley, L. A.; Fairbrother, D. H., Effect of Wet Chemical Treatments on the Distribution of Surface Oxides on Carbonaceous Materials. *Carbon* **2007,** *45*, (1), 47-54.

46. Langley, L. A.; Villanueva, D. E.; Fairbrother, D. H., Quantification of Surface Oxides on Carbonaceous Materials. *Chem Mater* **2006,** *18*, (1), 169-178.

47. Smith, B.; Yang, J.; Bitter, J. L.; Ball, W. P.; Fairbrother, D. H., Influence of Surface Oxygen on the Interactions of Carbon Nanotubes with Natural Organic Matter. *Environ Sci Technol* **2012,** *46*, (23), 12839-12847.

48. Haynes, W. M., Crc Handbook of Chemistry and Physics (92nd Edition). CRC Press: 2011.

49. Salam, M. A.; Al-Zhrani, G.; Kosa, S. A., Simultaneous Removal of Copper(Ii), Lead(Ii), Zinc(Ii) and Cadmium(Ii) from Aqueous Solutions by Multi-Walled Carbon Nanotubes. *Cr Chim* **2012,** *15*, (5), 398-408.

50. Ramana, D. K. V.; Yu, J. S.; Seshaiah, K., Silver Nanoparticles Deposited Multiwalled Carbon Nanotubes for Removal of Cu(Ii) and Cd(Ii) from Water: Surface, Kinetic, Equilibrium, and Thermal Adsorption Properties. *Chem Eng J* **2013,** *223*, 806-815.

51. Bohdziewicz, J.; Kaminska, G., Kinetics and Equilibrium of the Sorption of Bisphenol a by Carbon Nanotubes from Wastewater. *Water Science and Technology* **2013,** *68*, (6), 1306-1314.

52. Di Toro, D. M., A Particle Interaction Model of Reversible Organic Chemical Sorption. *Chemosphere* **1985,** *14*, (10), 1503 - 1538.

53. Di Toro, D. M.; Horzempa, L. M., Reversible and Resistant Components of Pcb Adsorption-Desorption. *Environmental Science and Technology* **1982,** *16*, (9), 594 - 602.

Chapter 3. Transport of Oxidized Multi-Walled Carbon Nanotubes through Silica Based Porous Media: Influences of Aquatic Chemistry, Surface Chemistry and Natural Organic Matter[1]

ABSTRACT

This chapter provides results from studies of the transport of oxidized multi-walled carbon nanotubes (O-MWCNTs) of varying surface oxygen concentrations under a range of aquatic conditions and through uniform silica glass bead media. In the presence of Na^+, the required ionic strength (IS) for maximum particle attachment efficiency (*i.e.*, the critical deposition concentration, or CDC) increased as the O-MWCNT's surface oxygen concentration or pH increased, following qualitative tenets of theories based on electrostatic interaction. In the presence of Ca^{2+}, CDC values were lower than those with Na^+ present, but were no longer sensitive to surface oxygen content, suggesting that Ca^{2+} impacts the interactions between O-MWCNTs and glass beads by mechanisms other than electrostatic alone. The presence of Suwannee River natural organic matter (SRNOM) decreased the attachment efficiency of O-MWCNTs in the presence of either Na^+ or Ca^{2+},

[1] This chapter has been published as Yang, J.; Bitter, J. L.; Smith, B. A.; Fairbrother, D. H.; Ball, W. P., Transport of Oxidized Multi-Walled Carbon Nanotubes through Silica Based Porous Media: Influences of Aquatic Chemistry, Surface Chemistry, and Natural Organic Matter. *Environ Sci Technol* **2013,** *47*, (24), 14034-14043. Julie L. Bitter and Billy A. Smith helped with the collection of preliminary data; D. Howard Fairbrother and William P. Ball helped with the data interpretation and editing.

but with more pronounced effects when Na^+ was present. Nevertheless, low concentrations of SRNOM (< 4 mg/L of dissolved organic carbon) were sufficient to mobilize all O-MWCNTs studied at $CaCl_2$ concentrations as high as10 mM. Overall, this study reveals that NOM content, pH and cation type have more importance than surface chemistry in affecting O-MWCNTs deposition during transport through silica-based porous media.

3.1 Introduction

Carbon nanotubes (CNTs), with their unique structure and properties,[1-5] have a widespread range of current and potential applications[6] and their production rates have steadily increased over the past decade.[7] Multi-walled CNTs (MWCNTs) cost less to produce and are sold in much greater quantities than single-walled CNTs (SWCNTs),[7] with correspondingly higher potential for environmental release. Although pathways for release have not yet been well established,[8-10] it is reasonable to assume that aqueous contamination may occur as the result of direct emissions to air or water through spills or misuse and also perhaps following long-term degradation of the commercial materials into which CNTs are embedded.[8-10] MWCNT surfaces are often oxidized during production to increase their stability in polar solvents such as water or polar solvents used with some polymeric resins,[11-16] or to improve their properties for use as drug delivery agents.[17] Surface oxides can also be introduced onto MWCNTs inadvertently during purification with acids or through exposure to UV radiation, reactive radicals, and/or ozone.[18-20] The existence of such oxides on MWCNT surfaces have been shown to dramatically influence environmentally relevant properties, such as homo-aggregation and sorption, in aquatic environments.[21-23]

To better understand MWCNT transport in groundwater or engineered processes of filtration it is useful to consider well-studied physical and chemical principles of colloid transport through porous media.[24-46] Chemical interactions between suspended particles and environmental collectors include London-van der Waals forces, electrostatic interactions, hydration forces, and steric interactions[24-36, 38-41] as well as some specific short-range interactions, such as the so-called "bridging" effects of Ca^{2+} with carboxylic groups.[42-46] All of these interactions are intimately dependent on surface and solution chemistry and have been extensively studied in prior work.[44-50] In prior studies of particle retention in porous media, researchers have found it useful to separately consider the case of "clean bed filtration" in which particle interactions with the solid media ("collectors") are studied under conditions where (1) the volume of particles (colloids) removed is low enough that collector surfaces have been negligibly covered, and (2) substantial amounts of straining are avoided. Here, we follow numerous others by defining straining as the "trapping of colloids in pore throats that are too small to allow their passage".[51] The avoidance of substantial amounts of straining helps to ensure depth filtration and is important for experimental studies where the goal is to isolate and understand the relative roles of single collector contact efficiency η_0 and attachment efficiency, α, as separate components of a first-order deposition rate coefficient, k_d that has been traditionally formulated in terms of the product $\alpha\eta_0$ and other coefficients that are constant for a given pore water velocity and porous media type.[24, 25, 38] In such a formulation, η_0 represents the fraction of approaching particles that can theoretically result in collision (due to interception, sedimentation and diffusion) and α represents the number of actual colloid-collector attachments that occur for a given number of collision opportunities).

Given the unique structure of MWCNTs, especially their small diameters, high aspect ratios, and varied surface chemistry, it is difficult to estimate η_0 from theory or to extrapolate its value from previous studies with other materials. Within this context, and to the best of our knowledge, no prior studies have specifically addressed the issue of surface oxygen and water chemistry impacts on deposition rate coefficients and attachment efficiencies during O-MWCNT transport through clean beds. In the study reported herein we focus on this issue through the estimation of attachment efficiencies between the glass surfaces of spherical filter "collectors" and the surfaces of individual O-MWCNTs of varying surface composition. Estimation on attachment efficiency is made possible through well-controlled conditions of transport under conditions that were designed to ensure so-called "clean bed filtration," where first-order irreversible removal rates apply for the majority of the observed fractional removal, as independently verified through spatial retention profiles and model simulation.

Although several prior studies have investigated CNT transport through porous media, most studies to date have been conducted with natural soil or quartz sand systems and none have quantified attachment efficiency as a function of both surface and solution chemistry. Moreover, given that size heterogeneity and surface roughness of the porous media tend to enhance straining,[51] it is not surprising that most prior work has been influenced by straining effects. For example, in their studies of the transport of oxidized SWCNTs through quartz sand as a function of ionic strength (IS), Jaisi *et al.*[52, 53] found that O-SWCNT transport followed predictions of conventional deposition theory under most conditions for quartz sand[52] but that straining was the primary means of O-SWCNT deposition with soils under all conditions[53]. In their study of functionalized MWCNT

tube-length effects on transport through quartz sand, Wang *et al.* [54] also reported that that straining played an important role – these investigators observed spatial retention profiles that deviated substantially from expectations based on simple first-order removal and attachment efficiencies could not be estimated. Other researchers have investigated the impact of CNT tube diameter[55] and flow velocity[56] on transport through quartz sand (and glass beads for flow velocity test) but these studies also did not focus on quantifying attachment efficiency.

Prior studies of solution chemistry effects on O-MWCNT surface properties in water have primarily focused on homo-aggregation (see Chen *et al.* for a review[57]), with relatively few studies conducted in transport systems. The prior homo-aggregation work has revealed a major impact of pH and ionic strength that is qualitatively consistent with DLVO theory[21, 58] as well as some important effects of calcium and natural organic matter (NOM). The effect of surface chemistry on the homo-aggregation of O-MWCNTs has also been studied.[21, 42] For example, Hyung *et al.*[59] reported that for any given mass of added MWCNT powder, the concentration of well-dispersed MWCNTs in solution increased systematically with concentration of Suwannee River natural organic matter (SRNOM). Prior work in our own laboratory[42] has revealed that NOM concentrations as low as 0.5 mg of dissolved organic carbon (DOC) /L can significantly enhance the stability of O-MWCNT dispersions and that these effects occur even in the presence of Ca^{2+} and in a manner largely independent of O-MWCNT surface oxygen concentration. Although the effect of aquatic chemistry and surface chemistry on CNT homo-aggregation has been widely reported,[25, 41, 42, 47, 48, 60-64] such effects on CNT attachment to other media during transport have been less well studied. Wang *et al.*[64] passed NOM-

stabilized MWCNT and SWCNT dispersions through sand packed columns at varied KCl and $CaCl_2$ concentrations and observed that substantial mass fractions CNTs passed through the column at KCl concentrations up to 1 mM and $CaCl_2$ up to 0.1 mM. Jaisi *et al.*[52] have reported that NOM presence can substantially decrease rates of SWCNT deposition onto quartz sand in the presence Ca^{2+}. Yi *et al.*[43] have studied deposition of MWCNTs with two different surface oxygen concentrations on quartz crystals, but did not study transport through packed columns.

In the study reported herein, we focused on quantifying the impacts of surface and solution chemistry on O-MWCNT attachment efficiency with amorphous silica surfaces during transport through porous media. It is noteworthy that our own focus was on *relative* alpha values as a reflection of the effects of aquatic chemistry and O-MWCNT surface chemistry, for a *consistently reproducible* media surface. In order to accurately measure attachment efficiencies in the absence of substantial straining effects, we used a well-defined system of uniformly sized spherical collectors and, to ensure "clean-bed" filtration conditions, we used very small input masses of CNTs. To enhance experimental reproducibility, we used rigorous and standardized methods of media cleaning. Studies were conducted on O-MWCNTs with five different oxygen contents in varied solution chemistry. Solution chemistry variables included ionic strength, pH, type of cations in the feed solution (sodium or calcium), and concentration of SRNOM.

3.2 Experimental Methods

3.2.1 *Surface Oxidation of MWCNTs*

Non-functionalized MWCNTs with diameters of 15 ± 5 nm and lengths of 1 - 5 μm were purchased from NanoLabs, Inc., who report 95% carbon purity with < 5% metal

content according to thermo-gravimetric analysis. (Such non-modified MWCNTs have sometimes been referred to as "pristine" MWCNTs in prior literature.) Oxidized MWCNTs (O-MWCNTs) were then prepared by refluxing the purchased materials in various acids using methods that have been described in detail elsewhere.[21] In our research, the conditions used were refluxing in HNO_3-water solutions at three different w/w concentrations (15%, 18%, and 53%) at 140 ºC for 1.5 h and refluxing in a 3:1 mixture of concentrated sulfuric and nitric acids at 70 ºC for 8 h.[21] We were thus able to create four O-MWCNT materials with different concentrations of oxygen-containing functional groups grafted onto the MWCNT surface. The resulting O-MWCNTs were subjected to an additional base purification process described elsewhere[65] to help remove amorphous carbon on the surface of the O-MWCNTs.

3.2.2 *Characterization of O-MWCNTs*

The length distribution of O-MWCNTs created by the methods described above has been characterized and reported in prior publications from our laboratory.[21, 66] Results showed that the length distribution of O-MWCNTs were independent of the O-MWCNTs' surface oxygen concentration.[21, 66] The total oxygen concentrations and distributions of oxygen functional groups present on the surfaces of the specific O-MWCNTs used in this work were determined using X-ray photoelectron spectroscopy (XPS) (PHI 5400 system) in conjunction with chemical derivatization methods for quantification of functional group concentrations.[67, 68] **Table 3.1** shows the total atomic oxygen concentrations of the studied O-MWCNTs (reported as % of XPS-accessed surface atoms). For the majority of the O-MWCNTs used, the percentages of surface oxygen atoms associated with different functional groups are also shown, as calculated

by the method of Wepasnick *et al.*[69] The total surface oxygen measured for O-MWCNTs treated with 15% HNO_3, 18% HNO_3, and 53% HNO_3 were 3.1%, 5.1%, and 7.1%, respectively; O-MWCNTs treated using a 3:1 mixture of concentrated H_2SO_4 and HNO_3 had the highest concentration at 11.5%. For the materials oxidized at JHU, concentrations of the carboxylate functional group (COO^-) also increased monotonically with % oxygen (**Table 3.1**). In addition to O-MWCNTs prepared at JHU, we also studied MWCNTs that had been oxidized (using 3:1 H_2SO_4 and HNO_3) by the commercial supplier (NanoLabs, Inc.). The purchased O-MWCNTs were also washed before use, using the previously described cleaning procedure to help reduce amorphous carbon.[65] The purchased O-MWCNTs exhibit total surface atomic concentration of 8.3%.

Table 3.1. Surface oxygen concentrations and oxide distribution of O-MWCNTs

Treatment method	O_T%	O_{COOH}%	$O_{C=O}$%	O_{OH}%	O_{others}%
10% HNO_3	3.0	1.5	0.6	0.8	0.1
18% HNO_3	5.1	2.0	2.9	0.6	-0.5
53% HNO_3	7.1	2.8	1.1	0.7	2.6
3:1 concentrated H_2SO_4/HNO_3	11.5	3.3	1.3	1.5	5.4
Purchased from Nanolab [a]	8.3	3.8	1.2	0.6	2.7

[a] O-MWCNTs purchased from Nanolab were thoroughly cleaned using the same acid-base cleaning procedure previously developed and used in our laboratory. See Smith *et al.* for details.[42]

3.2.3 *Preparation of O-MWCNT Dispersion*

Suspensions of well-dispersed O-MWCNTs were prepared by adding a small amount of MWCNTs (~ 4 mg) to 200 mL of de-ionized (DI) water and sonicating at low energy (70 W, Branson 1510) for 20 hours. For MWCNTs that had low surface oxygen concentrations (*i.e.*, $\leq$ 5.1%), it was necessary to increase the pH to above 9 to maintain a stable stock suspension. After sonication, the suspension was centrifuged at 1000 rpm for 5 minutes to remove any bundled O-MWCNTs that were not taken up into suspension.

The centrifugation also removed glass particles etched from the wall of the flask during sonication. The centrifuged suspension was then transferred to a clean glass bottle and sonicated for another 5 min to further disperse any bundled O-MWCNTs that may have remained after the prior steps.

The hydrodynamic diameters of the O-MWCNTs in our prepared stock solutions (as measured by Dynamic Light Scattering, DLS) were roughly 140 nm, which is quantitatively similar to the 150 ± 40 nm values observed by Smith *et al.*[21] who studied similarly prepared samples using both DLS and TEM and AFM analysis. These authors conducted their TEM analyses on samples that were carefully prepared by placing a drop of their dilute dispersed MWCNT water suspension on a holey-carbon TEM grid. Results were taken as evidence for the existence of individually dispersed nanoparticles in solution.[21] Prior to use in transport experiments, these well-dispersed stock suspensions were further diluted with DI water to a concentration of ~2.0 mg/L and adjusted to the designated pH of the transport experiment using either NaOH (for pH 10) or HCl (for pH 4). The final O-MWCNT concentration in a given suspension was determined by measuring its UV-Vis absorbance at 270 nm. Control studies showed good linear relationships ($R^2 > 0.998$) between absorbance at 270 nm and mass concentrations for the O-MWCNTs used this study – see **Table 3.2**. Our previous studies have shown that this approach creates a suite of O-MWCNTs which exhibit similar physical properties (*e.g.*, lengths, effective hydrodynamic diameters in solution) but different surface chemistry.[42, 70, 71]

Table 3.2. Linear regression parameters (extinction coefficients and R^2 values) of calibration curves for O-MWCNT dispersions using UV-Vis spectroscopy at 270 nm and 800 nm.

Total oxygen concentration of O-MWCNT, %	λa = 270 nm		λ = 800 nm	
	εb $L \cdot mol^{-1} \cdot cm^{-1}$	R^2	εb $L \cdot mol^{-1} \cdot cm^{-1}$	R^2
3.0	0.065	0.998	N/A	N/A
5.1	0.116	0.999	0.034	0.998
7.1	0.072	0.998	0.021	0.999
8.3	0.098	0.999	0.031	0.998
11.5	0.074	0.999	N/A	N/A

a. λ is the wavelength used in detecting MWCNT dispersion absorbance with UV-Vis.
b. ε is the extinction coefficient of MWCNT at corresponding wavelengths based on Beer's law.

3.2.4 *Preparation of Suwannee River Natural Organic Matter (SRNOM)*

SRNOM was purchased from the International Humic Substances Society. After dissolution into DI water the SRNOM was passed through a 0.22 μm polyethersulfone filter (EMD Millipore Corporation). The filtered stock solution was analyzed for total organic carbon content (Dohrmann 8000). This stock solution was subsequently diluted for calibration of DOC against UV absorbance at 254 nm and for preparation of various column feed solutions containing SRNOM concentrations between 0 and 4.1 mg DOC/L.

3.2.5 *Preparation of Glass Beads*

Soda lime glass spheres (0.355 - 0.425 mm, MO-SCI Corporation) were used as model collectors in transport experiments. Preliminary work showed that it was not possible to obtain consistent and accurate results unless the glass beads were pre-treated by a standardized process that involved multiple well-defined sonication steps, including not only the initial treatment (prior to drying for later use) but also again under more rigorous conditions immediately prior to use.

The initial preparation of glass beads involved sonication in mild base (0.1 M NaOH) for 20 minutes (for removal of anionic organic polymers), decantation, sonication in acid (1 M HNO_3) for 20 minutes (for removal of acid-soluble metal oxides), decantation, and final rinse with DI water until the resistance of the supernatant was higher than 0.5 MΩ. Beads were then dried at 70 ºC and stored under dry conditions until use.[72] This initial preparation of glass beads is referred to as "initial cleaning procedure" hereafter. For the studies presented in this manuscript, all columns were prepared using a wet-pack approach for which the beads were also subjected to a second cleaning step immediately prior to packing. To prepare a column, fixed and precisely measured quantities of initially cleaned beads (39.5 g for short columns (5.2 cm) and 79.5 g for long columns (10.2 cm)) were weighed out and again sonicated in the base and acid solutions described above for 20 minutes each, followed by sonication in DI water in 5 minute cycles no less than 12 times. After treatment the beads were kept saturated at all times before and during the column packing process.

This second cleaning step and a wet-pack approach were found to be necessary to achieve reproducible results in O-MWCNT transport experiments. Preliminary work showed that if these additional preparation steps were not taken, the observed results were many times less precise than the experiments reported in our paper. Such imprecision was evident as pronounced variability in either (1) plateau heights for experiments with "step-change" in CNT input concentrations (*i.e.*, those using a heavy-side function for input concentration); or (2) mass recoveries for experiments with pulse inputs of O-MWCNTs (*i.e.*, those using a dirac function for input concentration). We speculatively attribute such variability to the presence of varying amounts of fine

particulate material (silica and minor metal oxide particulates) and/or fine bubbles of air on the glass bead surfaces. This speculation has been at least qualitatively confirmed by Energy Dispersive X-ray (EDX) analysis of particles observed in the wash (rinse) water following sonication of the pre-treated glass beads. These analyses were conducted by Dr. Ken Livi (Director of the High-Resolution Analytical Electron Microbeam Facility of the Integrated Imaging Center at Johns Hopkins University) using a Philips CM 300 field emission gun TEM operating at 297 kV. Images were collected using a CCD camera mounted on a GIF 200 electron energy loss spectrometer. Samples chosen for imaging included both the uncentrifuged wash water and, for purposes of evaluating the potential influence of vacuum-induced precipitates, supernatant of the same water following centrifugation. (No evidence for such a confounding influence was observed.)

Figure 3.1 is an example image from the TEM analysis, showing some selected particles for EDX evaluation. Particles chosen for evaluation were based on visual clues of common morphology, with focus on those samples that dominated the fields of view. The image shown in **Figure 3.1** and other TEM images revealed that materials separated from the glass beads surface during the sonication process consisted primarily of silicon dioxide with variable amounts of Ca, Mg, and Na, together with lower quantities of other materials, primarily comprising magnesium silicates, and iron and lead oxides. With the exception of the lead, these materials were all expected based on the composition of the soda-lime glass beads that had been reported by the supplier (MO-SCI Corporation): 65~75% SiO_2, 0~5% Al_2O_3, 6~15% CaO, 1~5% MgO, 10~20% Na_2O and < 0.8% Fe_2O_3.) It is unclear whether the non-silica particles originated from either (a) dissolution

of surface impurities followed by re-precipitation upon drying or (b) dislodgement or

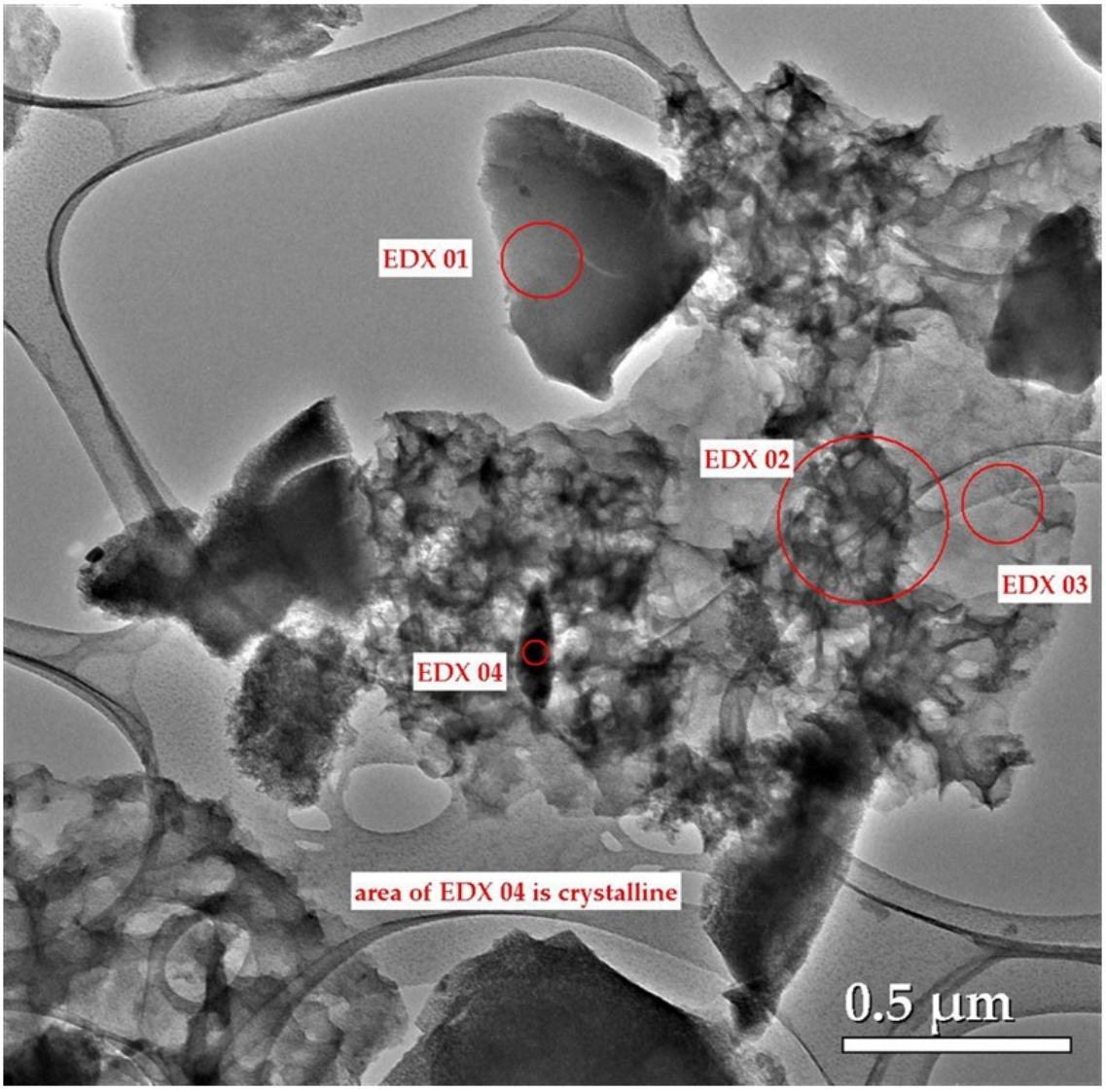

Figure 3.1. TEM image of unprocessed wash water from sonication of glass beads in DI water for one hour. EDX 01 is silica glass (similar to the expected glass bead composition). EDX 02 and 03 are poorly crystalline or amorphous magnesium silicate sheets, and EDX 04 is crystalline iron oxide. Particles similar to EDX 01 represented the majority of the material observed in the TEM images.

"breaking off" of small attached particles from the "as-received" glass beads. It is also unclear as whether the quantities of such impurities on the glass surfaces were fully eliminated by cleaning or whether they were merely "standardized" by the process. As noted in the primary manuscript, however, this cleaning treatment is known to have

contributed substantially to improvements in experimental reproducibility and, as also noted in the manuscript, achieving such reproducibility was our primary aim. In particular, we sought to create a reproducible media surface such that the *relative* alpha values among the various experimental runs could be safely interpreted as a reflection of only the effects of aquatic chemistry and O-MWCNT surface chemistry.

3.2.6 *Preliminary Study of Cleaning Effects on Reproducibility*

The selection of the final bead cleaning approach described above was based on comparative results of transport experiments conducted with 7.1% O-MWCNTs and using six different cleaning procedures for the glass beads. The six different cleaning procedures are described in the caption to **Figure 3.2**. For all six methods, the glass beads had been subjected previously to the initial cleaning and drying procedure described in the prior section prior to the final cleaning and wet packing of beds. **Table 3.3** and **Figure 3.2** show the attachment efficiencies obtained from these experiments, which were conducted under identical aquatic conditions and flow velocities. The results show that both base/acid wash and subsequent water wash were imperative to obtain reproducible results, and that a more diluted NaOH solution was not able to clean the beads as effectively as the more concentrated solution. As shown in **Figure 3.2** and **Table 3.3**, results obtained using procedure 1, where no further treatment of glass beads had been performed after initial cleaning, were comparatively irreproducible. In particular, the results obtained under these less rigorous cleaning conditions suggested an average α value of approximately 0.36 which was relatively high in comparison to that finally obtained with more reproducible methods ($\alpha = 0.15$) and with a comparatively

high uncertainty (±0.06). Similarly high α values with large uncertainties (0.38 ± 0.06, 0.36 ± 0.12) were obtained when glass beads were treated by Method 2 (sonication in

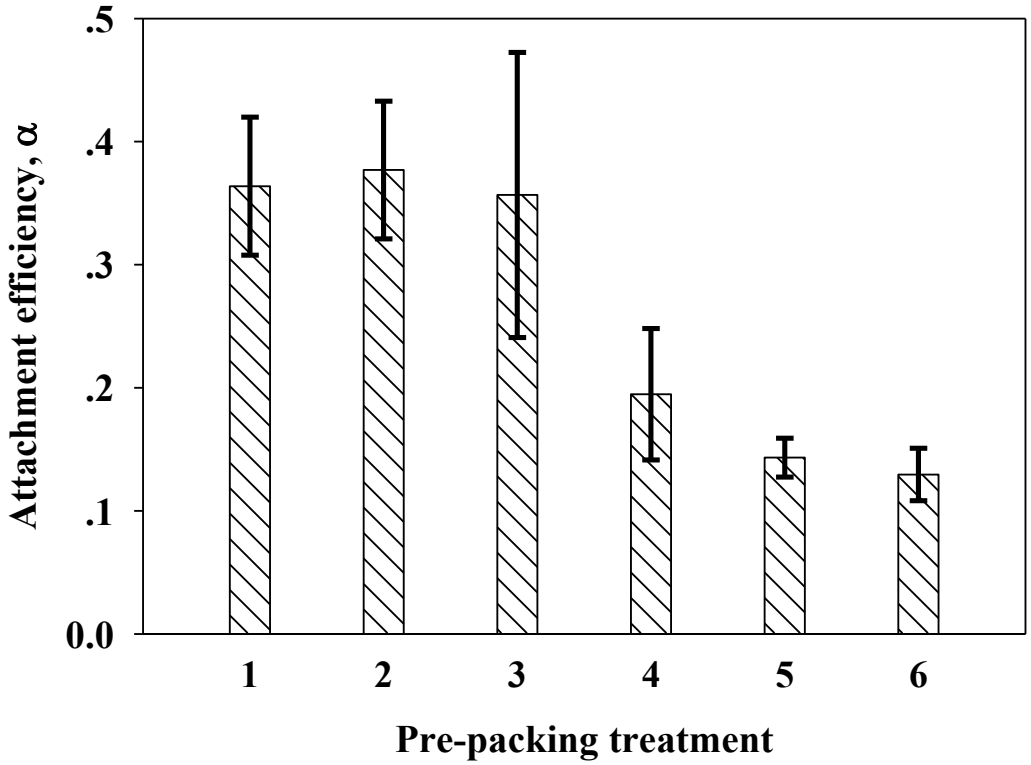

Figure 3.2. Effect of pre-packing treatment for glass beads on the magnitude and precision of attachment efficiency. Results shown were obtained from 7.1% O-MWCNT break through experiments conducted under the same experimental condition (column length = 10.2 cm, IS = 10.0 mM, pH = 5.8 ± 0.2). The treatment methods used were as followed: (1) no treatment before packing; (2) sonication in water for 60 min; (3) sonication in 0.01 M NaOH for 20 min, and then 1.0 M HNO_3 for 20min; (4) sonication in 0.1 M NaOH for 20 min, and then 1.0 M HNO_3 for 20 min; (5) sonication in 0.1 M NaOH for 20 min, 1.0 M HNO_3 for 20 min; and then water for 60 min; (6) sonication in 0.1 M NaOH for 20 min, 1.0 M HNO_3 for 20 min; 0.1 M NaOH again for 20 min, 1.0 M HNO_3 again for 20 min; and then water for 60 min.

water for 60 min) or Method 3 (sonication in a more dilute base solution of 0.01 M NaOH). The obtained α values decreased when sonication was in a more concentrated base solution (0.1 M NaOH) (Method 4), but this method still had a relatively high

uncertainty (0.19 ± 0.05) in comparison to methods 5 and 6, which were found to yield statistically equivalent results and with similarly small standard deviation (0.14 ± 0.02 and 0.13 ± 0.02, respectively). Both of these methods included a final sonication treatment in DI water and Method 6 also included a second sonication in base solution prior to the final DI treatment. The more aggressive treatment of method 6 was deemed to be unjustified based on the similarity of results with Method 5, which was selected and applied for routine use in this study.

Table 3.3. Attachment efficiencies of O-MWCNT transport through glass beads treated with different cleaning procedures.

Treatment Method [a] for Glass Beads	Replicates		
	1	2	3
1	0.47	0.33	0.29
2	0.31	0.49	0.34
3	0.59	0.25	0.23
4	0.24	0.09	0.26
5	0.13	0.17	0.12
6	0.15	0.11	

[a] Treatment methods used are in addition to the "initial cleaning procedure" described in the SI text and are identified as follows:
(1) no additional treatment before packing;
(2) sonication in water for 60 min;
(3) sonication in 0.01 M NaOH for 20 min, and then 1.0 M HNO_3 for 20min;
(4) sonication in 0.1 M NaOH for 20 min, and then 1.0 M HNO_3 for 20 min;
(5) sonication in 0.1 M NaOH for 20 min, 1.0 M HNO_3 for 20 min; and then water for 60 min;
(6) sonication in 0.1 M NaOH for 20 min, 1.0 M HNO_3 for 20 min; 0.1 M NaOH again for 20 min, 1.0 M HNO_3 again for 20 min; and then water for 60 min.

3.2.7 *Wet Packing of the Columns*

Final column packing and preparation of the columns was by means of a wet-pack method that was designed to avoid introducing air bubbles into the porous media. To build a column, the initial step was to vertically mount the column shell (a hollow quartz-walled cylinder of 25 mm inner diameter, 28 mm outer diameter and 100 or 150 mm

length), onto a stand. A silicone stopper (into which a length of silicone tubing had been previously inserted through its center) was then attached to the bottom of cylinder. The silicone tubing was clamped shut below the stopper, and the column was then filled with DI water. After expelling all of the air bubbles from the tubing and the exposed upper edge of the stopper by draining and pipetting, a water-saturated stainless steel mesh screen was dropped onto the stopper to ensure that all of the beads remained within the column. The previously hydrated and sonicated glass beads were then slowly added into the cylinder through the open top, making sure that the water level was always higher

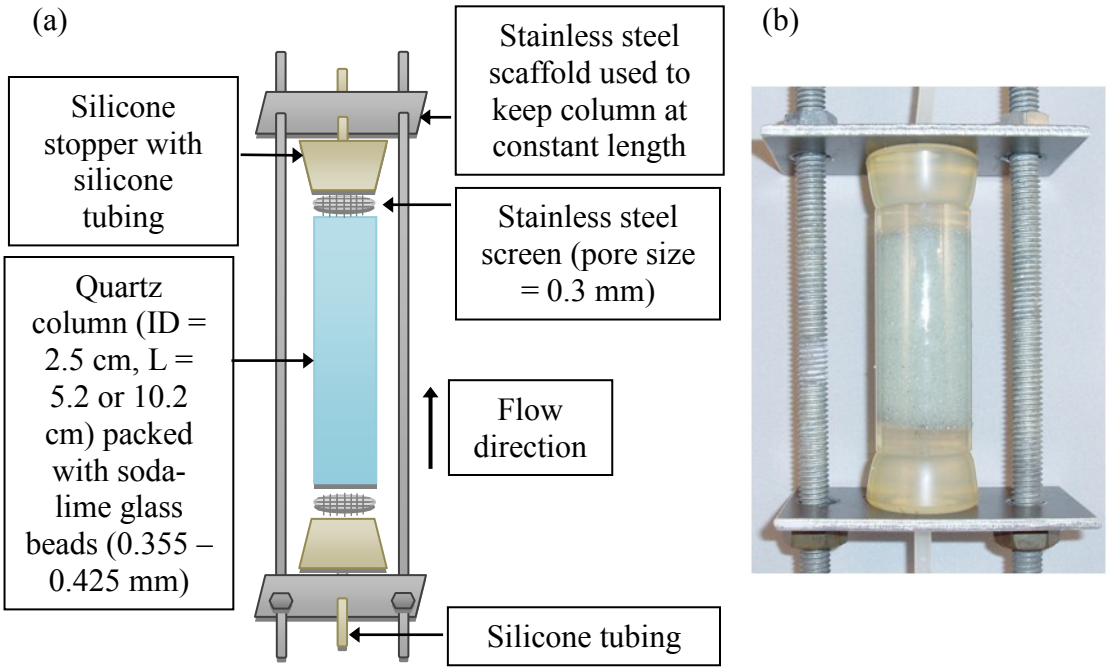

Figure 3.3. The schematic (a) and picture (b) of the packed-bed columns used in this study.

than the level of glass beads. During the filling process, the column was frequently tapped to ensure tight packing of the glass beads. Once the column had been filled with beads it was sealed at the top with another stainless steel screen and another silicone stopper with pre-inserted silicone tubing. A steel template/scaffold was used to ensure

that the length of the column remained exactly the same among all of the short or long columns used, with the lengths set to ensure that the porosity of the column was constant at 0.38, as calculated from the known volume of beads and inner diameter of the column. The pore volume of the packed columns was thus maintained at 9.73 cm^3 for short (5.2 cm) columns and 18.67 cm^3 for long (10.2 cm) columns. A schematic of the columns is provided as **Figure 3.3**.

3.2.8 *Transport Experiments*

A dual-pump system was used for transport experiments (**Figure 3.4**). Two feed solutions, one containing DI water ("DI line") and the other containing a sodium chloride or calcium chloride background electrolyte solution ("electrolyte line") were used. For most experiments these solutions were equilibrated with the ambient atmosphere without further pH adjustment (pH = 5.8 ± 0.2), although some solutions were adjusted with

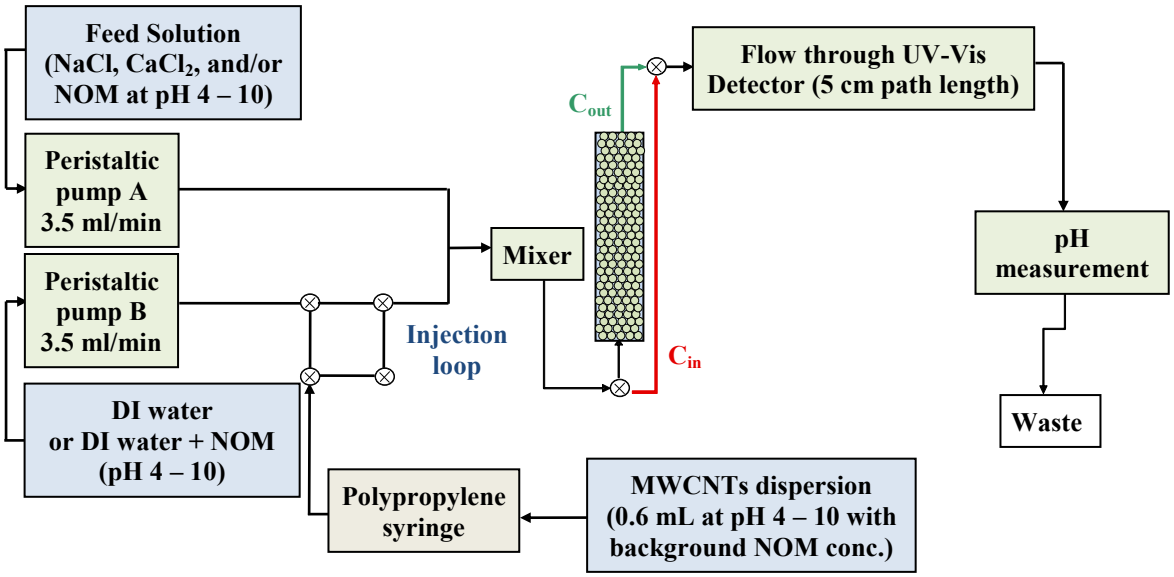

Figure 3.4. Dual-pump column filtration system with in-line mixer, column, and UV-Vis detection source for pulse-input method.

addition of 1.0 M HCl or 1.0 M NaOH to represent acidic (pH = 4.0 ± 0.2) or basic (pH = 10.0 ± 0.2) conditions, respectively. Buffers were avoided to eliminate their possible effects on O-MWCNT attachment efficiency. DI and electrolyte solutions were pumped at constant flow rate (each at 3.5 mL/min) by two peristaltic pumps operating in parallel. Immediately prior to the column inlet, these lines were combined in a custom-built Teflon® in-line mixing chamber of <1 mL internal volume that contains a tiny Teflon coated stir bar. Before each experiment, the column was conditioned first with DI water and then with background electrolyte, each for > 20 pore volumes. For experiments involving NOM both DI and electrolyte lines included a predetermined concentration of SRNOM.

To introduce O-MWCNTs into the feed solution we used a pulse-input approach. Relative to a step feed, pulse-inputs use a much smaller total mass of O-MWCNT particles so that conditions of clean bed filtration can be more easily maintained. During the pulse-input experiment a 0.6 mL pulse of O-MWCNT dispersion at a concentration of ~2.0 mg/L was injected into the DI line through an injection loop (**Figure 3.4**). The injection loop approach eliminates unwanted pressure spikes that can sometimes occur with syringe injections. O-MWCNT dispersions at the appropriate pH and NOM concentrations were then added into the DI line (as opposed to the electrolyte line) to minimize any aggregation or deposition prior to entering the column. Mixing of the DI and electrolyte lines occurred immediately prior to solution upflow through the column. For selected columns, separate runs were conducted using pulses of sodium nitrate for an independent measurement of a column's residence time distribution and hydraulic dispersivity.

To measure O-MWCNT concentrations in the column effluent, UV absorbance (at λ = 270 nm for O-MWCNTs and 302 nm for $NaNO_3$ tracer) was measured in real time as the effluent passed through a 5-cm path-length flow-through quartz cell (Starna Cells, Inc.) as shown in **Figure 3.4**. The advantage of the long-path-length cuvette (internal

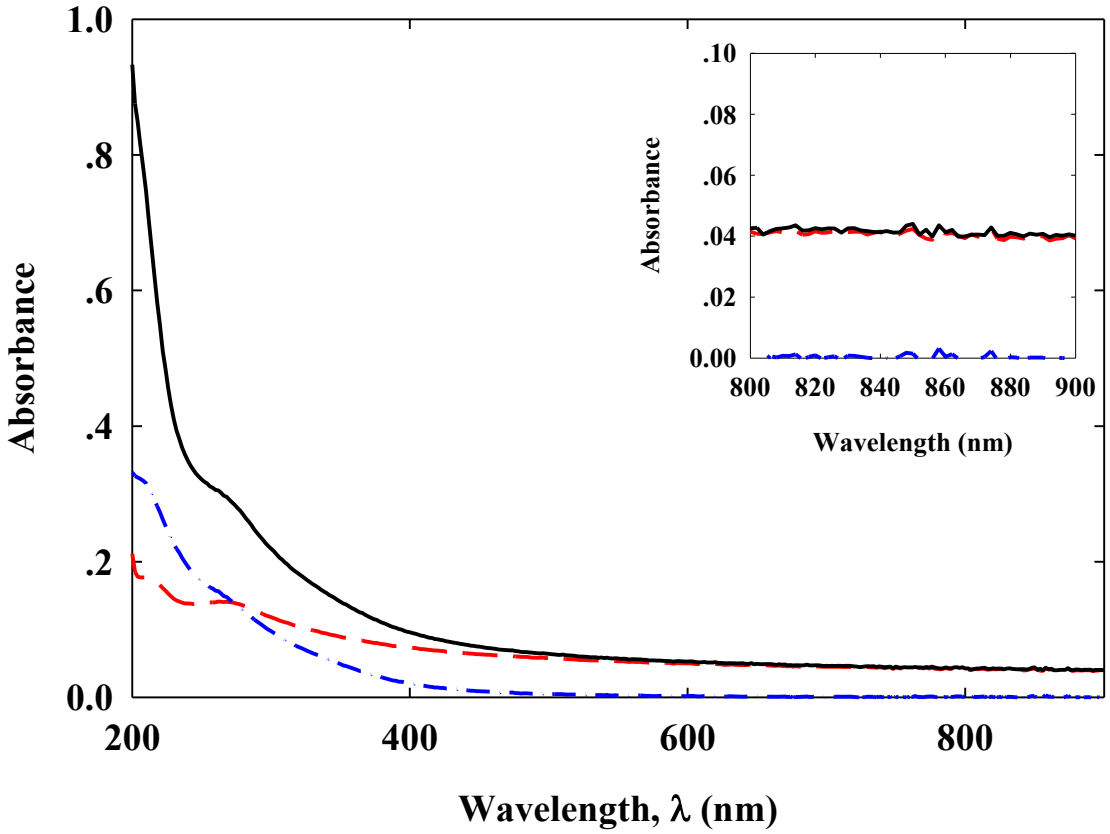

Figure 3.5. UV-Vis spectra of solutions containing 2.0 mg/L O-MWCNTs in water (red dashed line), 4.2 mg DOC/L NOM (blue dash-dot line) and 2.0 mg/L O-MWCNTs plus 4.2 mg DOC/L NOM (solid black line). The inset shows the region between 800-900 nm where NOM does not has absorption. Most results in experiments were obtained at λ = 270 nm (with subtraction of the background absorption due to NOM). However, comparisons of results were also made at λ = 800 nm where there is no interference from NOM.

volume ≈ 1.2 mL) is that O-MWCNT concentration can be more accurately measured at lower and more environmentally relevant concentrations (< 0.25 ppb). For experiments involving SRNOM, effluent concentrations of O-MWCNTs were quantified by

measuring absorption at 270 nm with subtraction of the constant background absorbance of NOM at this wavelength. O-MWCNT concentration values in these experiments were also verified using absorbance at 800 nm, where SRNOM does not absorb (**Figure 3.5**). Absorbance at 270 nm was used for subsequent calculation due to the higher sensitivity of UV response to concentration changes at this wavelength. The pH of the effluent was also closely monitored (Accumet Engineering Corp.) in all column experiments to ensure that it remained constant.

Prior to each O-MWCNT transport experiment, two preliminary control runs were conducted using the same initial mass of injected O-MWCNTs. The first of these control tests involved a "bypass" run (*i.e.*, at the designated IS but with all flow bypassing the column; **Figure 3.4**) in order to independently verify the injected mass. The mass estimates from these bypass runs were used to represent injected mass in subsequent data analysis. This mass was also used to calculate the "characteristic" concentration (C_0) for

Table 3.4. Deposition rate coefficients and mass balance obtained from columns conducted at selected background electrolyte concentrations

Background electrolyte concentrations, NaCl (mM)	**k_d (s^{-1})***		**Percentage recovery (%)**	
	Method 1	**Method 2**	**DI-pulse**	**Pulse in the presence of background electrolyte**
7	0.0013	0.0011	103.4	91.2
20	0.0094	0.0089	102.1	66.2
50	0.013	0.011	103.1	48.7
150	0.023	0.022	101.4	32.6
500	0.023	0.024	105.1	29.0

*k_d for a specific transport experiment was obtained by fitting the breakthrough curve using equation 2 (method 1) or by analyzing the percentage recovery of the breakthrough curve using equation 3.

normalization of column effluent concentrations. The second control test involved the removal of all electrolytes from the feed lines in order to confirm that the measured mass

recovered during DI water transport was reproducible and similar to that measured by the accompanying column bypass experiment. Mass recovery relative to by-pass was excellent (100% ± 5%;**Table 3.4**), thus confirming that we could reproducibly measure $\alpha = 0$ under conditions unfavorable to attachment.

3.2.9 *Quantitative Analysis of Column Effluent Data*

As confirmed through subsequent experiments conducted using step inputs and evaluation of spatial distributions of O-MWCNTs in our columns as described in **Chapter 5**, our transport experiments were characterized by good penetration of O-MWCNTs through-out the column depth. Although detailed numerical evaluation of the spatial concentration data is beyond the scope of the present chapter (and the subject of on-going analysis), our preliminary results are sufficient to show that the majority of CNT removal can be well-characterized by irreversible first-order removal – see **Chapter 5** for details.

With the above as justification and also given good fits of model simulations to observed O-MWCNT concentration data (further described in **Chapter 5**), our quantitative interpretation of transport results was based on an assumption of first-order irreversible deposition, as appropriate for clean-bed filtration in the absence of straining. More specifically, we applied the following one dimensional advection-dispersion equation [73] toward the estimation of k_d, a first-order coefficient for irreversible loss of O-MWCNTs during transport:

$$\frac{\partial C(x,t)}{\partial t} = D\frac{\partial^2 C(x,t)}{\partial x^2} - v_P\frac{\partial C(x,t)}{\partial x} - k_d C(x,t) \qquad \textbf{Eq. 3.1}$$

where $C(x, t)$ [M/L^3] is aqueous O-MWCNT concentration at position x within the column [L] and time t [T], D is the hydrodynamic dispersion coefficient [L^2/T]; v_p is the pore water velocity in the x direction [L/T], and k_d is the deposition rate coefficient [T^{-1}] for irreversible first-order loss from the pore water. The solution of **Eq. 3.1** for a column with fixed length is:[53]

$$C(t) = C_0 \tau \frac{L}{2\sqrt{\pi t^3 D}} \exp(-k_d t) \exp\left[\frac{(L - v_p t)^2}{4Dt}\right] \qquad \textbf{Eq. 3.2}$$

where C_0 is a characteristic concentration defined as M_0/V_{pore}, [M/L^3], M_0 is the mass recovery from the bypass experiment [M], V_{pore} is the aqueous pore volume within the column [L^3], τ is the mean hydraulic retention time ($\tau = V_{pore}/Q$, [T], where Q is the volumetric flow rate of the feed solution [L^3/T]), and L is the column length [L]. For a pulse-input method k_d can be calculated from the fraction of O-MWCNTs that are recovered, as follows:

$$k_d = -\frac{1}{\tau} \ln\left(\frac{Q}{M_0} \int_0^\infty C(t)\, dt\right) \qquad \textbf{Eq. 3.3}$$

The deposition rate coefficient, k_d, reaches a constant maximum value, $k_{d,fast}$, at high IS. We estimate this value from experiments conducted at the highest IS. The attachment efficiency α for all other runs can then be calculated using **Eq. 3.4**:

$$\alpha = \frac{k_d}{k_{d,fast}} = \frac{\alpha \eta_0}{\eta_0} \qquad \textbf{Eq. 3.4}$$

Note that the value used for τ does not affect the result so long as it is constant during the experiments where $k_{d,\,fast}$ and k_d are determined.

As an alternate approach, k_d can also be obtained by fitting **Eq. 3.2** to the effluent concentration data using independent estimates of L, v_p and D from prior analysis of tracer data. The mass recovery method of **Eq. 3.3** was used for the subsequently reported results; however, we applied both methods of determining k_d to five columns that represented a wide range of k_d values (**Table 3.4**). In all cases, the fits of the model to the data were generally good (data not shown) and, more importantly, the fitted results were approximately equivalent to those obtained on the basis of mass recovery (**Table 3.4**).

A plot of attachment efficiency (α) versus electrolyte concentration on a log-log scale creates an "attachment efficiency curve" and the concentration at which α approaches 1.0 is commonly referred to as the critical deposition concentration (CDC). A quantitative estimate of an approximate CDC can be made by applying the following empirical equation:

$$\alpha = \frac{1}{1+(\frac{CDC}{C_{electrolyte}})^b} \qquad \textbf{Eq. 3.5}$$

where $C_{\text{elctrolyte}}$ is the concentration of the background electrolyte (Na^+ or Ca^{2+}) [mg/L] and b is a fitted coefficient equal to the slope of the log-log curve in the reaction limited regime, where $C_{\text{elctrolyte}} << \text{CDC}$.

3.3 Results and Discussion

3.3.1 *Importance of Appropriately Preparing Porous Media*

As previously described, preliminary studies revealed that extensive and standardized methods of glass bead cleaning and packing were required to obtain reproducible column transport data. We hypothesize that this was because the ultrasonic cleaning approach removed small air bubbles and other colloids from the glass bead

surfaces, significantly improving the homogeneity of the surface. The presence of colloidal silica in the bead cleaning solution was confirmed using Energy Dispersive X-Ray (EDX) on particle types that were most commonly observed in the wash solution, as determined by visual observation of Transmission Electron Microscopy (TEM) images (**Figure 3.1**).

3.3.2 *O-MWCNT Transport in the Absence of Deposition*

The O-MWCNT transport experiments in DI water exhibited similar shape and average residence time as the $NaNO_3$ tracer (see **Figure 3.6**). On the basis of the 100% recovery of O-MWCNTs in DI water and identical values of τ to those determined from tracer studies, we conclude that straining is negligible under the transport conditions

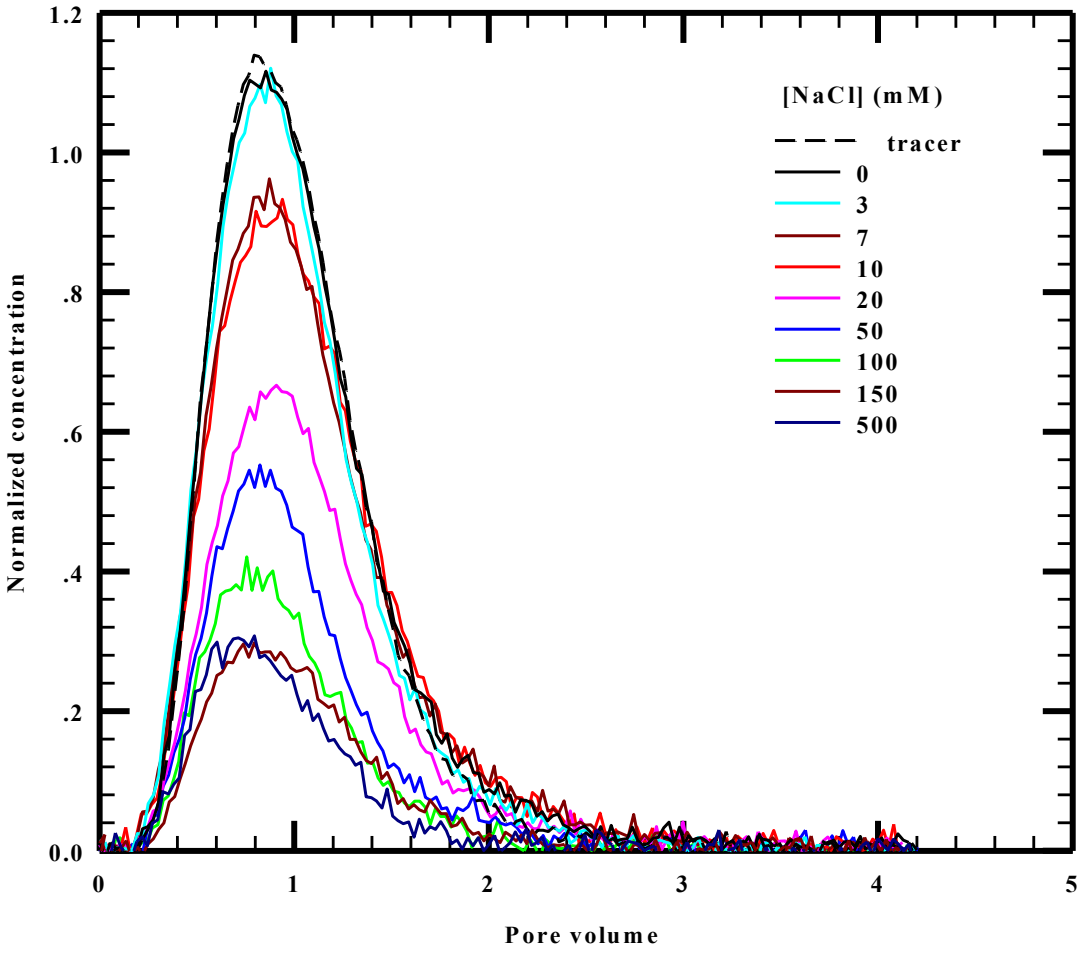

Figure 3.6. Breakthrough curves of 7.1% O-MWCNTs passing through 5.2 cm length columns at pH 5.8 ± 0.2, plotted as a function of NaCl concentration. The normalized concentration is determined as C/C_0, where C_0 is as defined in the text.

tested – *i.e.*, at low concentrations of well-dispersed O-MWCNTs and with the relatively uniform glass bead media. Absence of straining has also been observed by others studying CNT transport in well cleaned sands[56, 64, 74-76] but other investigators studying some quartz sands and soils have observed CNT retention at zero or low concentrations of background electrolyte and have attributed these observations to straining.[52-55] Clearly, the nature of the media is a critical factor that can control the relative importance of straining toward CNT transport.

3.3.3 *Evaluation of O-MWCNT Aggregation during Transport*

To evaluate possible in-column aggregation effects, we conducted a series of control experiments with varying masses of injected O –MWCNTs (7.1% O) at two conditions of aquatic chemistry: (a) 5.0 mM NaCl at pH 4.0 and (b) 40 mM NaCl at pH 5.8 ± 0.2. The mass range used (1.2 to 12.9 μg O-MWCNTs) was chosen to provide a 10 fold range that included (at the lowest mass) the 1.2 μg mass value used in most experiments. These two aqueous conditions were chosen to obtain attachment efficiencies of about 0.5 to 0.7, where the α value should be most sensitive to any change of O-MWCNTs condition. Our assumption was that if there was any aggregation and/or straining occurring within the porous media, input concentrations would affect the fractional rate of deposition (*i.e.*, k_d) and therefore α. Beside these experiments, particle size increase profile of 5.1% O-MWCNTs at pH 5.8 ± 0.2 were also tested.

Results from evaluation with varying mass (**Figure 3.7**) revealed that, within a 95% confidence interval the calculated attachment efficiency for 7.1% O-MWCNTs at pH 5.8 and pH 4.0 remained constant even as injected mass increased by over 10-fold. The aggregation profile of 7.1% O-MWCNT at pH 5.8 and pH 4.0, 3.0% O-MWCNT at pH 5.8 were subsequently shown in **Figure 3.8**. At pH 5.8 and IS 40 mM, particle size of

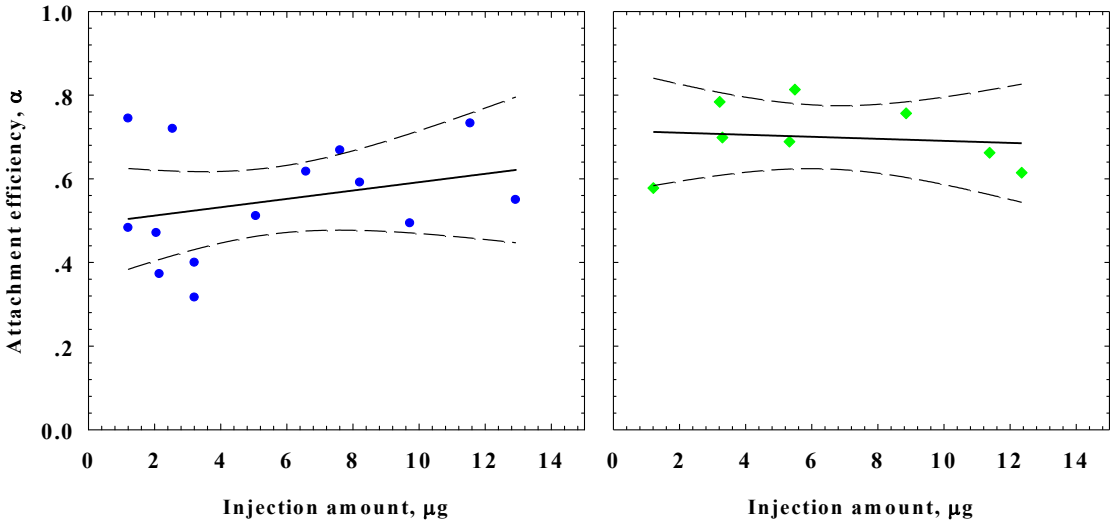

Figure 3.7. Change in attachment efficiency as a function of injected particle concentration for O-MWCNTs with total oxygen concentration of 7.1% at (a) pH 4.0 and 5.0 mM NaCl, and (b) pH 5.8 and 40 mM NaCl.

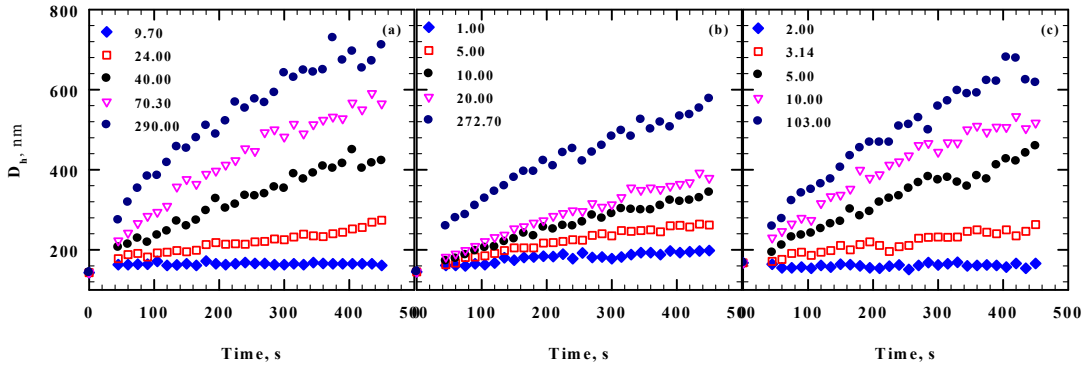

Figure 3.8. Aggregation profile of (a) 7.1% O-MWCNTs at pH 5.8 ± 0.2, (b) 7.1% O-MWCNTs at pH 4.0 ± 0.2, and (c) 3.0% O-MWCNTs at pH 5.8 ± 0.2 under varied NaCl concentrations as indicated by legends at the unit of mM. The aggregation profiles were obtained following method described in Smith *et al.*[1] All experiments were conducted under pH 6.0 ± 0.2 with O-MWCNT concentration of 0.8 mg/L.

7.1% O-MWCNTs increased from ~140 nm to ~240 nm during the retention time for column with length of 5.2 cm (83.4 s) and increased from ~140 nm to ~300 nm during the retention time for column with length of 10.2 cm (163.6 s). The potentially doubled

particle size did not to have a significant effect on their deposition onto the collectors. Considering the results shown in both **Figure 3.7** and **Figure 3.8**– and although the results are less precise at pH 4.0 than 5.8 (**Figure 3.7**) – we conclude that the effects of homo-aggregation and straining of O-MWCNTs is not substantial under either condition during the full time periods of transport.

Although the mass injection tests at $0.5< \alpha < 0.7$ do not confirm the complete absence of aggregation (and perhaps straining) where α values are higher, these results provide important assurance that aggregation and straining are not confounding the results in column experiments for 7.1% O-MWCNTs at the tested α values and below. This is significant because results under these conditions might be viewed as the principle evidence for subsequent conclusions about the impacts of pH, ionic strength, calcium and NOM. Moreover, these results, in combination with our independently conducted homo-aggregation studies (**Figure 3.8**), also serve as evidence against significant effect of aggregation and straining for other experiments at similar and lower α-value. This is certainly true for cases with O-MWCTs of higher surface oxygen content, since more highly oxidized O-MWCNTs are more stable against aggregation.

3.3.4 *Effect of IS*

The effects of IS on O-MWCNT transport are consistent with tenets of Derjaguin-Landau-Verwey-Overbeek (DLVO) theory and prior results observed by others.[52, 53, 64] In particular, the fractional mass recovery of O-MWCNTs in column effluent decreased systematically with increasing NaCl concentration down to a minimum value as the IS approached the CDC (≈ 150mM NaCl in **Figure 3.6** for example). Fractional removals and computed attachment efficiencies for these and all other reported experiments are

provided in **Table 3.5 – Table 3.7**. Above the CDC this minimum fractional mass recovery was constant to within experimental error (± 5% of C/C_0) as the NaCl concentration continued to increase. This minimum fractional recovery (maximum removal) corresponds to a maximum rate of O-MWCNT deposition in the regime where attachment is favorable (α =1) and fractional rates of deposition are controlled only by physical processes of diffusion and mass transfer. This is more clearly evident when data are interpreted in terms of attachment efficiency as shown in **Figure 3.9** for different O-MWCNTs over a range of different pH values. In this figure, the open triangles in panel (b) are derived from the transport effluent data shown in **Figure 3.6** (7.1% O-MWCNTs at pH 5.8). Within the unfavorable (below CDC) regime, **Figure 3.9** shows that a 10-fold increase in IS resulted in at least 5-fold increases in α for all MWCNTs tested. This observation is different from that of Jasi *et al.*[52], who observed that a 10-fold increase in the ionic strength produced only a 2-fold increase in α within the unfavorable deposition regime. We believe that this difference can be ascribed to the presence of straining in the results of Jasi *et al.* and to the fact that straining should be comparatively insensitive to the effects of ionic strength. We also observed that results for 3.0% O-MWCNTs at lower pH have greater uncertainty than other data in regard to the ionic strength required to obtain given α -- see **Figure 3.9(a)**. The cause of this uncertainty is unknown, but may relate to greater variability among samples at this lower oxidation extent.

Table 3.5. Fractional mass removals and associated α values for transport of O-MWCNTs through silica beads at varied pH and NaCl concentrations. (To be continued in next page)

NaCl concentration (mM)	Fractional mass	α	NaCl concentration (mM)	Fractional mass	α
3.0% O-MWCNTs					
pH 5.8, column length = 5.2 cm			**pH 5.8, column length = 10.2 cm**		
5.0	64%	0.23	1.0	90%	0.04
7.0	74%	0.23	2.0	88%	0.05
10.0	73%	0.24	4.0	75%	0.12
12.5	55%	0.45	750.0	9%	1.00
15.0	53%	0.48	**pH 10.0, column length = 10.2 cm**		
25.0	49%	0.53	5.0	91%, 87%	0.05, 0.07
30.0	40%	0.70	10.0	76%, 75%	0.14, 0.15
40.0	49%	0.53	20.0	72%, 70%	0.16, 0.19
50.0	47%	0.57	50	66%, 62%	0.21, 0.24
60.0	48%	0.55	75	40%	0.46
80.0	40%	0.69	100	45%	0.41
100.0	34%	0.81	150	29%	0.64
200.0	31%	0.89	300	18%	0.87
500.0	25%	1.05	500	15%	0.96
1000.0	28%	0.95	750	13%	1.04
NaCl concentration (mM)	**Fractional mass**	**α**	**NaCl concentration (mM)**	**Fractional mass**	**α**
7.1% O-MWCNTs					
pH 5.8, column length = 5.2 cm			**pH 5.8, column length = 10.2 cm**		
7.0	91%	0.07	5.0	92%	0.03
10.0	85%	0.13	7.0	84%	0.07
20.0	66%	0.33	10.0	77%	0.10
25.0	76%	0.22	20.0	48%	0.27
30.0	35%	0.84	60.0	11%	0.82
30.0	66%	0.34	200.0	7%	1.00
40.0	45%	0.64	500.0	7%	0.99
50.0	49%	0.58	**pH 10.0, column length = 10.2 cm**		
100.0	34%	0.87	20.0	94%	0.02
150.0	33%	0.91	30.0	89%	0.04
500.0	29%	1.00	30.0	91%	0.04
pH 4.0, column length = 5.2 cm			35.0	90%	0.04
1.0	75%	0.23	40.0	66%	0.16
2.0	79%	0.19	45.0	66%	0.16
3.5	44%	0.66	60.0	60%	0.19
3.5	62%	0.39	80.0	46%	0.29
5.0	47%	0.61	100.0	36%	0.38

Table 3.5. (continued from previous page) Fractional mass removals and associated α values for transport of O-MWCNTs through silica beads at varied pH and NaCl concentrations. (To be continued in next page)

NaCl concentration (mM)	Fractional mass	α	NaCl concentration (mM)	Fractional mass	α
pH 4.0, column length = 5.2 cm			**pH 10.0, column length = 10.2 cm**		
5.0	55%	0.48	150.0	29%	0.46
7.0	36%	0.84	200.0	18%	0.63
10.0	26%	1.09	350.0	13%	0.94
10.0	28%	1.02	500	7%	1.00
20.0	35%	0.84	700	7%	0.99
30.0	30%	0.98	-	-	-
100.0	39%	1.00	-	-	-
11.5% O-MWCNTs					
pH 5.8, column length = 5.2 cm					
5.0	95%	0.03	100.0	49%	0.50
10.0	86%	0.11	150.0	34%	0.74
20.0	79%	0.16	200.0	33%	0.77
40.0	66%	0.28	300.0	37%	0.69
60.0	69%	0.26	500.0	21%	1.07
80.0	56%	0.41	1000.0	26%	0.93

Table 3.6. Fractional mass removals and associated α values for transport of O-MWCNTs through silica beads at varied $CaCl_2$ concentrations (pH = 5.8, column length = 5.2 cm for all experiments)

$CaCl_2$ concentration (mM)	Fractional mass	α	$CaCl_2$ concentration (mM)	Fractional mass	α
5.1% O-MWCNTs					
0.7	87%	0.11	13.2	33%	0.90
1.3	68%	0.32	40.0	25%	1.15
2.6	53%	0.52	132.5	27%	1.08
6.6	38%	0.78			
7.1% O-MWCNTs					
0.7	80%	0.20	13.2	42%, 42%, 37%	0.76, 0.76, 0.81
1.3	72%, 69%, 67%, 67%	0.29, 0.33, 0.36, 0.36	53.1	36%, 36%	0.92, 0.92
2.6	57%	0.46	132.5	32%	0.92
6.6	47%, 46%	0.68, 0.69	200.0	29%	1.00
8.3% O-MWCNTs					
0.7	87%	0.11	13.2	31%	0.95
1.3	71%	0.28	40.0	31%	0.95
2.6	53%	0.52	132.5	31%	0.96
6.6	34%	0.87	200.0	30%	0.98

Table 3.7. Fractional mass removals and associated α values for transport of O-MWCNTs through silica beads in the presence of SRNOM (pH = 5.8 for all experiments) (To be continued in next page)

NOM concentration (mg DOC/L)		Fractional Mass Removals of O-MWCNTs and Associated α Values					
		5.1%O-MWCNTs		7.1%O-MWCNTs		8.3%O-MWCNTs	
		fractional removal	α	fractional removal	α	fractional removal (%)	α
5 mM $CaCl_2$	0.00	37%, 26%	0.81, 1.10	27%, 27%	1.07, 1.07	35%, 33%	0.85, 0.90
	0.02	56%, 54%	0.48, 0.49	36%, 36%	0.84, 0.84	57%, 55%	0.47, 0.49
	0.04	57%, 51%	0.45, 0.56	52%, 44%	0.54, 0.67	59%, 54%	0.44, 0.50
	0.06	N/A	N/A	50%	0.57	N/A	N/A
	0.08	N/A	N/A	67%	0.33	N/A	N/A
	0.16	74%, 70%	0.24, 0.29	68%, 68%	0.31, 0.32	59%, 53%	0.43, 0.51
	0.25	65%	0.35	N/A	N/A	N/A	N/A
	0.33	79%, 77%, 77%	0.19, 0.21, 0.22	75%, 55%, 32%	0.24, 0.48, 0.93	74%, 66%, 61%, 48%	0.24, 0.33, 0.40, 0.60
	0.49	72%, 67%, 62%, 57%	0.27, 0.33, 0.38, 0.44	68%, 55%	0.32, 0.48	72%, 71%, 70%, 68%	0.27, 0.28, 0.30, 0.31
	0.82	58%, 57%, 36%	0.45, 0.46, 0.84	79%, 60%, 57%	0.19, 0.41, 0.45	85%, 76%	0.13, 0.22
	1.64	N/A	N/A	83%, 80%	0.15, 0.18	81%, 77%	0.17, 0.21
	4.10	N/A	N/A	90%, 86%	0.09, 0.12	93%, 91%	0.05, 0.08

Table 3.7. (Continued form previous page) Fractional mass removals and associated α values for transport of O-MWCNTs through silica beads in the presence of SRNOM (pH = 5.8 for all experiments) (To be continued in next page)

NOM concentration (mg DOC/L)		Fractional Mass Removals of O-MWCNTs and Associated α Values					
		5.1%O-MWCNTs		7.1%O-MWCNTs		8.3%O-MWCNTs	
		fractional removal	α	fractional removal	α	fractional removal (%)	α
10 mM $CaCl_2$	0.00	35%, 31%	0.85, 0.95	35%, 30%	0.85, 0.98	34%, 28%	0.89, 1.05
	0.004	26%, 22%	1.08, 1.22	23%	1.20	N/A	N/A
	0.008	39%, 34%	0.76, 0.87	29%, 24%	1.00, 1.15	38%, 34%	0.79, 0.87
	0.02	41%	0.72	36%, 32%	0.83, 0.94	37%, 34%	0.81, 0.88
	0.04	N/A	N/A	38%	0.80	43%	0.68
	0.16	47%, 46%	0.62, 0.64	44%, 42%	0.66, 0.70	52%, 49%	0.53, 0.59
	0.33	48%, 33%	0.59, 0.91	N/A	N/A	N/A	N/A
	0.49	37%, 35%	0.80, 0.86, 0.91	39%, 39%	0.77, 0.78	55%, 53%, 51%	0.49, 0.51, 0.55
	0.82	53%, 53%, 52%	0.51, 0.52, 0.54	44%, 41%	0.67, 0.74	54%, 54%, 48%	0.50, 0.50, 0.59
	1.64	N/A	N/A	54%, 50%	0.50, 0.55	66%, 66%	0.34, 0.34
	4.10	N/A	N/A	81%, 81%	0.17, 0.17	83%, 79%	0.16, 0.19
100 mM NaCl	0.00	N/A	N/A	34%	0.88	49%	0.59
	0.33	N/A	N/A	75%, 67%	0.23, 0.32	85%, 80%	0.13, 0.19
	0.82	N/A	N/A	78%	0.21	87%	0.11

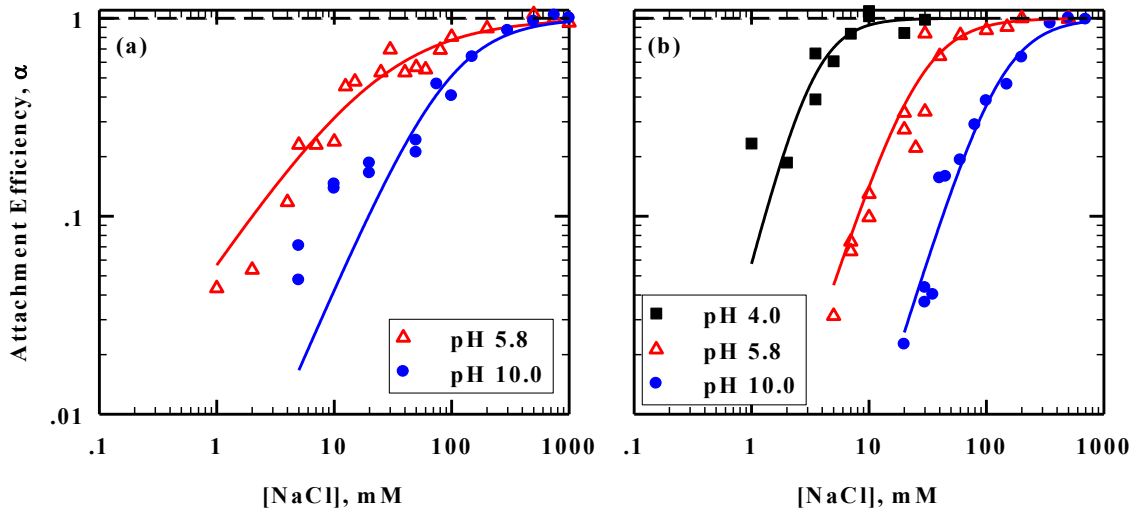

Figure 3.9. Critical deposition curves for O-MWCNTs with total oxygen concentrations of (a) 3.0% and (b) 7.1% measured at pH 10 (filled blue circles), pH 5.8 (open red triangles), and pH 4 (filled black squares).

3.3.5 *Effect of pH*

Few researchers have systematically studied the effect of pH on MWCNT deposition.[75] In this paper, the effect of pH on the transport of two different types of O-MWCNTs (3.0% O and 7.1% O) was studied with NaCl as the electrolyte. As shown in **Figure 3.9**, the data reveal that CDC values for O-MWCNTs increased systematically with pH between 4.0 and 10.0 for both types of O-MWCNTs. All of the CDC curves could be well fit by Equation 4, yielding estimated CDC values for 3.0% O-MWCNTs of 24.4 mM and 96.8 mM at pH 5.8 and 10.0, respectively. CDC values for 7.1% O-MWCNTs were 3.4 mM, 27.3 mM, and 134.4 mM at pH 4.0, 5.8 and 10.0, respectively. As with the previously described IS effects, these results are qualitatively consistent with DLVO theory.[32, 33, 39] More specifically, reduced barriers to attachment with decreasing pH correspond to the fact that higher proton concentration in solution will lead to reduced surface charge on both the collectors (glass beads) and particles (O-MWCNTs) due to

protonation of negatively charged functional groups – that is, principally carboxyl groups on the O-MWCNTs and silanol groups on the amorphous silica beads. The effect of pH on surface charge for the O-MWCNTs produced in our laboratories is well understood, as previously reported by Smith *et al.*[21, 66]– see Figure 2(a) in Ref 21 and Figure 5 in Ref 66 These materials were very similar to those used in our research and were produced by identical methods. Moreover, we also confirmed the presence of more negative surface charge at higher pH for one of our materials (7.1% O-MWCNTs) by means of zeta potential measurement -- see **Figure 3.10**. Unfortunately, however, direct quantitative testing of DLVO theory is not possible for O-MWCNTs owing to the complexities of their shape and size and the unknown aspects of charge distribution on the various interacting

surfaces.

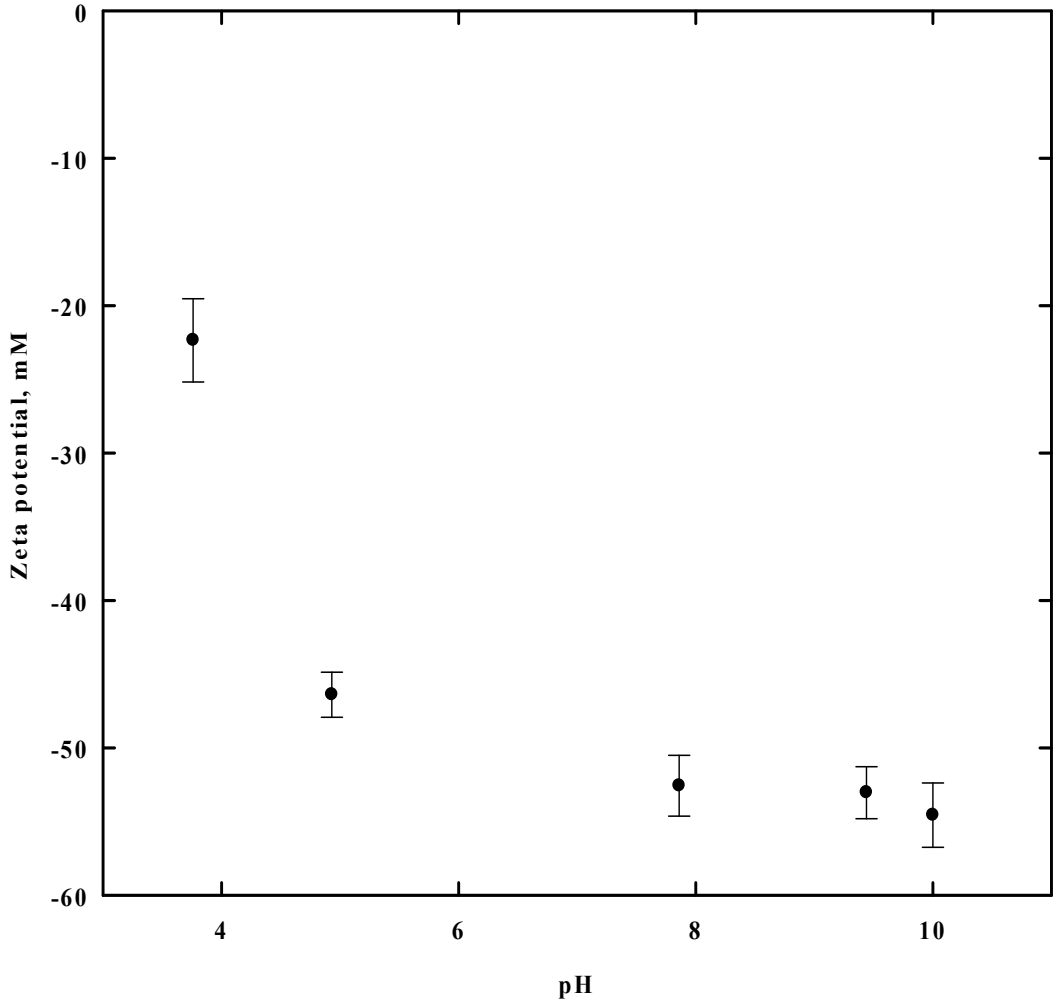

Figure 3.10. Zeta potential of 7.1% O-MWCNTs at varied pH and at the NaCl concentration of 1 mM. The zeta potential profile obtained for 7.1% O-MWCNTs is similar to those obtained in our previous studies[1] using O-MWCNTs from the same supplier (Nanolab) and prepared with identical functionalization method.

3.3.6 *Effect of Surface Oxygen on O-MWCNTs*

O-MWCNTs with different total surface oxygen concentrations were selected to investigate the effect that surface chemistry has on attachment efficiency during transport. NaCl and $CaCl_2$ were both used separately as background electrolytes in these studies. For the NaCl based experiments, CDC curves for O-MWCNTs with 3.0% O,

7.1% O and 11.5% O at pH 5.8 are shown in **Figure 3.11(a)**. Fitting these stability curves to Equation 4 yielded CDC values of 24.4, 27.3 and 93.7 mM NaCl, respectively. As previously discussed in the context of **Figure 3.9(a)**, data for 3.0% O-MWCNTs (**Figure 3.11 (a)**) show greater uncertainty than do other data, perhaps because of greater variability among samples at this lower oxidation extent. This may also partially explain observed overlap of α-values among O-MWCNTs with 3.0% and 7.1% oxygen at higher NaCl concentrations (**Figure 3.11 (a)),** although aggregation and/or straining of either material could also be affecting results in this high α region. In any case, however, the more heavily oxidized O-MWCNTs are clearly more stable towards attachment for conditions at $\alpha < 0.6$ where the possible influence of aggregation and straining can be reliably neglected. (See prior discussion of **Figure 3.7**). The data also reveal that CDC is clearly less sensitive to changes in surface oxygen content than to solution pH. This is not surprising in that pH has impacts on surface potential of both the O-MWCNTs and the collectors whereas changes in surface oxygen only affect the O-MWCNTs.

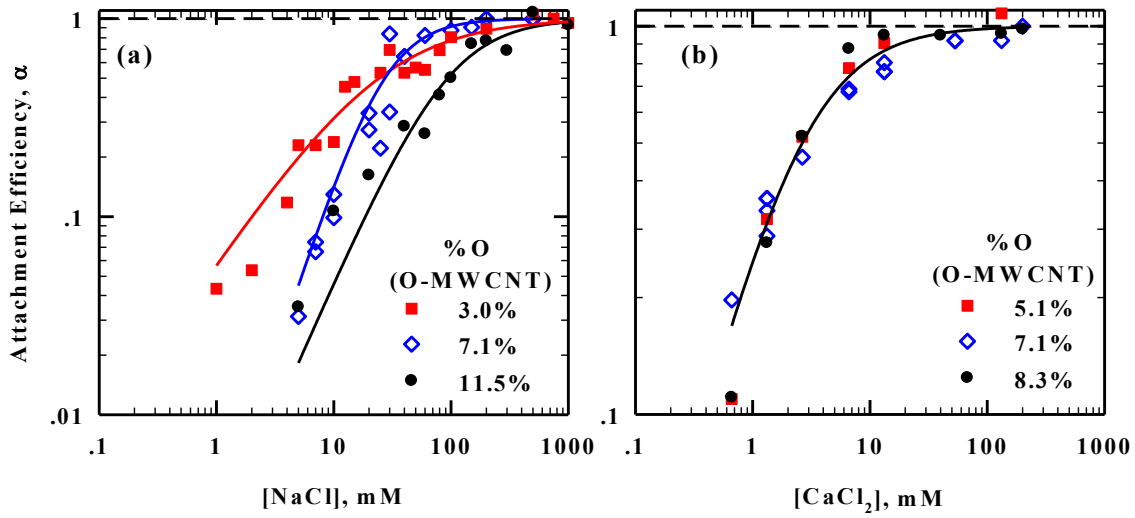

Figure 3.11. Critical deposition curves of O-MWCNTs with varied surface oxygen concentration at pH 5.8 ± 0.2 in the presence of (a) NaCl and (b) $CaCl_2$ as background electrolytes.

For experiments conducted with $CaCl_2$ as background electrolyte, CDC curves for three O-MWCNTs are plotted in **Figure 3.11(b)**. In contrast to the obvious effect of surface oxygen concentration on α in NaCl solution, almost no effect was observed in $CaCl_2$ solution. Estimated CDC values for O-MWCNTs at 5.1% O, 7.1% O, and 8.3% O are almost identical at 2.5 mM, 3.0 mM, and 2.4 mM, respectively. As expected, these CDC values are all significantly smaller than those observed in NaCl due to the ability of the divalent calcium ions to more effectively screen the negative surface charges, thereby facilitating attachment. The differences in CDC between Ca^{2+} and Na^{+} based solutions for O-MWCNTs correspond to roughly 9 fold to 39 fold differences, which are substantially less than the 64-fold differences previously observed by Grolimund *et al.*[73] for spherical carboxylate latex particles and naturally occurring particles during transport through soil. Although the observed difference from Grolimund *et al.* roughly followed expectations of the empirical Schulze-Hardy rule,[73] we note that the Schulze-Hardy rule was developed

from homo-aggregation studies and not deposition. Moreover, in light of the relative complexity of O-MWCNT surface charge and morphology we would not necessarily expect these materials to follow this simple rule. More surprising to us was the lack of CDC dependence on O-MWCNT surface oxygen content when Ca^{2+} was present. Similar effects of independence of CNT – silica CDC to O-MWCNT surface charge in the presence of Ca^{2+} has also been observed by Yi *et al.* in their studies of O-MWCNT deposition onto quartz crystal using QCM-D.[43] We follow those authors in suggesting that the existence of multiple Ca^{2+} binding energies with COO^- functional groups on O-MWCNTs (*e.g.*, mono-dentate or multi-dentate) could cause a relative insensitivity of CDC to O-MWCNT surface charge.[43] Note that other authors have also discussed how Ca^{2+} may participate in additional short-range interactions with anionic surfaces such as silica,[77] anionic polymers,[45] and O-MWCNTs.[23, 42, 78]

3.3.7 *Effect of Natural Organic Matter (NOM)*

The results reported above suggest that O-MWCNTs' attachment efficiencies with amorphous silica can be quite high in clean (organic free) water systems that are mildly brackish (NaCl > 30 mM) or with Ca^{2+} concentrations (> 5 mM) commonly found in groundwater environments.[79] Also relevant, however, will be the background dissolved organic matter that is almost ubiquitously present in natural waters. In this regard, it is now widely understood that the presence of NOM can substantially increase particle stabilities and decrease rates of attachment.[42, 52, 54]

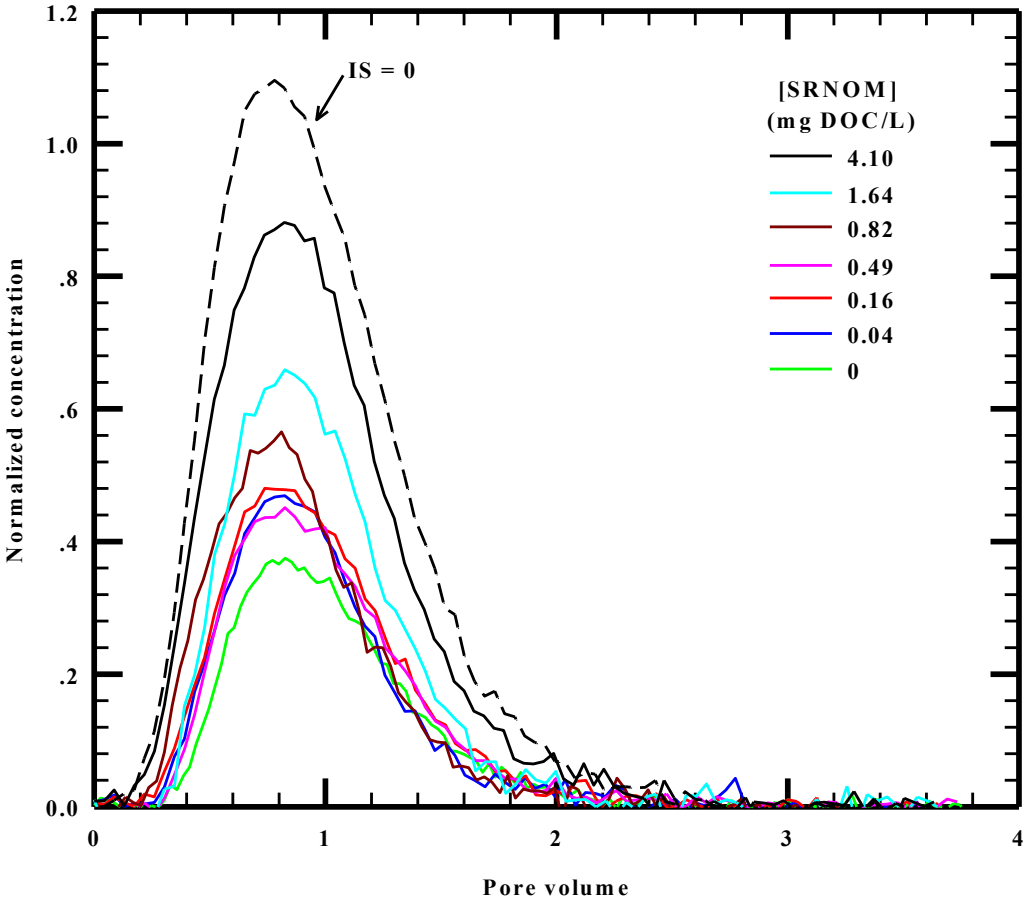

Figure 3.12. Breakthrough curves of 7.1% O-MWCNTs passing through 5.2 cm long columns at 10 mM $CaCl_2$ and pH 5.8 ± 0.2, plotted as a function of SRNOM concentration (mg DOC/L). The dashed line shows a breakthrough curve of O-MWCNTs (SRNOM was present at 0.82 mg DOC/L for this experiment.) in the absence of any added background electrolyte. The normalized concentration is determined as C/C_0, where C_0 is as defined in the text.

The present investigation builds on the above noted prior work by providing a more quantitative estimate of fractional deposition rates of O-MWCNTs to amorphous silica under conditions of varying NOM concentration. This was done under carefully controlled conditions of pH and IS using both sodium and calcium chloride as background electrolyte. By determining the deposition rate coefficient, k_d, in the presence of a known concentration of SRNOM and taking the ratio of this value to the previously

calculated $k_{d,\,fast}$ (*i.e.*, at the highest Na^+ (500 mM) or Ca^{2+} (132 mM) but in the absence of SRNOM), our work provides a first quantitative metric regarding the effect of SRNOM on α for different types of O-MWCNTs.

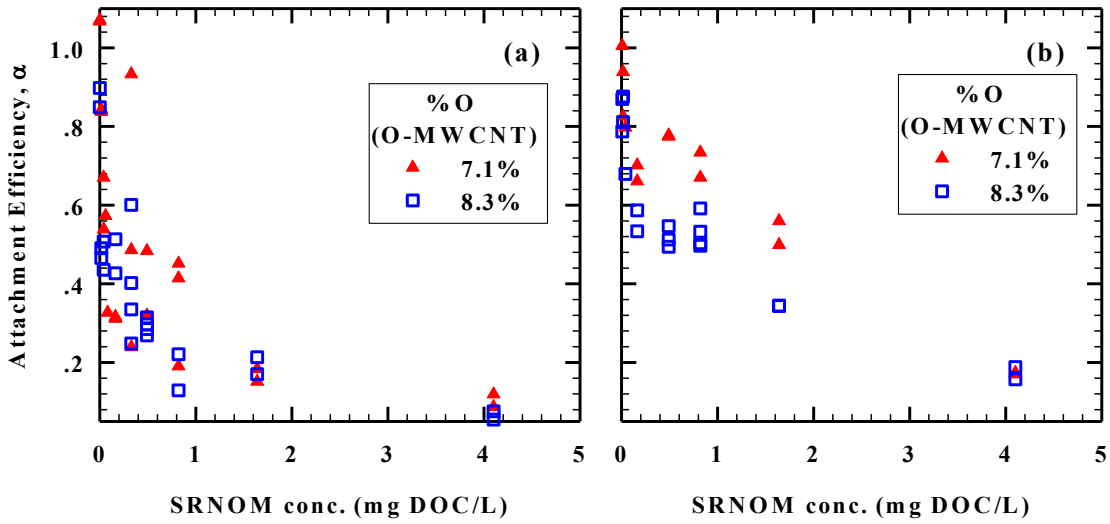

Figure 3.13. Attachment efficiencies obtained using 7.1% O-MWCNTs (filled red triangles) and 8.3% O-MWCNTs (open blue squares) from breakthrough experiments conducted at pH 5.8 ± 0.2 and in the presence of (a) 5 mM $CaCl_2$ and (b) 10 mM $CaCl_2$ plotted as a function of SRNOM concentration.

As expected, SRNOM was observed to facilitate the transport of O-MWCNTs through glass beads for all three O-MWCNTs studied. Selected (typical) column effluent data for one of the three materials are shown in **Figure 3.12**. These results were obtained with 7.1% O-MWCNTs at pH 5.8 and 10 mM $CaCl_2$ over a range of SRNOM concentrations (0 – 4.1 mg DOC/L). Also shown for comparison is the O-MWCNT curve obtained at 0.0 IS and a fixed SRNOM concentration of 0.84 mg DOC/L (dashed line). The 0.0 IS curve is provided for purposes of comparison as a control that has 100% mass recovery (α =0). The *α* values obtained through experiments of this type for two O-MWCNTs are plotted as a function of SRNOM concentration (mg DOC/L) in **Figure**

3.13(a) and **(b)**, using 5 mM Ca^{2+} and 10 mM Ca^{2+} background electrolyte, respectively. Data for the third less oxidized material (5.1% O-MWCNTs) under these same conditions are provided in **Figure 3.14**. The attachment coefficients under each condition and also under a third electrolyte condition of 100 mM NaCl are detailed in **Table 3.7**.

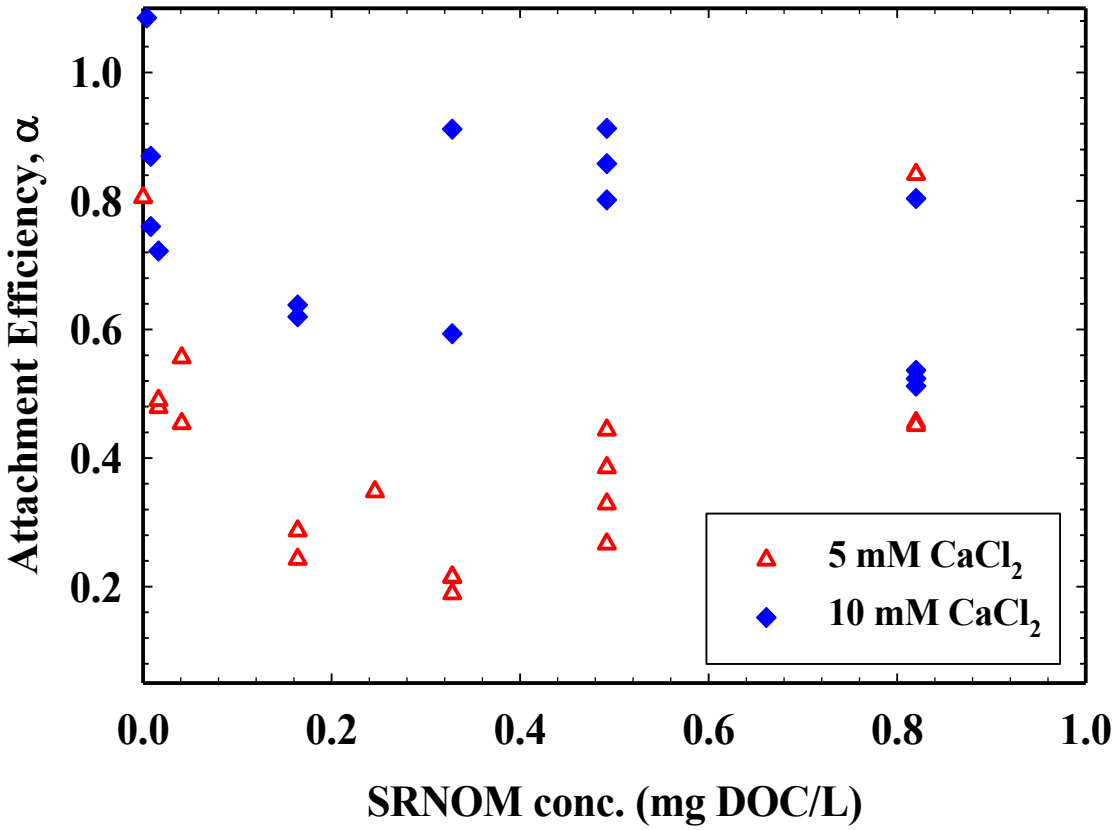

Figure 3.14. Attachment efficiencies of O-MWCNTs with a total surface oxygen concentration of 5.1% as a function of SRNOM concentration at pH 5.8 ± 0.2 with 5mM $CaCl_2$ (red triangles), and 10mM $CaCl_2$ (blue diamonds).

For all three O-MWCNTs and under all aquatic conditions tested, increasing SRNOM concentration led to decreasing α (*i.e.*, decreasing rates of deposition). With 100 mM NaCl as the background electrolyte, deposition was sensitive to SRNOM as well as

O-MWCNT surface oxygen – for example, 0.82 mg DOC/L of NOM causes a 4 fold decrease in α (from 0.88 to 0.21) for 7.1% O-MWCNTs and a 3-fold decrease (from 0.59 to 0.11) for 8.3% O-MWCNTs (**Table 3.7**).

With $CaCl_2$ as background electrolyte, deposition was sensitive to SRNOM but not to O-MWCNT surface oxygen. For both O-MWCNTs shown in **Figure 3.13** results were almost identical. In the presence of 5 mM Ca^{2+} (**Figure 3.13(a)**), α values for two O-MWCNTs tested decreased sharply for SRNOM concentrations between 0.02 and 0.82 mg DOC/L; however, the decline of α at higher concentrations of NOM was somewhat more gradual. More specifically, α values dropped from 1.0 to 0.2 with addition of 0.82 mg DOC/L, but then gradually decreased thereafter, requiring 4.1 mg DOC/L for $\alpha \sim 0.1$. For the 10 mM Ca^{2+} scenarios (**Figure 3.13(b)**), the same trend was observed but with α dropping only to 0.6 at very low values of SRNOM and then gradually decreasing only to ~ 0.2 at 4.1 mg DOC/L of added SRNOM. Results with the less oxidized 5.1% O-MWCNTs (**Figure 3.14**) show similar trends as discussed above for low DOC values although with much greater variability of results owing to the lower stability of these materials. For these reasons, SRNOM concentrations above 0.82 DOC mg/L were not studied for the 5.1% O-MWCNTs.

We postulate that the rapid drop in α at low NOM concentrations (< 0.82 mg DOC/L) correspond monolayer coverage of all available O-MWCNT surfaces. Simple calculations confirm that this is a realistic possibility – with roughly 1.2 μg of O-MWCNTs injected (corresponding to $C_0 = M_0/V_{pore} = 0.12$ mg/L) and assume 283.3 m^2 surface area per g MWCNT (based on BET measurement from Cho *et al.*[23]) we estimate that each mg of SRNOM DOC would need to occupy only 0.04 m^2. This is much lower

than the value of 1 m^2 that has been previously estimated as the amount needed to achieve full monolayer coverage of a mineral surface by moderately sized organic molecules.[80] Thus, our postulation lies well within the realm of possibility. We further postulate that the lower sensitivity of α to DOC at SRNOM concentrations above 0.2 mg DOC/L reflects a change in dominant mechanism from one of surface charge screening as DOC monolayer adsorption blocks O-MWCNT surfaces to steric interaction as the adsorbed layer of SRNOM thickens.

Considering the effects of surface oxygen on attachment efficiencies in the presence of SRNOM, the results show that such effects were much less substantial in Ca^{2+} based than Na^{+} based electrolyte–see **Table 3.5**. These findings are qualitatively similar to those found in the absence of SRNOM (**Figure 3.11(b)**). Moreover, similar effects have been previously reported by Smith *et al.* who studied homo-aggregation in the presence of SRNOM in both simple NaCl solution and in a "synthetic groundwater" containing Ca^{2+}. In that work, as in this, SRNOM dramatically reduced attachment efficiencies in both types of electrolyte, but the impact of surface oxygen was more pronounced in the simple Na^{+} solution.[42]

In natural environments where both Ca^{2+} and NOM are present, O-MWCNT transport may be largely independent of O-MWCNT surface oxidation, with attachment efficiencies of dispersed O-MWCNTs being instead controlled primarily by the amount of adsorbed NOM and other aquatic conditions such as pH, ionic strength, and ionic composition. Importantly, the results showed that the presence of even low concentrations of natural organic matter caused low particle attachment efficiencies ($\alpha <$ 0.2) under all conditions tested. Together, these findings suggest that O-MWCNT

attachment efficiencies in porous media may be very low in many natural situations where straining is not important, with commensurate implications for deposition. We believe that these findings may be directly relevant for environmental transport under some conditions, such as in subsurface sand and gravel aquifers where grain size and uniformity are sufficient to exclude straining mechanisms.

3.4 Acknowledgements

We would like to express our acknowledge to professor Nathalie Tufenkji (Department of Chemical Engineering, McGill University) for her advise and scientific discussion regarding the experimental method of column dissection. We would also like to thank Dr. Kenneth Livi (Department of Earth and Planetary Sciences and Biology, Johns Hopkins University) for his help on TEM analysis. Financial support for this effort was from the National Science Foundation (Grant # BES0731147) and the Environmental Protection Agency (Grant # RD – 83385701-1). Its contents are solely the responsibility of the grantee and do not necessarily represent the official views of the USEPA. Further, USEPA does not endorse the purchase of any commercial products or services mentioned in the publication.

3.5 Cited References

1. Ebbesen, T. W., Carbon Nanotubes. *Annual Review of Materials Science* **1994,** *24*, (1), 235-264.

2. Iijima, S., Helical Microtubules of Graphitic Carbon. *Nature* **1991,** *354*, (6348), 56-58.

3. Ebbesen, T. W.; Hiura, H.; Fujita, J.; Ochiai, Y.; Matsui, S.; Tanigaki, K., Patterns in the Bulk Growth of Carbon Nanotubes. *Chemical Physics Letters* **1993,** *209*, (1-2), 83-90.

4. Dresselhaus, M. S.; Dresselhaus, G.; Eklund, P. C., Science of Fullerenes and Carbon Nanotubes. Academic Press: San Diego, 1996; p xviii, 965 p.

5. Gallagher, M. J.; Chen, D.; Jacobsen, B. P.; Sarid, D.; Lamb, L. D.; Tinker, F. A.; Jiao, J.; Huffman, D. R.; Seraphin, S.; Zhou, D., Characterization of Carbon Nanotubes by Scanning Probe Microscopy. *Surface Science* **1993,** *281*, (3), L335-L340.

6. Klaine, S. J.; Alvarez, P. J. J.; Batley, G. E.; Fernandes, T. F.; Handy, R. D.; Lyon, D. Y.; Mahendra, S.; Mclaughlin, M. J.; Lead, J. R., Nanomaterials in the Environment: Behavior, Fate, Bioavailability, and Effects. *Environ Toxicol Chem* **2008,** *27*, (9), 1825-1851.

7. Parish, A. Production and Application of Carbon Nanotubes, Carbon Nanofibers, Fullerenes, Graphene and Nanodiamonds: A Global Technology Survey and Market Analysis; Innovative research and products (iRAP), Inc: 2011.

8. Mueller, N. C.; Nowack, B., Exposure Modeling of Engineered Nanoparticles in the Environment. *Environ Sci Technol* **2008,** *42*, (12), 4447-4453.

9. Nowack, B.; Bucheli, T. D., Occurrence, Behavior and Effects of Nanoparticles in the Environment. *Environ Pollut* **2007,** *150*, (1), 5-22.

10. Petosa, A. R.; Jaisi, D. P.; Quevedo, I. R.; Elimelech, M.; Tufenkji, N., Aggregation and Deposition of Engineered Nanomaterials in Aquatic Environments: Role of Physicochemical Interactions. *Environ Sci Technol* **2010,** *44*, (17), 6532-6549.

11. Marrs, B.; Andrews, R.; Pienkowski, D., Multiwall Carbon Nanotubes Enhance the Fatigue Performance of Physiologically Maintained Methyl Methacrylate-Styrene Copolymer. *Carbon* **2007,** *45*, (10), 2098-2104.

12. Breuer, O.; Sundararaj, U., Big Returns from Small Fibers: A Review of Polymer/Carbon Nanotube Composites. *Polymer Composites* **2004,** *25*, (6), 630-645.

13. Vaisman, L.; Marom, G.; Wagner, H. D., Dispersions of Surface-Modified Carbon Nanotubes in Water-Soluble and Water-Insoluble Polymers. *Advanced Functional Materials* **2006,** *16*, (3), 357-363.

14. Sluzarenko, N.; Heurtefeu, B.; Maugey, M.; Zakri, C.; Poulin, P.; Lecommandoux, S., Diblock Copolymer Stabilization of Multi-Wall Carbon Nanotubes in Organic Solvents and Their Use in Composites. *Carbon* **2006,** *44*, (15), 3207-3212.

15. Bourlinos, A. B.; Georgakilas, V.; Zboril, R.; Dallas, P., Preparation of a Water-Dispersible Carbon Nanotube-Silica Hybrid. *Carbon* **2007,** *45*, (10), 2136-2139.

16. Liu, P., Modifications of Carbon Nanotubes with Polymers. *European Polymer Journal* **2005,** *41*, (11), 2693-2703.

17. Yusof, A. M.; Buang, N. A.; Yean, L. S.; Ibrahim, M. L., The Use of Multi-Walled Carbon Nanotubes as Possible Carrier in Drug Delivery System for Aspirin. In *Nanoscience and Nanotechnology*, Rusop, M.; Soga, T., Eds. 2009; Vol. 1136, pp 390-394.

18. Li, L.; Xing, Y., Pt-Ru Nanoparticles Supported on Carbon Nanotubes as Methanol Fuel Cell Catalysts. *Journal of Physical Chemistry C* **2007,** *111*, (6), 2803-2808.

19. Penza, M.; Cassano, G.; Aversa, P.; Antolini, F.; Cusano, A.; Cutolo, A.; Giordano, M.; Nicolais, L., Alcohol Detection Using Carbon Nanotubes Acoustic and Optical Sensors. *Applied Physics Letters* **2004,** *85*, (12), 2379-2381.

20. Savage, T.; Bhattacharya, S.; Sadanadan, B.; Gaillard, J.; Tritt, T. M.; Sun, Y. P.; Wu, Y.; Nayak, S.; Car, R.; Marzari, N.; Ajayan, P. M.; Rao, A. M., Photoinduced Oxidation of Carbon Nanotubes. *Journal of Physics Condensed Matter* **2003,** *15*, (35), 5915-5921.

21. Smith, B.; Wepasnick, K.; Schrote, K. E.; Cho, H. H.; Ball, W. P.; Fairbrother, D. H., Influence of Surface Oxides on the Colloidal Stability of Multi-Walled Carbon Nanotubes: A Structure-Property Relationship. *Langmuir* **2009,** *25*, (17), 9767-9776.

22. Cho, H. H.; Smith, B. A.; Wnuk, J. D.; Fairbrother, D. H.; Ball, W. P., Influence of Surface Oxides on the Adsorption of Naphthalene onto Multiwalled Carbon Nanotubes. *Environ Sci Technol* **2008,** *42*, (8), 2899-2905.

23. Cho, H. H.; Wepasnick, K.; Smith, B. A.; Bangash, F. K.; Fairbrother, D. H.; Ball, W. P., Sorption of Aqueous Zn[Ii] and Cd[Ii] by Multiwall Carbon Nanotubes: The Relative Roles of Oxygen-Containing Functional Groups and Graphenic Carbon. *Langmuir* **2010,** *26*, (2), 967-981.

24. Rajagopalan, R.; Tien, C., Trajectory Analysis of Deep-Bed Filtration with Sphere-in-Cell Porous-Media Model. *Aiche J* **1976,** *22*, (3), 523-533.

25. Yao, K. M.; Habibian, M. M.; Omelia, C. R., Water and Waste Water Filtration - Concepts and Applications. *Environ Sci Technol* **1971,** *5*, (11), 1105-1112.

26. Mccarthy, J. F.; Mckay, L. D., Colloid Transport in the Subsurface: Past, Present, and Future Challenges. *Vadose Zone J* **2004,** *3*, (2), 326-337.

27. Tobiason, J. E.; Omelia, C. R., Physicochemical Aspects of Particle Removal in Depth Filtration. *J Am Water Works Ass* **1988,** *80*, (12), 54-64.

28. Hahn, M. W.; O'melia, C. R., Deposition and Reentrainment of Brownian Particles in Porous Media under Unfavorable Chemical Conditions: Some Concepts and Applications. *Environ Sci Technol* **2004,** *38*, (1), 210-220.

29. Elimelech, M.; Omelia, C. R., Effect of Particle Size on Collision Efficiency in the Deposition of Brownian Particles with Electrostatic Energy Barriers. *Langmuir* **1990,** *6*, (6), 1153-1163.

30. Veerapaneni, S.; Wiesner, M. R., Role of Suspension Polydispersivity in Granular Media Filtration. *J Environ Eng-Asce* **1993,** *119*, (1), 172-190.

31. Frimmel, F. H.; Von Der Kammer, F.; Flemming, H.-C., Colloidal Transport in Porous Media. Springer: Berlin, Heidelberg, 2007.

32. Derjaguin, B., On the Repulsive Forces between Charged Colloid Particles and on the Theory of Slow Coagulation and Stability of Lyophobe Sols. *Transactions of the Faraday Society* **1940,** *35*, (0), 203-215.

33. Derjaguin, B.; Landau, L., Theory of the Stability of Strongly Charged Lyophobic Sols and of the Adhesion of Strongly Charged-Particles in Solutions of Electrolytes. *Prog Surf Sci* **1941,** *14*, 633.

34. Elimelech, M.; Omelia, C. R., Kinetics of Deposition of Colloidal Particles in Porous-Media. *Environ Sci Technol* **1990,** *24*, (10), 1528-1536.

35. Franchi, A.; O'melia, C. R., Effects of Natural Organic Matter and Solution Chemistry on the Deposition and Reentrainment of Colloids in Porous Media. *Environ Sci Technol* **2003,** *37*, (6), 1122-1129.

36. Mcdowell-Boyer, L. M.; Hunt, J. R.; Sitar, N., Particle Transport through Porous Media. *Water Resour Res* **1986,** *22*, (13), 1901-1921.

37. Stumm, W., Chemistry of the Solid-Water Interface: Processes at the Mineral-Water and Particle-Water Interface in Natural Systems. Wiley-Interscience: New York, 1992.

38. Tufenkji, N.; Elimelech, M., Correlation Equation for Predicting Single-Collector Efficiency in Physicochemical Filtration in Saturated Porous Media. *Environ Sci Technol* **2004,** *38*, (2), 529-536.

39. Verwey, E. J. W.; Overbeek, J. T., Theory of the Stability of Lyophobic Colloids. Elsevier: Amsterdam, 1948.

40. Yao, K. M. Influence of Suspended Particle Size on the Transport Aspect of Water Filtration. University of North Carolina at Chapel Hill, 1968.

41. Saleh, N. B.; Pfefferle, L. D.; Elimelech, M., Aggregation Kinetics of Multiwalled Carbon Nanotubes in Aquatic Systems: Measurements and Environmental Implications. *Environ Sci Technol* **2008,** *42*, (21), 7963-7969.

42. Smith, B.; Yang, J.; Bitter, J. L.; Ball, W. P.; Fairbrother, D. H., Influence of Surface Oxygen on the Interactions of Carbon Nanotubes with Natural Organic Matter. *Environ Sci Technol* **2012,** *46*, (23), 12839-12847.

43. Yi, P.; Chen, K. L., Influence of Surface Oxidation on the Aggregation and Deposition Kinetics of Multiwalled Carbon Nanotubes in Monovalent and Divalent Electrolytes. *Langmuir* **2011,** *27*, (7), 3588-3599.

44. Qu, X. L.; Hwang, Y. S.; Alvarez, P. J. J.; Bouchard, D.; Li, Q. L., Uv Irradiation and Humic Acid Mediate Aggregation of Aqueous Fullerene (Nc(60)) Nanoparticles. *Environ Sci Technol* **2010,** *44*, (20), 7821-7826.

45. Li, Q. L.; Elimelech, M., Organic Fouling and Chemical Cleaning of Nanofiltration Membranes: Measurements and Mechanisms. *Environ Sci Technol* **2004,** *38*, (17), 4683-4693.

46. Davis, C. J.; Eschenazi, E.; Papadopoulos, K. D., Combined Effects of Ca2+ and Humic Acid on Colloid Transport through Porous Media. *Colloid Polym Sci* **2002,** *280*, (1), 52-58.

47. Chen, K. L.; Elimelech, M., Interaction of Fullerene (C-60) Nanoparticles with Humic Acid and Alginate Coated Silica Surfaces: Measurements, Mechanisms, and Environmental Implications. *Environ Sci Technol* **2008,** *42*, (20), 7607-7614.

48. Chen, K. L.; Mylon, S. E.; Elimelech, M., Enhanced Aggregation of Alginate-Coated Iron Oxide (Hematite) Nanoparticles in the Presence of Calcium, Strontium, and Barium Cations. *Langmuir* **2007,** *23*, (11), 5920-5928.

49. Yoon, S. H.; Lee, C. H.; Kim, K. J.; Fane, A. G., Effect of Calcium Ion on the Fouling of Nanofilter by Humic Acid in Drinking Water Production. *Water Res* **1998,** *32*, (7), 2180-2186.

50. Iler, R. K., Coagulation of Colloidal Silica by Calcium-Ions, Mechanism, and Effect of Particle-Size. *J Colloid Interf Sci* **1975,** *53*, (3), 476-488.

51. Auset, M.; Keller, A. A., Pore-Scale Visualization of Colloid Straining and Filtration in Saturated Porous Media Using Micromodels. *Water Resour Res* **2006,** *42*, (12).

52. Jaisi, D. P.; Saleh, N. B.; Blake, R. E.; Elimelech, M., Transport of Single-Walled Carbon Nanotubes in Porous Media: Filtration Mechanisms and Reversibility. *Environ Sci Technol* **2008,** *42*, (22), 8317-8323.

53. Jaisi, D. P.; Elimelech, M., Single-Walled Carbon Nanotubes Exhibit Limited Transport in Soil Columns. *Environ Sci Technol* **2009,** *43*, (24), 9161-9166.

54. Wang, Y. G.; Kim, J. H.; Baek, J. B.; Miller, G. W.; Pennell, K. D., Transport Behavior of Functionalized Multi-Wall Carbon Nanotubes in Water-Saturated Quartz Sand as a Function of Tube Length. *Water Res* **2012,** *46*, (14), 4521-4531.

55. O'carroll, D. M.; Liu, X.; Mattison, N. T.; Petersen, E. J., Impact of Diameter on Carbon Nanotube Transport in Sand. *J Colloid Interf Sci* **2013,** *390*, 96-104.

56. Liu, X. Y.; O'carroll, D. M.; Petersen, E. J.; Huang, Q. G.; Anderson, C. L., Mobility of Multiwalled Carbon Nanotubes in Porous Media. *Environ Sci Technol* **2009,** *43*, (21), 8153-8158.

57. Chen, K. L.; Smith, B. A.; Ball, W. P.; Fairbrother, D. H., Assessing the Colloidal Properties of Engineered Nanoparticles in Water: Case Studies from Fullerene C-60 Nanoparticles and Carbon Nanotubes. *Environ Chem* **2010,** *7*, (1), 10-27.

58. Hu, H.; Yu, A. P.; Kim, E.; Zhao, B.; Itkis, M. E.; Bekyarova, E.; Haddon, R. C., Influence of the Zeta Potential on the Dispersability and Purification of Single-Walled Carbon Nanotubes. *J Phys Chem B* **2005,** *109*, (23), 11520-11524.

59. Hyung, H.; Fortner, J. D.; Hughes, J. B.; Kim, J. H., Natural Organic Matter Stabilizes Carbon Nanotubes in the Aqueous Phase. *Environ Sci Technol* **2007,** *41*, (1), 179-184.

60. Chen, K. L.; Elimelech, M., Envr 92-Influence of Humic Acid on the Aggregation Kinetics of Fullerene Nanoparticles in Monovalent and Divalent Electrolyte Solutions. *Abstr Pap Am Chem S* **2007,** *234*.

61. Chen, K. L.; Elimelech, M., Influence of Humic Acid on the Aggregation Kinetics of Fullerene (C-60) Nanoparticles in Monovalent and Divalent Electrolyte Solutions. *J Colloid Interf Sci* **2007,** *309*, (1), 126-134.

62. Saleh, N. B.; Pfefferle, L. D.; Elimelech, M., Influence of Biomacromolecules and Humic Acid on the Aggregation Kinetics of Single-Walled Carbon Nanotubes. *Environ Sci Technol* **2010,** *44*, (7), 2412-2418.

63. Hyung, H.; Kim, J. H., Natural Organic Matter (Nom) Adsorption to Multi-Walled Carbon Nanotubes: Effect of Nom Characteristics and Water Quality Parameters. *Environ Sci Technol* **2008,** *42*, (12), 4416-4421.

64. Wang, P.; Shi, Q.; Liang, H.; Steuerman, D. W.; Stucky, G. D.; Keller, A. A., Enhanced Environmental Mobility of Carbon Nanotubes in the Presence of Humic Acid and Their Removal from Aqueous Solution. *Small* **2008,** *4*, (12), 2166-2170.

65. Smith, B. Y., Jin; Bitter, Julie; Ball, William; Fairbrother, D. Howard;, Influence of Surface Oxygen on the Interactions of Carbon Nanotubes with Natural Organic Matter. *Environ Sci Technol* **2012**.

66. Smith, B.; Wepasnick, K.; Schrote, K. E.; Bertele, A. H.; Ball, W. P.; O'melia, C.; Fairbrother, D. H., Colloidal Properties of Aqueous Suspensions of Acid-Treated, Multi-Walled Carbon Nanotubes. *Environ Sci Technol* **2009,** *43*, (3), 819-825.

67. Langley, L. A.; Fairbrother, D. H., Effect of Wet Chemical Treatments on the Distribution of Surface Oxides on Carbonaceous Materials. *Carbon* **2007,** *45*, (1), 47-54.

68. Langley, L. A.; Villanueva, D. E.; Fairbrother, D. H., Quantification of Surface Oxides on Carbonaceous Materials. *Chem Mater* **2006,** *18*, (1), 169-178.

69. Wepasnick, K. A.; Smith, B. A.; Schrote, K. E.; Wilson, H. K.; Diegelmann, S. R.; Fairbrother, D. H., Surface and Structural Characterization of Multi-Walled Carbon Nanotubes Following Different Oxidative Treatments. *Carbon* **2011,** *49*, (1), 24-36.

70. Cho, H.-H.; Smith, B. A.; Wnuk, J. D.; Fairbrother, D. H.; Ball, W. P., Influence of Surface Oxides on the Adsorption of Naphthalene onto Multiwalled Carbon Nanotubes. *Environmental Science & Technology* **2008,** *42*, (8), 2899-2905.

71. Smith, B.; Wepasnick, K.; Schrote, K. E.; Cho, H.-H.; Ball, W. P.; Fairbrother, D. H., Influence of Surface Oxides on the Colloidal Stability of Multi-Walled Carbon Nanotubes: A Structure-Property Relationship *Langmuir* **2009,** *25*, (17), 9767-9776.

72. Litton, G. M.; Olson, T. M., Colloid Deposition Rates on Silica Bed Media and Artifacts Related to Collector Surface Preparation Methods. *Environ Sci Technol* **1993,** *27*, (1), 185-193.

73. Grolimund, D.; Elimelech, M.; Borkovec, M.; Barmettler, K.; Kretzschmar, R.; Sticher, H., Transport of in Situ Mobilized Colloidal Particles in Packed Soil Columns. *Environ Sci Technol* **1998,** *32*, (22), 3562-3569.

74. Kasel, D.; Bradford, S. A.; Simunek, J.; Heggen, M.; Vereecken, H.; Klumpp, E., Transport and Retention of Multi-Walled Carbon Nanotubes in Saturated Porous Media: Effects of Input Concentration and Grain Size. *Water Res* **2013,** *47*, (2), 933-944.

75. Tian, Y.; Gao, B.; Wang, Y.; Morales, V. L.; Carpena, R. M.; Huang, Q. G.; Yang, L. Y., Deposition and Transport of Functionalized Carbon Nanotubes in Water-Saturated Sand Columns. *J Hazard Mater* **2012,** *213*, 265-272.

76. Mattison, N. T.; O'carroll, D. M.; Rowe, R. K.; Petersen, E. J., Impact of Porous Media Grain Size on the Transport of Multi-Walled Carbon Nanotubes. *Environ Sci Technol* **2011,** *45*, (22), 9765-9775.

77. Sulpizi, M.; Gaigeot, M. P.; Sprik, M., The Silica-Water Interface: How the Silanols Determine the Surface Acidity and Modulate the Water Properties. *J Chem Theory Comput* **2012,** *8*, (3), 1037-1047.

78. Chen, C. L.; Wang, X. K., Adsorption of Ni(Ii) from Aqueous Solution Using Oxidized Multiwall Carbon Nanotubes. *Ind Eng Chem Res* **2006,** *45*, (26), 9144-9149.

79. Briggs, J. C.; Ficke, J. F., Quality of Rivers of the United States, 1975 Water Year: Based on the National Stream Quality Accounting Network (Nasqan). U.S. Geological Survey: 1977.

80. Mayer, L. M., Extent of Coverage of Mineral Surfaces by Organic Matter in Marine Sediments. *Geochimica Et Cosmochimica Acta* **1999,** *63*, (2), 207-215.

Chapter 4. Transport of Oxidized Multi-Walled Carbon Nanotubes through Silica Based Porous Media: Investigation of Removal Mechanisms and Mathematical Modeling

ABSTRACT

To better understand the nature of oxidized multi-walled carbon nanotube (O-MWCNT) interaction with the surfaces of silica glass bead collectors, additional transport studies were conducted with special focus on removal mechanism. These studies included both investigations of velocity effects on deposition rate under pulse-input conditions and investigations of spatial distribution of O-MWCNTs through column dissection under step-input conditions. For studies of the effect of approach velocity on the estimated deposition rate coefficient, k_d, the mathematical relationship between k_d and approach velocity followed expectations of interception theory, which would be consistent with the notion that, for purposes of collision prediction, O-MWCNTs effectively occupy a spherical volume with a diameter on the order of the CNT length. Other experiments were conducted with a step-input approach to allow examination of in-situ concentrations of O-MWCNTs and better understand deviations from conventional clean-bed filtration theory (CBFT). Both breakthrough curves (BTCs) and retention profiles at five different ionic strengths (IS) were analyzed. Although the trends of the experimental observations followed the general expectations from traditional theory based on electrostatic interactions, the BTCs as well as retention profiles exhibited features that could not be quantitatively well explained by simple CBFT, including BTC plateaus that either

increased (low IS) or decreased (high IS) with time as well as hypo-exponential decay in spatial profiles of retained particles. Modified models incorporating terms for straining, site-blocking, and multilayer deposition effects were applied to simulate experimental results that deviated from simple CBFT and to investigate the mechanisms of O-MWCNT removal. Results showed that all of the additional terms were needed in order to explain the full set of data, although there were conditions under which one or more of the terms could be neglected.

4.1 Introduction

As illustrated by the O-MWCNT transport studies described in Chapter 3, observation of breakthrough curves in laboratory columns can be an effective approach to study the movement of particulate and dissolved contaminants through porous media, and thus to better understand their transport in groundwater systems.[1-8] One important reason for the widespread use of breakthrough curves in transport studies is that they are comparatively straight forward to conduct and usually require less analytical effort than other methods of observation, such as direct imaging of in-situ concentrations[9, 10] or post-experiment dissection for measurement of in-situ solid concentrations.[4, 8, 11] Moreover, it is also usually the case that aqueous-phase concentrations of contaminants can be measured with greater sensitivity and accuracy than in-situ solid concentrations, which facilitates quantitative interpretation of results. On the other hand, breakthrough experiments provide no direct observation of the collector-contaminant interaction at the physical locations of removal within the column, but only provide information regarding the rate at which the contaminants enter and leave the porous media. By contrast, direct observations of retained contaminants can provide valuable additional information

regarding their in-column distribution. Consequently, column dissection is sometimes applied in conjunction with transport experiments to gather more information and enable a more mechanistically based analysis of results.[4, 8, 11-14]

When the column dissection approach is used with colloidal transport experiments, columns are cut into small segments, each of which is separately analyzed to obtain the amount (usually mass) of deposited particles. The amount of particles for each segment is usually normalized by the mass of the collectors in the segment to calculate a solid-phase concentration (mass/mass), which is then plotted with respect to the distance of the segment location from the column inlet. The resulting plot, called a retention profile or spatial distribution profile, exhibits the distribution of deposited particles after the completion of an experiment and can shed light on the deposition mechanism. Compared to methods such as direct imaging, column dissection does not require advanced detection instruments such as high resolution microscopy, but still provides abundant information regarding the behavior of colloidal particles in the porous media.

Many prior publications have reported on investigations of the transport of engineered nanomaterials through porous media, including some that were conducted using column dissection.[4, 8, 11, 13, 15] For example, Wang *et al.*[8] analyzed retention profiles of 4-ethoxybenzoic acid functionalized MWCNTs through saturated media composed of quartz sands. The authors found that the amount of deposited MWCNTs was exceptionally high at the column inlet and postulated that the effects of straining were significant.[8] Li *et al.*[11] used porous media composed of quartz sands to examine the breakthrough curves and retention profiles of C_{60}. They observed phenomena consistent with their hypothesis of a site-blocking mechanism, *i.e.*, that some of the most favorable

sites for deposition were of limited quantity and were blocked against further deposition once they were initially occupied. Lanphere *et al*.[13] investigated the fate of graphene oxide nanoparticles (GONPs) through packed bed columns at varied ionic strengths (IS) by using transport experiments. Mass balances and column dissections revealed that as concentrations of KCl increased from 0.01 to 0.1 M, the portion of GONPs retained within the media increased from 5% to 100%, the majority of which were retained within the first centimeter of the column.

To more quantitatively interpret experimental results, test their understanding and make predictions of as yet untested circumstances, investigators and engineers often use mathematical representations (i.e., quantitative simulation models) of the underlying physical and chemical processes of transport. Such models are usually solved through computer-based analysis and can be used to obtain additional understanding of system properties. Such computer modeling has been widely used in the interpretation of colloidal particle transport.

In the context of aquatic particle transport through beds of porous media, Yao *et al*.[16] were among the first to apply clean-bed filtration theory (CBFT) to data interpretation. Focus of the study was on physical mechanisms of collision in terms of "single collector contact efficiencies" (η_0). In addition, the authors also applied the Derjaguin-Landau-Verwey-Overbeek (DLVO) theory[17-19] in an effort to understand particle-particle forces that were not incorporated into the physical collector efficiency term. The effects of such interactions were instead lumped into a separate term, called the "sticking probability" or "attachment efficiency" (α).

Since the early work of Yao *et al.*[16], numerous improvements of the clean bed filtration (CBF) model have been proposed and applied to simulate the transport of colloidal particles in porous media.[5, 16, 20, 21] In their own work, Yao *et al.*[16], provided individual analytical solutions for single collector contact efficiencies caused by diffusion (η_D), interception (η_I), and sedimentation (η_G). They also proposed that the numerical solution of the total single-collector contact efficiency (η_0) can be approximated as the sum of the solutions for the three primary mechanisms.[16] In 1976, Rajagopalan and Tien improved Yao's equation by developing a semi-empirical correlation equation for η_0.[20] In 2004, Tufenkji and Elimelech further improved the equation by including additional particle-removal mechanisms and interaction forces, such as the previously omitted hydrodynamic and van der Waals interactions, into their calculation of η_0, thereby providing a more accurate solution.[21]

In addition to the traditional CBFT, other researchers have provided additional mathematical expressions in efforts to mechanistically account for observations in experiments where the clean bed assumption appeared not to hold.[6, 7, 22-31] For example, Bradford *et al.* [23] added a first order straining rate coefficient, k_{str}, together with a depth-dependent term in the convection-diffusion equation to address the straining effect. Tufenkji *et al*.[24] developed a power law distribution of the deposition rate coefficient k_d into the CBFT to model a hyper-exponential retention profile of bacteria in glass beads. Ryde *et al*.[29, 31] applied a multilayer deposition model to study the transport of uniform spherical hematite particles through glass beads, reporting that their model was successful in fitting the breakthrough curves obtained at varied ionic strength (IS) and that multilayer deposition was only significant at high IS conditions.

Despite abundant research on traditional colloidal particles such as soil-mobilized colloids or latex particles[22, 32-36], it is still challenging to estimate the aquatic movement of complex colloids including many engineered nanomaterials, such as carbon nanotubes (CNTs), fullerenes, and quantum dots, owing to their unique shapes and/or extremely high aspect ratios. In these cases, new modeling approaches are needed, as may be obtained either by altering existing models or proposing new ones.

Several research groups have attempted to explain experimental results with engineered nano-particles (ENPs) through modification of traditional models. Liu *et al.*[5] applied traditional CBF model in conjunction with site-blocking and detachment terms to model the breakthrough of sulfuric/nitric acid treated MWCNTs through quartz sand columns. The authors also took the non-spherical shape of MWCNTs into consideration and re-calculated the single collector efficiency by revising all three contact efficiencies (η_I, η_G, and η_D).[5] This calculation was conducted using the assumption that dispersed MWCNTs existed in water flow in a form similar to cylindrically shaped rods that can come into contact with collectors by means of end-on or side-on interactions.[5] This model was able to provide good agreement with the experimental observations, using only attachment efficiency α and maximum solid concentration (or maximum adsorption capacity of the solid phase according to the authors) as fitting parameters for the model.[5] Wang *et al.*[8] also successfully applied a modified CBF model to model their transport experimental results for the transport of 4-ethoxybenzoic acid functionalized MWCNTs through porous media composed of Ottawa sands, including breakthrough curves and retention profiles. Their modified version included additional terms for a straining rate coefficient and time-dependent site-blocking kinetics, as well as a nanotube shape factor.

Li *et al.*[11] used a mathematical model incorporating non-equilibrium attachment kinetics and a maximum retention capacity to simulate the effluent breakthrough curves and retention profiles obtained by passing C_{60} through columns packed with quartz sands. Their attachment efficiencies, estimated from fitted attachment rate coefficients, were more than one order of magnitude larger than the theoretical attachment efficiencies computed from DLVO theory.[11] Similar issues had been observed previously with latex particles by O'melia et al.[ref]. Li et al. followed Elemelech and O'melia to postulate that this discrepancy was due to the patch-wise surface charge heterogeneity on the sand grains.[11][ref] More investigations are still needed to better estimate the transport behavior of engineered nanoparticles (ENPs) in porous media. In comparison with prior studies on the transport of more traditional colloidal particles, there are as yet few studies focused on ENPs.

In this work, transport of 7.1% O-MWCNTs through columns packed with glass beads was investigated and analyzed by both of the previously discussed methods: breakthrough curves and retention profiles. A conventional CBF model, as well as modified models incorporating straining, site-blocking, and multilayer deposition terms were applied to simulate experimental results and investigate the mechanisms of O-MWCNT removal.

4.2 Experimental Methods

4.2.1 *Surface Oxidation, Characterization, and Preparation of Colloidal O-MWCNTs.*

MWCNTs (15 ± 5 nm diameter, 1 - 5 μm length) purchased from NanoLabs, Inc. (Waltham, MA) were used in this study. The oxidation and characterization processes for

these materials, as well as details for the preparation of O-MWCNT colloidal dispersions have been described in previous work.[37-44] To summarize, oxidized MWCNTs (O-MWCNTs) were prepared by refluxing in 53% w/w HNO_3, followed by an additional base purification process. X-ray photoelectron spectroscopy (XPS) (PHI 5400 system) in conjunction with chemical derivatization[45, 46] was employed to characterize the resulting O-MWCNTs and obtain total surface oxygen concentrations, as well as the distribution of oxygen-containing functional groups. To prepare O-MWCNT stock dispersions, a small amount of O-MWCNTs (~ 4 mg) was added into ~ 200 mL de-ionized (DI) water and sonicated (Branson 1510, 70 W) for 20 hours. The suspension was then subjected to repeated centrifugation cycles (1000 rpm, 5 min) to remove any un-dispersed O-MWCNTs bundles and glass particles etched from the wall of the flask during sonication. An additional sonication (5 min) of the supernatant was conducted afterward to further disperse some bundled O-MWCNTs that may have remained suspended. Dynamic light scattering (DLS) was employed to measure the hydrodynamic diameters of O-MWCNTs in stock suspensions.

4.2.2 *Preparation of Glass Beads and Packed Columns.*

Columns with diameters of 2.5 cm and lengths of 5.2 cm or 10.2 cm were prepared using soda lime glass spheres (0.355 - 0.425 mm, MO-SCI Corporation) as model collectors. Details regarding preparation of glass beads and column packing were the same as for the studies described in **Chapter 3**. The careful cleaning and preparation were necessary in order to achieve good reproducibility. Mild sonication of glass spheres in base (0.1 M NaOH), acid (1 M HNO_3), and de-ionized (DI) water was performed both upon receipt and again immediately prior to use. A wet-pack method was used during

column assembly, maintaining the porosity of columns at 0.38 and the pore volume at 9.7 cm^3 (short column) or 19.0 cm^3 (long columns). The porosity of the porous media in each packed column was calculated based on the quartz column inner diameter, the weight of packed glass beads, and the column length.

4.2.3 *Transport Experiments*

Transport experiments were conducted using a dual-pump system as described earlier. (See **Chapter 3**) Pulse-input and step-input methods were used to study O-MWCNTs deposition onto model collectors. Pulse-input experiments use a smaller total mass of O-MWCNT particles so that the conditions for clean bed filtration can be more easily maintained. Step-input experiments use a much greater volume of O-MWCNT suspension and therefore more O-MWCNTs are retained in the column at a specific background electrolyte concentration. A higher solid concentration of O-MWCNTs within the column is necessary to obtain the retention profile within each column after each transport experiment.

a. Pulse-input method.

The pulse-input method was employed in the study described in this chapter to analyze the effect of flow-rate on O-MWCNT deposition. During a pulse-input experiment, two separate feed solutions, one containing DI water ("line I") and another containing sodium chloride background electrolyte solution ("electrolyte line") were pumped into the column at a constant flow rate by two separate peristaltic pumps operating in parallel. In each experiment, both feed lines were kept at identical and constant flow-rates. Among the various experiments, these flows ranged between 0.5 mL/min and 7 mL/min to achieve a final total flow rate of 1 mL/min to 14 mL/min for

the mixed solution flowing through the column. When the column reached steady-state with the intended solution and flow rate, a 0.6 mL pulse of O-MWCNT dispersion (~2.0 mg/L) was injected into the DI line through an injection loop as described in **Chapter 3**. O-MWCNT dispersions were added into the DI line instead of the electrolyte line to minimize any aggregation or deposition that could occur before entering the column. The two lines were mixed immediately prior to the column inlet in a custom-built Teflon® in-line mixing chamber (<1 mL internal volume) inside of which a tiny Teflon coated stir bar was placed. Please refer to **Chapter 3**, including **Figure 3.4** for details regarding the experimental set-up.

b. Step-input method

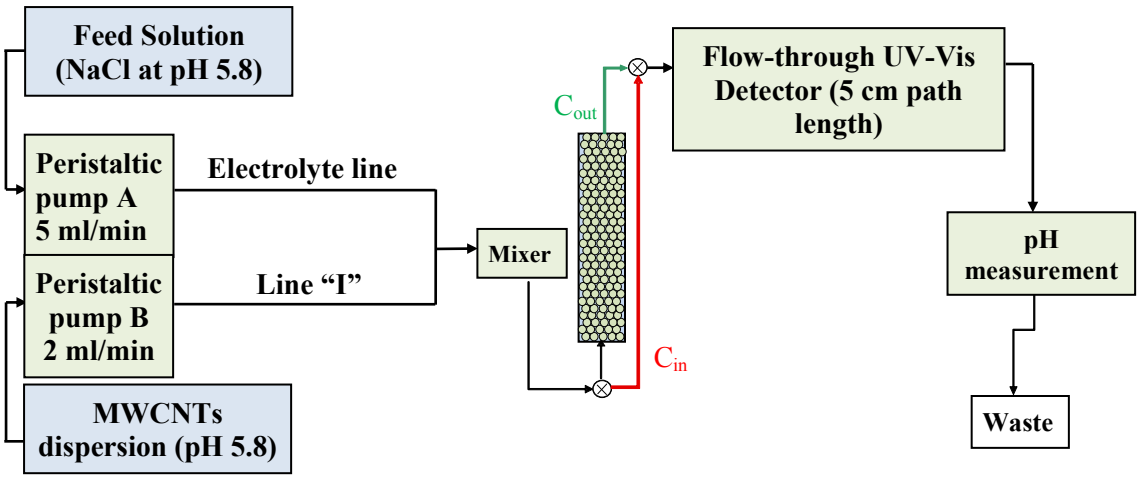

Figure 4.1. Dual-pump column filtration system with in-line mixer, column, and UV-vis detection source for step-input method.

As shown in **Figure 4.1**, when the step-input method was employed, an O-MWCNT dispersion (~1.23 mg/L) replaced the DI water at the "line I" and was pumped into the column at a constant flow-rate of 2.0 mL/min. A sodium chloride solution was pumped into the column at a flow-rate of 5.0 mL/min through the "electrolyte line". These two lines were also mixed immediately before entering the column, resulting in a

final concentration of 0.35 mg/L O-MWCNTs. The O-MWCNT dispersions were passed through columns for a prescribed amount of time ranging from 10-28 pore volumes fed (PVF). The length of the feeding time was chosen based on the availability of the O-MWCNT stock dispersion and the background ionic strength. For BTCs with increasing plateaus (low IS), the O-MWCNT dispersion was fed until a flat plateau was obtained or the dispersion stock was emptied. For BTCs with decreasing plateaus (high IS), a lower PVF was selected to avoid the plateaus from decreasing to the same level of system noise, so that features of the BTCs could be better captured. Afterwards, DI water without O-MWCNTs was pumped through "line I" at the same flow rate while electrolyte pumping continued as before. This was maintained for another five pore volumes (PV).

All solutions or dispersions used in this study were equilibrated with ambient atmosphere before use so as to keep the pH at 5.8 ± 0.2 without the addition of any buffering agent. Before each experiment, columns were conditioned with DI water and then background electrolyte, each for 20 pore volumes. As described previously (**Chapter 3**), sodium nitrate was used as a pulse-input tracer for selected columns in order to obtain independent information about residence time distribution and hydraulic dispersivity.

O-MWCNT dispersions exiting the columns were passed through a 5 cm light path flow-through quartz cell (Starna Cells, Inc.) and detected using UV-Vis (Cary 50) at 270 nm; $NaNO_3$ tracers were measured at 302 nm. The pH of the effluent was measured to be 5.8 ± 0.2 throughout all experiments. Two preliminary runs, one using only DI water and no electrolyte ("DI" run) and another "bypass" run that circumvented the column completely, were conducted prior to each O-MWCNT breakthrough experiment

as described in our previous study (see **Chapter 3**). For column experiments conducted with the pulse-input method, "DI" and "bypass" runs were performed using identical volumes of O-MWCNT dispersions to those used in the experimental runs under the designated background electrolyte concentration and both preliminary test yielded 100% mass balance (±5%) (see **Chapter 3**). For consistency, the mass of O-MWCNTs estimated from "bypass" run (M_{bypass}) was used as the *injected mass* (M_I) in the data analysis. For column experiments conducted with the step-input method, however, both "DI" and "bypass" runs were performed for only five PVF, i.e., the O-MWCNT dispersion was passed through the system for 5 PVF before switching to DI water. The injected mass (M_I) for each experiment was then calculated by multiplying the mass estimated from the corresponding bypass run (M_{bypass}) by the ratio of feed times (in PVF). Details of the normalization are provided in **Eq. 4.1** below,

$$M_I = M_{bypass} \frac{PVF_{expt}}{PVF_{bypass}} \qquad \textbf{Eq. 4.1}$$

where M_I [M] is the injected mass of O-MWCNTs in the actual transport experiment; M_{bypass} [M] is the mass of O-MWCNTs estimated from the bypass run; PVF_{ex} is the total number of pore volumes fed in the actual experiment, and PVF_{bypass} is the total number of pore volumes fed in the bypass run.

For the pulse-input and step-input method, as with the pulse-input method, the mass of O-MWCNTs recovered from the effluent in "DI" runs was reproducible and similar to the mass obtained in bypass runs (mass balance is 95% - 105%).

4.2.4 *Dissection of Columns*

To promote further understanding of the deposition properties of O-MWCNTs, the amount of O-MWCNTs deposited on each unit mass of glass spheres was obtained by

analyzing the O-MWCNT retention profile after each step-input transport experiment through dissection of the column. As previously mentioned, the step-input method was used in these experiments to increase the recoverable amount of deposited O-MWCNTs. After completion of a transport experiment, the column was kept vertical while the stopper and stainless steel screen at the bottom of the column was removed. The stopper at the top of the column was kept in place during this process and a feed solution of the same background electrolyte concentration as the one used during the transport experiment was then pumped into the column from the top at a flow rate of 1 mL/min. The in-flowing water did not flow through the porous media, but rather created a region of high pressure at the top of the column that served to push the glass beads downward without distorting their relative position or affecting the deposited O-MWCNTs' locations relative to the beads. Glass beads pushed out of the column were collected in 0.25- to 0.5-cm increments as they emerged from the bottom end by slicing the beads with a thin-edged razor blade. These samples were then stored in small 20-mL screw-cap vials for analysis.

To determine the quantity of CNTs deposited during a transport experiment, the collected samples of O-MWCNT-laden glass beads were first immersed in 3 mL of 1% Triton X100 solution and shaken for 3 hours. The supernatant was then transferred into another clean vial and sonicated for 10 min to ensure that all the O-MWCNTs were dispersed. After sonication the solutions were injected into the 5-cm path-length cell and scanned using UV-Vis over the wavelength range of 200 nm to 900 nm. As shown in **Figure 4.2,** the O-MWCNT concentration in a

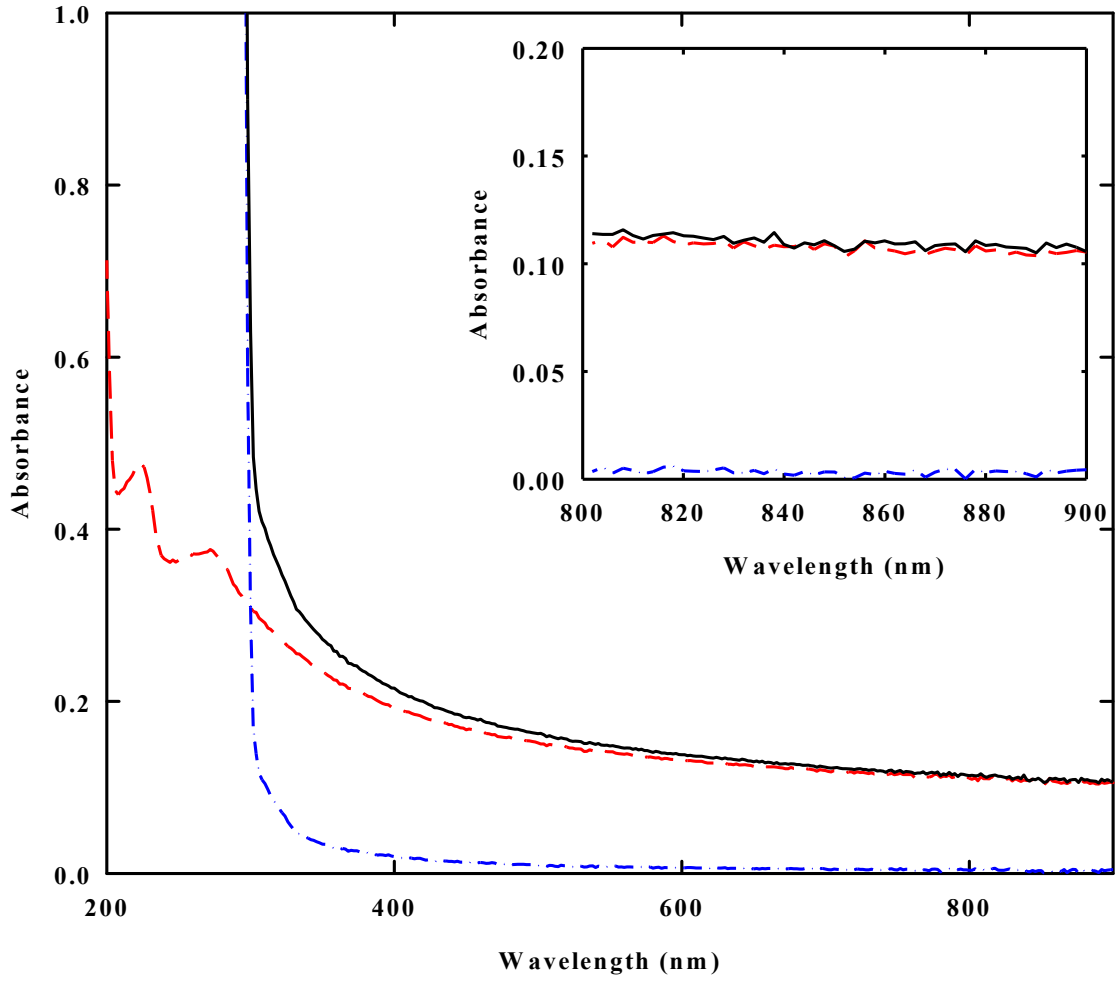

Figure 4.2. UV-vis spectra of solutions containing 5.2 mg/L O-MWCNTs in water (red dashed line), 1% Triton X-100 (blue dash-dot line) and 5.2 mg/L O-MWCNTs plus 1% Triton X-100 (solid black line). The inset shows the region between 800 and 900 nm where Triton X-100 does not show absorption.

sample could be determined by measuring the sample's average UV-Vis absorbance in the wavelength region between 800 nm and 900 nm, where there was no overlapping absorbance from the surfactant or high baseline noise. In this regard, the use of the long path length UV-Vis cell was important because of its ability to increase the sensitivity of O-MWCNT detection. Once the concentration of O-MWCNTs (C_L) in the supernatant from each column segment had been ascertained, the mass of O-MWCNTs per unit mass

of glass beads (solid concentration of O-MWCNTs, C_s) could be determined using **Eq. 4.2**:

$$C_s = \frac{M_D}{M_{Glass\ beads}} = \frac{C_L V_S}{M_{Glass\ beads}} \quad \textbf{Eq. 4.2}$$

where M_D is the mass of deposited O-MWCNTs, V_S is the volume of the supernatant, $M_{Glass\ beads}$ is the mass of glass beads. These results were then plotted against the distance of each glass bead segment from the column inlet to obtain a retention profile of O-MWCNTs.

The total mass balances of O-MWCNTs in the transport experiments were calculated in **Eq. 4.3** as follows:

$$\text{Mass balance} = \frac{M_{BTC} + M_{RP}}{M_I} \times 100\% \quad \textbf{Eq. 4.3}$$

where M_{BTC} [M] is the total mass of effluent O-MWCNTs estimated from breakthrough curves; M_{RP} [M] is the total mass of retained O-MWCNTs estimated from retention profiles. The mass balance for transport experiments with both BTCs and retention profiles is showing in **Table 4.1**.

Table 4.1. Mass balance of transport experiments with BTCs and retention profiles

Background ionic strength (mM)	Input mass of O-MWCNTs (µg)	Mass of O-MWCNTs obtained from BTC ((µg)	Mass of O-MWCNTs obtained from retention profile ((µg)	Mass balance (%)
5	92.9	80.4	17.5	105.3%
10	123.2	88.6	36.3	101.4%
40	92.1	36.0	47.6	90.9%
60	46.3	11.0	29.1	86.5%
375	76.0	6.25	55.5	81.3%

4.3 Interpretive Models and Quantitative Analysis

4.3.1 *Estimation of Dispersion in the Column System*

a. Exclusion of dispersion introduced by flow-through cuvette

Breakthrough curves in transport experiments were obtained by monitoring a 5-cm flow-through cuvette. The flow-through cuvette is a chamber with an inner volume of ~1.2 mL. Given that the total flow-rate was 7 mL/min for all experiments except those conducted to investigate velocity effects, it is reasonable to assume that the cuvette acted as a completely mixed flow reactor. With the assumption that no dead space was present in the reactor, the relationship between concentrations in the influent to the cuvette (C_{in}) and the effluent from the cuvette (C_e) would be expressed by **Eq. 4.4**,

$$\frac{dC_e(t)}{dt}V = QC_{in}(t) - QC_e(t) \qquad \textbf{Eq. 4.4}$$

where Q [L^3/T] is the volumetric flow-rate in experiments and V [L^3] is the volume in the flow-through cuvette.

The effect of the flow-through cuvette on the breakthrough curves can then be corrected using a numerical simulation method as shown in **Eq. 4.5** as follows:

$$QC_{in,ave} = QC_{e,ave} + \frac{\Delta C_e}{\Delta t}V \qquad \textbf{Eq. 4.5}$$

where $C_{in,ave} = \frac{C_{in}(t) + C_{in}(t+\Delta t)}{2}$, $C_{e,ave} = \frac{C_e(t) + C_e(t+\Delta t)}{2}$.

b. Estimation of diffusion coefficient using tracer breakthrough curves

As mentioned above, $NaNO_3$ was occasionally employed as a tracer to explore the hydrodynamic characteristics of the columns used in this study. Since O-MWCNT breakthrough in the "DI" run were found to exhibit shapes identical to those in the tracer runs (**Figure 3.6** in **Chapter 3**) and since such DI runs were conducted prior to every

column experiment and showed excellent mass balance, breakthrough curves from these "DI" runs were used to estimate the dispersion coefficient, *D*, for each column. The one-dimensional convection-diffusion equation for inert compounds (i.e., no decay or production processes during transport)[36] used for the simulation is shown in **Eq. 4.6**,

$$\frac{\partial C(x,t)}{\partial t} = D\frac{\partial^2 C(x,t)}{\partial x^2} - v\frac{\partial C(x,t)}{\partial x} \qquad \textbf{Eq. 4.6}$$

where $C(x, t)$ [M/L^3] stands for the aqueous concentration of O-MWCNT at time t [T] in a water parcel whose distance from the column inlet is x [L]; D [L^2/T] is the hydrodynamic dispersion coefficient; and v [L/T] is the pore water velocity. The effluent concentration of O-MWCNTs from a column with fixed length L at time t after a dirac pulse-input method can then be expressed in **Eq. 4.7** by solving for **Eq. 4.6**,[47]

$$C(t) = C_0\tau\frac{L}{\sqrt{\pi t^3 D}}\exp\left[\frac{(L-vt)^2}{4Dt}\right] \qquad \textbf{Eq. 4.7}$$

where C_0 [M/L^3] is a characteristic concentration defined as M_0/V_{pore}; M_0 [M] is the injected mass of O-MWCNTs in the transport experiment, which is recovery from the bypass experiment; V_{pore} is the aqueous pore volume within the column [L^3]; τ is the mean hydraulic retention time ($\tau = V_{pore}/Q$, [T], where Q is the volumetric flow rate of the feed solution [L^3/T]); and L is the column length [L]. The dispersion coefficient D for transport experiments using pulse-input method can then be estimated by fitting breakthrough curves from "DI" runs with **Eq. 4.7**. At a flow-rate of 7 mL/min, ten breakthrough curves obtained from columns of each length (5.2 cm or 10.2 cm) were fit to obtain the average value of D in order to ensure the most accuracy. Since the hydrodynamic dispersion coefficient D is identical for columns with identical physical characteristics at identical flow-rates, the values of D obtained from pulse-input method

were also used in quantitative estimation of results obtained using step-input methods. For experiments conducted at a flow-rate other than 7 mL/min, values of *D* were estimated specifically for each column using breakthrough curves from the "DI" runs.

4.3.2 *Estimations of O-MWCNT Deposition Mechanism for Experiments Using Pulse-Input Method*

a. Estimation of first order deposition rate coefficient, k_d

The presence of background electrolyte causes O-MWCNTs to deposit onto the surface of collectors. The one-dimensional convection-diffusion equation that includes the deposition process is as shown in **Eq. 4.8**.[36]

$$\frac{\partial C(x,t)}{\partial t} + \frac{\rho_b}{\varepsilon}\frac{\partial S(x,t)}{\partial t} = D\frac{\partial^2 C(x,t)}{\partial x^2} - v\frac{\partial C(x,t)}{\partial x} \qquad \textbf{Eq. 4.8}$$

where the effect of deposition is accounted by $S(x, t)$ [M/M], which is the solid-associated concentration of O-MWCNTs at time t and distance x from the column inlet. In this equation,, ρ_b [M/L^3] and ε are the bulk density and porosity of the porous media, respectively.

Conventional CBF model was applied to quantitatively interpret results obtained from transport experiments using the pulse-input method. The assumption of first-order irreversible deposition (clean bed) can be held for transport experiments conducted at low IS (< 40 mM) using the pulse-input method because of the combination of small mass of O-MWCNTs injected into the column and α <1. (See **Chapter 3**) Under CBF conditions, the removal or the accumulation rate of the deposited O-MWCNTs can be calculated through the use of **Eq. 4.9**,

$$\frac{\rho_b}{\varepsilon}\frac{\partial S(x,t)}{\partial t} = k_d C(x,t) \qquad \textbf{Eq. 4.9}$$

where k_d [T^{-1}] is the deposition rate coefficient. Therefore, the convection-diffusion equation becomes **Eq. 4.10** as shown below,

$$\frac{\partial C(x,t)}{\partial t} = D\frac{\partial^2 C(x,t)}{\partial x^2} - v\frac{\partial C(x,t)}{\partial x} - k_d C(x,t) \qquad \textbf{Eq. 4.10}$$

The analytical solution to **Eq. 4.10** for column subjected to a dirac pulse-input method is well-known.[8, 47] The expression, which applies towards modeling the effluent concentration of O-MWCNTs under conditions of CBF, is shown in **Eq. 4.11**:

$$C(t) = C_0\tau\frac{L}{\sqrt{\pi t^3 D}}\exp(-k_d t)\exp\left[\frac{(L - v_p t)^2}{4Dt}\right] \qquad \textbf{Eq. 4.11}$$

The estimation of k_d can then be obtained by fitting the breakthrough curves from the pulse-input method to **Eq. 4.11** using a nonlinear least-squares analysis.

b. <u>Relationship of single collector removal efficiency and approach velocity</u>

Once the deposition rate coefficient (k_d) is obtained, the single collector removal efficiency $\eta\eta$ can be calculated using **Eq. 4.12**, [48, 49]

$$k_d = \frac{3}{4}\frac{(1-\varepsilon)^{1/3}}{a_c}\eta v \qquad \textbf{Eq. 4.12}$$

where a_c [L] is the collector radius. As mentioned previously, the attachment efficiency, α, is an empirical parameter used to explain the effect of double layer interactions while predicting the experimental single collector removal efficiency η from the η_0 values (single collector contact efficiencies) that are presumed by filtration theory to apply for conditions of favorable deposition:[48, 50]

$$\eta = \alpha\eta_0 \qquad \textbf{Eq. 4.13}$$

where η_0 is the theoretical single collector contact efficiency, as can be calculated for ideal collectors and particles using approaches such as those described by Tufenkji *et*

al.[50] At constant pH and IS, α is a constant, so η is then proportional to η_0. As mentioned earlier, η_0 can be approximately calculated by adding individual contributions of different transport mechanisms,[50]

$$\eta_0 = \eta_D + \eta_I + \eta_G \quad \textbf{Eq. 4.14}$$

where η_D is the single collector contact efficiency contributed from diffusion, η_I is that from interception, and η_G η_G is that from sedimentation. Based on theoretical calculations that assume spherical collectors and particles, the relationships between the three η_i (i = D, I, G) and the fluid interstitial velocity (v) are given by **Eq. 4.15** through **Eq. 4.17**:[50]

$$\eta_D \propto v^{-0.715} \quad \textbf{Eq. 4.15}$$

$$\eta_I \propto v^{-0.125} \quad \textbf{Eq. 4.16}$$

$$\eta_G \propto v^{-1.11} \quad \textbf{Eq. 4.17}$$

Combining **Eq. 4.12** with **Eq. 4.15** through **Eq. 4.17**, the relationships between k_d and v can be easily obtained:

$$k_d \propto v^{0.285} \quad \textbf{Eq. 4.18}$$

$$k_d \propto v^{0.875} \quad \textbf{Eq. 4.19}$$

$$k_d \propto v^{-0.11} \quad \textbf{Eq. 4.20}$$

Although the above equations were derived using calculations that assume spherical particles and collectors, it is unclear as to how sensitive the exponents will be to particle shape.[21] For our current purpose, we assume that O-MWCNTs will rotate in sheared flow and effectively occupy a spherical volume. We therefore believe that the above exponents may be reasonably correct. If so, one can examine the observed relationship between k_d

and *v*, to make a reasonable speculation in regard to the dominant mechanism(s) of the transport behavior.

4.3.3 *Quantitative Analysis for Results Obtained from Transport Experiments Using Step-Input Method*

When step-input methods are employed and injected amounts of O-MWCNTs are much greater, the tenets of CBFT may no longer hold, even for the idealized and uniform spherical beads used in this work. Under these circumstances, the mathematical simulation of O-MWCNT removal can become much more complicated. In particular, other mechanisms need to be taken into account and mathematically approximated in order to explain the breakthrough curves and retention profiles obtained from experiments using this method.

In this study, a numerical method was applied to quantitatively simulate and analyze the breakthrough curves and retention profiles. Modification of the CBF model involved applying additional terms to the transport equation (**Eq. 4.10**) and then using numerically generated solutions under varied experimental conditions. Toward this end, identical parameter sets were applied to the paired combinations of (1) temporal breakthrough curve results and (2) final spatial profile of retained particles at the end of the breakthrough test. As mentioned above, the value of *D* was obtained by analyzing breakthrough curves obtained using pulse-input method at an identical flow-rate and column lengths. The injected mass of O-MWCNTs was estimated from the "bypass" run of each transport experiment.

Estimation of deposition rate and other mechanistic parameters of deposition were then conducted by first simulating the BTC and retention profile with numerical

integration and then minimizing the combined errors between model simulations and data for both the breakthrough and retention profile concentration results with optimization routine. Optimization was achieved using the non-constrained optimization function fmin in MATLAB, which achieves minimization based on golden section search parabolic interpolation.[51] Since the numbers of data points in breakthrough curves were much greater than those in retention profiles, the objective function for optimization was the sum of the *weighted* total error, in which the total relative squared error for breakthrough curves and retention profiles were each divided by their sample sizes as a means of weighting prior to combination.

a. CBF model

The conventional CBF model was the first one applied to analyze the step-based breakthrough curves and retention profiles. The value of the deposition rate coefficient k_d was obtained by fitting **Eq. 4.10** using the aforementioned weighted optimization method.

b. CBF model with additional site-blocking

As discussed subsequently, CBF modeling alone could only partially explain the experimental results. One major case when the method failed was at low IS (< 40 mM), where the BTCs showed increasing plateaus. The increasing plateaus seem to imply that rates of deposition are decreasing over time, as might be associated with decreasing availability of deposition sites. In this regard, it is possible that there is only limited (finite) supply of the "preferred" cites at low IS. As previously discussed in **Chapter 3**, the soda-lime glass beads used to simulate porous media contained ~15% impurities, including magnesium oxides, calcium oxides, magnesium silicate, and other metal oxides according to the manufacturer and shown in the TEM images (**Figure 3.1**). These

impurities are likely to be associated with heterogeneity of surface charge on the collectors (glass beads), most of which are metal oxides as detected in the supernatant after sonicating glass beads (**Figure 3.1**). In this regard, the intensive cleaning procedure seemed to reduce the amount of metal oxides (**Figure 3.1**). and homogenize the collector surface at least sufficiently for consistent results to be obtained for different batches of collectors. Nonetheless, however, the relatively dilute acid was unable to completely remove all impurity sites on the collector surface. A reasonable hypothesis may be that experiments with the pulse-input method would be relatively less affected by these heterogeneities than step-input experiments because of the much smaller amount of injected O-MWCNTs with the pulse approach. In this regard, the hypothesis is that deposition sites formed by metal oxides and silica could be mathematically simulated as effectively "infinite" for the Dirac pulse experiment – that is, their concentrations are sufficiently high as to be unaffected by "blocking." With this reasoning, the assumption of CBFT could be satisfied for the pulse experiments and a combined first-order deposition rate coefficient would be obtained. By contrast, however, the step-input method leads to injected amounts of O-MWCNTs that are 20 or more times greater than those in the pulse-input methods such that the clean-bed assumption may no longer be valid. In particular, one may speculate that the numbers of retained O-MWCNTs can be sufficiently high as to effectively block some important fraction of the higher energy deposition sites, as perhaps associated with iron and other metallic impurities on the collector surface. This phenomenon has been reported in prior literature, some of which has reported effective use of a site-blocking model to explain the effects.[11, 22]

In terms of simulation of deposition-site blocking, the Langmuirian isotherm model has been one of the most commonly used approaches.[11] With this approach, a maximum capacity of sites on the collector is assumed, and the "filling" of these sites by deposited particles is assumed to affect on-going deposition rate in ways similar to the monolayer coverage assumed in the Langmuir adsorption model. For the study reported here, for example, we may assume that the amount of surface area comprised of metal oxides is limited, but that the total amount of silica surface is sufficiently large as to be effectively modeled as infinite. This is reasonable given that the total estimated surface area of deposited O-MWCNTs is less than 1% of the total surface area of the glass beads. With this model, then, the combined first order deposition rate coefficient needs to be separated into two terms as shown in **Eq. 4.21**,

$$\frac{\partial C(x,t)}{\partial t} = D\frac{\partial^2 C(x,t)}{\partial x^2} - v\frac{\partial C(x,t)}{\partial x} - k_d C(x,t) - k_b \psi_b C(x,t) \qquad \textbf{Eq. 4.21}$$

where k_b [T^{-1}] is the deposition rate coefficient due to the limited sites and ψ_b is the ratio of *available* number of metal-oxide deposition sites on the collector surface relative to the *total* number of metal-oxide deposition sites on the collector surface. ψ_b can be quantitatively expressed as shown in **Eq. 4.22**,

$$\psi_b = \frac{S_{max} - S_b(x,t)}{S_{max}} \qquad \textbf{Eq. 4.22}$$

where S_{max} [M/M] is the maximum solid-associated concentration of O-MWCNTs on the impurity sites of collectors, and $S_b(x,t)$ [M/M] is the solid-associated concentration of O-MWCNTs on such sites at time t and distance x from the column inlet.

c. CBF model with additional straining effects

Due to the large aspect ratio of O-MWCNTs and their unique shape as one-dimensional nanomaterials, it is likely that straining may occur. Moreover, the effects of such straining may perhaps represent an even more important fraction of total removal for step feed conditions, owing to the longer period of feed and a perhaps greater initial accumulation of materials at the column inlet. Bradford *et al.*[52] have reported that straining was likely to occur within the first 20% of a column's length and to diminish with distance. In their later research, these authors proposed a straining term in addition to the CBF model as shown in **Eq. 4.23** below, which includes a first-order straining rate coefficient and a factor related to the distance from column inlet:[23]

$$\frac{\partial C(x,t)}{\partial t} = D\frac{\partial^2 C(x,t)}{\partial x^2} - v\frac{\partial C(x,t)}{\partial x} - k_d C(x,t) - k_s \psi_s C(x,t) \qquad \textbf{Eq. 4.23}$$

where k_s [T^{-1}] is the straining rate coefficient and ψ_s [-] is a dimensionless colloid straining function:

$$\psi_s = \left(\frac{a_c + d}{a_c}\right)^{-\beta} \qquad \textbf{Eq. 4.24}$$

Here, d is the distance from the porous medium (column) inlet, and β is a fitting parameter controlling the shape of the colloid spatial distribution.

d. CBF model with additional ripening effects

The large aspect ratio of O-MWCNTs not only increases the likelihood of straining after long-time feeding of O-MWCNT dispersions, but also increases the tendency of interactions between deposited and dispersed O-MWCNTs. In particular, the deposited O-MWCNTs may be likely to have a portion of their length extending out into

the solution and could thus possibly retain dispersed O-MWCNTs as they pass by. This interaction would be significant at high IS, when the electrostatic repulsion between O-MWCNTs is screened and multiple layers of O-MWCNTs can deposit onto collector surfaces. Under these circumstances, breakthrough curves and retention profiles would exhibit decreasing plateaus and hypo-exponential decay, respectively. These phenomena have been reported in prior literature,[30, 31] where they have been modeled by the addition of a "ripening" term to the convection-diffusion. In this study, a simplified deposition coefficient k_r [T^{-1}·M/M], is applied to characterize the ripening phenomenon:

$$\frac{\partial C(x,t)}{\partial t} = D\frac{\partial^2 C(x,t)}{\partial x^2} - v\frac{\partial C(x,t)}{\partial x} - k_d C(x,t) - k_r C(x,t)S(x,t) \qquad \textbf{Eq. 4.25}$$

Note that the ripening effect is a function of both the aqueous concentration of O-MWCNTs, $C(x,t)$, and the concentration of deposited O-MWCNTs, $S(x, t)$. Therefore, the deposition rate coefficient for ripening effect (k_r) has the units [T^{-1}·M/M] ([g/(mg·s]].

e. Combining CBF model with three additional models

An equation employing all three terms of the above has been used in this research and is shown below as **Eq. 4.26**.

$$\frac{\partial C(x,t)}{\partial t} = D\frac{\partial^2 C(x,t)}{\partial x^2} - v\frac{\partial C(x,t)}{\partial x} - k_d C(x,t) - k_b \psi_b C(x,t) - k_s \psi_s C(x,t) - k_r C(x,t)S(x,t)$$

Eq. 4.26

4.4 Results and Discussion

4.4.1 *Estimation of Dispersion*

a. Effect of flow-through cuvette on breakthrough curves

Because the inner volume of the flow-through cuvette is small (1.2 mL), the mixture of solution in the cuvette should not have major impact on the shape of the BTC.

This was proven to be the case by our results. As shown in **Figure 4.3**, the shape of breakthrough curves before and after numerical modification for the exclusion of the flow-through cuvette effect (**Eq. 4.5**) did not change significantly. The BTC did, however, move forward (i.e., forward on the PVF axis) due to the removal of the measurement delay caused by the flow-through cuvette. Since breakthrough curves after this correction represented the actual shape of effluent, these were used in future calculation.

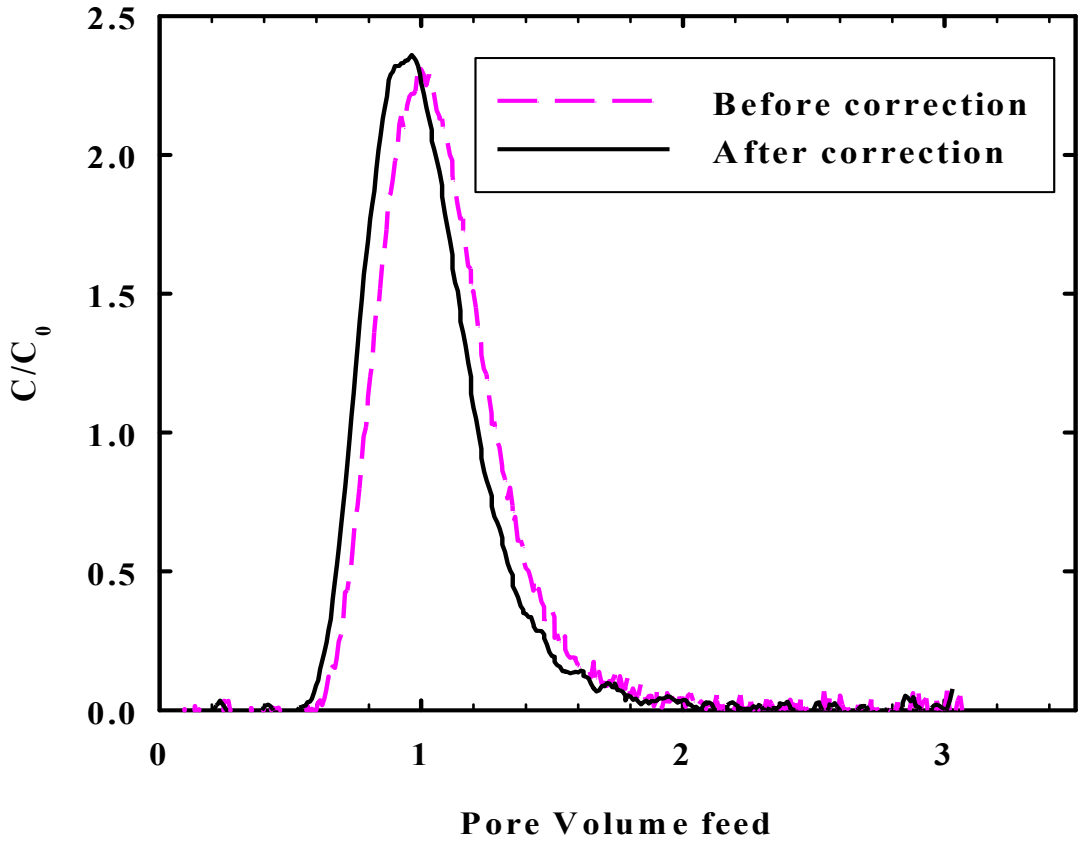

Figure 4.3. Typical breakthrough curves obtained through 10.2 cm column using pulse-input method before and after the correction for the effect of flow-through cuvette using **Eq. 4.5**.

b. Estimation of dispersion coefficient D using "DI" run and O-MWCNTs on "tracers"

As shown in **Figure 4.4**, breakthrough curves from O-MWCNT

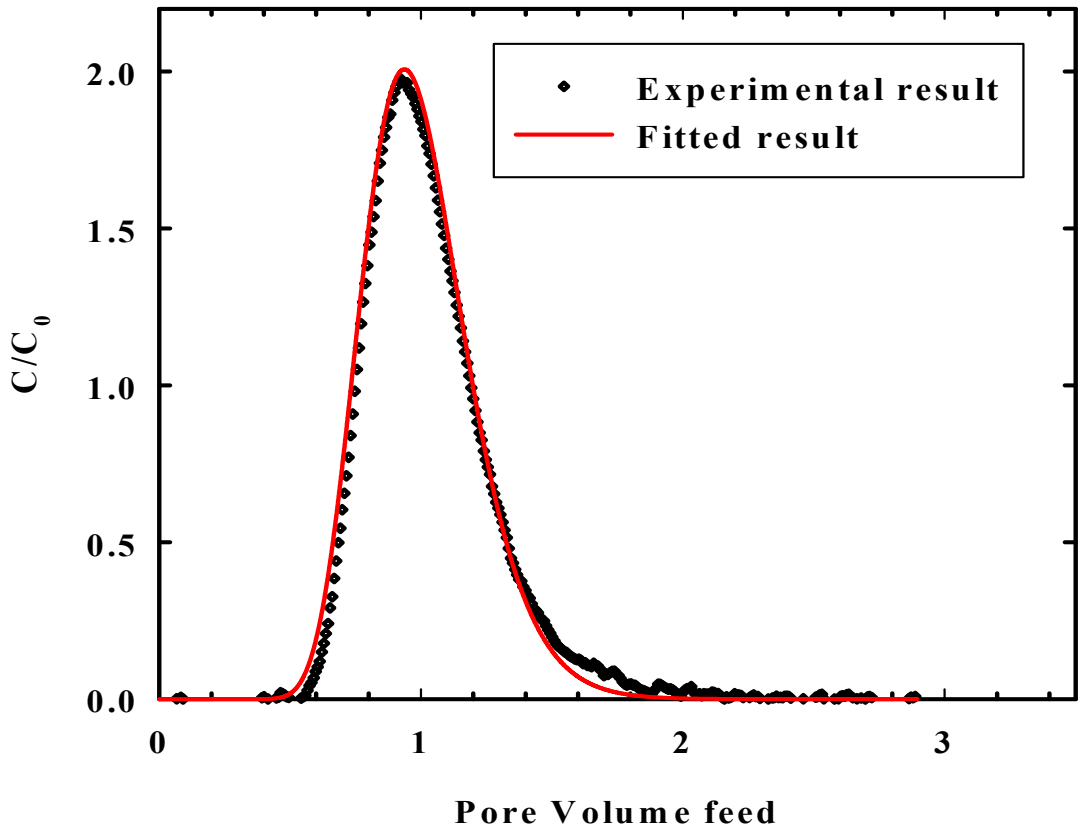

Figure 4.4. Breakthrough curves obtained by passing 7.1% O-MWCNTs through a 10.2 cm column at the flow rate of 7 mL/min and IS of 0 mM. The BTC was fitted using **Eq. 4.7** to obtain the hydrodynamic dispersion coefficient *D*.

transport during the "DI" run could be well fit by **Eq. 4.7**. The values of the hydrodynamic dispersion coefficient *D* for short (5.2 cm) and long (10.2 cm) columns were $(4.24 \pm 0.2) \times 10^{-7}$ m^2/s and $(1.42 \pm 0.15) \times 10^{-6}$ m^2/s, respectively for a flow velocity of 0.0238 cm/s, implying a dipersivity, α_D, of roughly 1.78×10^{-5} m and 5.97×10^{-4} m, respectively, if we assume $D = \alpha_D v^{1.0}$. These values were used subsequently when estimating other parameters such as deposition rate coefficients. Values of D for experiments at flow-rate other than 7 mL/min are provided in **Table 4.2**. α_D values are calculated for all runs and are seen to agree to within roughly a factor of 2.

Table 4.2 Summary of dispersion coefficient D and deposition rate coefficient k_d at varied approach velocity v for transport experiments conducted using 5.2 cm columns at pH 5.8 ± 0.2 and 30 mM NaCl as shown in **Figure 4.5**.

Approach velocity v (m/s)	**Dispersion coefficient D (m^2/s)**	**Dispersivity α_D (m)**	**Deposition rate coefficient k (s^{-1})**
0.007	1.7E-07	2.5E-05	0.015
0.007	1.2E-07	1.8E-05	0.015
0.010	1.9E-07	2.0E-05	0.020
0.012	2.2E-07	1.8E-05	0.023
0.012	2.1E-07	1.7E-05	0.024
0.012	2.4E-07	1.9E-05	0.024
0.018	2.8E-07	1.6E-05	0.033
0.024	4.3E-07	1.8E-05	0.044
0.034	5.8E-07	1.7E-05	0.060
0.048	7.1E-07	1.5E-05	0.082
0.068	7.5E-07	1.1E-05	0.111

4.4.2 *Effect of Approach Velocity on the Deposition Rate Coefficient*

The change of deposition coefficients k_d as a function of approach velocity is shown in **Figure 4.5.** Experiments with altered flow-rate (and therefore changed velocity of

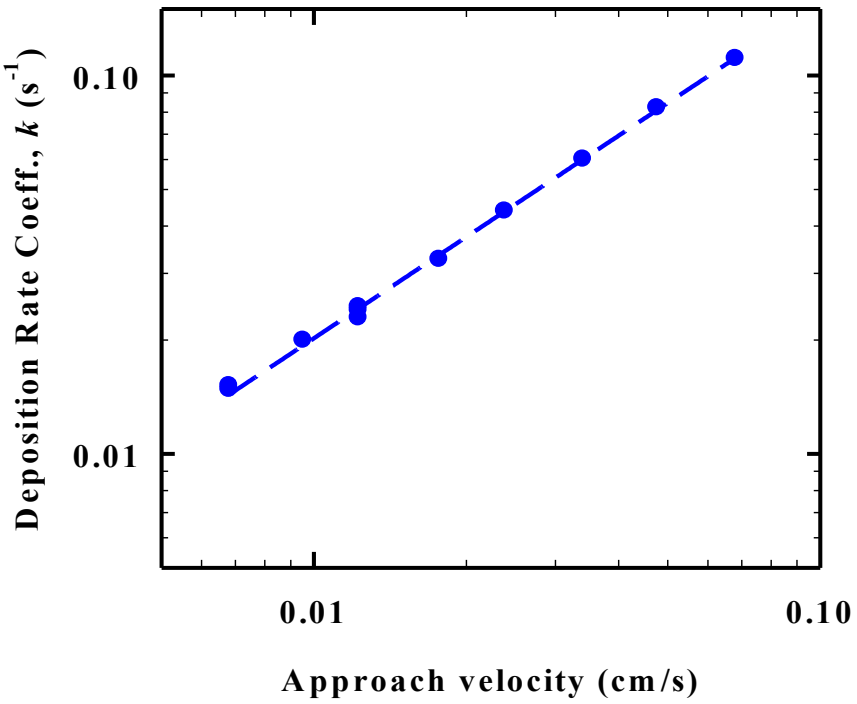

Figure 4.5. Change of deposition rate coefficients of 7.1% O-MWCNTs as a function of approach velocity. The O-MWCNTs were passed through 5.2 cm columns at pH 5.8 ± 0.2 and 30 mM NaCl.

approach) revealed that the deposition rate coefficient of O-MWCNTs increased with approach velocity in a manner found to be consistent with $k_d = 1.22v^{0.89}$. The exponent can be compared with that of the theoretical relation of $k_d \sim v^{-0.875}$ shown in **Eq. 4.19**. The coincidence of the exponent with that derived independently from theory for mechanisms of interception[21] suggests that interception may be the primary removing mechanism of O-MWCNT deposition in the model column used in this study (0.355 – 0.425 mm soda lime silica spheres). This result would not be predicted if the O-MWCNTs were spherical particles with diameters equivalent to their diameters. For spherical particles within the same range of diameter (15 ± 5 nm), diffusion instead of interception is calculated to be the primary removing mechanism.[21] On the other hand, if

O-MWCNTs are considered as spheres with diameters equivalent to their lengths, then the interception mechanism would not be surprising. As shown in previous study, the same type of O-MWCNTs after identical treatment (oxidation and 20 h sonication) exhibited a length distribution ranging from 0.09 μm to 5.81 μm.[44] The majority of O-MWCNTs had diameters between 0.3 μm and 0.7 μm.[44] Thus, interception is the expected collision mechanism if O-MWCNTs rotate out of stream lines of flow and can collide onto the collector by way of "end-on" contact, where the ends of O-MWCNTs contact the collector during deposition. Alternatively, this is also conceivable if the dispersed O-MWCNTs re-aggregated during transport to form small bundles prior to contact and if the effective diameters of these bundles were equal or larger than the length of individual O-MWCNTs such that interception could occur. The hydrodynamic diameter D_h of dispersed O-MWCNT was tested to be ~120 nm and ~180 nm before and after transport experiments, indicating slight aggregation of O-MWCNTs, which suggested the possible formation of small bundles. Although it is possible that some O-MWCNT aggregates with larger D_h might deposite onto the porous media, separately conducted aggregation experiments showed **(Chapter 3)** that severe aggregation would not occur during the time of transport experiments under the given conditions (IS = 30 mM, pH 5.8, O% = 7.1 for O-MWCNTs). Nevertheless, the formation of small bundles is possible. It is noteworthy that Jaisi and Elimelech[47] also conducted similar experiments to investigate the relationship of approach velocity with the deposition rate coefficient of SWCNTs onto columns packed with soil. The authors observed a relationship of $k_d \sim v^{-0.65}$, closely consistent with the deposition of soil-mobilized colloids observed in prior literature ($k_d \sim v^{-0.6}$)[36], but substantially different from the diffusion dominated removal

($k_d \sim v^{-0.33}$) or the interception dominated removal ($k_d \sim v^{-0.875}$).[21, 36] Jaisi and Elimelech attributed this discrepancy to a straining effect, which they assumed to be a dominant effect in columns packed with soil.[47] In the case of this study, however, we believe that the straining effect is not the primary contributor to O-MWCNT removal due to the application of spherical glass beads as collectors, A more detailed analysis of the potential role of straining under different conditions is provided in section 4.4.4(c).

4.4.3 *Analysis of Breakthrough Curves and Retention Profiles*

Breakthrough curves and retention profiles of transport experiments conducted at IS of 5, 10, 40, 60 and 357 mM are shown in **Figure 4.6**. As mentioned above and seen in **Figure 4.6**, the total PVF were different for varied experiments. The discrepancy in PVF

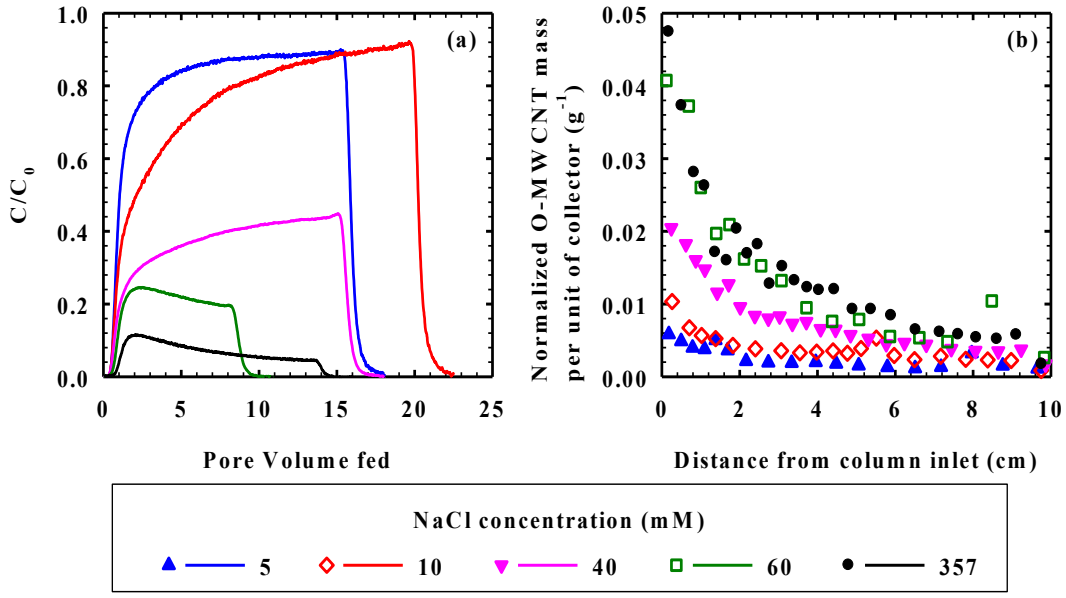

Figure 4.6. (a) Breakthrough curves and (b) retention profiles obtained by passing 7.1% O-MWCNTs through 10.2 cm columns at varied NaCl concentrations (pH = 5.8± 0.2).

as well as the varied IS in those experiments resulted in discrepancy in the total mass of deposited O-MWCNTs. Larger amount of O-MWCNTs were deposited for experiments

that were conducted at higher IS or that ran for a longer period of time. In order to compare the pattern of retention profiles obtained under different experimental conditions, the solid concentrations of O-MWCNTs (mass of O-MWCNTs per unit mass of glass beads) were normalized by dividing absolute solid concentrations by the total injected mass of O-MWCNTs. Results shown in **Figure 4.6** provide evidence that the assumption of CBFT, which was previously found to be valid for the pulse-input method, was partially violated for results using step-input method. As previously discussed, this is presumed to be the result of the long pore volume applied in these experiments. Both blocking (for IS of 5, 10 and 40 mM) and ripening (for IS of 60, 357 mM) phenomena were observed in breakthrough curves. At the same time, hypo-exponential decay phenomenon was observed in the retention profiles, especially for those at high IS (for IS of 60, 357 mM).

4.4.4 *Numerical Simulation Using Traditional CBF Model and Additional Models*

As mentioned above, site-blocking, straining and ripening terms in addition to simple means of CBF have been reported in previous research.[4, 5, 8, 23, 27, 29, 31] Such terms were employed in this study to interpret observations of increasing or decreasing plateau and hypo-exponential decay in retention profiles. Simulations conducted using CBF model alone, CBF and each of three additional models (site-blocking model, straining model and ripening model), as well as CBF and all three additional models are summarized in **Table 4.3** and shown in **Figure 4.7**. The advantages and disadvantages of each model are discussed as below.

Table 4.3. Simulated results using traditional CBFT, CBFT and site-blocking model, CBFT and straining model, CBFT and ripening model and all four models.

Simulation using CBFT					
IS (mM)	5	10	40	60	357
k_d (s^{-1})	0.032	0.040	0.076	0.092	0.12
$k_{d,ex}$ (s^{-1})	0.032	0.040	0..075	0.095	0.12
Simulation using CBFT and site-blocking model					
k_d (s^{-1})	0.029	0.031	0.072	0.095	0.12
k_b (s^{-1})	0.041	0.070	0.054	0.065	0
S_{max} (mgCNT/kg glassbeads)	0.26	0.71	1.00	0.057	N/A
Simulation using CBFT and straining model					
k_d (s^{-1})	0.032	0.040	0.075	0.095	0.12
k_s (s^{-1})	0.58	0.41	11.6	11.1	0
B	1.61	1.61	2.12	2.1	N/A
Simulation using CBFT and ripening model					
k_d (s^{-1})	0.032	0.040	0.076	0.092	0.115
k_r (s^{-1})	0	0	0	0.015	0.015
Simulation using all four models					
k_d (s^{-1})	0.019	0	0.043	0.082	0.11
k_b (s^{-1})	0.042	0.072	0.056	0.064	0.096
S_{max} (mgCNT/kg glassbeads)	0.23	0.69	0.85	0.12	0.046
k_s (s^{-1})	0.11	0.25	0.17	0.41	0
β	0.64	1.2	0.48	1.25	N/A
k_r (s^{-1})	0	0.011	0	0.019	0.016

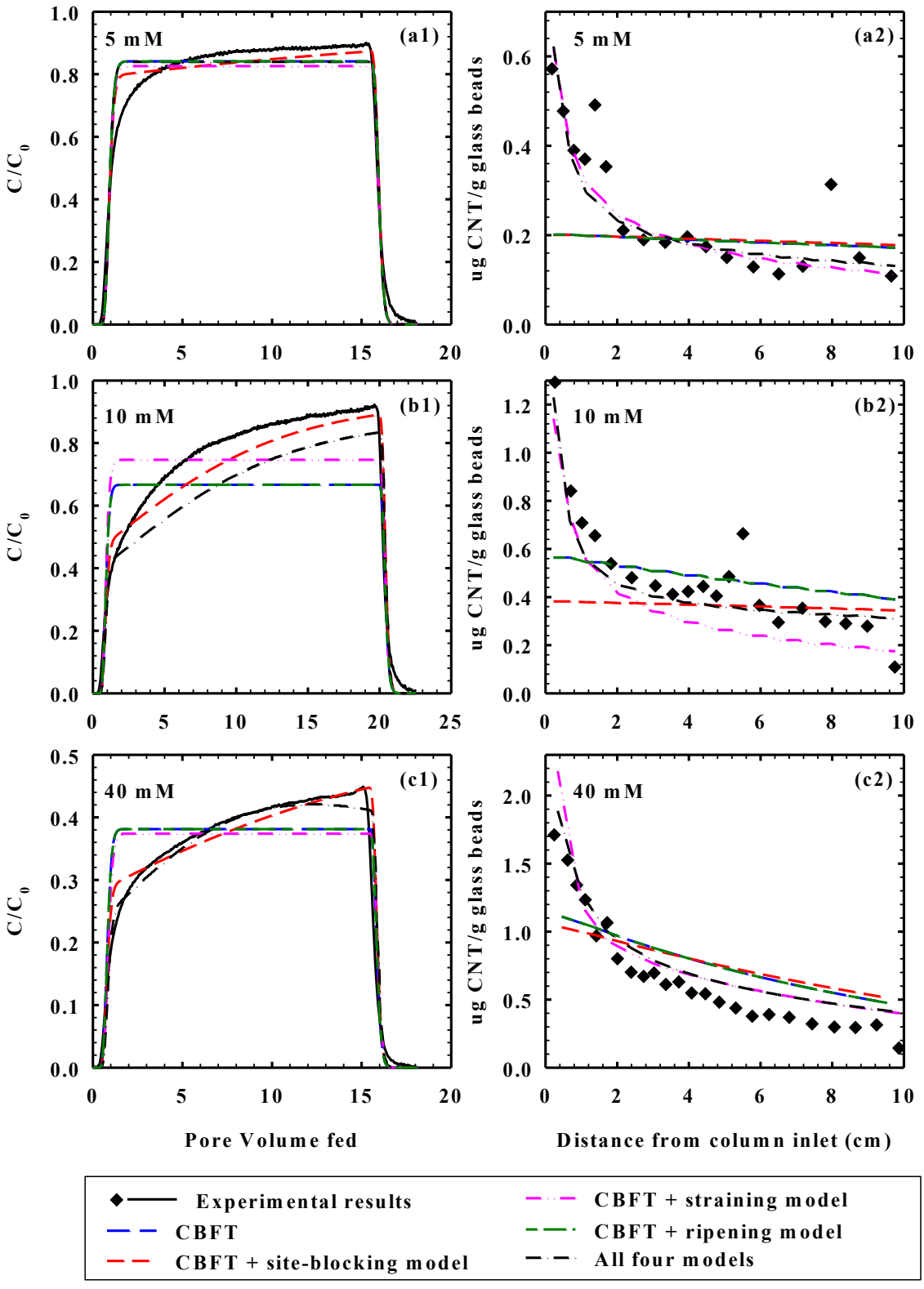

Figure 4.7. (continued on next page)

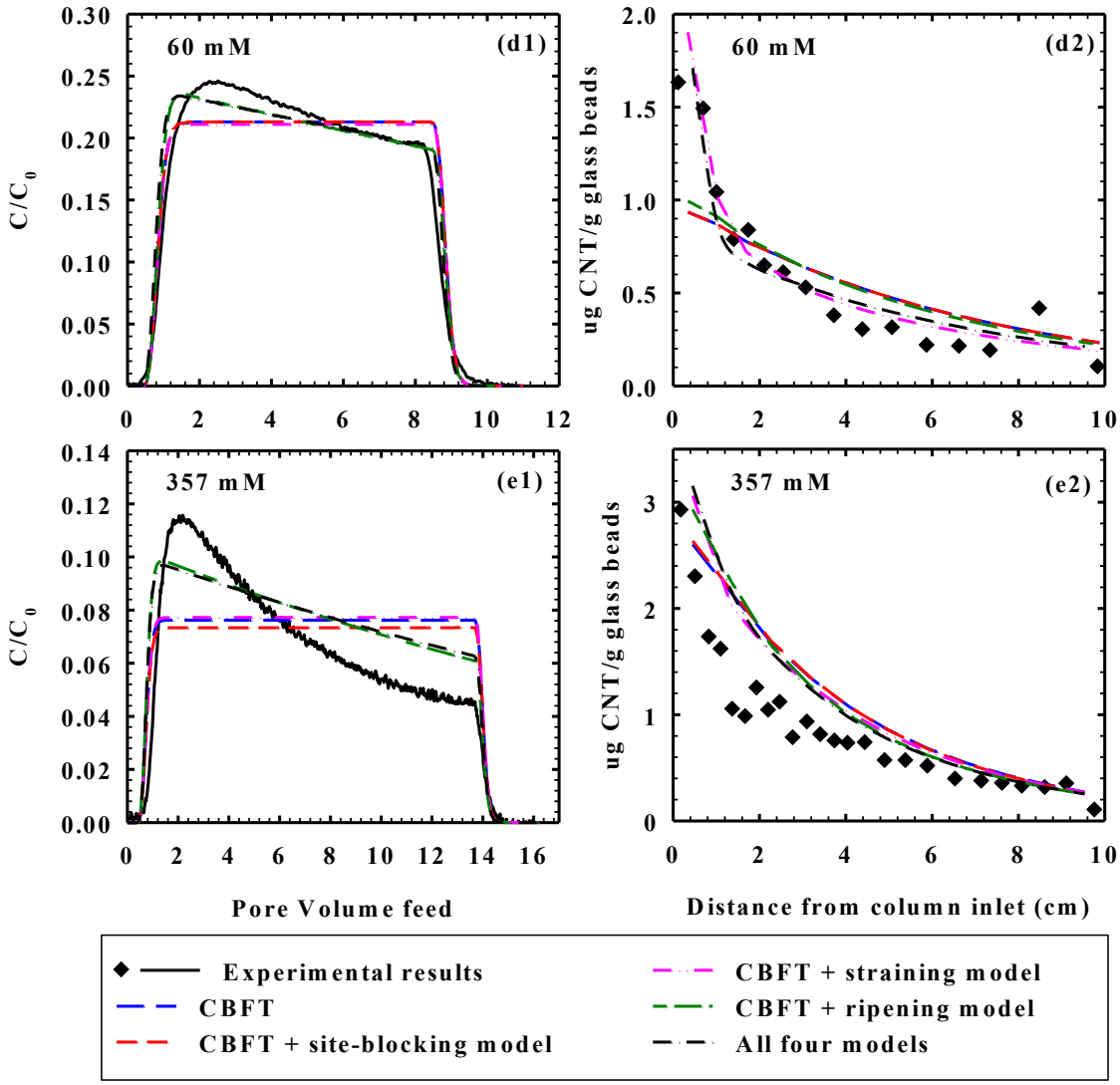

Figure 4.7. (Continued from prior page) Breakthrough curves and retention profiles obtained by passing 7.1% O-MWCNTs through 10.2 cm columns at pH 5.8± 0.2 and NaCl concentrations of (a) 5 mM, (b) 10 mM, (c) 40 mM (d) 60 mM and (e) 357 mM. Experimental results were each fitted with four models as illustrated in text.

a. Numerical Simulation Using CBF Model

The breakthrough curves simulated using this theory exhibited a completely flat plateau, and were thus not consistent with many of the experimental results obtained with step-input (**Figure 4.7**). The retention profiles simulated using this theory exhibited a

trend of exponential decay with increasing distance from column inlet. The decay rates observed in the retention profiles were found to be higher than theoretical. Although the simulation was not accurate, the fitted deposition rate coefficient k_d still exhibited a clear increasing trend with increasing IS as shown in **Table 4.3**, indicating that the DLVO theory still played a significant role in deposition of O-MWNTs onto glass beads. However, additional model components are needed to fully explain the observed results.

b. Numerical simulation using CBF and an additional site-blocking term

As shown in Figure 2.2, the breakthrough curves obtained at low IS ($\leqslant$ 40 mM) all exhibited obvious blocking phenomena. The site-blocking model (**Eq. 4.21**) was therefore applied. For results obtained from each transport experiment, k_d, k_b, and S_{max} were all obtained by fitting experimental data with **Eq. 4.21**. Since the amount of impurity on collector surfaces should be effectively identical for all of the columns, and given that the parameter S_{max} represents the total concentration of sites from the impurities (known to be mostly metal oxides or metal silicates), S_{max} should be identical regardless of the background ionic strength. Therefore, the simulation was conducted using a fixed amount of the impurity sites, $S_{max,f}$. Since, there was no available experimental approach to independently quantify $S_{max,f}$, the maximum S_{max} obtained by fitting the model to 5 batches of experimental was adopted to be the fixed parameter $S_{max,f}$. Results obtained with $S_{max,f}$ are plotted in **Figure 4.7**. The simulation results of the BTC at IS of 40 mM are also re-plotted in **Figure 4.8** to more clearly show the effects of each model.

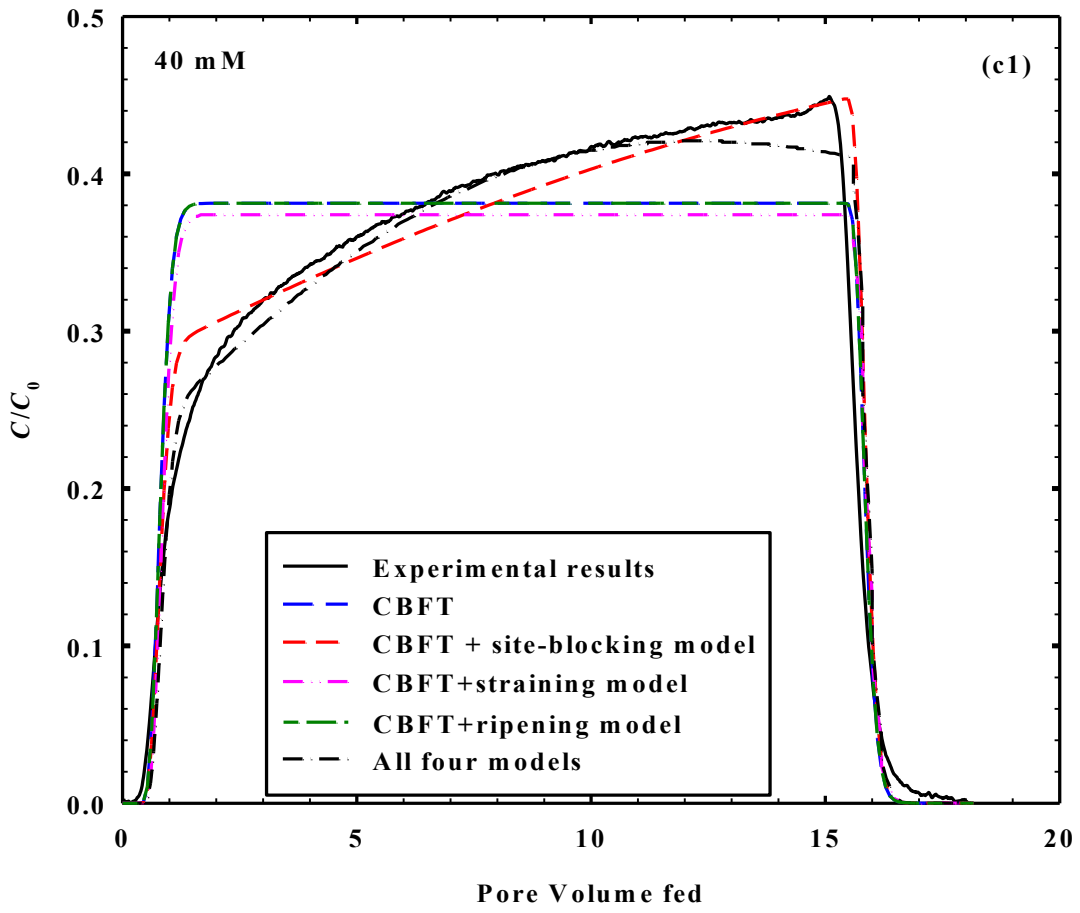

Figure 4.8. Simulation results of BTC obtained at IS = 40 mM. (Same as **Figure 4.7(c1)).**

The site-blocking model was able to catch the phenomena of increasing plateau of the breakthrough curves successfully. However, due to the existence of the maximum capacity of collectors, the simulated retention profile (Figure 4.7(c2)) has a curve that is less steep than the typical exponential decay curve, thus showing that the model still fails to agree with all experimental observations. The results suggest that although blocking is one of the important mechanisms at play, there are other considerations as well. Li *et al.*[11] successfully used a similar model for the quantitative explanation of the transport of C_{60} through quartz sand. In their study, the breakthrough curves of C_{60} showed significantly

increasing plateaus and the retention profiles were flat for observation points at the first several centimeters from the column inlet. Both of these phenomena were consistent with the blocking mechanism. Since C_{60} particles used in their experiments were spherical particles with diameters of 92 ± 0.3 nm, and the IS applied was low enough to prevent multilayer deposition, the site-blocking model in conjunction with CBFT was sufficient to simulate the transport behavior of C_{60}. In the case of O-MWCNTs, however, blocking is apparently not the only mechanism other than CBFT that contributes to the removal of O-MWCNTs.

c. Numerical simulation using CBFT plus straining

Straining has been reported by numerous prior investigators to be a potentially important factor in O-MWCNT transport.[1, 8, 26-28] Although straining effects were not found to be especially significant in the prior pulse-based transport experiments, they appear to have played a relatively more important role in transport experiments of O-MWCNTs under the conditions of step-input, i.e., using a long feeding time and a large total amount of O-MWCNTs. As shown in **Figure 4.7** and re-plotted in **Figure 4.9** (pink dash-dot line), the straining model (**Eq. 4.23**) could explain the high solid concentration of deposited O-MWCNTs at the beginning of columns, especially for results obtained at low IS. It has been reported by Bradford *et al.*[27, 53] that straining effects are only significant at the beginning of the column and should quickly decay with distance from the column inlet since after a certain distance an exclusion effect would force water and remaining particles through larger pores and therefore reduce the straining effect.[23, 52] The decay parameter, β, was used to simulate the diminishing effect of the straining effect with distance. For this study, evidence suggests that the diminishment of straining effects

with distance was particularly pronounced. The values of β obtained by fitting **Eq. 4.23** to experimental results were all significantly larger than those reported by Bradford *et al.*[23] or Wang *et al.*[8], indicating a faster diminishment of the straining effect which effectively limits the role of straining to the first several centimeters of columns. This may relate to our use of spherical collectors -- compared to quartz sands, spherical collectors have more evenly distributed pores that may provide fewer regions conductive to straining. It is conceivable that most straining in our system is due to the fact that water distribution is initially imperfect.

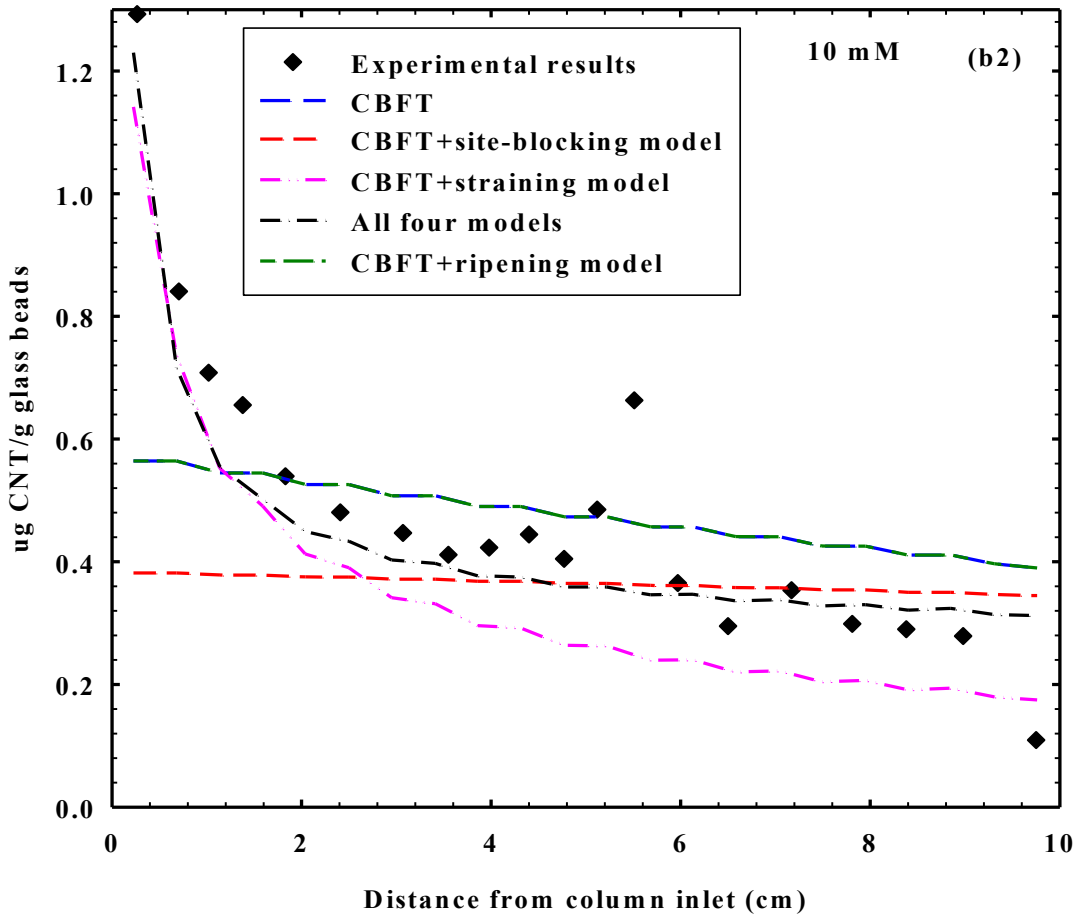

Figure 4.9. Simulation results of retention profiles obtained at IS = 10 mM. (Same as **Figure 4.7(b2)**).

For experiments conducted at high IS, because straining and multilayer deposition could both potentially cause the hypo-exponential decay of the retention profile, the contribution of straining cannot be accurately isolated without also understanding the possible influence of ripening. However, at low IS (< 40 mM) where multilayer effects can be presumed as negligible, it is reasonable to fully attribute the higher O-MWCNT deposition at the beginning of the retention profile to straining.

d. Simulation using CBFT plus ripening

The ripening model used in this research is based on the concept of multi-layer deposition. Since such multi-layer deposition would involve an interaction between the dispersed O-MWCNTs and the deposited O-MWCNTs, the deposition rate coefficient due to ripening (k_r) is considered as a second-order rate coefficient for a rate equation based on the product of both aqueous- and solid-phase concentrations of O-MWCNTs (**Eq. 4.25**). As shown in **Table 4.3**, the fitted values of k_r were large enough to be important only in experiments conducted at high IS (60 mM and 357 mM). This finding is consistent with prior results obtained by other researchers.[29, 31] With the addition of this term, the transport model was able to explain the decreasing plateau of the BTC obtained at high IS as well as the hypo-exponential decay trend exhibited in some retention profiles -- see **Figure 4.7**.Thus, the results suggest that multi-layer deposition becomes the most dominant effect at high IS, where it can be used to explain most of the BTC and retention profile data. As with other models, however, the ripening model alone cannot completely account for all phenomena observed in all transport experiments or even for all aspects of high IS results.

e. Simulation of experimental results using all four models

All three process mechanisms (site-blocking, straining, and ripening) have been proved to be necessary additions to CBFT in interpreting the various experimental results observed in this study. Therefore, **Eq. 4.25** was used to simulate all results as shown in **Figure 4.7**. During the simulation, k_d, k_b, k_s, β, and k_r from **Eq. 4.25** were all fitting parameters but $S_{max,f}$ was fixed at a value of 0.9929 μg/g with method illustrated above. As shown in **Figure 4.7**, experimental results were all reasonably well fit by this combined model.

4.5 Conclusions

Overall, four models, describing including CBF effect, straining effect, site-blocking effect and ripening effect, are all needed to fit the experimental results. The requirement of all four models indicates that transport of O-MWCNTs through soda-lime glass beads is a complex process which can be affected by numerous factors, including the heterogeneous surface of the collectors, the morphology of the dispersed O-MWCNTs, and the interactions among O-MWCNTs and between O-MWCNTs and collectors.

4.6 Cited References

1. Jaisi, D. P.; Saleh, N. B.; Blake, R. E.; Elimelech, M., Transport of Single-Walled Carbon Nanotubes in Porous Media: Filtration Mechanisms and Reversibility. *Environ Sci Technol* **2008,** *42*, (22), 8317-8323.

2. Lecoanet, H. F.; Bottero, J. Y.; Wiesner, M. R., Laboratory Assessment of the Mobility of Nanomaterials in Porous Media. *Environ Sci Technol* **2004,** *38*, (19), 5164-5169.

3. Lecoanet, H. F.; Wiesner, M. R., Velocity Effects on Fullerene and Oxide Nanoparticle Deposition in Porous Media. *Environ Sci Technol* **2004,** *38*, (16), 4377-4382.

4. Wang, Y.; Li, Y.; Fortner, J. D.; Hughes, J. B.; Abriola, L. M.; Pennell, K. D., Transport and Retention of Nanoscale C60 Aggregates in Water-Saturated Porous Media. *Environ Sci Technol* **2008,** *42*, (10), 3588-3594.

5. Liu, X. Y.; O'carroll, D. M.; Petersen, E. J.; Huang, Q. G.; Anderson, C. L., Mobility of Multiwalled Carbon Nanotubes in Porous Media. *Environ Sci Technol* **2009,** *43*, (21), 8153-8158.

6. Rajagopalan, R.; Chu, R. Q., Dynamics of Adsorption of Colloidal Particles in Packed-Beds. *J Colloid Interf Sci* **1982,** *86*, (2), 299-317.

7. Song, L.; Elimelech, M., Dynamics of Colloid Deposition in Porous-Media - Modeling the Role of Retained Particles. *Colloid Surface A* **1993,** *73*, 49-63.

8. Wang, Y. G.; Kim, J. H.; Baek, J. B.; Miller, G. W.; Pennell, K. D., Transport Behavior of Functionalized Multi-Wall Carbon Nanotubes in Water-Saturated Quartz Sand as a Function of Tube Length. *Water Res* **2012,** *46*, (14), 4521-4531.

9. Liu, Y. Y.; Zhang, C. Y.; Hilpert, M.; Kuhlenschmidt, M. S.; Kuhlenschmidt, T. B.; Nguyen, T. H., Transport of Cryptosporidium Parvum Oocysts in a Silicon Micromodel. *Environ Sci Technol* **2012,** *46*, (3), 1471-1479.

10. Baumann, T.; Werth, C. J., Visualization and Modeling of Polystyrol Colloid Transport in a Silicon Micromodel. *Vadose Zone J* **2004,** *3*, (2), 434-443.

11. Li, Y. S.; Wang, Y. G.; Pennell, K. D.; Abriola, L. M., Investigation of the Transport and Deposition of Fullerene (C60) Nanoparticles in Quartz Sands under Varying Flow Conditions. *Environ Sci Technol* **2008,** *42*, (19), 7174-7180.

12. Tufenkji, N.; Elimelech, M., Spatial Distributions of Cryptosporidium Oocysts in Porous Media: Evidence for Dual Mode Deposition. *Environ Sci Technol* **2005,** *39*, (10), 3620-3629.

13. Lanphere, J. D.; Luth, C. J.; Walker, S. L., Effects of Solution Chemistry on the Transport of Graphene Oxide in Saturated Porous Media. *Environ Sci Technol* **2013,** *47*, (9), 4255-4261.

14. Tufenkji, N.; Elimelech, M., Deviation from the Classical Colloid Filtration Theory in the Presence of Repulsive Dlvo Interactions. *Langmuir* **2004,** *20*, (25), 10818-10828.

15. Chowdhury, I.; Hong, Y.; Honda, R. J.; Walker, S. L., Mechanisms of Tio2 Nanoparticle Transport in Porous Media: Role of Solution Chemistry, Nanoparticle Concentration, and Flowrate. *J Colloid Interf Sci* **2011,** *360*, (2), 548-555.

16. Yao, K. M.; Habibian, M. M.; Omelia, C. R., Water and Waste Water Filtration - Concepts and Applications. *Environ Sci Technol* **1971,** *5*, (11), 1105-1112.

17. Derjaguin, B., On the Repulsive Forces between Charged Colloid Particles and on the Theory of Slow Coagulation and Stability of Lyophobe Sols. *Transactions of the Faraday Society* **1940,** *35*, (0), 203-215.

18. Derjaguin, B.; Landau, L., Theory of the Stability of Strongly Charged Lyophobic Sols and of the Adhesion of Strongly Charged-Particles in Solutions of Electrolytes. *Prog Surf Sci* **1941,** *14*, 633.

19. Verwey, E. J. W.; Overbeek, J. T., Theory of the Stability of Lyophobic Colloids. Elsevier: Amsterdam, 1948.

20. Rajagopalan, R.; Tien, C., Trajectory Analysis of Deep-Bed Filtration with Sphere-in-Cell Porous-Media Model. *Aiche J* **1976,** *22*, (3), 523-533.

21. Tufenkji, N.; Elimelech, M., Correlation Equation for Predicting Single-Collector Efficiency in Physicochemical Filtration in Saturated Porous Media. *Environ Sci Technol* **2004,** *38*, (2), 529-536.

22. Johnson, P. R.; Elimelech, M., Dynamics of Colloid Deposition in Porous-Media - Blocking Based on Random Sequential Adsorption. *Langmuir* **1995,** *11*, (3), 801-812.

23. Bradford, S. A.; Simunek, J.; Bettahar, M.; Van Genuchten, M. T.; Yates, S. R., Modeling Colloid Attachment, Straining, and Exclusion in Saturated Porous Media. *Environ Sci Technol* **2003,** *37*, (10), 2242-2250.

24. Tufenkji, N.; Redman, J. A.; Elimelech, M., Interpreting Deposition Patterns of Microbial Particles in Laboratory-Scale Column Experiments. *Environ Sci Technol* **2003,** *37*, (3), 616-623.

25. Li, X. Q.; Lin, C. L.; Miller, J. D.; Johnson, W. P., Role of Grain-to-Grain Contacts on Profiles of Retained Colloids in Porous Media in the Presence of an Energy Barrier to Deposition. *Environ Sci Technol* **2006,** *40*, (12), 3769-3774.

26. Xu, S. P.; Liao, Q.; Saiers, J. E., Straining of Nonspherical Colloids in Saturated Porous Media. *Environ Sci Technol* **2008,** *42*, (3), 771-778.

27. Bradford, S. A.; Simunek, J.; Walker, S. L., Transport and Straining of E-Coli O157 : H7 in Saturated Porous Media. *Water Resour Res* **2006,** *42*, (12).

28. Cushing, R. S.; Lawler, D. F., Depth Filtration: Fundamental Investigation through Three Dimensional Trajectory Analysis. *Environ Sci Technol* **1998,** *32*, (23), 3793-3801.

29. Ryde, N.; Kallay, N.; Matijevic, E., Particle Adhesion in Model Systems .14. Experimental Evaluation of Multilayer Deposition. *J Chem Soc Faraday T* **1991,** *87*, (9), 1377-1381.

30. Privman, V.; Frisch, H. L.; Ryde, N.; Matijevic, E., Particle Adhesion in Model Systems .13. Theory of Multilayer Deposition. *J Chem Soc Faraday T* **1991,** *87*, (9), 1371-1375.

31. Ryde, N.; Kihira, H.; Matijevic, E., Particle Adhesion in Model Systems .15. Effect of Colloid Stability in Multilayer Deposition. *J Colloid Interf Sci* **1992,** *151*, (2), 421-432.

32. Adamczyk, Z.; Siwek, B.; Zembala, M.; Weronski, P., Kinetics of Localized Adsorption of Colloid Particles. *Langmuir* **1992,** *8*, (11), 2605-2610.

33. Davis, C. J.; Eschenazi, E.; Papadopoulos, K. D., Combined Effects of Ca2+ and Humic Acid on Colloid Transport through Porous Media. *Colloid Polym Sci* **2002,** *280*, (1), 52-58.

34. Elimelech, M., Indirect Evidence for Hydration Forces in the Deposition of Polystyrene Latex Colloids on Glass Surfaces. *J Chem Soc Faraday T* **1990,** *86*, (9), 1623-1624.

35. Elimelech, M.; Omelia, C. R., Effect of Electrolyte Type on the Electrophoretic Mobility of Polystyrene Latex Colloids. *Colloid Surface* **1990,** *44*, 165-178.

36. Grolimund, D.; Elimelech, M.; Borkovec, M.; Barmettler, K.; Kretzschmar, R.; Sticher, H., Transport of in Situ Mobilized Colloidal Particles in Packed Soil Columns. *Environ Sci Technol* **1998,** *32*, (22), 3562-3569.

37. Smith, B.; Wepasnick, K.; Schrote, K. E.; Cho, H. H.; Ball, W. P.; Fairbrother, D. H., Influence of Surface Oxides on the Colloidal Stability of Multi-Walled Carbon Nanotubes: A Structure-Property Relationship. *Langmuir* **2009,** *25*, (17), 9767-9776.

38. Fogden, S.; Verdejo, R.; Cottam, B.; Shaffer, M., Purification of Single Walled Carbon Nanotubes: The Problem with Oxidation Debris. *Chemical Physics Letters* **2008,** *460*, (1-3), 162-167.

39. Price, B. K.; Lomeda, J. R.; Tour, J. M., Aggressively Oxidized Ultra-Short Single-Walled Carbon Nanotubes Having Oxidized Sidewalls. *Chem Mater* **2009,** *21*, (17), 3917-3923.

40. Salzmann, C. G.; Llewellyn, S. A.; Tobias, G.; Ward, M. a. H.; Huh, Y.; Green, M. L. H., The Role of Carboxylated Carbonaceous Fragments in the Functionalization and Spectroscopy of a Single-Walled Carbon-Nanotube Material. *Advanced Materials* **2007,** *19*, (6), 883-887.

41. Wang, Z. W.; Shirley, M. D.; Meikle, S. T.; Whitby, R. L. D.; Mikhalovsky, S. V., The Surface Acidity of Acid Oxidised Multi-Walled Carbon Nanotubes and the Influence of in-Situ Generated Fulvic Acids on Their Stability in Aqueous Dispersions. *Carbon* **2009,** *47*, (1), 73-79.

42. Worsley, K. A.; Kalinina, I.; Bekyarova, E.; Haddon, R. C., Functionalization and Dissolution of Nitric Acid Treated Single-Walled Carbon Nanotubes. *J Am Chem Soc* **2009,** *131*, (50), 18153-18158.

43. Chen, K. L.; Smith, B. A.; Ball, W. P.; Fairbrother, D. H., Assessing the Colloidal Properties of Engineered Nanoparticles in Water: Case Studies from Fullerene C-60 Nanoparticles and Carbon Nanotubes. *Environ Chem* **2010,** *7*, (1), 10-27.

44. Smith, B.; Wepasnick, K.; Schrote, K. E.; Bertele, A. H.; Ball, W. P.; O'melia, C.; Fairbrother, D. H., Colloidal Properties of Aqueous Suspensions of Acid-Treated, Multi-Walled Carbon Nanotubes. *Environ Sci Technol* **2009,** *43*, (3), 819-825.

45. Langley, L. A.; Villanueva, D. E.; Fairbrother, D. H., Quantification of Surface Oxides on Carbonaceous Materials. *Chem Mater* **2006,** *18*, (1), 169-178.

46. Wepasnick, K. A.; Smith, B. A.; Schrote, K. E.; Wilson, H. K.; Diegelmann, S. R.; Fairbrother, D. H., Surface and Structural Characterization of Multi-Walled Carbon Nanotubes Following Different Oxidative Treatments. *Carbon* **2011,** *49*, (1), 24-36.

47. Jaisi, D. P.; Elimelech, M., Single-Walled Carbon Nanotubes Exhibit Limited Transport in Soil Columns. *Environ Sci Technol* **2009,** *43*, (24), 9161-9166.

48. Elimelech, M.; Gregory, J.; Jia, X.; Williams, R. A., Particle Deposition and Aggregation : Measurement, Modelling, and Simulation. Butterworth-Heinemann: Oxford ; Boston, 1995; p xv, 441 p.

49. Kretzschmar, R.; Barmettler, K.; Grolimund, D.; Yan, Y. D.; Borkovec, M.; Sticher, H., Experimental Determination of Colloid Deposition Rates and Collision Efficiencies in Natural Porous Media. *Water Resour Res* **1997,** *33*, (5), 1129-1137.

50. Tufenkji, N.; Elimelech, M., Correlation Equation for Predicting Single-Collector Efficiency in Physicochemical Filtration in Saturated Porous Media. *Environmental Science and Technology* **2004,** *38*, (2), 529-536.

51. Forsythe, G. E.; Malcolm, M. A.; Moler, C. B., Computer Methods for Mathematical Computations. Prentice-Hall: 1976.

52. Bradford, S. A.; Yates, S. R.; Bettahar, M.; Simunek, J., Physical Factors Affecting the Transport and Fate of Colloids in Saturated Porous Media. *Water Resour Res* **2002,** *38*, (12).

53. Bradford, S. A.; Bettahar, M., Straining, Attachment, and Detachment of Cryptosporidium Oocysts in Saturated Porous Media. *J Environ Qual* **2005,** *34*, (2), 469-478.

Chapter 5. Sensitivity Analysis of Simulations Conducted for Experimental Results Obtained Using Step-Input Method under Varied Ionic Strengths.

ABSTRACT

Sensitivity analyses were conducted on the modeling approaches presented in Chapter 4 to investigate the contribution and physical meaning of each term in the models and thus to better understand the relative importance of each process under different conditions of aquatic chemistry. Results showed that at ionic strength (IS) < 40 mM, model modifications for site-blocking and straining effects were more important than other effects for simulating observed data. At higher IS (≥ 60 mM), the ripening modification was the only important component needed beyond clean-bed filtration theory (CBFT). Site-blocking, straining and ripening models were all found to be important for accurately simulating O-MWCNT removal at IS = 40 mM. Thus, the sensitivity results suggest that ionic strength is a key variable in determining which mechanistic processes are most important to consider when quantitatively simulating O-MWCNT interactions with silica-based porous media.

5.1 Introduction

As illustrated in **Chapter 4**, good simulation of the transport and retention of oxidized multi-walled carbon nanotubes (O-MWCNTs) under step input conditions required that numerical models based on clean bed filtration theory (CBFT) be amended with terms to account for the additional processes of site-blocking, straining and ripening.

Although each of these three processes was relevant to at least one of our experimental runs, there were many circumstances under which adequate simulation could be achieved with inclusion of only one or two of the additional processes in the model. Therefore, sensitivity analyses were conducted in order to better understand the relative importance of each process under different conditions of aquatic and surface chemistry and to gain more understanding about model sensitivity to parameter values. The results of these sensitivity analyses are presented in this chapter.

5.2 Methodological Approach to Sensitivity Analysis

The analyses presented in this chapter are based on systematic study of the generalized form of the O-MWCNT transport equation that was developed and discussed in **Chapter 4.** The generalized equation is the convection-dispersion equation of transport with three additional terms to account for a second set of site types with site-blocking (term including "k_b" and "ψ"), a new term to account for a possible straining mechanism of removal (*"k_s"* term), and a new term to account for the removal by deposition onto already deposited O-MWCNTs and often referred to as "ripening" ("k_r" term). The overall equation was previously presented as **Eq. 4.26** and is reproduced below as **Eq. 5.1**:

$$\frac{\partial C(x,t)}{\partial t} = D\frac{\partial^2 C(x,t)}{\partial x^2} - v\frac{\partial C(x,t)}{\partial x} - k_{\mathrm{d}}C(x,t) - k_{\mathrm{b}}\psi_{\mathrm{b}}C(x,t) - k_{\mathrm{s}}\psi_{\mathrm{s}}C(x,t) - k_{\mathrm{r}}C(x,t)S(x,t)$$

Eq. 5.1

The contributions of all four processes, first-order "normal" clean-bed deposition (k_{d}), blocking-affected deposition on a sub-set of sites (k_{b}), straining (k_{s}) and ripening (k_{r}) were analyzed by separately lowering each of the identified rate constants to 10% and

50% of its initially fit value. Simulation curves based on those revised values were then plotted together with the best fit of the experimental results as a means of observing the relative influence of the varied term. The effect of the maximum available deposition sites of impurities (S_{max}) used in the term accounting for site-blocking mechanism was also analyzed by increasing its value to infinity, thus fixing the parameter ψ_b at 1.0 as per its definition given below in **Eq. 5.2**. (This was previously provided as **Eq. 4.22**)

$$\psi_b = \frac{S_{max} - S_b(x,t)}{S_{max}} \qquad \textbf{Eq. 5.2}$$

Thus, setting S_{max} to infinity effectively eliminates site-blocking as a mechanism but still includes deposition onto high energy sites as a component of "clean-bed" deposition – in other words, the total deposition rate constant under this condition is effectively $k_d + k_b$.

5.3 Results and Discussions

5.3.1 *Contribution of "Clean-Bed" Deposition*

Figure 5.1 shows a sensitivity analysis in which the contribution of the "clean-bed" deposition term ("k_d" term) is reduced to 10% and 50% of its initial value. This term is referred to as "clean-bed filtration" or CBF hereafter. A clear trend of increasing contribution of CBF with increasing IS was observed. At relatively lower IS (**Figure 5.1** (a) through (c)), the contribution of CBF was negligible, as reflected in no apparent change in model simulated results with major changes in k_d. For IS values of 60 mM and 357 mM, on the other hand, the C/C_0 values associated with the plateaus of the breakthrough curves (BTCs) were found to increase dramatically with decreasing k_d. (from ~0.1 and ~0.2 up to ~0.8 respectively). These results imply that CBF accounts for

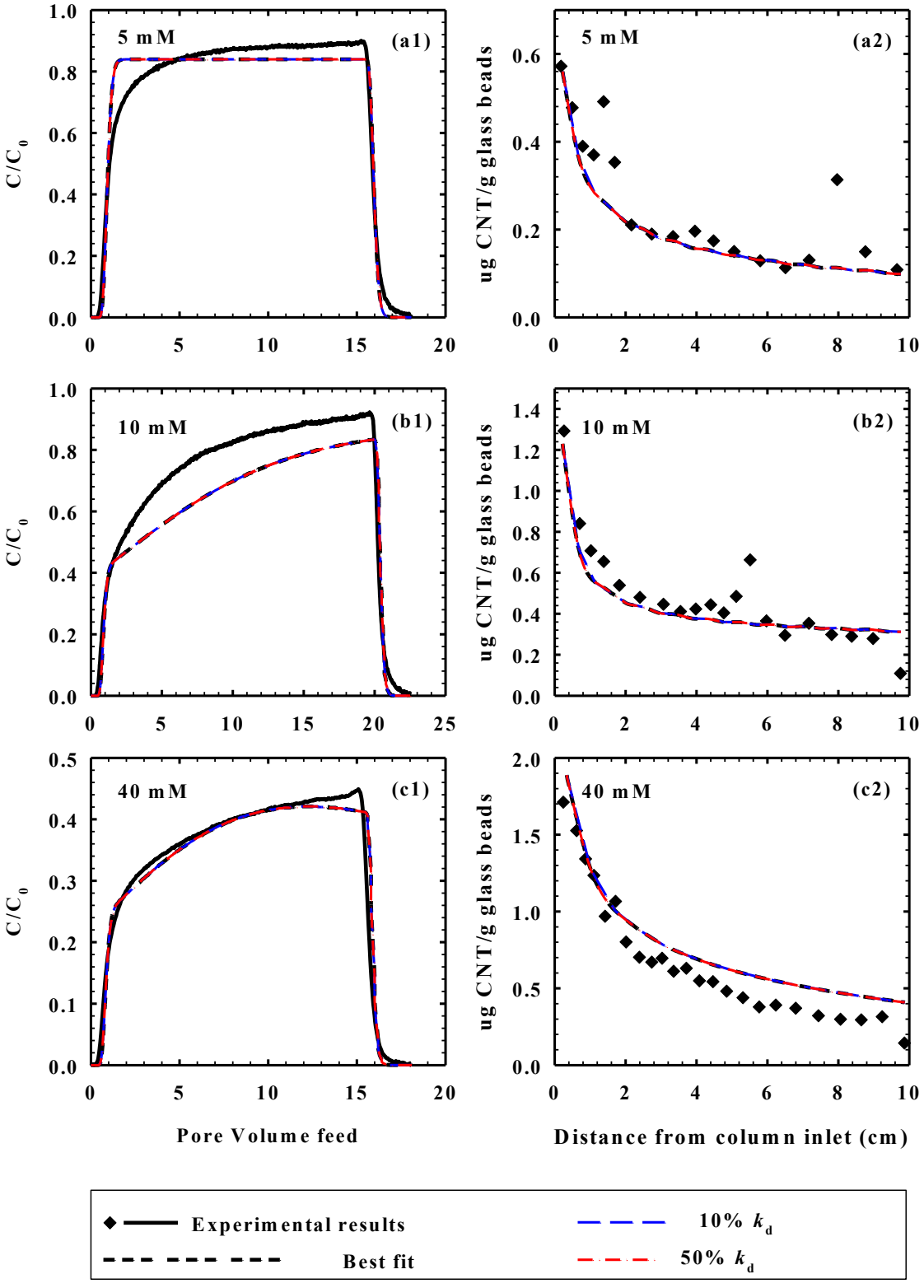

Figure 5.1 (This figure is continued on the next page, where its caption is provided.)

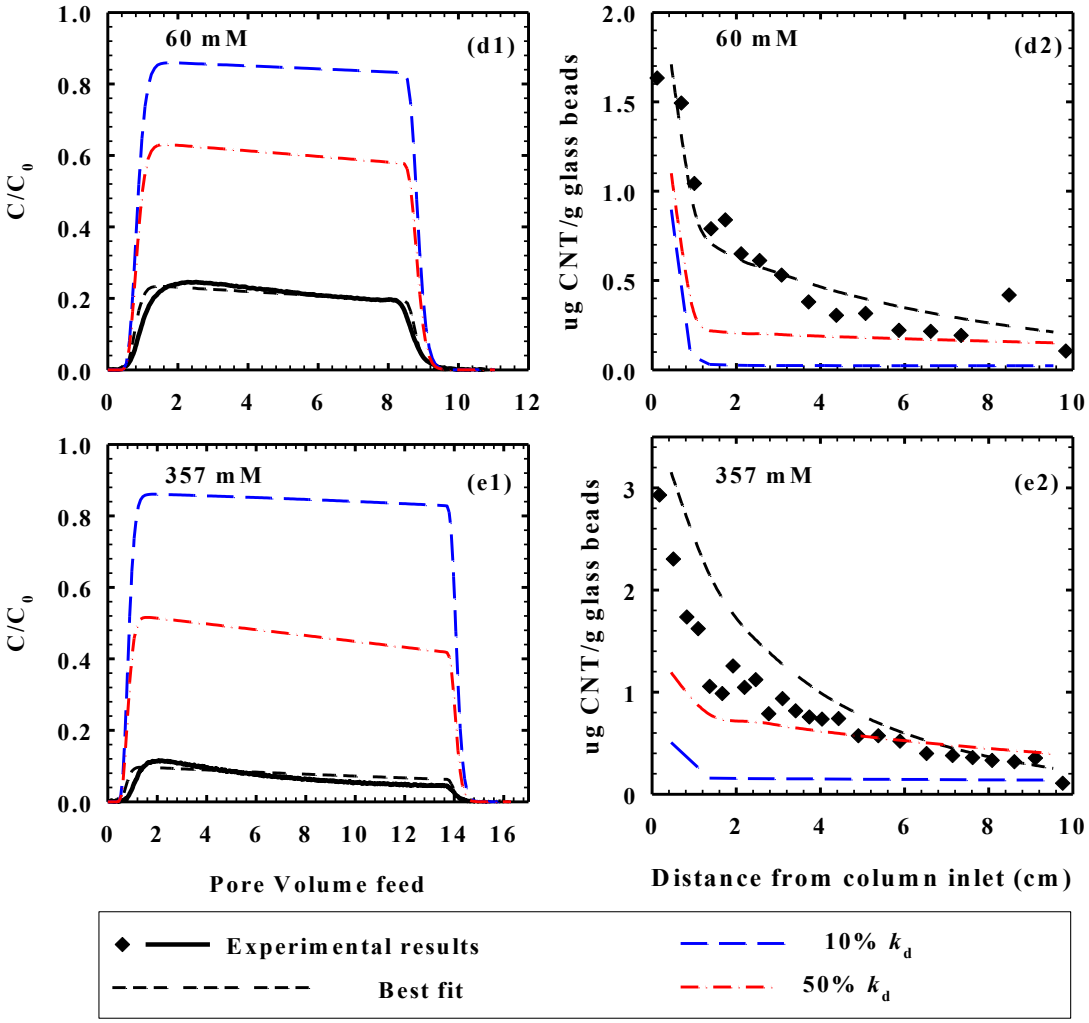

Figure 5.1. (continued from prior page) Analysis of the contributions of CBF for experimental results obtained at pH 5.8± 0.2 and NaCl concentrations of (a) 5 mM, (b) 10 mM, (c) 40 mM, (d) 60 mM and (e) 357 mM. The CBF term k_d under each condition was reduced to 10% and 50% of its original value to analyze its importance and contribution.

the majority of the O-MWCNT removal under these high IS conditions and the direction of change is consistent with expectations based on DLVO theory. In particular, increased rates of CBF are expected at higher IS where surface charges on the collectors (glass beads) and particles (O-MWCNTs) are more effectively screened by cations (Na^+) at

relatively higher IS. Therefore, the results support a conclusion that CBF was the primary removal mechanism for the observed O-MWCNT retention in our study at IS > 60 mM. This further corroborates the assumptions and interpretations presented in Chapter 3 for pulse input conditions, where CBF is even more likely to hold. On the other hand, the results presented in Figures 5.1(a) through (c) reveal that our simulations of transport experiments conducted at lower IS were dominated by mechanisms other than CBF.

5.3.2 *Contribution of Site-Blocking Removal Mechanism*

The results of our analysis of contributions from site-blocking component of the model are shown in **Figure 5.2**. Unlike CBF, which has a clear trend of IS dependency, the relationship between IS and the site- blocking removal mechanism is more complicated.

As evident from Figure 5.2(a), the value of k_b did not affect the simulations for IS = 5 mM (where very low alpha is manifest) but variation of k_b does affect the simulation substantially for the "best fit" simulations of experiments conducted at IS of 10 mM and 40 mM, especially at 40 mM.

Particularly important to note is **Figure 5.2**(c). These results clearly show that the model's ability to simulate rising plateau over time was strongly dependent on the value of k_b. Only at the initially fitted k_b (and not at the 10% or 50% k_b values used in sensitivity test) did the effects of blocking cause accurate simulation of this rising plateau phenomenon.

On the other hand, model results were once again fairly insensitive to k_b for the simulation of results obtained at IS above 60 mM. At IS < 60 mM, the effect of IS on

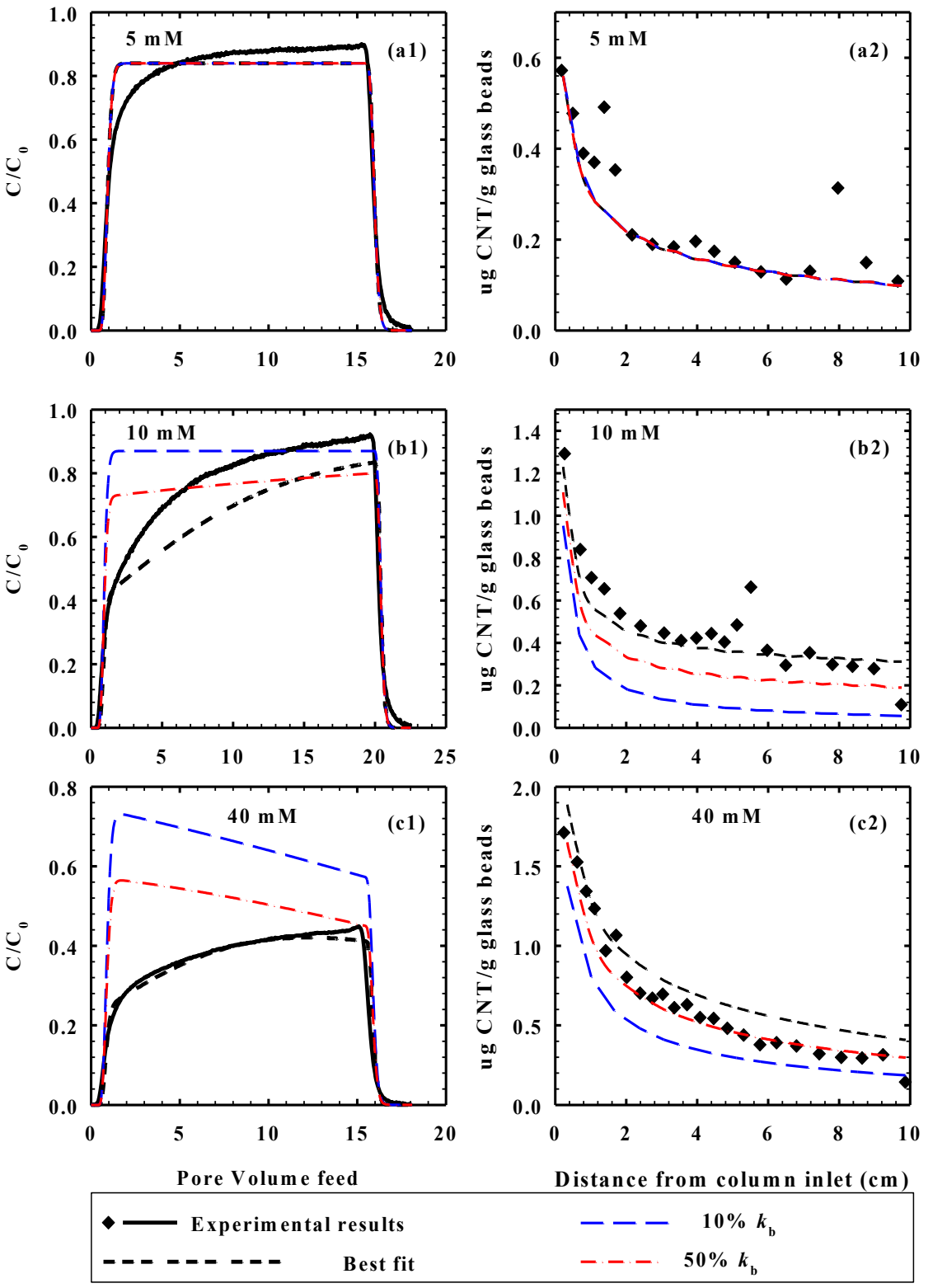

Figure 5.2 (This figure is continued on the next page, where its caption is provided.)

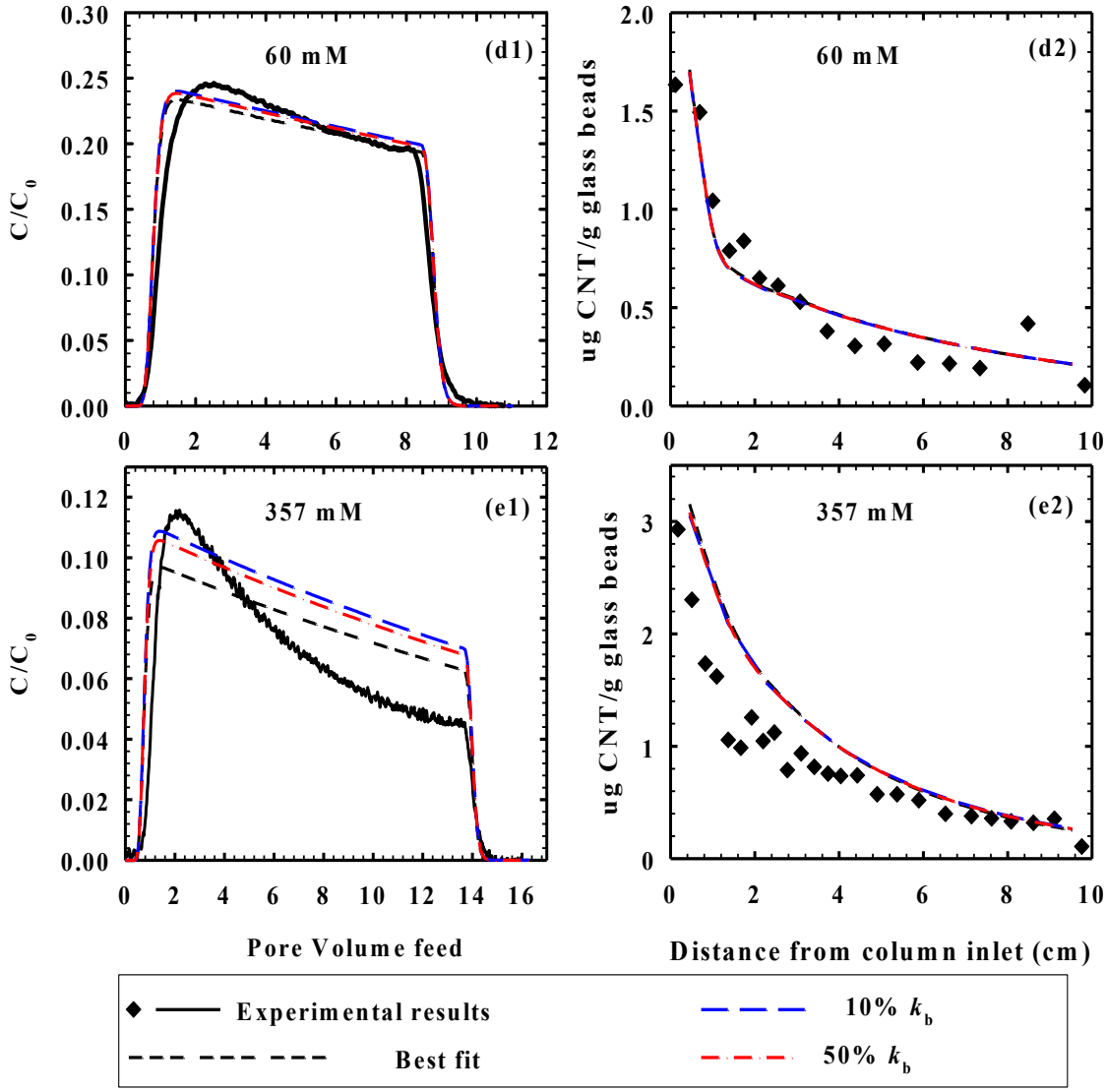

Figure 5.2. (continued from prior page) Analysis of the contributions of site-blocking removal mechanism for experimental results obtained at pH 5.8± 0.2 and NaCl concentrations of (a) 5 mM, (b) 10 mM, (c) 40 mM, (d) 60 mM and (e) 357 mM. The blocking term k_b under each condition was reduced to 10% and 50% of its original value to analyze its importance and contribution.

modeling sensitivity to k_b (deposition rate on the "blockable" high affinity sites) increased with increasing IS, similar to (but not quite as strong as) the effect on sensitivity to k_d,

As discussed in Chapter 4, the "blockable" high-affinity sites are most likely associated with impurities on the glass. Such impurities are reported in the compositional data provided by the manufacturer and have been further characterized through TEM imaging by Dr. Ken Livi in the Electron Microscope Laboratory located within the Department of Earth and Planetary Sciences at JHU (**Figure 3.1**). The surfaces of impurities, mostly metal oxide or silicate, may be less likely to have negative charge at the given pH (5.8 ± 0.2). Based on the amounts observed, it is reasonable to assume that these sites were relatively sparse and surrounded by the more dominant silica sites. Given the large size of O-MWCNTs, it is therefore likely that their deposition is affected by their interaction with silica sites as well as the alternative site types, and that screening of charge repulsion is still relevant to the overall forces of interaction. I speculate that this is the cause of the IS effects at 10 mM and 40 mM. At > 60 mM, on the other hand, the repulsive interaction between O-MWCNT particles and collector surface is effectively diminished for all sites, making the deposition rate coefficient influenced by site-blocking effect (k_b), identical to that due to CBFT (k_d). The sites with or without impurities were equally preferred by O-MWCNTs. Under these conditions, the inclusion of k_b (as a separate component from k_d) is no longer important to the modeling and its value has little impact on the simulation. It is noteworthy that at the beginning of each experiment, where $S_{max} \gg S$, no site-blocking is occurring and the full impact of k_b is at play. Under these conditions, which are likely to apply for the pulse input case, the overall deposition rate coefficient measured using CBF alone will represent the added sum of deposition to both site types – that is, $k_{d,CBF\text{-}pulse} = k_{d,} + k_b$). Moreover, because these two mechanisms were the dominant mechanisms responsible for O-MWCNT removal at most depths and

at all IS tested except for 5 mM (which will be discussed later), it was appropriate to apply CBF to the analysis of results obtained by pulse-input method In this regard, however, we note that the α-values estimated in **Chapter 3** are "combined" values that reflect the overall effect of chemistry on the multiple site types present.

5.3.3 *Contribution of the Limited S_{max}*

As mentioned above, the site-blocking model was proposed based on the assumption that certain types of sites (presumed to be associated with metal oxide impurities) were limited in number and that rates of deposition to these sites would decrease over the course of the column run. The value of S_{max} was then used to represent the maximum available concentration (number per unit volume of porous medium) of such surface sites on the collectors. The finite value of S_{max} is thus the key factor that differentiates a model with CBF plus site-blocking from a model with CBF alone. At the beginning of experiments, however, the solid concentration of deposited O-MWCNTs, S, was much smaller than S_{max}, and a combined deposition rate coefficient $k_{d,total} = k_d + k_b$ can then be applied to account for the removal of O-MWCNTs caused by CBF to both non-blockable and blockable sites. In this study, since the value of S_{max} was small (0.9929 ug/g), the beginning period, where $S_{max} \gg S$, was too short for a constant (full value) of k_b to apply over any part of the step-input BTCs or retention profiles. In this sensitivity analysis, S_{max} was set to be large enough so that the value of ψ was approximately equal to 1.

As shown in **Figure 5.3 (b)** and **Figure 5.3 (c)**, the use of higher (unlimited) S_{max} with the same k_b value caused the BTC plateaus to be significantly lower than those in actual experiments, and the retention profiles significantly higher. This is of course expected, because when S_{max} is infinitely large, the effective rate of deposition to blockable sites

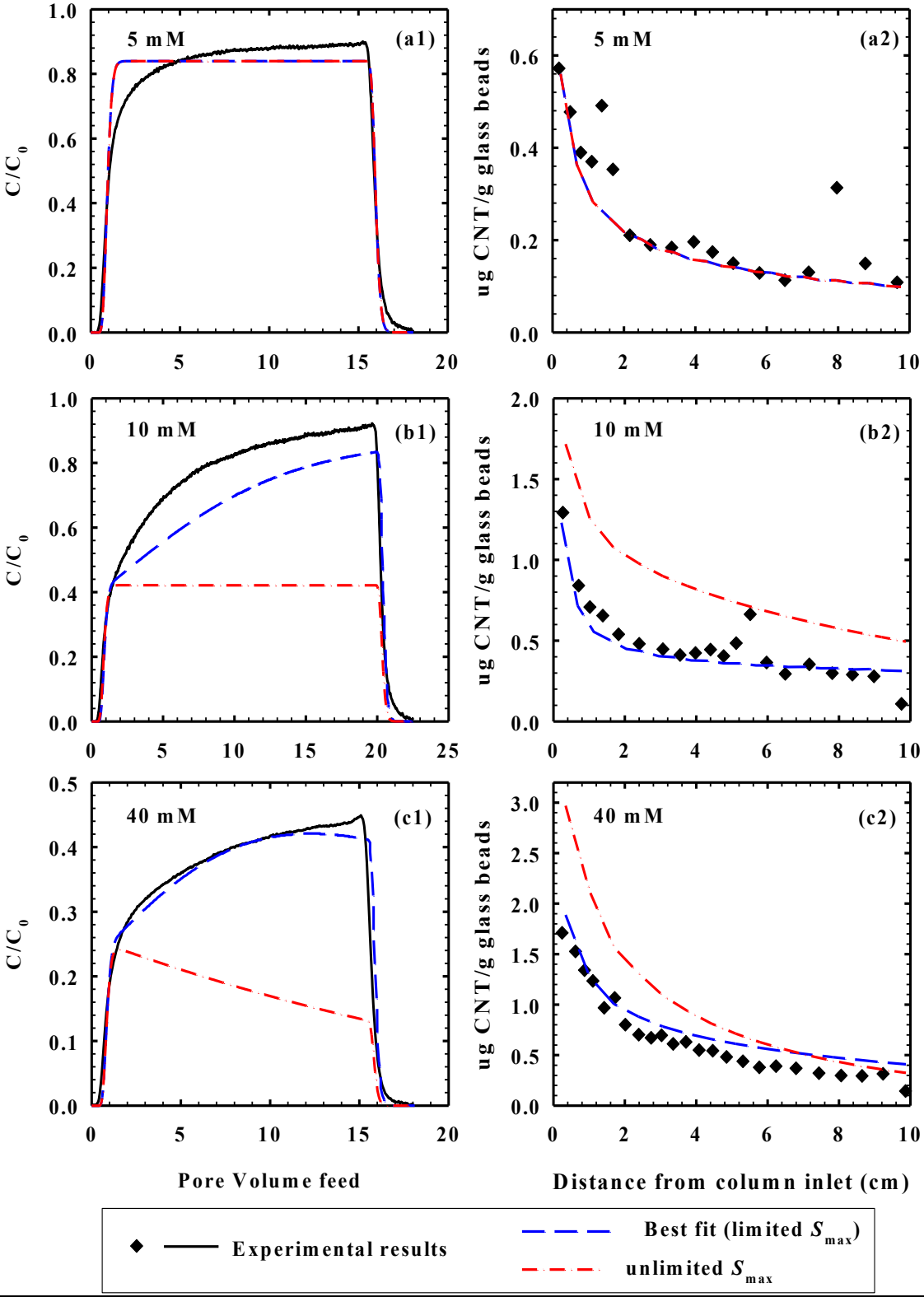

Figure 5.3 (This figure is continued on the next page, where its caption is provided.)

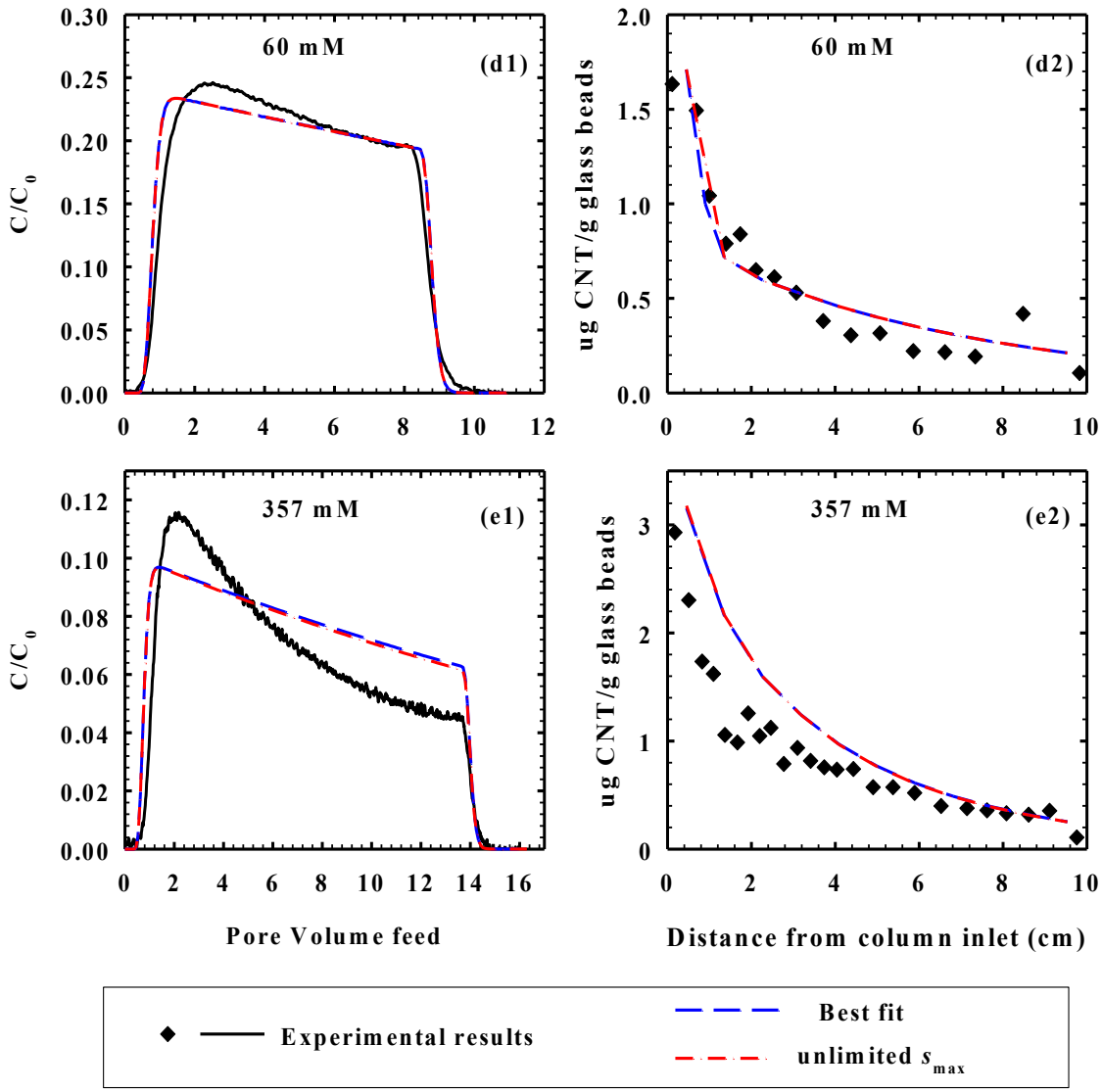

Figure 5.3. (continued from prior page) Analysis of the S_{max} effect on experimental results obtained at pH 5.8± 0.2 and NaCl concentrations of (a) 5 mM, (b) 10 mM, (c) 40 mM, (d) 60 mM and (e) 357 mM. The S_{max} under each condition was increased to infinitely large to analyze its importance and contribution.

will be fully equal to k_b at all times and locations and thus greater than assumed in the prior simulations for any site where blocking was high enough to be relevant. Under this circumstance, $C/C_0 \sim 0.42$ for IS = 10 mM and $C/C_0 \sim 0.25$ for IS = 40 mM. These values were important to simulate results obtained with pulse-input method. The simulation of

unlimited S_{max} further revealed the function of CBF and blocking removal mechanisms and could also help to explain the observation with pulse-input method. In experiments where site-blocking mechanism was not important, the change of S_{max} didn't alter the simulation results as shown in **Figure 5.3 (a), (d), (e)**.

5.3.4 *Contribution of Straining Removal Mechanism*

Unlike deposition under conditions of CBF and deposition to blockable sites, the contribution of straining was unaffected by IS, with almost identical experimental results obtained at IS of 5 mM, 10 mM, and 40 mM as shown in **Figure 5.4**. For results at IS = 40 mM, the plateau increased from ~ 0.1 at the beginning to ~ 0.3 in the end with the diminishing removal rates over time presumable due to the existence of substantial site-blocking effects. Although the contribution of k_b and site-blocking was a strong function of IS in this low IS range as discussed above, the total contribution of straining (as evident from the changes observed with changing k_s) was similar at 5, 10, and 40 mM . For results obtained at 60 mM and 357 mM, however, the contribution of straining was very limited. This is presumably because the effects of straining are overwhelmed by the depositional removal mechanisms of CBF and multilayer deposition, both of which are quite rapid at higher IS.

As shown in **Table 4.3**, the value of β -- a parameter obtained by fitting and used to describe the distance-dependent decay of the straining effect -- was always below 1 at IS $\leq$ 40 mM, but was as high as 4 at IS $\geq$ 60 mM,. These higher values indicate a much faster decay of straining with distance for the high IS simulations. This is consistent with the idea that other mechanisms are relatively more important at high IS and that straining is only a major contributor early in the column.

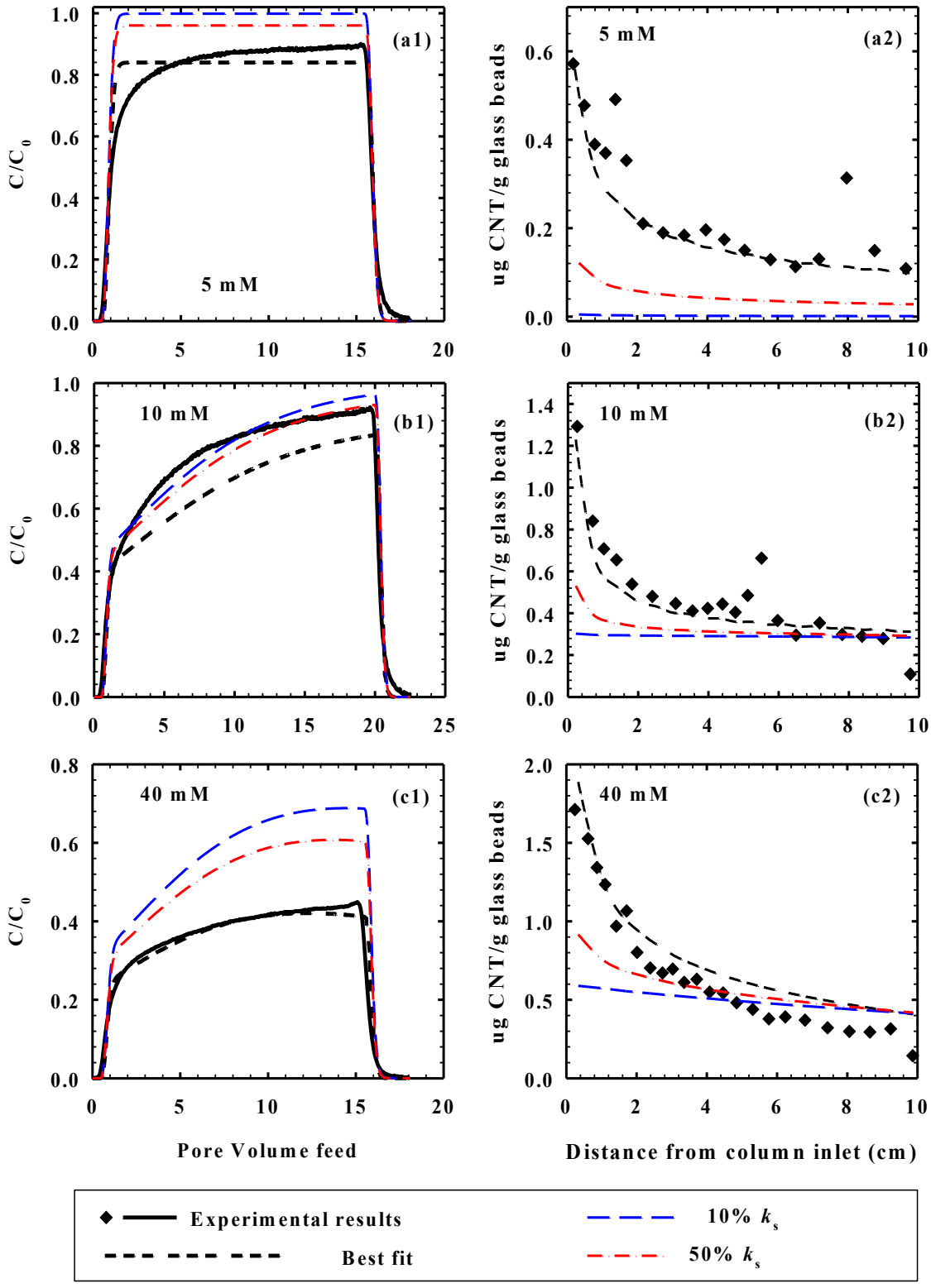

Figure 5.4 (This figure is continued on the next page, where its caption is provided.)

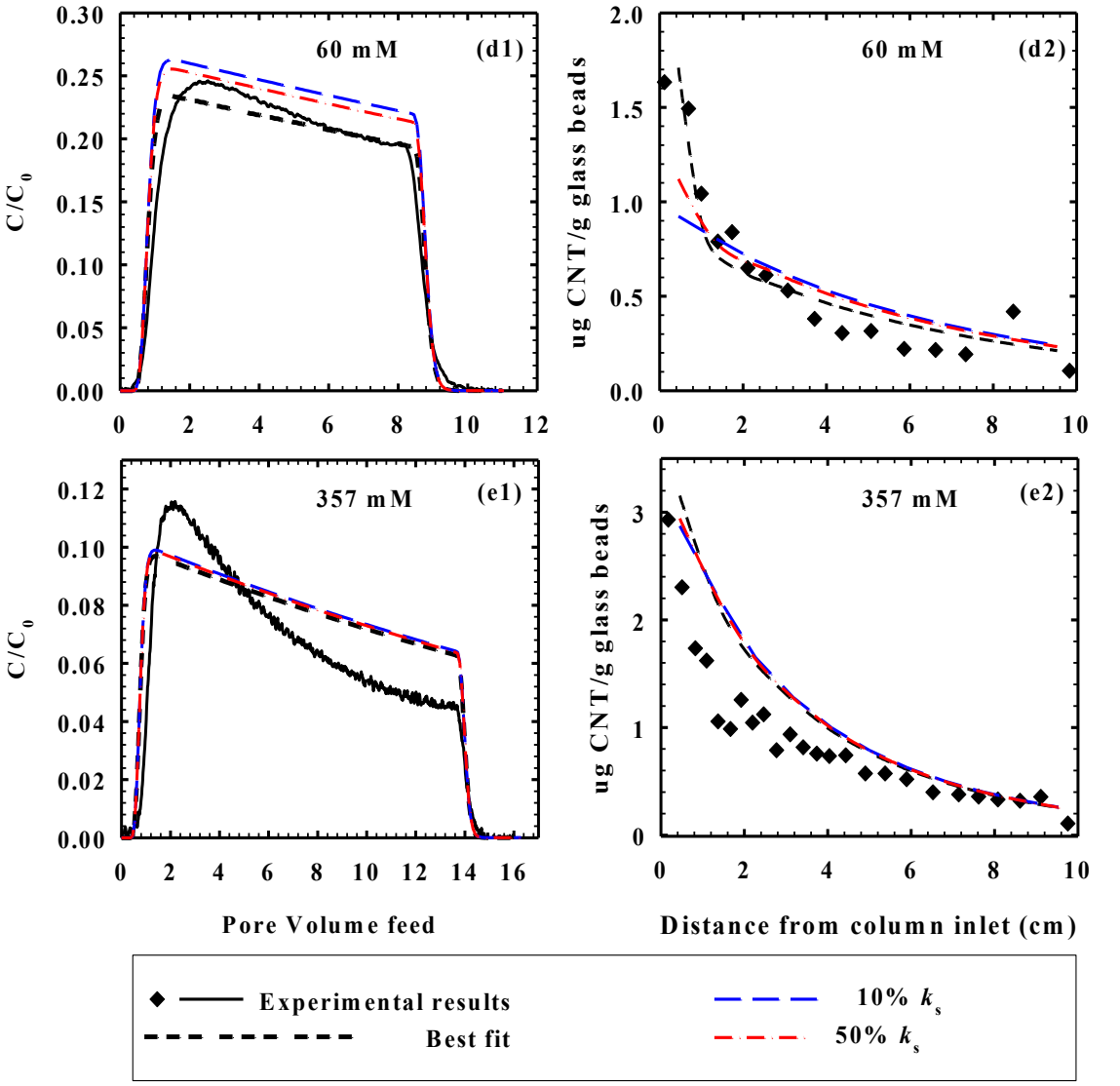

Figure 5.4. (continued from prior page) Analysis of the contributions of straining removal mechanism for experimental results obtained at pH 5.8± 0.2 and NaCl concentrations of (a) 5 mM, (b) 10 mM, (c) 40 mM, (d) 60 mM and (e) 357 mM. The straining term k_s under each condition was reduced to 10% and 50% of its original value to analyze its importance and contribution.

5.3.5 *Contribution of Ripening Removal Mechanism*

The results of our sensitivity analyses with regard to the relative magnitude of the ripening term are shown in **Figure 5.5**. The inclusion of a ripening term in the modeling was found to manifest itself through the appearance of decreasing plateaus in the BTCs

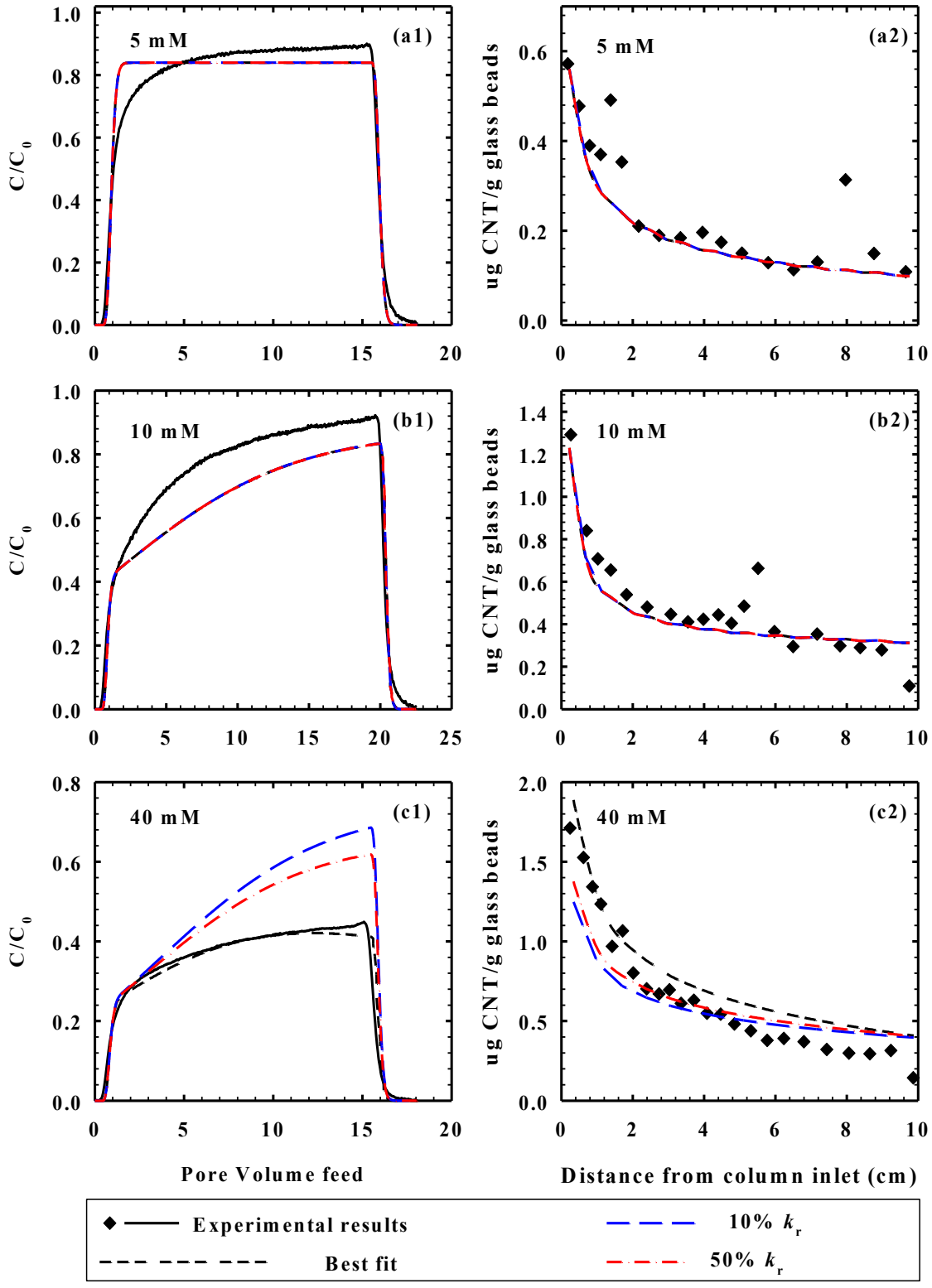

Figure 5.5 (This figure is continued on the next page, where its caption is provided.)

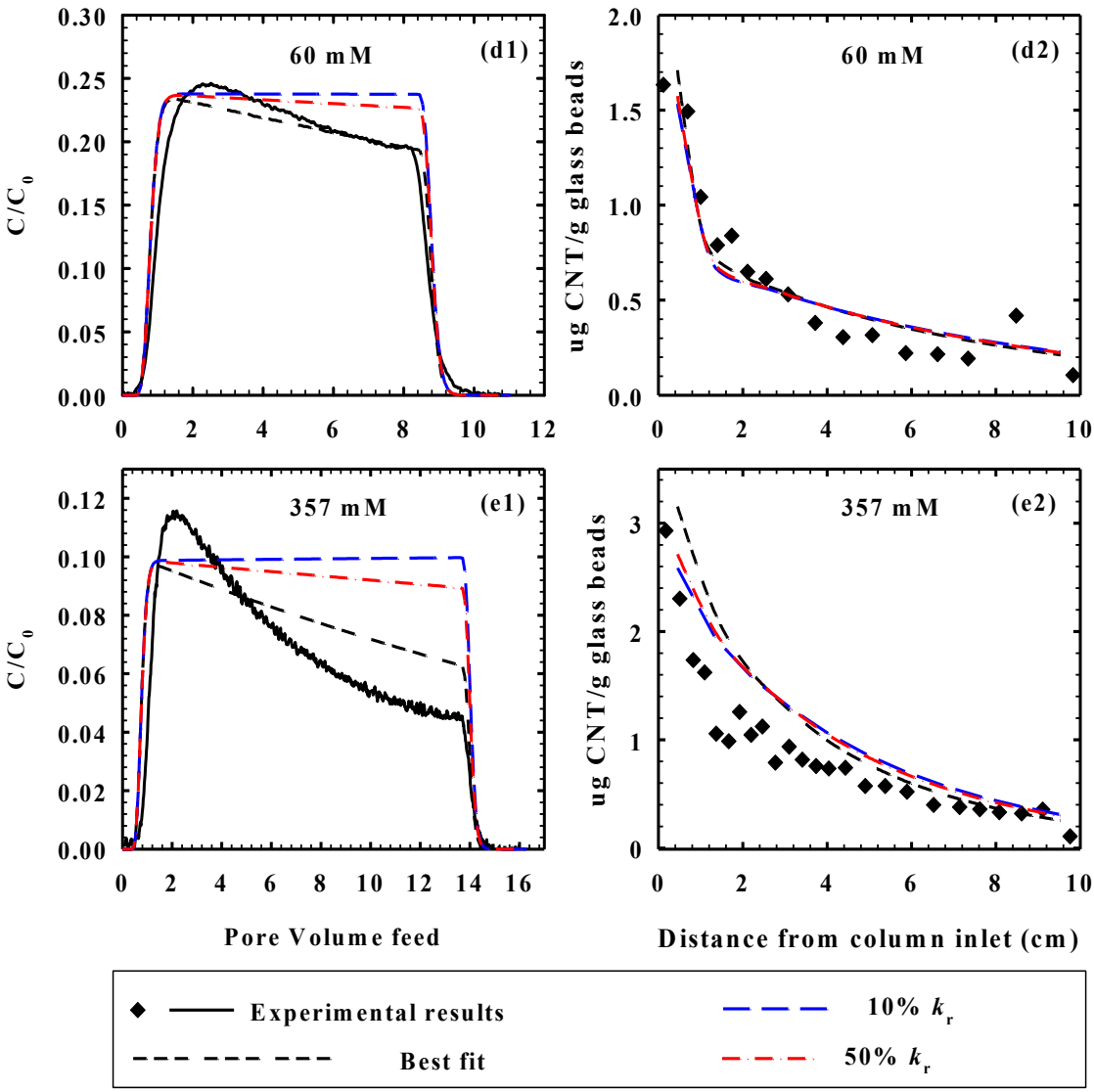

Figure 5.5. (continued from prior page) Analysis of the contributions of ripening removal mechanism for experimental results obtained at pH 5.8± 0.2 and NaCl concentrations of (a) 5 mM, (b) 10 mM, (c) 40 mM, (d) 60 mM and (e) 357 mM. The ripening term k_r under each condition was reduced to 10% and 50% of its original value to analyze its importance and contribution.

and hypo-exponential decay rates in the retention profiles. These effects were only found to be important for experimental data simulation at high IS (≥ 60 mM). As shown in **Figure 5.5**, the ripening mechanism only contributed to the modeled O-MWCNT removal for IS above 40 mM. This is consistent with theory in that these conditions of

high IS are those where repulsive interaction between O-MWCNT particles would be screened, allowing strong attractive interactions between dispersed O-MWCNTs and those on collector surfaces. Also under the circumstance of high IS, the collector surfaces would be more quickly occupied by O-MWCNTs such that more pre-existing O-MWCNTs would be present. **Figure 5.5 (c)** shows that the ripening removal mechanism accounted for only a small part of the simulated O-MWCNT removal at 40 mM NaCl. As previously discussed in the context of **Figure 5.2** and **Figure 5.4** , mechanisms of site-blocking and straining were found to play important roles in the simulation of O-MWCNT removal at IS = 40 mM. Note that, although the concurrent application of all three mechanisms can complicate the modeling exercise, each mechanism has a vastly different type of effect on results, and each is relevant under its own specific set of conditions. We postulate that 40 mM was not high enough to completely screen the surface charges on o-MWCNTs and glass beads, and therefore O-MWCNTs still preferred sites containing impurities of metal oxides, the gradual blocking of which causes the plateau of the BTC to increase (as previously discussed). On the other hand, it can be clearly observed that at 40 mM, much more O-MWCNTs were retained within the column compared to experiments conducted at lower IS (see **Figure 5.5 (a), (b) and (c)**). The large amount of deposited O-MWCNTs occupied most available glass bead surfaces after a period of time and caused multi-layer deposition. The presence of the ripening effect decreased the BTC plateau significantly relative to what would have occurred with blocking alone (**Figure 5.5 (c)**), but still not profoundly enough to cause a decreasing plateau over time, as in the higher IS cases (**Figure 5.5(d)** and **5.5.(e)**. Since the straining effect existed under all conditions, and the amount of deposited O-MWCNTs at 40 mM

was not large enough to negate the losses caused by straining, the contribution of straining could be easily observed. For BTCs and retention profiles obtained at higher IS (60 mM, 357 mM), normal CBF and deposition and ripening were the two removal mechanisms that dominated the simulations, with other mechanisms being relatively unimportant.

5.3.6 *Contributions of all effects at varied background IS*

During the simulation, the specific contribution of CBF, straining, blocking, and ripening effect can be calculated using **Eq. 5.1**. The summaries of the relative and absolute contributions of each effect on the overall rate of O-MWCNT removal are shown in **Figure 5.6** and **Figure 5.7**, respectively.

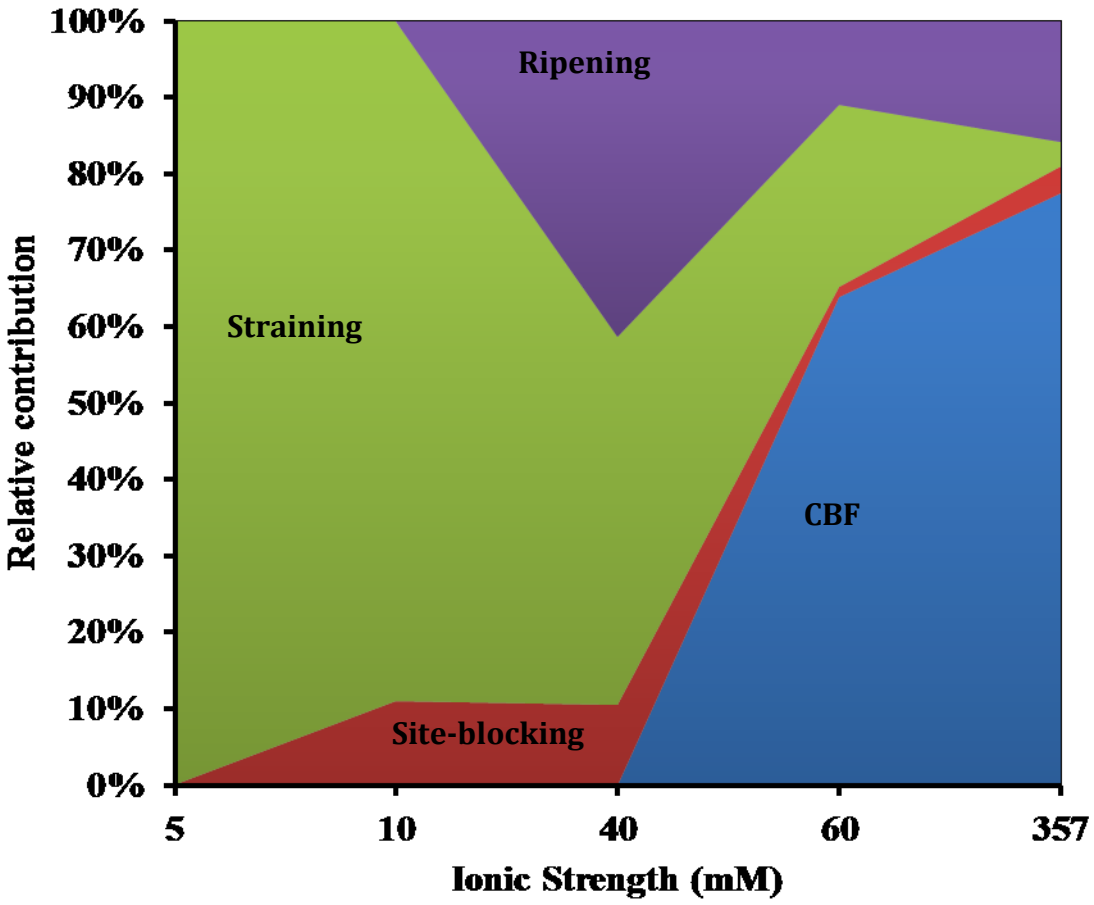

Figure 5.6. Relative contributions of CBF, site-blocking, straining, and ripening effects on 8% O-MWCNT removal at varied ionic strength.

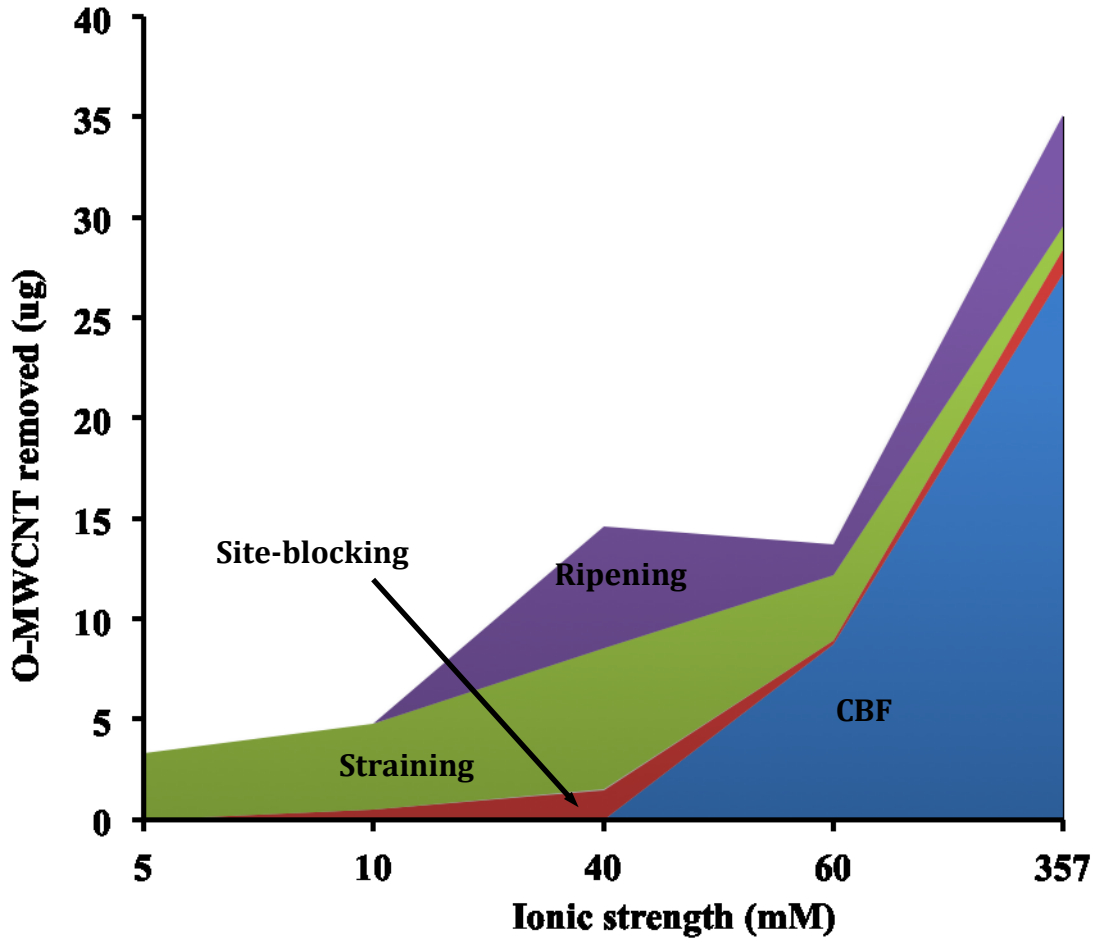

Figure 5.7. Amount of 8% O-MWCNT removed by CBF, site-blocking, straining, and ripening effects at varied ionic strength.

As shown in those figures, deposition (both k_d and k_b) played an important role in O-MWCNT removal at IS ≥ 60 mM, but the separation k_d and k_b (i.e., of specific separate consideration of a site-blocking model) was found to be most important at IS of 10 mM and 40 mM. Although its effect was still noticeable above 60 mM, its importance was much less profound. Overall, the combination of CBF and deposition to "blockable" sites was found to account for the majority of O-MWCNT removal at IS ≥ 60 mM and the combined first-order deposition rate was the one detected in pulse-input method. The straining effect was less IS sensitive and was responsible for an almost consistent amount of the modeled O-MWCNT removal except at 357 mM, where the effect of straining

could not be clearly separated from the ripening effect. This effect was responsible for all of the simulated removal at IS of 5 mM, which is consistent with the idea that all other mechanisms will be effectively absent at such low IS. Ripening removal mechanisms were found relevant to modeling only at high IS and provided reasonable explanation of the decreasing plateaus at high IS. This mechanism also had a noticeable impact on simulated O-MWCNT removal at IS $\geq$ 40 mM.

5.4 Conclusion

In general, the sensitivity analyses were very effective at revealing the relative contributions of each removal mechanism on O-MWCNT removal at varied experimental conditions. Overall, each of the four removal mechanisms had conditions where it was relevant, such that consideration of all four was important in order to accurately simulate the transport of O-MWCNTs through porous media under all of the conditions studied.

Chapter 6. Summary, Application, and Future Work

6.1 Summary

In this work, I established quantitative relationships between the surface composition of oxidized multi-walled carbon nanotubes (O-MWCNTs) and their sorption and transport properties under varying aquatic chemical conditions. Mathematical models and computations were applied to test whether the hypothesized conceptual understanding was useful for interpreting and predicting experimental observations.

6.1.1 *Sorption Properties of O-MWCNTs*

In work reported in this dissertation, the adsorption of divalent zinc and nickel ions (Zn^{2+} and Ni^{2+}) onto O-MWCNTs under varied conditions was investigated (**Chapter 2**). Effects of "aquatic chemistry", surface chemistry, O-MWCNT aggregation state and concentration, as well as competitive effects of naphthalene on the adsorption of Zn^{2+} onto O-MWCNTs were studied.

The chemistry of the experimental aquatic environment, including pH, and ionic strength (IS), affected the adsorption capacity of O-MWCNTs for Zn^{2+} and Ni^{2+} in ways consistent with those previously reported in our research group.[1] The adsorption of both Zn^{2+} and Ni^{2+} increased with increasing pH and decreasing IS. The observed effects of O-MWCNT surface chemistry on the adsorption of Zn^{2+} was also similar to those observed in a prior study.[1] O-MWCNTs with higher total oxygen concentrations and higher concentrations of carboxylic groups exhibited higher adsorption capacity on Zn^{2+}. All isotherms conducted using O-MWCNTs at 4 different surface oxygen concentrations could be well fit by the traditional Langmuir isotherm model. The two-site Langmuir

model developed by Cho *et al.*[1] and as described in **Chapter 2** was applied to mathematically analyze the role of carboxyl functional groups. This model fit the experimental results reasonably well, indicating that the adsorption capacity of O-MWCNTs comprised contributions primarily from graphene and carboxylic groups on the surface. The presence of 5 mg/L naphthalene did not have any effect on the adsorption of Zn^{2+} onto 8% O-MWCNTs, in contrast to the obvious suppressing effect of other competing metallic ions on the adsorption of metallic ions onto O-MWCNTs.[2] These results indicated that the primary adsorption mechanism for Zn^{2+} and similar divalent cations is different from that for naphthalene, and therefore the competing naphthalene did not effectively suppress the adsorption of cations.

Studies of aggregation state and solid-to-liquid ratio on adsorption were also conducted. Ranges of S/L were studied for both the "original-powder-state" (aggregated) and fully dispersed O-MWCNTs, as discussed in the paragraph below. Unfortunately, however, there was only a single S/L value (0.061 g/L) at which the both aggregation states could be studied, because of limits on both (1) the minimum amount of O-MWCNT that could be accurately weighed in "powder-addition" systems (and therefore minimum S/L values with experimentally practical volumes of liquid); and (2) maximum S/L values that could be used for dispersed phase systems without reducing final aqueous concentrations below detection limits.

Results obtained in the studies at the common identical solid-to-liquid ratio (S/L) (0.061 g/L) revealed that there was no statistical difference in the adsorption isotherms between aggregated and dispersed forms at the studied S/L. These results indicate that, at the S/L value studied (0.061 g/L) no significant difference in adsorption extent exists

between O-MWCNTs that are still in their initial aggregated state, relative to when they are sonicated and well dispersed. I interpret these results to mean that mechanism of sorption is not dependent on aggregation state.

Although the aggregation state of the O-MWCNTs did not have any major effect on the adsorption capacity of O-MWCNTs at S/L of 0.061 g/L, the solid-to-liquid ratio showed significant effect on adsorption characteristics for both types of O-MWCNTs studied, whose surface oxygen concentrations were 5.1% and 8.0%. For both types of O-MWCNTs, isotherms obtained at lower solid-to-liquid ratios were significantly higher than those obtained at relatively higher solid-to-liquid ratios, and this phenomenon was observed with both the orginial-state-powders and the fuly dispersed tubes, albeit over different S/L ranges, as previously discussed. We also observed that the effects of S/L were primarily on sorption affinity at low C_e (*i.e.,* the product of $K_L q_{max}$) rather than on adsorption capacity (q_{max}). Although there are numerous prior reports of similar findings by other researchers on adsorption reactions of trace metals with soils and clays[3-6], the source for the S/L effect remains unclear. Much prior work has focused on alternative "artifactual" explanations for these findings, but there remain many cases where all imagined explanations have been disproven[3-5, 7] and I am also unable to posit a good mechanistic explanation for results in the current case.

6.1.2 *Transport Properties of O-MWCNTs*

I also investigated numerous transport properties of O-MWCNTs of varying surface oxygen concentrations through columns of uniform silica glass beads under a wide range of aquatic conditions. Both pulse-input and step-input methods were employed in these studies and analyses were conducted of both the aqueous

(breakthrough curves, BTCs) and adsorbed phases (retention profiles). A pulse-input method was employed to investigate effects of aquatic and surface chemistry on O-MWCNT transport, using temporal histories of O-MWCNT effluent concentrations, i.e., breakthrough curves (BTCs), under conditions where the overall removal of O-MWCNTs was dominated by clean-bed filtration. Comparisons of results under these conditions with those obtained under conditions of perfectly unfavorable attachment (distilled water) allowed me to determine the effects of system chemistry on attachment efficiency, α. (**Chapter 3**). In other experiments described in **Chapter 4**, a step-input method was employed to investigate effects of site blocking, straining, and ripening, which come to have major effects with prolonged loading, and especially at the frontal ends of columns. For these studies, data were obtained in the forms of both temporal histories of O-MWCNT concentration in column effluent water (BTCs) as well as in-situ spatial distributions of retained O-MWCNTs (retention profiles), as obtained through column dissection at each experiment's end. More complex mathematical models were developed for the simulation and interpretation of experimental results (**Chapter 4**), and these models were further tested to better understand their sensitivity to the various mechanistic sub-models (**Chapter 5**)."

In regard to the effects of aquatic and surface chemistry on the transport of O-MWCNTs (**Chapter 3**), our results provided important new data about O-MWCNT attachment efficiencies as a function of aquatic and surface chemistry In the presence of Na^+, the required ionic strength (IS) for maximum particle attachment efficiency (*i.e.*, the critical deposition concentration, or CDC) increased as the O-MWCNT's surface oxygen concentration or pH increased, following qualitative tenets of theories based on

electrostatic interaction. In the presence of Ca^{2+}, CDC values were lower than those with Na^{+} present, but were no longer sensitive to surface oxygen content. Because surface oxygen groups are known to affect electrostatic interactions, these suggest that Ca^{2+} influences the interactions between O-MWCNTs and glass beads by mechanisms other than electrostatics alone. The presence of Suwannee River natural organic matter (SRNOM) decreased the attachment efficiency of O-MWCNTs in the presence of either Na^{+} or Ca^{2+}, but with more pronounced effects when Na^{+} was present. Nevertheless, low concentrations of SRNOM (< 4 mg/L of dissolved organic carbon) were sufficient to mobilize all O-MWCNTs studied at $CaCl_2$ concentrations as high as10 mM. Overall, results from these studies revealed that NOM content, pH and cation type have more importance than the surface characteristics of O-MWCNTs in affecting O-MWCNTs deposition during transport through silica-based porous media.

Chapter 4 contains findings in regard to the transport of O-MWCNTs through columns packed with glass beads, including analysis of both breakthrough curves (BTCs) and retention profiles at five different ionic strengths (IS). As previously noted, a step-input method was employed, which allowed more O-MWCNTs to deposit onto glass beads and both (a) ensured a sufficient quantity of deposited O-MWCNTs for the creation of retention profiles and (b) caused a violation of the assumptions of clean-bed filtration for some sets of conditions, and especially at the frontal end of the column. Although the general trend of the experimental observation followed the expectation of traditional theory based on clean-bed filtration and electrostatic interactions, the BTCs as well as retention profiles exhibited features that could not be well explained by such simple theory alone. Such features included BTC "plateaus" that either increased (low IS)

or decreased (high IS) over time as well as hypo-exponential decay in retention profiles. Conventional CBFT models were first applied and shown not to simulate all of these effects. Improved simulations were then obtained using modified models that incorporate straining, site-blocking, and multilayer deposition (ripening). Simulation results indicated that all four effects were necessary to explain the experimental observations. Sensitivity analysis regarding simulation results (**Chapter 5**) revealed that at IS < 40 mM, site-blocking and straining effects played relatively more significant roles than other effects. For experiments conducted at higher IS (≥ 60 mM), CBF together with ripening effect were the primary removal mechanisms. Site-blocking, straining and ripening effects all made significant contributions in O-MWCNT removal at IS = 40 mM.

6.2 Application

The purpose of this study was to understand the behavior of O-MWCNTs and their interactions with other contaminants, so as to help researchers better estimate risks O-MWCNTs may pose on human and ecosystems. Findings from this study have partially fulfilled this purpose and outputs from model development can also be used to estimate the transport of colloidal particles other than O-MWCNTs.

Findings from the adsorption study (**Chapter 2**) have furthered the understanding of the interactions of trace metals with O-MWCNTs. Effects of aquatic and surface chemistry estimated in this study were consistent with prior findings obtained in our laboratory and elsewhere[1, 8-10] Importantly, however, this work also made new discoveries about the effect of experimental conditions on measured sorption isotherms. In particular, a significant effect of S/L was revealed, indicating that the adsorption capacity of well-dispersed O-MWNCTS (for at least Zn^{2+} and possibly many other types

of low-molecular weight adsorbates) may be underestimated by studies conducted with high O-MWCNT concentrations, as has been the case in much prior work. Adsorption results developed in this study using O-MWCNTs at environmentally relevant concentrations provide necessary information for the estimation of O-MWCNT interactions with Zn^{2+} in natural environments and suggests a more appropriate method for obtaining adsorption isotherms for dispersed O-MWCNTs with other adsorbates in future research.

Transport properties of O-MWCNTs were investigated using columns packed with spherical glass beads as porous media. The rigid methods of glass-bead preparation and column packing developed in this study as described in **Chapter 3** are necessary to create stable and consistent experimental conditions and therefore to guarantee the output of reliable results. These methods are useful for future researchers conducting similar column experiments to investigate the transport properties of colloidal particles as well as aqueous contaminants. Findings from the transport study not only provide a thorough analysis of the effects of aquatic and surface chemistry, but also provide a valuable source of new data for estimating O-MWCNT behavior in aquatic environments. Results indicated that in natural environments where both Ca^{2+} and NOM are present, O-MWCNT transport may be largely independent of O-MWCNT surface oxidation, with attachment efficiencies of dispersed O-MWCNTs being instead controlled primarily by the amount of adsorbed NOM and other aquatic conditions such as pH, ionic strength, and ionic composition. The observed independence of the transport of O-MWCNTs on their surface chemistry suggests that, for purposes of generalized risk estimation under these common aquatic conditions (of NOM presence), it may be possible to treat O-

MWCNTs with varied surface characteristics as a single kind of model colloid. Moreover, the reported values of attachment efficiency may be directly useful for making gross estimates of environmental transport under some conditions, such as in subsurface sand and gravel aquifers where grain size and uniformity are sufficient to exclude straining mechanisms.

In this study, I also investigated a variety of filtration-related mechanisms of O-MWCNTs using both experimental approaches and mathematical simulations (**Chapter 4**). Developments in both regards should be useful to future researchers. The method of column dissection was found useful for developing retention profiles of colloidal particles after transport experiments. This method has been used in similar studies such as the studies of O-MWCNT[11], fullerene[12] or graphene oxide[13] transport through porous media. The models used for the simulation of experimental results were developed from basic concepts of traditional clean bed filtration theory,[14-16] in combination with prior approaches suggested by others for simulating the effects of site-blocking,[17] straining,[18, 19] and multilayer deposition.[20, 21] In scenarios where multiple removal mechanisms control the movement of colloidal particles, the new combined model could be a useful tool to others for estimating the contribution of each removal mechanism under varied conditions.

6.3 Future Work

The environmental implication of O-MWCNTs has been intensively investigated in study presented in this dissertation in terms of the effects of varied environmental conditions on their transport properties and their adsorption properties for heavy metals as typical aquatic contaminants. Experimental approaches and mathematical simulation

are also applied to study the mechanisms of O-MWCNT removal through porous media. More studies, however, need to be conducted especially at several aspects as shown below.

6.3.1 *Investigation on Physical Meaning of Solid-to-Liquid Effect*

Although the effect of solid-to-liquid ratio in adsorption studies has been reported previously, the reason for such effect is still to be investigated. Several hypothesized explanations were provided in prior literature. McKinley *et al.*[6] have summarized them as follows: (1) adsorption by "non-settling" colloids that remain suspended in the aqueous phase after centrifugation or filtration;[22-25] (2) competition for adsorbate by complexing agents (particularly organic carbon) desorbed from the adsorbent;[23-26] (3) implicit adsorbate competition;[26, 27] (4) increased solid aggregation (e.g., flocculation) to produce a net decrease in readily available adsorption sites;[22, 28-31] and (5) extraneous chemical reactions.[32] For example, Di Toro *et al.*[4, 5] proposed particle interaction model to explain the increasing adsorption of heavy metals onto montmorillonite and quartz with decreasing adsorbent concentration. The model could fit experimental data well but the proposed physical explanation for this model is questionable and solid mechanistic underpinnings for the observations have yet to be well developed. Zhang *et al.*[7] attributed increasing amounts of adsorbed pyrene onto CNTs after sonication to the presence of more exposed surface in dispersed CNTs that were broken down from aggregates during sonication. In our current study, however, we observed little difference on adsorption ability between dispersed and non-disaggregated O-MWCNTs when the experiments were conducted at similar S:L. As with the prior observations summarized by Di Toro *et al.*, a mechanistically defensible theory is still needed to explain the solid-to-liquid effects

observed in our current study. This is a potentially intriguing area for further research but we unfortunately do not have a strong hypothesis to test at this time.

6.3.2 *Investigation of O-MWCNT Transport Properties under More Environmentally Relevant Conditions*

In this study, the transport of O-MWCNTs was investigated using spherical glass beads as model porous media under simple aquatic environment (single cation, limited impurities). In this simplified experimental environment, the behavior of O-MWCNTs could be observed with limited interference and the removal mechanisms could be easily separated. In order to better relate these results to O-MWCNT transport in the environment, however, additional studies are needed under more complex circumstances. In particular, it would be useful to systematically increase the complexity of the porous medium, for example by introducing non-spherical grains and grain-size distributions. More complex media that includes a wide range of mineral surfaces and particulate organic matter would also add complications deserving of direct study. Such complications will undoubtedly have major impact on transport and it is currently unclear whether the trends and mechanisms identified in dissertation work will always apply.

6.3.3 *Further Improvement and Testing of the Developed Model*

The multi-process filtration models developed in this work could be used more widely for simulating other types of colloidal transport. Although this model was able to fit the experimental results well in this study, it should be further tested with other kinds of colloidal particles for verification. A particular result that needs further testing is the issue of deposition mechanism for rod-like colloid such as O-MWCNTs. In the work presented here, the transport of initially dispersed O-MWCNTs showed velocity effects

consistent with deposition by interception, suggesting that the O-MWCNTs behaved as spherical particles with effective diameters equal to their lengths. It is unclear, however, as to whether this finding was the result of re-aggregation of the tubes during transport (perhaps into bundles of roughly this size) or whether rotation of the tubes during transport may have caused them to occupy effectively spherical volumes defined by their length. Additional testing with other rod-like or thread-like particles would be useful in testing this and other assumptions, and for investigating the role of aspect ratio and size on the effect.

6.4 Cited References

1. Cho, H. H.; Wepasnick, K.; Smith, B. A.; Bangash, F. K.; Fairbrother, D. H.; Ball, W. P., Sorption of Aqueous Zn[Ii] and Cd[Ii] by Multiwall Carbon Nanotubes: The Relative Roles of Oxygen-Containing Functional Groups and Graphenic Carbon. *Langmuir* **2010,** *26*, (2), 967-981.

2. Li, Y. H.; Ding, J.; Luan, Z. K.; Di, Z. C.; Zhu, Y. F.; Xu, C. L.; Wu, D. H.; Wei, B. Q., Competitive Adsorption of Pb^{2+}, Cu^{2+} and Cd^{2+} Ions from Aqueous Solutions by Multiwalled Carbon Nanotubes. *Carbon* **2003,** *41*, (14), 2787-2792.

3. Di Toro, D. M., A Particle Interaction Model of Reversible Organic Chemical Sorption. *Chemosphere* **1985,** *14*, (10), 1503 - 1538.

4. Di Toro, D. M.; Horzempa, L. M., Reversible and Resistant Components of Pcb Adsorption-Desorption. *Environmental Science and Technology* **1982,** *16*, (9), 594 - 602.

5. Di Toro, D. M.; Mahony, J. D.; Kirchgraber, P. R.; O'byrne, A. L.; Pasquale, L. R.; Piccirilli, D. C., The Effects of Nonreversibiliy, Particle Concentration, and Ionic Strength on Heavy Metal Sorption. *Environmental Science and Technology* **1986,** *20*, (1), 55 - 61.

6. Mckinley, J. P.; Jenne, E. A., Experimental Investigation and Review of the "Solids Concentration" Effect in Adsorption Studies. *Environmental Science and Technology* **1991,** *25*, (12), 2082 - 2087.

7. Zhang, X.; Kah, M.; Jonker, M. T. O.; Hofmann, T., Dispersion State and Humic Acids Concentration-Dependent Sorption of Pyrene to Carbon Nanotubes. *Environ Sci Technol* **2012,** *46*, (13), 7166-7173.

8. Chen, C. L.; Wang, X. K., Adsorption of Ni(Ii) from Aqueous Solution Using Oxidized Multiwall Carbon Nanotubes. *Ind Eng Chem Res* **2006,** *45*, (26), 9144-9149.

9. Chen, G. C.; Shan, X. Q.; Wang, Y. S.; Pei, Z. G.; Shen, X. E.; Wen, B.; Owens, G., Effects of Copper, Lead, and Cadmium on the Sorption and Desorption of Atrazine onto and from Carbon Nanotubes. *Environ Sci Technol* **2008,** *42*, (22), 8297-8302.

10. Velickovic, Z. S.; Bajic, Z. J.; Ristic, M. D.; Djokic, V. R.; Marinkovic, A. D.; Uskokovic, P. S.; Vuruna, M. M., Modification of Multi-Wall Carbon Nanotubes for the Removal of Cadmium, Lead and Arsenic from Wastewater. *Dig J Nanomater Bios* **2013,** *8*, (2), 501-511.

11. Wang, Y. G.; Kim, J. H.; Baek, J. B.; Miller, G. W.; Pennell, K. D., Transport Behavior of Functionalized Multi-Wall Carbon Nanotubes in Water-Saturated Quartz Sand as a Function of Tube Length. *Water Res* **2012,** *46*, (14), 4521-4531.

12. Wang, Y.; Li, Y.; Fortner, J. D.; Hughes, J. B.; Abriola, L. M.; Pennell, K. D., Transport and Retention of Nanoscale C60 Aggregates in Water-Saturated Porous Media. *Environ Sci Technol* **2008,** *42*, (10), 3588-3594.

13. Lanphere, J. D.; Luth, C. J.; Walker, S. L., Effects of Solution Chemistry on the Transport of Graphene Oxide in Saturated Porous Media. *Environ Sci Technol* **2013,** *47*, (9), 4255-4261.

14. Yao, K. M.; Habibian, M. T.; O'melia, C. R., Water and Waste Water Filtration: Concepts and Applications. *Environmental Science and Technology* **1971,** *5*, (11), 1105-1112.

15. Rajagopalan, R.; Tien, C., Trajectory Analysis of Deep-Bed Filtration with Sphere-in-Cell Porous-Media Model. *Aiche J* **1976,** *22*, (3), 523-533.

16. Tufenkji, N.; Elimelech, M., Correlation Equation for Predicting Single-Collector Efficiency in Physicochemical Filtration in Saturated Porous Media. *Environ Sci Technol* **2004,** *38*, (2), 529-536.

17. Liu, X. Y.; O'carroll, D. M.; Petersen, E. J.; Huang, Q. G.; Anderson, C. L., Mobility of Multiwalled Carbon Nanotubes in Porous Media. *Environ Sci Technol* **2009,** *43*, (21), 8153-8158.

18. Bradford, S. A.; Bettahar, M., Straining, Attachment, and Detachment of Cryptosporidium Oocysts in Saturated Porous Media. *J Environ Qual* **2005,** *34*, (2), 469-478.

19. Bradford, S. A.; Simunek, J.; Bettahar, M.; Van Genuchten, M. T.; Yates, S. R., Modeling Colloid Attachment, Straining, and Exclusion in Saturated Porous Media. *Environ Sci Technol* **2003,** *37*, (10), 2242-2250.

20. Ryde, N.; Kallay, N.; Matijevic, E., Particle Adhesion in Model Systems .14. Experimental Evaluation of Multilayer Deposition. *J Chem Soc Faraday T* **1991,** *87*, (9), 1377-1381.

21. Ryde, N.; Kihira, H.; Matijevic, E., Particle Adhesion in Model Systems .15. Effect of Colloid Stability in Multilayer Deposition. *J Colloid Interf Sci* **1992,** *151*, (2), 421-432.

22. Li, Y. H.; Burkhardt, L.; Buchholtz, M.; Ohara, P.; Santschi, P. H., Partition of Radiotracers between Suspended Particles and Seawater. *Geochimica Et Cosmochimica Acta* **1984,** *48*, (10), 2011-2019.

23. Gschwend, P. M.; Wu, S. C., On the Constancy of Sediment Water Partition-Coefficients of Hydrophobic Organic Pollutants. *Environ Sci Technol* **1985,** *19*, (1), 90-96.

24. Voice, T. C.; Rice, C. P.; Weber, W. J., Effect of Solids Concentration on the Sorptive Partitioning of Hydrophobic Pollutants in Aquatic Systems. *Environ Sci Technol* **1983,** *17*, (9), 513-518.

25. Voice, T. C.; Weber, W. J., Sorbent Concentration Effects in Liquid Solid Partitioning. *Environ Sci Technol* **1985,** *19*, (9), 789-796.

26. Higgo, J. J. W.; Rees, L. V. C., Adsorption of Actinides by Marine-Sediments - Effect of the Sediment Seawater Ratio on the Measured Distribution Ratio. *Environ Sci Technol* **1986,** *20*, (5), 483-490.

27. Curl, R. L.; Keoleian, G. A., Implicit-Adsorbate Model for Apparent Anomalies with Organic Adsorption on Natural Adsorbents. *Environ Sci Technol* **1984,** *18*, (12), 916-922.

28. Grover, R.; Hance, R. J., Effect of Ratio of Soil to Water on Adsorption of Linuron and Atrazine. *Soil Sci* **1970,** *109*, (2), 136-&.

29. Chang, C. C. Y.; Davis, J. A.; Kuwabara, J. S., A Study of Metal-Ion Adsorption at Low Suspended-Solid Concentrations. *Estuar Coast Shelf S* **1987,** *24*, (3), 419-424.

30. Santschi, P. H., Factors Controlling the Biogeochemical Cycles of Trace-Elements in Fresh and Coastal Marine Waters as Revealed by Artificial Radioisotopes. *Limnol Oceanogr* **1988,** *33*, (4), 848-866.

31. Nyffeler, U. P.; Li, Y. H.; Santschi, P. H., A Kinetic Approach to Describe Trace-Element Distribution between Particles and Solution in Natural Aquatic Systems. *Geochimica Et Cosmochimica Acta* **1984,** *48*, (7), 1513-1522.

32. Avotins, P.; Jenne, E. A., Time Stability of Dissolved Mercury in Water Samples .2. Chemical Stabilization. *J Environ Qual* **1975,** *4*, (4), 515-519.

Curriculum Vitae

Jin Yang

2526 Rellim Rd, Apt B, Baltimore, MD 21209 jyang59@jhu.edu (410)350-5387

Education

Ph.D., Environmental Engineering (3/2014) Johns Hopkins University, Baltimore, MD GPA 3.7/4.0
M.S., Environmental Engineering (5/2008) Johns Hopkins University, Baltimore, MD GPA 3.9/4.0
B.S., Environmental Science (7/2007) Peking University, Beijing, China GPA 3.3/4.0
B.S., Economics (7/2007) Peking University, Beijing, China GPA 3.0/4.0

Skills

Computation and data analysis: MATLAB, Mathematica, Sigma-plot, SPSS, C
Sample Analysis: Chemical detection (GC/MS, ICP-MS, AAS, UV-Vis, TOC, LSC), material characterization (BET surface area analysis, DLS)
Language: English (fluent), Mandarin Chinese (Native)

Research Projects

Project I: Implication of oxidized multi-walled carbon nanotubes (O-MWCNTs) to aquatic environments: aggregation, adsorption and transport of MWCNTs and their interaction with pre-existing co-contaminants
Advisor: Prof. William P. Ball Sep, 2008 – present
Johns Hopkins University, Baltimore, MD
Developed a reliable experimental set-up to analyze the transport of O-MWCNTs in simulated porous media;
Summarized and improved currently available theoretical models for O-MWCNT removal and successfully conducted simulation using MATLAB;
Discovered an important effect of the solid-to-liquid ratio on adsorption of Zn^{2+} and Ni^{2+} onto O-MWCNTs and proposed theoretical explanation;
Collaborated with graduate students and a professor from Chemistry department and advised 7 undergraduate or graduate lab assistants on the investigation of O-MWCNT transport and adsorption properties.

Project II: Analysis on the Interdependency of Infrastructure networks
Advisor: Prof. Seth Guikema Sep, 2013 – present
Applied graph theory, Monte Carlo method, and Dijkstra's algorithm in the analysis of infrastructure networks;
Learnt new knowledge regarding optimization and graph theory within one semester and successfully created simulated networks for infrastructure systems.

Project III: Investigation of effect of UV light exposure on the stability of CNTs – redox reaction in the presence of radicals
Advisor: Prof. Howard Fairbrother Aug. 2012 – Jan. 2013
Investigated the effect of UV light on the stability of dispersed O-MWCNTs and the possible mechanism for these effects;
Collaborated with Graduate students and professors from Chemistry Department in JHU and Department of Environmental Engineering in Purdue Univesrity.

Publications and Presentations

Yang, J.; Bitter, J. L.; Smith, B. A.; Fairbrother, D. H.; Ball, W. P., Transport of multi-walled carbon nanotubes through porous media: influences of aquatic chemistry, surface oxidation, and natural organic matter. *Environ Sci Technol* **2013,** *47*, (24), 14034-14043.
Smith, B.; **Yang, J.**; Bitter, J. L.; Ball, W. P.; Fairbrother, D. H., Influence of Surface Oxygen on the Interactions of Carbon Nanotubes with Natural Organic Matter. *Environ Sci Technol* **2012,** *46*, (23), 12839-12847.

Yang, **J.**; Smith, B. A.; Bitter, J. L.; Fairbrother, D. H.; Ball, W. P., Transport mechanism of multi-walled carbon nanotubes through porous media**,** (manuscript in preparation)

Platform Presentations

"Aggregation, Sorption and Transport Properties of Carbon Nanotubes as Influenced by Surface Oxides"
SETAC North America 33rd Annual meeting (EPA grantee meeting), Long Beach, CA, Nov, 11 – 15, 2012
"Transport of Multi-Walled Carbon Nanotubes through Porous Media"
The 86th ACS Colloid & Surface Symposium, Baltimore, MD, Jun, 10 – 13, 2012
"Transport properties of Multi-Walled Carbon Nanotubes: Influence of Surface Oxides and Aquatic Chemistry"
The 2011 Association of Environmental Engineering and Science Professors (AEESP) Education & Research Conference, Tampa, FL, Jul, 10 – 12, 2011
"Transport of Oxidized Multi-Walled Carbon Nanotubes through Porous Media"
The 240th ACS National Meeting (Hot Topic Talk), Boston, MA, Aug, 22 – 26, 2010

Poster Presentations

"Transport of Oxidized Multi-Walled Carbon Nanotubes (O-MWCNTs) through porous media"
The 2nd Gordon Research Conference on Environmental Nanotechnology, Stoweflake Resort and Conference Center, Stowe, VT, Jun, 2-7, 2013
"Transport of Oxidized Multi-Walled Carbon Nanotubes through Porous Media"
The 1st Gordon Research Conference Environmental Nanotechnology, Waterville Valley Resort, NH, May, 29 – Jun, 3, 2011
"Challenges in Experimental Studies with Nanomaterials: Sorption and Transport Studies with Carbon Nanotubes"
The 2010 Gordon Research Conference Environmental Sciences: Water, Jun, 20 – 25, 2010
"Adsorption of Divalent Aquatic Contaminants by Oxidized Multi-Walled Carbon Nanotubes: Modeling and Measurements"
The 4th Annual Symposium of the Institute of NanoBioTechnology (INBT), Baltimore, MD, Apr, 29, 2010
"Influence of Surface Oxidation on Divalent Cations Sorption Properties of Multi-Walled Carbon Nanotubes in Single- and Binary-Solute System"
The 2009 Association of Environmental Engineering and Science Professors (AEESP) Education & Research Conference, Iowa City, IA, Jul, 26 – 29, 2009

Honors and Awards

The Lee Albert H. Halff Doctoral Student Award (Sep, 2012- Dec, 2012)
Department of Geography and Environmental Engineering, Johns Hopkins University